



Julian Swatler

**Role of leukemic extracellular vesicles in differentiation
and suppressive activity of regulatory T cells**

PhD thesis
Completed at the Laboratory of Cytometry
of the Nencki Institute of Experimental Biology
Polish Academy of Sciences

SUPERVISOR:
Dr hab. Katarzyna Piwocka
Professor of the Nencki Institute

Auxiliary supervisor:
Dr Ewa Kozłowska
Department of Immunology, Faculty of Biology,
University of Warsaw

Warsaw, 2021



Work included in the thesis was supported by grants from
the National Science Centre and Foundation for Polish Science:

NCN: 2013/10/E/NZ3/00673 SONATA BIS to KP

NCN: 2018/29/N/NZ3/01754 PRELUDIUM to JS

FNP: TEAM-TECH Core Facility PLUS „FlowPROSPER - Flow Cytometry Protein
Signature platform for Personalized Therapies”
2017-2/2 (POIR.04.04.00-00-23C2/17-00) to KP



ACKNOWLEDGEMENTS

Science is always a group effort and so has been this project. Therefore, I would like to thank:

My incredible Supervisor, Professor **Katarzyna Piwocka**, for her constant, multidimensional support throughout the entire time of my PhD studies. From investing in me and my development as an immunologist, all the way to her patience, motivation, always finding time to discuss different scientific and non-scientific issues, invaluable advice and engaging me in many exciting ventures of our Lab.

Ewa Kozłowska, for teaching me about mouse studies, patience and tenacity, as well as help with in vivo mouse experiments.

My incredible colleagues from the lab:

Laura Tuross-Korgul, for her constant, unconditional and selfless support, both in and outside the lab, indispensable help in countless experiments, constant laughter and an amazing friendship.

Wiola Dudka and **Magda Wołczyk** for insightful advice, support, teaching me multiple laboratory techniques and all the highly enjoyable times together, either at work or outside.

Marta Brewińska-Olchowik, **Agata Kominek** and **Łukasz Bugajski** for long hours of sorting cells and other flow cytometric endeavors. **Bac Viet Le**, **Piotr Chrościcki**, **Milena Wiech** and **Kuba Janiec**, **Paulina Podrzywałow-Bartnicka**, **Zosia Dąbrowska** for joint projects, experiments and discussions.

Collaborators:

Salwador Cyranowski for help with in vivo mouse studies, joint projects in glioma immunology, fruitful discussions and a great friendship.

Sara de Biasi for teaching me so much about cytometry, immunology, science and always being a supportive, friendly figure through my journey.

Mrs Lidia Malchar for constant, selfless help and support and always kind discussions.

Professor Andrea Cossarizza for generous support in several cytometric and immunological endeavors.

Paulina Pilanc for help with in vivo mouse studies.

Jakub Mieczkowski and **Elyas Mohammadi** for bioinformatic analyses of transcriptomic data.

Dominik Cysewski for proteomic analysis.

Agata Klejman for support in lentiviral transductions of cell lines.

People I have met during conferences and courses, who have changed my outlook on science, inspired me and gave invaluable advice on several aspects of my project:

Esther Nolte-t Hoen, **Guillaume van Niel**, **Sten Libregts**, **Jan van Deun**, **Marca Wauben**, **Enrico Lugli**, **Zosia Maciorowski**, **Steffen Jung**, **Diane Mathis**, **Erika Pearce**, **Noah Palm**, **Lara Gibellini**, **Sofie van Gassen**, **Martin Williams**, **Nicola Cahill**, **Estefanía Lozano-Andrés**.

My incredible Friends, who have been a terrific support system and have patiently listened to me both praising and complaining about work: **Tosia**, **Ania**, **David** and **Marta**.

Last, but definitely not least, my Parents, **Anna** and **Aleksander Swatler**, for always being there to help and support me, for sharing their life wisdom and invaluable advice on several non-scientific aspects of my work. They have been the true Heroes behind the scenes and I dedicate this thesis to them.

ABBREVIATIONS

Abbreviation	Description
4-1BBL	4-1BB ligand
ALL	Acute lymphocytic leukemia
AML	Acute myeloid leukemia
APOA1	Apolipoprotein A1
Arg1	Arginase-1
BATF	Basic leucine zipper transcription factor, ATF-like
BCR-ABL1	Breakpoint Cluster Region protein and Abelson murine Leukemia viral oncogene homolog 1
BM	Bone marrow
Breg	Regulatory B cell
CCL	Chemokine (C-C motif) ligand
CCR	Chemokine (C-C motif) receptor
CD	Cluster of differentiation
CFSE	Carboxyfluorescein succinimidyl ester
CLL	Chronic lymphocytic leukemia
CML	Chronic myeloid leukemia
CNS	Conserved non-coding sequence
CRISPR/Cas9	Clustered regularly interspaced short palindromic repeats/CRISPR associated protein 9
CTLA-4	Cytotoxic T-lymphocyte-associated protein 4
DC	Dendritic cell
DEG	Differentially expressed gene
DT/DTR	Diphtheria toxin/diphtheria toxin receptor
ESCRT	Endosomal sorting complexes required for transport
eTreg(s)	Effector regulatory T cell(s)
EV(s)	Extracellular vesicle(s)
FACS	Fluorescence-activated cell sorting
FBS	Fetal bovine serum
FlowSOM	Flow cytometry algorithm basen on SOMs (self organising maps)
FLT3-ITD	Fms like tyrosine kinase 3-internal tandem duplication
Foxp3	Forkhead box P3
GFP	Green fluorescent protein
GM130	Cis-Golgi Marker
(g)MFI	(Geometric mean)/median fluorescence intensity
gRNA	Guide RNA
HSC	Hematopoietic stem cell
ICOS	Inducible T-cell costimulator
IFN	Interferon
IL	Interleukin
IL-2R α	Interleukin 2 receptor alpha chain
IL1R2	Interleukin 1 receptor, type II
IL21R	Interleukin 21 receptor
ILV(s)	Intraluminal vesicle(s)

Abbreviation	Description
IRF4	Interferon regulatory factor 4
ISAC	International Society for Advancement of Cytometry
ISEV	International Society for Extracellular Vesicles
iTreg(s)	Induced regulatory T cell(s)
LAG-3	Lymphocyte-activation gene 3
LSC	Leukemic stem cell
MDSC	Myeloid-derived suppressor cells
MHC	Major histocompatibility complex
mTOR	Mammalian target of rapamycin
MVB(s)	Multivesicular body(bodies)
NFκB	Nuclear factor kappa-light-chain-enhancer of activated B cells
NK	Natural killer (cell)
nSMAse2	Neutral sphingomyelinase 2
NTA	Nanoparticle tracking analysis
PBMC(s)	Peripheral blood mononuclear cell(s)
PD-1/PD-L	Programmed cell death protein 1/Programmed death-ligand 1
pTreg(s)	Peripheral regulatory T cell(s)
Rab27a	Ras-related protein Rab-27A
RelA	V-rel avian reticuloendotheliosis viral oncogene homolog A
RFP	Red fluorescent protein
RT	Room temperature
S6	Ribosomal protein S6
SEC	Size exclusion chromatography
SMAD2/3	Mothers against decapentaplegic homolog 2/3
STAT5	Signal transducer and activator of transcription 5
Tconv	Conventional T cell
TCR	T cell receptor
TEM	Transmission electron microscopy
TFBM(s)	Transcription factor binding motif(s)
TGF-β	Transforming growth factor β
Th	T helper
TIGIT	T cell immunoreceptor with Ig and ITIM domains
TIM-3	T-cell immunoglobulin and mucin-domain containing-3
TKI	Tyrosine kinase inhibitor
TNF	Tumor necrosis factor
TNFR2	Tumor necrosis factor receptor 2
TNFSF9	Tumor necrosis factor ligand superfamily member 9
Treg(s)	Regulatory T cell(s)
Tresp	Responder T cell
TSDR	Treg-specific demethylated region
Tsg101	Tumor susceptibility gene 101
tSNE	T-distributed stochastic neighbor embedding
tTreg(s)	Thymic regulatory T cell(s)

ABSTRACT

Chronic and acute myeloid leukemia (CML/AML) constitute cancers that arise in the bone marrow, due to malignant transformation (by oncogenic mutations such as *BCR-ABL1*, *FLT3-ITD* and others) of myeloid progenitor cells. As myeloid leukemias develop, they expand outside the bone marrow and engraft other tissues, such as the spleen or blood. Development and expansion of myeloid leukemias has been recently shown to be significantly facilitated by immunosuppression - a state when anti-tumor immunity is attenuated and dysfunctional. Immunosuppression is largely established by suppressive cell subsets of the immune system, such as regulatory T cells (Tregs) - a type of T cells that express transcription factor Foxp3 and perform tolerogenic/suppressive function. Tregs have been shown to be upregulated in blood and bone marrow of patients with myeloid leukemias. However, as this has only recently been described, mechanisms that drive expansion and suppressive activity of Tregs in leukemias remain largely unexplored. This thesis has aimed at dissecting modulation of Tregs by leukemic extracellular vesicles (EVs) - small, lipid bilayer-enclosed structures released outside cells as mediators of intercellular communication. As EVs have been demonstrated to modulate non-immune components of the leukemic bone marrow niche and have been shown to interact with Tregs in solid tumors, they might also constitute drivers of Foxp3+ regulatory T cells in myeloid leukemias.

Using *ex vivo* cultures of murine and human Tregs with EVs released by CML and AML cell lines, leukemic EVs were shown to upregulate suppressive phenotype and activity of Tregs, as well as level of Foxp3. Leukemic EVs also induced Foxp3 expression in non-regulatory, conventional T cells. Leukemic EVs have upregulated phosphorylation of STAT5 and downregulated mTOR-S6 signaling in T cells to promote Treg induction, activity and stability. RNA-sequencing has revealed significant remodeling of Treg transcriptome by leukemic EVs, upregulated expression of tumor Treg genes and several transcription factors engaged in this regulation. Furthermore, 23-color spectral flow cytometry and unsupervised clustering tools have revealed 2 subsets of human effector Tregs (eTreg) expanded by leukemic EVs - CD30+CCR8^{hi}TNFR2^{hi} eTreg1 and CD39+TIGIT^{hi} eTreg2. Mass spectrometric analysis of leukemic EVs' proteome revealed presence of TNF superfamily protein 4-1BBL, which was engaged in modulation of expression of effector molecules (CD30, TNFR2, LAG-3) on Tregs. Finally, in a developed immunocompetent mouse model of CML-like disease, influence of EVs on Tregs and leukemic progression was validated by development of leukemia by Rab27a-deficient cells, with attenuated secretion of EVs. Rab27a-deficient leukemia has exhibited reduced engraftment in animals, whereas Tregs were less abundant and exhibited a less activated, less suppressive phenotype than in wild-type counterparts.

Altogether, data presented in this thesis pin-point extracellular vesicles, released by chronic and acute myeloid leukemia cells, as significant modulators of regulatory T cells - their induction, suppressive phenotype, function and effector subsets. *In vivo*, in a mouse model of leukemia-like disease, Rab27a-mediated secretion of EVs was shown to modulate Tregs and leukemic engraftment. Therefore, EVs and EVs-Tregs interaction may be evaluated as potential therapeutic targets in myeloid neoplasms.

STRESZCZENIE

Przewlekła i ostra białaczka szpikowa są nowotworami powstającymi w szpiku kostnym w wyniku transformacji nowotworowej (mutacji onkogennych takich jak *BCR-ABL1*, *FLT3-ITD* i innych) komórek progenitorowych linii mieloidalnej. Wraz z rozwojem choroby, komórki białaczkowe ulegają ekspansji poza szpik kostny, do innych tkanek, takich jak śledziona czy krew. Ostatnie badania wykazały, że rozwój białaczek szpikowych jest wspierany przez immunosupresję - stan, w którym przeciwnowotworowa odpowiedź immunologiczna jest zaburzona. Immunosupresja jest w dużej mierze modulowana przez supresyjne komórki układu odpornościowego, w tym regulatorowe limfocyty T (Tregs) - populację limfocytów T, która charakteryzuje się ekspresją czynnika transkrypcyjnego Foxp3 i pełni tolerogenną/supresyjną funkcję. Ilość Tregs jest podwyższona we krwi i szpiku kostnym pacjentów chorujących na białaczki szpikowe. Obserwacja ta została dokonana stosunkowo niedawno i stąd wciąż słabo poznane są czynniki, które powodują wzrost ilości i aktywności Tregs w białaczkach szpikowych. Celem badań przedstawionych w niniejszej rozprawie było określenie, jaką rolę w modulacji Tregs odgrywają białaczkowe pęcherzyki zewnątrzkomórkowe (EVs) - małe struktury, otoczone dwuwarstwową błoną lipidową, wydzielane na zewnątrz komórek i pełniące rolę w komunikacji międzykomórkowej. Wcześniejsze badania pokazały, że białaczkowe EVs mogą wpływać na komórki niszy szpiku kostnego, a EVs z nowotworów litych mogą wpływać na biologię regulatorowych limfocytów T. Stąd w poniższej rozprawie postawiono hipotezę, że białaczkowe EVs również mogą kontrolować regulatorowe limfocyty T.

W hodowlach *ex vivo* mysich i ludzkich regulatorowych limfocytów T z białaczkowymi pęcherzykami zewnątrzkomórkowymi pokazano, że białaczkowe EVs wzmacniają fenotyp i aktywność supresyjną Treg oraz poziom czynnika Foxp3. Białaczkowe EVs doprowadziły też do indukcji Foxp3 w nieregulatorowych, konwencjonalnych limfocytach T. Białaczkowe EVs doprowadziły do wzrostu fosforylacji czynnika transkrypcyjnego STAT5 oraz zahamowania szlaku mTOR-S6 w limfocytach T, promując w ten sposób indukcję, aktywność i stabilność Tregs. Sekwencjonowanie RNA wykazało znaczące zmiany w transkryptomie Treg, podwyższoną ekspresję genów specyficznych dla Tregs w nowotworach oraz wskazało szereg czynników transkrypcyjnych zaangażowanych w regulację Tregs przez białaczkowe EVs. Za pomocą 23-parametrycznej spektralnej cytometrii przepływowej oraz analizy bioinformatycznej danych cytometrycznych, zidentyfikowano dwie subpopulacje ludzkich efektorowych Tregs (eTreg), które ulegały ekspansji pod wpływem białaczkowych EVs - CD30+CCR8^{hi}TNFR2^{hi} eTreg1 oraz CD39+TIGIT^{hi} eTreg2. Za pomocą spektrometrii masowej przeanalizowano skład białkowy białaczkowych EVs i zidentyfikowano w nich białko 4-1BBL (z rodziny TNF). 4-1BBL, znajdujące się w białaczkowych EVs, odpowiadało za wzrost cząsteczek efektorowych CD30, TNFR2 i LAG-3 na Tregs. W ostatniej części, z wykorzystaniem mysiego modelu przewlekłej białaczki szpikowej zbadano wpływ EVs na Tregs i

progresję choroby, poprzez porównanie rozwoju białaczki wywołanej przez komórki typu dzikiego oraz przez komórki pozbawione białka Rab27a, która wydzielają mniejszą ilość białaczkowych EVs. Brak ekspresji Rab27a przez komórki białaczkowe doprowadził do niższego nacieku komórek białaczkowych w myszach, a regulatorowe limfocyty T wyizolowane z tych zwierząt wykazywały mniej aktywowany i mniej supresyjny fenotyp, niż w przypadku białaczki wywołanej przez komórki typu dzikiego (niezmienione).

Podsumowując, wyniki przedstawione w poniższej rozprawie wykazały, że pęcherzyki zewnątrzkomórkowe, wydzielane przez komórki przewlekłej i ostrej białaczki szpikowej, stanowią istotny czynnik modulujący regulatorowe limfocyty T - doprowadzając do indukcji Tregs, wzrostu fenotypu i aktywności supresyjnej oraz ekspansji silnie efektorowych subpopulacji. W mysim modelu przewlekłej białaczki szpikowej, regulowane przez Rab27a wydzielanie pęcherzyków zewnątrzkomórkowych przez komórki białaczkowe również wpływało na regulatorowe limfocyty T oraz rozwój choroby. Tym samym, białaczkowe pęcherzyki zewnątrzkomórkowe i ich interakcja z regulatorowymi limfocytami T mogą stanowić potencjalny cel terapeutyczny w białaczkach szpikowych.

TABLE OF CONTENTS

ACKNOWLEDGEMENTS	3
ABBREVIATIONS	4
ABSTRACT	6
STRESZCZENIE	8
TABLE OF CONTENTS	10
1 INTRODUCTION	13
1.1 Chronic and acute myeloid leukemia (CML/AML)	13
1.1.1 Pathogenesis and treatment	13
1.1.2 Immune system evasion in myeloid leukemias	15
1.2 Regulatory T cells (Tregs)	17
1.2.1 Thymic and extrathymic origin and differentiation	18
1.2.2 Biological function and phenotype of Tregs.....	20
1.2.3 Molecular regulation of Foxp3 and Treg function	22
1.2.4 Regulatory T cells in cancer.....	25
1.2.5 Regulatory T cells in myeloid leukemias	28
1.3 Extracellular vesicles (EVs)	30
1.3.1 Characteristics, composition and biogenesis of EVs	30
1.3.2 Isolation and methods in extracellular vesicles research	32
1.3.3 Extracellular vesicles in immunity and cancer.....	34
1.3.4 Extracellular vesicles as modulators of T cells and Tregs in cancer	36
1.3.5 Extracellular vesicles in myeloid leukemias	37
2 AIMS	39
3 MATERIALS AND METHODS	40
3.1 Cell lines and cell culture	40
3.1.1 Mouse cell lines 32D, 32D BCR-ABL1+ and modifications	40
3.1.2 Human cell lines K562, MOLM-14 and modifications	41
3.1.3 Cell line modification by CRISPR/Cas9-mediated genome editing.....	42
3.2 Cell cycle and population doubling time analysis, clonogenic assay	43
3.3 Extracellular vesicles isolation and characterization	43
3.3.1 Isolation by differential ultracentrifugation	43
3.3.2 Isolation by density gradient ultracentrifugation	45
3.3.3 Primary EVs from plasma of CML/AML patients and isolation by size exclusion chromatography	47
3.3.4 Transmission electron microscopy.....	48
3.3.5 Western blot analysis of proteins.....	48
3.3.6 Nanoparticle tracking analysis	50
3.3.7 Uptake of extracellular vesicles by mouse and human T lymphocytes	51
3.4 Primary cells and cell culture	53
3.4.1 Primary mouse lymphocytes	53
3.4.2 Primary human lymphocytes	55
3.5 Flow cytometry	56
3.5.1 Antibodies and dyes used for flow cytometry.....	56
3.5.2 Staining and analysis of surface and intracellular proteins	59
3.5.3 Analysis of phosphorylated signaling proteins	60

3.5.4 Phenotyping of human Tregs by 23-color spectral flow cytometry.....	60
3.5.5 Computational analysis of flow cytometry data.....	62
3.6 Treg/T cell assays with extracellular vesicles.....	63
3.6.1 Mouse <i>in vitro</i> suppression assay and analysis of Foxp3 level.....	63
3.6.2 Human iTreg inducing culture.....	66
3.6.3 Human Treg/T cell expansion culture.....	67
3.6.4 Human <i>in vitro</i> suppression assay.....	69
3.7 Soluble cytokine analysis.....	70
3.8 RNA sequencing, RT-qPCR, methylation-specific PCR.....	71
3.9 Proteomics.....	73
3.10 <i>In vivo</i> mouse model of CML-like disease.....	74
3.10.1 Development of CML-like disease.....	74
3.10.2 Bioluminescent imaging of entire animals.....	75
3.10.3 Isolation of tissues, engraftment analysis.....	75
3.10.4 Cell phenotyping.....	76
3.10.5 <i>Ex vivo</i> culture of splenocytes and intracellular cytokine staining.....	78
3.11 Statistics.....	79
4 RESULTS.....	80
4.1 Chronic myeloid leukemia-derived extracellular vesicles upregulate suppressive activity and Foxp3 level in mouse thymic regulatory T cells.....	80
4.1.1 Characterization of 32D and 32D BCR-ABL1+ extracellular vesicles.....	80
4.1.2 Mouse thymocytes take up/bind CML EVs.....	81
4.1.3 CML EVs amplify suppressive activity of mouse tTregs.....	83
4.1.4 CML EVs do not inhibit proliferation of effector CD8+ and CD4+ T cells.....	86
4.1.5 CML EVs increase Foxp3 expression in mouse tTregs.....	87
4.2 Chronic and acute myeloid leukemia extracellular vesicles, containing 4-1BBL protein, promote human immunosuppressive regulatory T cells.....	89
4.2.1 Characterization of K562 and MOLM-14 extracellular vesicles.....	89
4.2.2 Human T cells take up/bind leukemic EVs.....	90
4.2.3 Leukemic extracellular vesicles induce Foxp3 and iTregs from non-regulatory cells.....	93
4.2.4 Leukemic extracellular vesicles upregulate suppressive phenotype and activity of human regulatory T cells.....	94
4.2.5 Leukemic extracellular vesicles induce exhausted phenotype and attenuate secretion of inflammatory cytokines in effector, non-regulatory T cells.....	99
4.2.6 Leukemic extracellular vesicles modulate STAT5 and mTOR signaling to induce Foxp3 and upregulate suppressive Tregs.....	102
4.2.7 Leukemic EVs maintain genetic and functional stability of Tregs <i>ex vivo</i>	105
4.2.8 Treg transcriptome is globally affected by leukemic EVs.....	106
4.2.9 Leukemic EVs drive specific signature of human Tregs, including two effector subsets - CD30+CCR8 ^{hi} TNFR2 ^{hi} eTreg1 and CD39+TIGIT ^{hi} eTreg2.....	112
4.2.10 Leukemic EVs from plasma of CML and AML patients induce Foxp3 and promote effector signature of Tregs.....	116
4.2.11 Leukemic EVs contain 4-1BBL/CD137L protein.....	119
4.2.12 4-1BBL protein in leukemic EVs partially regulates effector Treg phenotype.....	123
4.3 Rab27a-dependent extracellular vesicles promote development of leukemia and expand immunosuppressive regulatory T cells <i>in vivo</i>.....	125
4.3.1 Mouse model of CML-like disease.....	125
4.3.2 Rab27a-deficient 32D BCR-ABL1+ cells demonstrate unaffected cell growth and clonogenicity.....	127
4.3.3 Rab27a-deficient CML-like disease leads to CD3+ T cell compartment remodeling.....	129

4.3.4 Rab27a-dependent EVs secretion <i>in vivo</i> modulates Tregs in the spleen and bone marrow of leukemia bearing mice	132
4.3.5 Regulatory B cells and suppressive CD11b+ myeloid cells are not upregulated in CML-like disease and are not affected by Rab27a-dependent EVs	135
4.3.6 Rab27a-dependent EVs secretion <i>in vivo</i> promotes leukemic engraftment.....	137
5 DISCUSSION.....	139
5.1 Relevance of extracellular vesicles in driving immunosuppressive Tregs and myeloid leukemia development	139
5.1.1 Influence of leukemic extracellular vesicles on Tregs and immunosuppression.....	140
5.1.2 Influence of leukemic EVs and Tregs on myeloid leukemia development <i>in vivo</i> – EVs as potential therapeutic targets	142
5.2 Significance of leukemic EVs as drivers of effector, immunosuppressive Tregs, including different Treg subsets	146
5.2.1 Functional relevance of effector Treg subsets driven by leukemic EVs	146
5.2.2 Do effector Treg subsets driven by leukemic EVs resemble Treg subsets identified in solid tumors?	148
5.2.3 Influence of leukemic EVs on Tregs of thymic and peripheral origin	151
5.2.4 Molecular pathways in Tregs influenced by leukemic EVs.....	152
5.3 Significance of 4-1BBL, shuttled by EVs, in leukemia and activity of Tregs	154
6 SUMMARY AND CONCLUSIONS.....	159
7 LITERATURE.....	161
8 PUBLICATIONS - OUTCOME OF THE THESIS.....	176

1 INTRODUCTION

The presented thesis investigates the role of leukemic extracellular vesicles (EVs) in immunity and immunosuppression in myeloid leukemias. Chronic myeloid leukemia was the main malignancy studied in this dissertation, followed by validation of crucial results in acute myeloid leukemia. The focus is directed at influence of EVs on biology of Foxp3+ regulatory T cells - their differentiation, suppressive phenotype, function and molecular pathways, using *ex vivo* (human, mouse) and *in vivo* mouse models. The following introductory chapter will describe pathology and immunology of myeloid leukemias, biology of regulatory T cells and current knowledge of extracellular vesicles in immunity.

1.1 Chronic and acute myeloid leukemia (CML/AML)

1.1.1 Pathogenesis and treatment

Leukemias constitute a group of heterogenous hematological cancers that arise due to malignant transformation of hematopoietic stem cells (HSCs) or multipotent progenitor cells. In normal hematopoiesis, HSCs either self-renew or further differentiate into lymphoid or myeloid progenitor cells. Lymphoid progenitors further give rise to T and B cells, whereas myeloid progenitors give rise to granulocytes, monocytes, platelets and erythrocytes. Altogether, normal hematopoiesis leads to formation of blood cells and platelets, as well as immune cells in the tissues. Oncogenic transformation of HSCs or progenitor cells leads to formation of malignant, abnormal cells - leukemic stem cells (LSCs), and eventually development of leukemia¹. Depending on the type of mutated progenitor cells and disease intensity, leukemia can be classified into 4 main subtypes: chronic myeloid leukemia (CML), acute myeloid leukemia (AML), chronic lymphocytic leukemia (CLL) and acute lymphocytic leukemia (ALL). Myeloid leukemias (CML and AML) are in the scope of presented thesis.

Among leukemias, AML and CLL constitute most common types in adults which has been well documented in both the United States and European population^{2,3}. The average incidence rate for myeloid neoplasms is 4-5/100.000 people for AML⁴ and 1-2/100.000 people for CML⁵. Both CML and AML are mainly diagnosed in adults, with highest incidence among individuals over 65 years old^{5,6}. In terms of deaths due to leukemia, both total amount and death rate is highest for AML^{2,4}. While over 76% of patients with AML will eventually die till 5 years after diagnosis^{4,7}, only 25-30% of CML patients will not survive 5 years^{5,8}. Deaths due to AML constitute over 3% of morbidity due to all cancers^{9,10}. This difference is largely an outcome of different advances in therapy of both types of myeloid leukemia. AML has been mainly treated with chemotherapy and (in some cases) allogeneic stem cells transplantation^{6,7} which do not yield high efficiency. On the other hand, CML

treatment has become significantly more efficient due to introduction of imatinib - a tyrosine kinase inhibitor (TKI) of BCR-ABL1 oncoprotein - a well-established molecular driver of CML¹¹.

Both chronic and acute myeloid leukemia arise in the bone marrow, due to oncogenic alterations in myeloid progenitor cells. CML is a disease driven by one, well-studied abnormality - namely the Philadelphia (Ph) chromosome. Ph chromosome is formed due to reciprocal translocation between chromosomes 9 and 22 which leads to formation of a fusion gene consisting of *BCR* and *ABL1* genes. The *BCR-ABL1* gene encodes a constitutively active tyrosine kinase - BCR-ABL1. BCR-ABL1 over-activates several signaling pathways (among others: JAK/STAT, Ras/MEK, PI3K/Akt, mTOR), inducing robust proliferation and inhibition of apoptosis, as well as simultaneous differentiation arrest of myeloid progenitors¹². CML firstly develops relatively slowly during a chronic phase, predominantly in the bone marrow. However, amplified activity of BCR-ABL1 and activation of other pro-survival pathways lead to accelerated phase and, finally, blast crisis. During blast crisis, immature myeloblasts are present in high numbers in peripheral blood and peripheral tissues, at which stage disease is tougher to control and treat^{5,12,13}. As CML is primarily driven by a single oncogene, it has enabled targeted treatment of the disease. Development of imatinib, a tyrosine kinase inhibitor of BCR-ABL1¹¹, has revolutionized treatment of chronic phase CML and contributed to relatively low morbidity. Moreover, next generation TKIs have been developed, such as dasatinib or nilotinib, enabling treatment of some imatinib-resistant patients⁵. On the other hand, blast crisis CML is still hard to treat which urges the need to look for novel, alternative therapeutic modalities.

On the other hand, genetic background of acute myeloid leukemia is more complex and heterogenous. The most common cause is internal tandem duplication of surface kinase FLT3 (FLT3-ITD), but also mutations in *NPM1*, *DNMT3*, *NRAS*, *TET2*, *RUNX1* and others^{7,14}. Moreover, these mutations are often present simultaneously which constitutes a significant challenge for diagnosis and treatment of AML. As already mentioned, AML is mainly treated with chemotherapy (cytarabine, daunorubicin), but improvements in genetic testing and advancing knowledge of molecular drivers enable attempts to develop novel therapies. Evaluated treatments include: FLT3 inhibitors (such as sorafenib or quizartinib), IDH1/2 inhibitors or CD33-targeting monoclonal antibodies. However, they are yet to yield high efficiency simultaneously with low toxicity⁶.

For both types of myeloid leukemias, a significant obstacle of effective treatment is established by leukemic stem cells (LSCs). LSCs maintain ability to self-renew and constitute an especially drug-resistant subset of leukemic cells. Typically, they are characterized by a CD34+CD38- phenotype^{15,16}, though recent studies have identified new markers of LSCs¹⁶, as well as identified CD34- LSCs¹⁷. Leukemia stem cells reside in a strongly pro-survival bone marrow niche, which constitutes a heterogenous microenvironment, supportive of quiescence and therapy-resistance of LSCs. One of important components of this niche is established by immunosuppressive immune cells¹⁸.

1.1.2 Immune system evasion in myeloid leukemias

Immune evasion is a well-recognized hallmark of cancer. Immune system cells can destroy malignant (including cancer) cells and perform this function daily. However, as cancer eventually develops, it evades immune response and leads to a state of immunosuppression (reduced efficacy of the immune system). Immune evasion and immunosuppression have recently been well documented also in myeloid leukemias. Importantly, though CML and AML constitute genetically distinct diseases, the immune landscape and predominant immunosuppression are similar for both types of myeloid neoplasms.

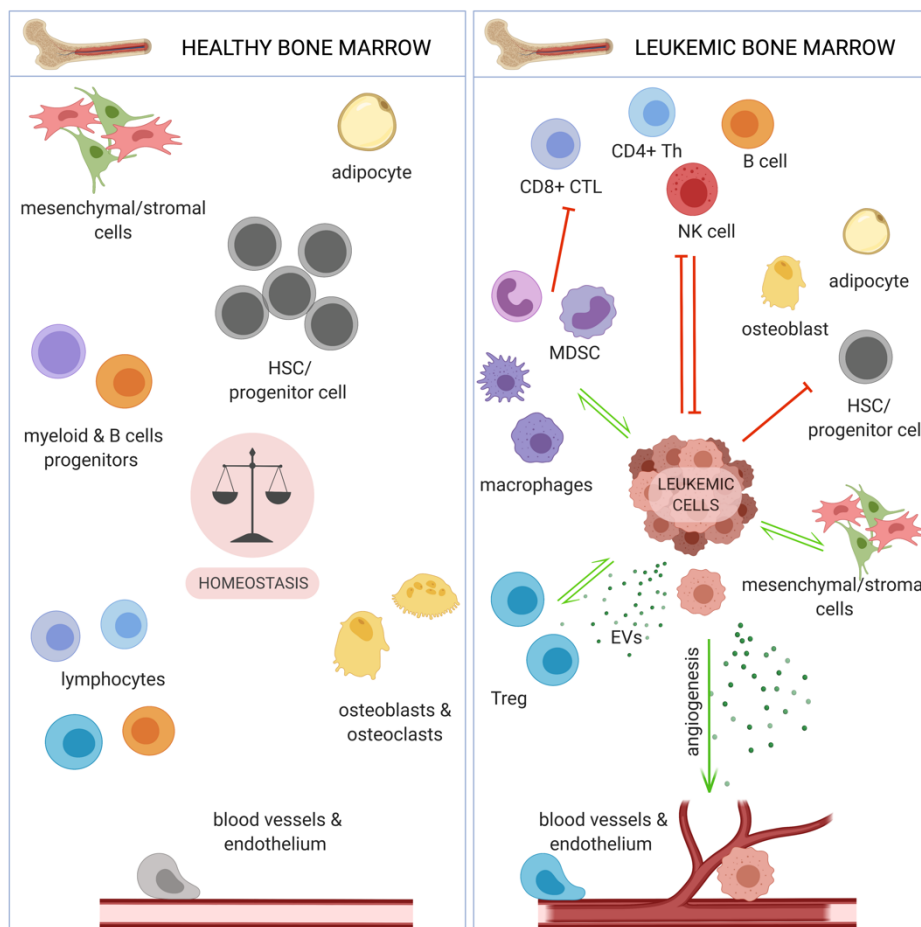


Figure 1.1 Bone marrow (immune) microenvironment at steady state and during leukemia development. In healthy homeostasis (left), bone marrow constitutes a well-balanced tissue, enabling maintenance of hematopoietic stem cells (HSC), normal hematopoiesis and development of leukocytes. During leukemia (right), this equilibrium is disturbed, and the microenvironment is dominated by immunosuppressive cells, leukemia-promoting cells and characterized by abnormal hematopoiesis (figure from Swatler *et al.*, 2021¹⁸). Abbreviations: CTL—cytotoxic T lymphocyte; EVs—extracellular vesicles; HSC—hematopoietic stem cell; MDSC—myeloid derived suppressor cell; NK—natural killer; Treg—regulatory T cell;

At steady state, bone marrow microenvironment is a well-balanced tissue, allowing proper maintenance of HSCs/progenitor cells and differentiation of blood cells (Figure 1.1, left). Apart from hematopoietic compartment, bone marrow is also comprised of stromal cells, osteoblast,

osteoclasts, endothelial cells and adipocytes. During leukemia development, this equilibrium is disturbed, leading to disturbed hematopoiesis¹⁹, expansion of immunosuppressive immune cells (regulatory T cells, suppressive myeloid cells) and dysfunctional effector immunity (dysfunctional CD8+ cytotoxic T cells and natural killer (NK) cells)^{20,21} (Figure 1.1, right).

CD8+ cytotoxic T cells and NK cells are main effector immune cells that eliminate malignant cancer cells and are crucial for tumor clearance, e.g. after immunotherapy. In myeloid leukemias, as in solid tumors, they become dysfunctional and are no longer capable of eradicating cancer cells. In AML, higher CD8+ T cells counts were observed in both bone marrow (BM) and blood of patients²². However, functional and phenotypic studies of CD8+ T cells in AML revealed an exhausted phenotype (expression of PD-1, LAG-3, TIGIT)²³ and disturbances in formation of functional immune synapse by these cells²⁴. CD8+ T cells from CML patients also exhibited limited cytotoxic activity, lower secretion of proinflammatory cytokines IFN- γ and TNF- α and lower expression of TCR ζ ^{25,26}. Natural killer (NK) cells are also less abundant in blood of CML patients at diagnosis²⁵. Functionally, in both chronic and acute myeloid leukemia, NK cells have lower degranulating capacity and express lower levels of effector molecules, such as NKG2D, KIR, NKp30 and NKp46^{27,28}. Detailed changes in biology of antitumor cells - CD8+ T cells and NK cells in myeloid leukemias are summed up in Table 1.1. The lab of Satu Mustjoki (University of Helsinki) has evaluated anti-leukemic immunity in a large immunogenomic study of several hematological malignancies²⁹. By bulk and single-cell RNA sequencing they have globally evaluated expression of genes responsible for cytotoxic activity towards tumor cells and, by bioinformatic and mathematic tools, assessed "cytolytic infiltrate" into respective niches of leukemias and lymphomas. Both CML and AML exhibited significantly lower infiltrate of cytotoxic cells, as compared to CLL and B cell lymphomas, showing they constitute one the most immunosuppressed hematological cancers²⁹. Multiplex histology analyses (also by Mustjoki lab) of bone marrow biopsies of CML and AML patients have confirmed these findings at protein level and revealed dysfunction of other immune cells with anti-tumor potential, such as CD4+ helper T cells, M1-polarized macrophages or DC1/DC2 subsets of dendritic cells^{20,21}. Importantly, antigen-specific studies of CD8+ T cells from CML patients have identified CD8+ T cells specific for leukemic antigens (proteins from leukemic cells)²⁵, which proves that direct anti-leukemic immunity is possible. However, as these cells express PD-1, they are not capable of strong anti-tumor function³⁰.

Collectively, though anti-leukemic immunity is possible, during disease development it becomes attenuated by several immunosuppressive mechanisms. These include immunosuppressive factors expressed directly by leukemic cells (such as inhibitory receptors, enzymes or extracellular vesicles) and immunosuppressive immune cells (suppressive myeloid cells and regulatory T cells). As regulatory T cells and extracellular vesicles are the subject of studies presented in this thesis, they will be further described in detail in the next chapters of this introduction. Myeloid suppressive

cells and factors expressed by leukemic cells have been described in detail in a review article Swatler *et al.*, 2021¹⁸.

Table 1.1 Changes in abundance, phenotype and function of cytotoxic CD8+ T cells and NK cells in myeloid leukemias. Specific phenotypic and functional changes of anti-tumor CD8+ T cells and NK cells are indicated separately for AML and CML, though in both leukemias these cells are dysfunctional. Green and red arrows indicate upregulation or downregulation, respectively, of specified feature. Equal sign indicates no change in a parameter (table from Swatler *et al.*, 2021¹⁸).

Cell Type	Malignancy	Trend	Observation (Number/Functionality)
CD8+ T cells	AML	↑	absolute number in PB
		↓	amount in BM
		↑	terminally differentiated/exhausted
		↑	PD-1, 2B4, LAG-3, TIGIT, CD57
CD8+ T cells	AML	=	cytokine secretion
		↓	formation of immune synapse
		↓	granzyme B, CD27
		↓	
CD8+ T cells	CML	↓	TCRζ
		↓	cytotoxicity, secretion of IFN-γ, TNF-α
		↓	CD62L
		↓	granzyme B, CD27, OX40, LAG-3
CD8+ T cells	CML	↓	CTLA-4, TIM-3, PD-1
		↑	
		↓	
		↓	
NK cells	AML	↓	NCRs (NKp30, NKp44, NKp46)
		↓	secretion of IFN-γ
		↓	
		↓	
NK cells	CML	↓	amount in PB
		↓	NKG2D, NKG2A, NKG2C
		↓	degranulating capability (CD107a)
		↓	NCRs (NKp30, NKp46), KIR

Abbreviations: PB–peripheral blood; BM–bone marrow; PD-1–programmed cell death protein 1; LAG-3–lymphocyte activation gene 3; TIGIT–T cell immunoglobulin and ITIM domain; TCR–T cell receptor; IFN-γ–interferon γ; TNF-α–tumor necrosis factor α; CTLA-4–cytotoxic T- lymphocyte antigen 4; TIM-3–T cell immunoglobulin and mucin domain 3; NCRs–natural cytotoxicity receptors; NKG2D/NKG2A/NKG2C– natural killer group 2D/2A/2C; KIR–killer cell immunoglobulin-like receptor.

1.2 Regulatory T cells (Tregs)

T lymphocytes constitute one of the most abundant and crucial subsets of immune cells. They develop in the thymus and are characterized by expression of CD3 and the T cell receptor (TCR), which enable interaction with antigen presenting cells and development of specific, adaptive immunity. In general T cells are divided into CD4+ helper T cells and CD8+ cytotoxic T cells, which jointly perform defensive immune function against pathogens and malignant cells. However, CD4+ T cells constitute a heterogeneous population consisting of functionally distinct subsets, including regulatory T cells - Tregs. Contrary to effector CD4+ T cells, Tregs perform a tolerogenic function, maintaining self-tolerance and preventing autoimmunity. Early studies by Sakaguchi have revealed that thymectomy, resulting in depletion of a "T cell subset" (which later turned out to be Tregs), leads to autoimmunity in mice³¹. Further studies performed by this group have identified CD25-expressing T cells (named regulatory T cells) as a subset that prevents autoimmunity³². Finally, Ramsdell, Sakaguchi and Rudensky groups have discovered Foxp3 as a hallmark transcription factor and molecular driver of regulatory T cells^{33–36}. Therefore, regulatory T cells

(Tregs) are now recognized as a tolerogenic, anti-inflammatory T cells subset, phenotypically described as CD4⁺CD25^{hi}Foxp3⁺ (in humans additionally CD127^{lo}).

1.2.1 Thymic and extrathymic origin and differentiation

Regulatory T cells can have a dual origin - they can differentiate either in the thymus (thymic/thymus-derived Tregs - tTregs) or in the periphery (peripheral/peripherally derived Tregs - pTregs). In the latter case, environmental cues can drive Foxp3 expression in non-regulatory, conventional CD4⁺CD25⁻ T cells. T cell subsets, including tTregs, differentiate in the thymus firstly from double negative thymocytes (CD4⁻CD8⁻), through double positive cells (CD4⁺CD8⁺) to finally either CD4⁺(CD8⁻) or CD8⁺(CD4⁻) single positive lymphocytes. tTregs mainly arise among the single positive CD4⁺ lineage, although Foxp3⁺ cells can be found at the double positive³⁷ or even double negative stage³⁸. According to the current paradigm, tTregs arise in a two-step process. Firstly, stimulation of the TCR (by MHC complex) leads to upregulation of IL-2R α (CD25), whereas in the second step cytokines (such as IL-2, IL-15, which drive STAT5 signaling) promote Foxp3 expression. Though still a matter of controversy^{39,40}, it is generally established that Tregs in the thymus (tTregs) arise after interaction of TCR with MHC-self-peptide complex, which makes them specific for self-antigens and thus predisposes them to tolerogenic function and prevention of autoimmunity⁴¹. Therefore, tTregs have a different TCR repertoire than conventional CD4⁺ T cells, which have a rather pro-inflammatory function⁴². Self-antigens are predominantly presented by medullar thymic epithelial cells (mTEC), in a process regulated by autoimmune regulatory (Aire) protein⁴³.

On the other hand, peripheral regulatory T cells are generated outside the thymus in peripheral tissues. Foxp3 can be induced in conventional CD4⁺CD25⁻ T cells by factors such as cytokine TGF- β or retinoic acid, in a process which also requires TCR stimulation and a costimulatory signal⁴⁴. However, in this case Tregs are specific to foreign-antigens and thus promote tolerance towards foreign factors⁴⁵. Prime example includes peripheral Tregs induced in the gut in response to short chain fatty acids released by commensal microbiota. This way, tolerance to human gut microbiome is maintained, which is beneficial to human homeostasis⁴⁶. On the other hand, this process may not be beneficial when Tregs are induced in the tumor microenvironment, to attenuate immunity towards tumor cells. In some cases, pTregs or iTregs (induced/*in vitro*-induced Tregs, a term which historically has been referred to Tregs induced in the periphery, but now is mainly attributed to Tregs induced experimentally *in vitro*⁴⁷) exhibit unstable expression of Foxp3, lack a specific Treg epigenetic signature and can "reverse" back to a non-regulatory phenotype⁴⁸. In terms of molecular regulation (which will be described in more detail in Chapter 1.2.3), tTregs and pTregs undergo distinct regulation of the Foxp3 promoter. pTregs are driven by CNS1 intronic regulatory

element, which contains binding sites for SMAD3 (downstream of TGF- β) and retinoic acid receptor. On the other hand, lack of CNS1 does not affect differentiation of tTregs⁴⁹.

Tregs in blood and peripheral tissues are highly heterogenous depending on the niche and, also depending on the tissue, constitute a mix consisting of different amounts of tTregs and pTregs. This may also differ depending on the type of cancer. To elucidate that, several phenotypic and molecular markers have been investigated to enable distinguishing of these populations. Identification of stable tTregs is also of high relevance in adoptive Treg therapies in transplantation or autoimmune diseases. Initially, neuropilin-1 and Helios were proposed as markers of tTregs^{50,51}. However, some studies have suggested otherwise and shown that neuropilin-1 does not distinguish human tTregs⁵². Nevertheless, multiple studies confirmed Helios as a marker of tTregs and up to date it is probably the most used protein to distinguish this population. An experiment performed as a part of this thesis on mouse Tregs has confirmed that Helios expression can be used to reliably describe Tregs as thymic (Figure 4.3B). Moreover, CD31 can be used as a marker of recent thymic emigrant cells⁵³ and a very recent study has selected a transmembrane protein GPA33 as a marker of stable Tregs of thymic origin⁵⁴.

Group of Sakaguchi has proposed a classification of human Tregs according to stability and functionality, rather than arbitrary division into tTregs and pTregs. Foxp3/CD25 may be expressed at low levels in non-Treg cells, as well as unstable Tregs. Thus, Sakaguchi group has proposed to divide Tregs into 3 fractions based on CD45RA and Foxp3/CD25 expression (blue frames on Figure 1.2, orange frames represent non-Treg, Foxp3⁻ conventional T cells - Tconv). Fraction I Tregs exhibit a naive, CD45RA⁺Foxp3^{lo} phenotype. They are natural, stable Tregs, mostly of thymic origin. However, they have not proliferated and are yet to perform effector, suppressive function. Fraction II Tregs (CD45RA⁻CD45RO⁺Foxp3^{hi}) constitute an effector fraction of cells, with high expression of effector molecules CCR4, CTLA-4 and a strong suppressive activity. They also constitute a stable Treg subset. Both fraction I and fraction II Tregs have demethylated TSDR (Treg-specific demethylated region) in the *Foxp3* gene, which is an epigenetic trait specific for stable Tregs^{48,55}. Fraction III Tregs exhibit a CD45RA⁻CD45RO⁺Foxp3^{lo} phenotype, weaker suppressive activity, partially methylated TSDR, as well as secrete inflammatory cytokines. They probably constitute a mixture of unstable Tregs and non-Tregs with transient, low expression of Foxp3⁴⁸. This classification points out that human CD25⁺CD127^{lo}Foxp3⁺ cells may include unstable Tregs. This signifies that experiments on human Treg cells should not only include analysis of suppressive function and phenotype, but also deliver insight into stability of analyzed cells.

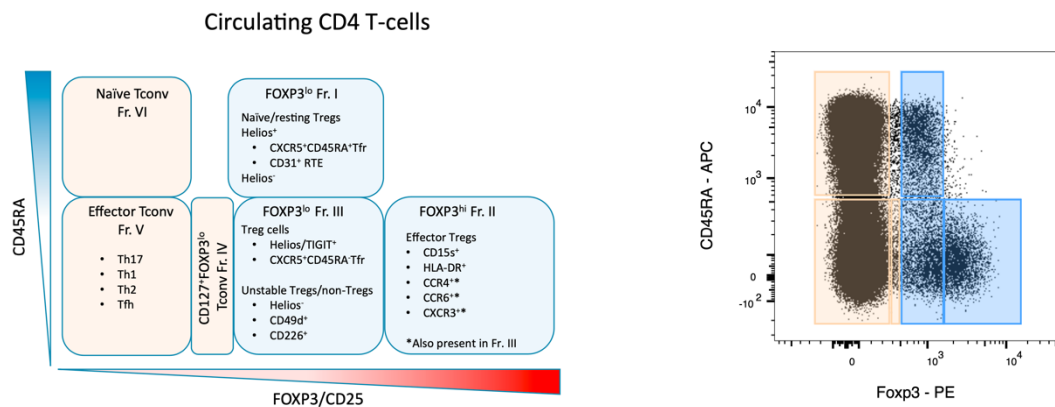


Figure 1.2. Human regulatory T cells contain subsets of different maturation and stability. Human regulatory T cells can be divided into three fractions (Fr. I-III, blue frames, Fr. IV-VI in orange are non-Treg, Fcpx3- conventional T cells - Tconv), based on expression of CD45RA and Fcpx3/CD25. Fractions I and II constitute stable subsets, whereas fraction III are unstable Tregs, which may lose Treg identity. Left panel shows schematic division and short characteristics of Treg fractions (figure from Wine *et al.*, 2019⁴⁸). Right panel shows distribution of CD4⁺ subsets on an actual blood sample analyzed by flow cytometry, based on CD45RA and Fcpx3 staining. Abbreviations: Fr.-fraction; RTE-recent thymic emigrant; Tconv-conventional T cells; Tfh-T follicular helper; Tfr-T follicular regulatory; Th-T helper; Tregs-regulatory T cells.

1.2.2 Biological function and phenotype of Tregs

Regulatory T cells perform several tolerogenic functions to maintain homeostasis. These processes include prevention of autoimmunity (tolerance to self-antigens), attenuation of allergic reactions and chronic infections, control of acute infections (inflammation resolution), tissue repair following injury, as well as tolerance to commensal microbiota, transplanted organs and fetus during pregnancy. All these functions are beneficial to a human body. On the other hand, Tregs may also create the state of immunosuppression and thus hamper anti-tumor immunity, which is far from beneficial⁵⁶. High relevance and beneficial role of Tregs have been confirmed by phenotypes of Fcpx3 knock-out mice (Fcpx3^{-/-}, *scurfy* mice) or CTLA-4^{-/-} animals (CTLA-4 is a functional molecule characteristic for Tregs). Both animal strains develop lymphoproliferative disease - phenotype that is lethal by 3 weeks of age³⁶. Similarly, humans with deficiencies in *Fcpx3* gene develop immunodysregulation polyendocrinopathy and enteropathy, X-linked (IPEX) syndrome - a fatal autoimmune disease³⁷. Moreover, less severe mutations in *FOXP3*, *IL2RA* (encoding CD25) or *CTLA4* genes affect Treg development and enhance the risk of developing autoimmune type 1 diabetes or rheumatoid arthritis⁵⁷.

Tregs are characterized by a specific phenotype (described below), which enables their identification (for example by multiparameter flow cytometry) and functional characteristics. While Fcpx3, a hallmark Treg transcription factor, is rather a molecular driver of these cells, most surface receptors/molecules and soluble factors (cytokines) characteristic for Tregs are functional and

orchestrate the tolerogenic, suppressive function (Figure 1.3). CD25 (α chain of the IL-2 receptor), together with β and γ chain of the IL-2 receptor, effectively binds IL-2 in the environment. Tregs themselves do not produce IL-2, but require it for survival, Foxp3 expression, expansion and suppressive activity. As IL-2 is produced by activated, effector CD4⁺ conventional T cells and, to a lesser extent, CD8⁺ T cells, binding of IL-2 by Tregs sequesters this cytokine from the environment and blocks a positive activating loop of effector T cells, simultaneously leading to Treg expansion⁵⁸. CTLA-4 is a coinhibitory receptor, which binds costimulatory proteins CD80/CD86 on antigen presenting cells. Normally, binding of CD80/CD86 on antigen presenting cells (such as dendritic cells) to CD28 on T cells leads to T cell activation. However, CTLA-4 binds CD80/CD86 with higher affinity and thus blocks an activating costimulatory signal to attenuate T cell activation⁵⁹. Crucially, inhibition of CTLA-4 by blocking antibodies may restore/amplify effector immunity and enable anti-tumor responses - such approach has been largely successful and a CTLA-4 blocking antibody ipilimumab (Yervoy) is now used in the clinic in treatment of cancers, such as melanoma⁶⁰. Another suppressive mechanism employed by Tregs is degradation of extracellular ATP. Normally, extracellular ATP can enhance immune response. Ectoenzymes (ectonucleosidases) CD39 and CD73 on Treg surface catalyze degradation of ATP to AMP (by CD39) and then AMP to adenosine (by CD73), which inhibits activation of effector and antigen presenting cells^{61,62}. Though CD39 and CD73 are preferentially expressed by Tregs (though they exhibit different expression pattern between mice and humans), they may also be present on dysfunctional CD8⁺ T cells in the tumor microenvironment⁶³.

Tregs secrete several cytokines that contribute to their tolerogenic function - IL-10, IL-35 and TGF- β . TGF- β displays a pleiotropic function, as it not only inhibits effector T cells and induces Tregs from non-regulatory cells, but can also influence tumor cells and facilitate therapy resistance by activating pro-survival signaling, as shown by our group in myeloid leukemias⁶⁴. IL-10, on the other hand, apart from well recognized function in immunosuppression in cancers, plays a significant role in the gut. Treg-derived IL-10 inhibits pathogenic Th17 T cells and induces tolerogenic dendritic cells in the gut, which attenuates inflammation in the intestinal mucosa⁶⁵. Finally, Treg cells can directly kill effector CD4⁺ and CD8⁺ T cells by cytotoxic mechanisms, involving granzyme B and perforin⁶⁶. Described phenomena constitute well-recognized mechanisms of Treg action. Recent years have discovered even more molecules (for example coinhibitory proteins) involved in Treg function, especially in the tumor microenvironment, which will be introduced and described in the following chapter on Treg in cancer.

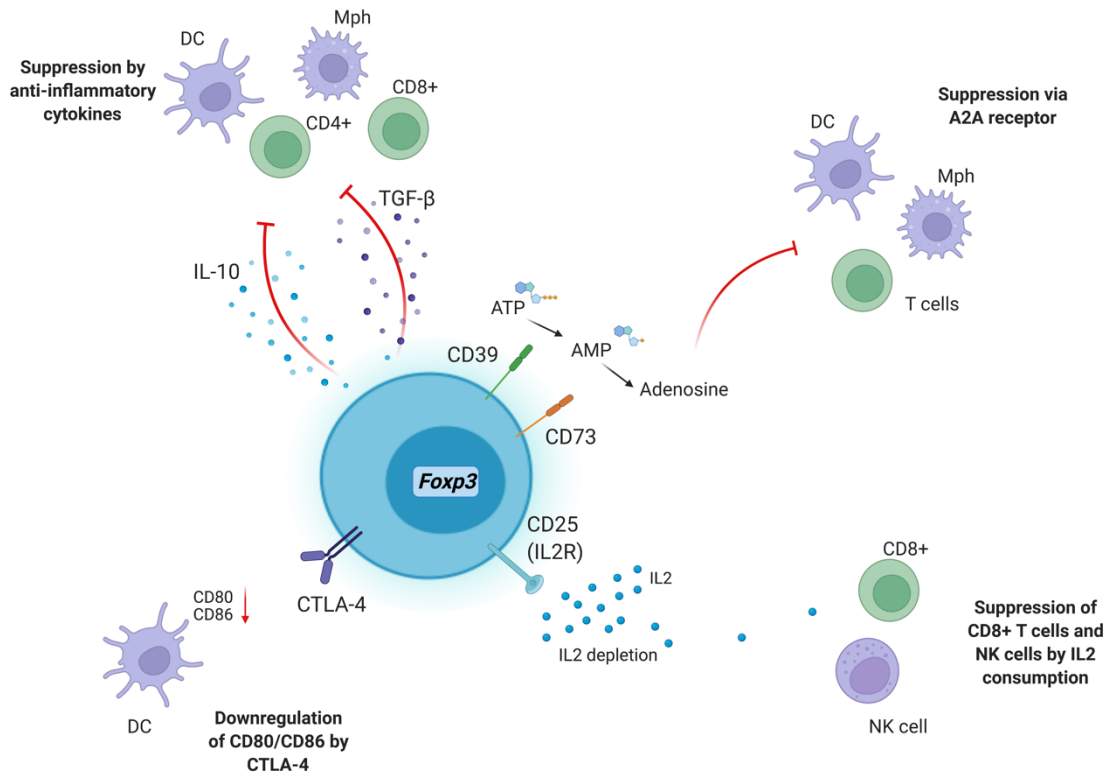


Figure 1.3. Mechanism of Treg suppressive activity. Tregs can perform their suppressive function via suppressive receptors (CTLA-4), IL-2 depletion via CD25, ectonucleosidases CD39 and CD73, as well as suppressive cytokines, such as IL-10 and TGF- β . All these mechanisms lead to attenuated effector function of CD4 and CD8 effector T cells, dendritic cells and macrophages (figure based on Plitas & Rudensky, 2016⁵⁶). Figure created with BioRender.com. Abbreviations: DC-dendritic cell; Mph-macrophage; IL-interleukin; CTLA-4-cytotoxic T cell antigen 4; ATP-adenosine triphosphate; AMP-adenosine monophosphate; TGF- β -transforming growth factor β ; NK-natural killer.

Apart from strictly immune functions (tolerogenic and immunosuppressive), Tregs also establish homeostasis in the peripheral tissues by influencing non-immune cells. This includes interaction with several types of cells in the brain. Tregs can prevent astrogliosis and neuronal apoptosis in the injured brain, interact with neurons by expressing serotonin receptors, as well as promote neuronal remyelination by modulating oligodendrocytes⁶⁷. Crucially for the scope of this thesis, Tregs can also perform non-immune functions in the bone marrow. Tregs in the healthy bone marrow enforce quiescence of hematopoietic stem cells (HSCs), in a process regulated by ectonucleosidase CD39. Indeed, inhibited migration of Tregs into bone marrow by CXCR4 deletion resulted in amplified HSCs proliferation⁶⁸.

1.2.3 Molecular regulation of Foxp3 and Treg function

Transcription factor Foxp3 is constitutively expressed in regulatory T cells and establishes a main driver of expression of genes crucial to suppressive function of Tregs. *Foxp3* gene itself is under complex molecular regulation, as well as downstream effects of Foxp3 activity are affected by several mechanisms.

Foxp3 itself can bind almost 3000 genomic sites to directly regulate 700-1400 genes. However, these include only less than 10% of genes under Foxp3 control. The rest requires interaction and formation of large complexes of Foxp3 and other transcription factors⁶⁹. Foxp3 can exist and function in different multimolecular complexes, which can localize in different regions of the nucleus and determine either activator or repressor function of Foxp3⁷⁰. These can include transcription factors such as NFAT, RUNX1 and IRF4, though interaction with each one of them controls expression of different genes relevant to distinct functions⁷¹⁻⁷³. Foxp3 can also act through inducing epigenetic changes in target loci of regulated genes. Indeed, during development Treg cells acquire a specific epigenetic signature that enables their stability and expression of Treg specific genes⁷⁴. For example, expression of genes encoding CD25 and CTLA-4 is regulated by acetylation of histones next to their gene promoters⁷⁵. Tregs are also characterized by a specific CpG hypomethylation pattern, including Treg-specific genes such as *Il2ra* (encoding CD25), *Foxp3*, *Ctla4* and *Ikzf4* (encoding EOS). Interestingly, specific hypomethylation pattern is generated in Tregs independent of Foxp3, which signifies relevance of epigenetic signature, alongside Foxp3, for Treg function⁷⁶.

Foxp3 itself is under complex molecular regulation. *Foxp3* gene is highly conserved between humans and mice, which enables use of both human and mouse models for studies of *Foxp3* gene expression. *Foxp3* consists of 11 exons and is regulated by binding of transcription factors to either gene promoter or enhancer conserved non-coding sequences (CNS). A landmark study by Rudensky lab has identified three CNS sequences - CNS1, CNS2, CNS3. CNS3 is only required for tTreg development in the thymus, but not engaged in Treg biology in the periphery. CNS2 is required for maintaining *Foxp3* expression in tTregs after leaving the thymus. CNS2 is highly hypomethylated and contains the TSDR region, which demethylation is an indicator of stable Tregs^{48,55}. CNS2 binds several transcription factors such as REL, STAT5, RUNX1, CREB-ATF1 and Foxp3 itself to maintain Treg stability and activity. Finally, CNS1 is responsible for peripheral induction of *Foxp3* expression, such as Foxp3 induction in non-regulatory CD4+ T cells⁴⁹.

Foxp3 gene regulation in the periphery via CNS2 and CNS1 maintains Treg stability and function in response to several extracellular factors (Figure 1.4). IL-2, following binding of its receptor CD25, activates JAK kinases to induce phosphorylation of STAT5 (pSTAT5). pSTAT5 binds CNS2 to maintain *Foxp3* expression. Importantly, phosphorylated STAT5 can maintain *Foxp3* expression and Treg function independently of IL-2 and STAT5 deficiency leads to lower Treg amount⁷⁷. CNS1 activity is mainly driven by TGF- β and SMAD signaling, but also retinoic acid (vitamin A metabolite) and short chain fatty acids released by commensal microbiota. On the other hand, proinflammatory cytokines destabilize *Foxp3* expression - for example IL-6 recruits DNMT1 methyltransferase and leads to CNS2 methylation⁷⁸. Also engagement of TLR ligands provides Treg destabilizing signals, as it activates PI3K-Akt-mTOR pathway and switches Treg metabolism into glycolysis, leading to

impaired suppressive function⁷⁹. Moreover, mTOR pathway inhibition promoted SMAD3 activity (independent of TGF- β) and Treg differentiation⁸⁰. An interesting, recently reported aspect of Foxp3/Treg molecular control is the role of costimulation via TNF superfamily and TNF receptors. While most-recognized cytokine in this family - TNF- α - is rather a proinflammatory factor, TNF- α itself and other cytokines/proteins from TNF superfamily can be beneficial for Treg biology. Several recent studies have observed that stimulation of Tregs with ligands for TNFRSF members (TNF receptor superfamily members), such as GITRL, OX-40L, 4-1BBL and agonists for TNFR2 and DR3 led to increased Treg proliferation, viability and significant transcriptomic remodeling^{81,82}. On signaling level, TNF pathway was dependent on a NF- κ B family protein RelA. Induction of RelA activity in Treg by 4-1BB, TNFR2, DR3 and GITR costimulation was demonstrated by electrophoretic mobility shift assay (EMSA)⁸². On the other hand, phosphorylation of RelA was only promoted by TNFR2 and GITR agonists⁸¹. Tregs deficient in RelA had downregulated expression of genes encoding effector molecules (*Icos*, *Tigit*, *Il10*, *Ctla4*)⁸¹ and CD44+CD62L- activated Treg were less abundant in mice with RelA-deficient Treg⁸³. Finally, RelA was required for development of Tregs in the intestine⁸¹ and costimulation via TNF superfamily receptors has promoted Treg-mediated suppression of colitis in mice⁸²

Foxp3 and Treg function are also regulated at a protein level by several posttranslational modifications (Figure 1.4). Acetylation stabilizes Foxp3 protein, as it prevents lysine residues from ubiquitylation (and subsequent proteasomal degradation), as well as facilitates chromatin binding and transcription factor function. Interestingly, Foxp3 acetylation can be partially induced by TGF- β and short-chain fatty acids secreted by commensal microbiota⁶⁹. Phosphorylation of Foxp3 can have a dual effect, either stimulating or inhibiting Treg function. On the other hand, ubiquitylation targets Foxp3 towards proteasomal degradation and causes loss of Treg-identity. Foxp3 can become polyubiquitylated after exposure to inflammatory cytokines, LPS or heat-shock, in a process mediated by ubiquitin ligase STUB1⁸⁴. On the contrary, deubiquitinates are a Foxp3 stabilizing factor⁸⁵.

Collectively, molecular identity of Treg cells is very complex, thus requires study of several aspects of these cells to gain information even partially about regulated processes in a certain biological setting. Though Foxp3 is the main driver of Treg cells, it can cooperate with several other transcription factors to determine the final functional phenotype. Finally, Foxp3 itself undergoes a multilayer regulation on transcriptional and post-transcriptional levels.

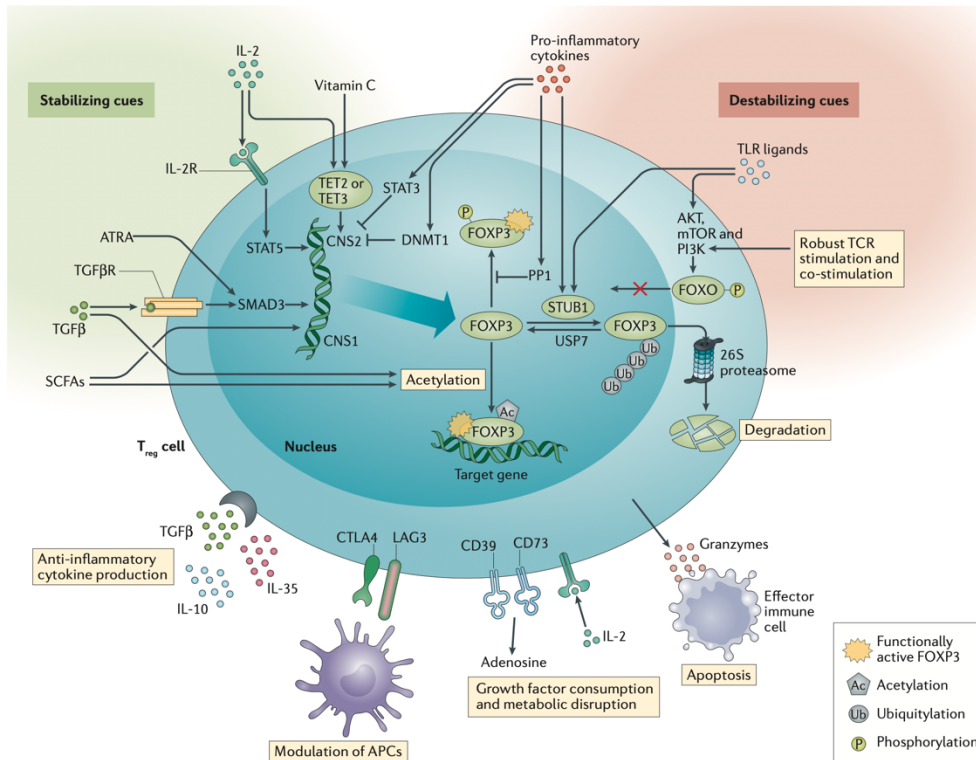


Figure 1.4. Mechanisms that stabilize (green) and destabilize (red) Treg identity and function. Treg cells respond to extracellular signals, via signaling cascades and epigenetic mechanism, to either maintain stable phenotype or lose Treg identity and suppressive function. Examples of these signaling pathways, extracellular signals and epigenetic modifications are shown in the upper part of the Figure. Following stable Foxp3 expression, they can perform suppressive function via surface molecules (CTLA-4, LAG-3, CD39, CD73) or secretory factors (TGF- β , IL-10, IL-35, granzymes), shown in the bottom part of the Figure (figure from Lu *et al.*, 2017⁶⁹).

1.2.4 Regulatory T cells in cancer

Analyses of human solid cancers have shown that large amounts of Foxp3+ regulatory T cells infiltrate tumors, where they hamper anti-tumor immunity and promote cancer growth. High ratio of Tregs to CD8+ cytotoxic T cells has been associated with poor prognosis of patients^{86,87}. In animal models of cancer, Treg depletion by administration of anti-CD25 antibody or diphtheria toxin/DT (to deplete Tregs in Foxp3^{DTR} animals, which express DT receptor in Foxp3-expressing cells) has slowed down growth of tumors. Moreover, Treg depletion in mouse models has potentiated effect of immunotherapy by anti-CTLA-4/anti-PD-1 blockade^{88–91}.

Regulatory T cells in tumors usually exhibit effector phenotype (fraction II - Figure 1.2), thus exhibit high level of Foxp3, CD25 and lack expression of markers of naive Tregs, such as CD45RA and CCR7⁴⁸. Tregs in tumors exhibit high levels of molecules associated with Treg activation and suppression, such as CTLA-4, PD-1, LAG-3, TIGIT and ICOS⁹². LAG-3 is an inhibitory receptor which binds MHC-II with higher affinity than the TCR complex and thus inhibits T cell activation⁹³. TIGIT is also a coinhibitory receptor, as it blocks costimulatory interaction of CD155 with CD226

and thus inhibits proinflammatory Th1 and Th17 responses^{94,95}. Another group of markers highly upregulated on tumor Tregs are TNF receptor superfamily members OX-40, 4-1BB, TNFR2, GITR⁹² and CD30⁹⁶. As described in the previous chapter, engagement of these receptors by their ligands promotes Treg proliferation and tolerogenic function. Tregs in cancer are also characterized by high expression of chemokine receptors CCR4 and CCR8. CCR4 is expressed by effector Tregs, not only in the tumor microenvironment. Chemokines CCL17 and CCL22 can be expressed in the tumor milieu and induce Treg chemotaxis via CCR4⁹⁷. CCR8 has been identified as a tumor Treg marker in a high-throughput RNA-sequencing (RNA-seq) study of Tregs in breast cancer. The study carried out in the Rudensky lab constituted one of the first studies when high-throughput RNA-seq enabled identification of novel effector/tumor Treg markers. CCR8 expression by Tregs may facilitate their migration into the tumor following CCL1 chemokine secreted by myeloid cells in the tumor⁹⁸. CCR8 has been established as one of most specific markers of Tregs in cancer and Treg depletion via CCR8 targeting has proven to be of therapeutic value⁹⁹.

Further studies by RNA-sequencing revealed another set of markers upregulated on Tregs in tumors¹⁰⁰. Study by De Simone *et al.*⁹⁶ in non-small cell lung cancer and colorectal cancer has compared transcriptomes of tumor Tregs to Tregs in blood and Tregs of healthy donors, but also Tregs in adjacent healthy tissues of cancer patients (e.g. healthy lung fragment from a patient with lung cancer). Tumor Treg cells exhibited elevated expression of well-recognized *ICOS*, *CTLA-4*, *TNFRSF4* (encoding OX-40), *TNFRSF9* (4-1BB) and *TIGIT*, but also novel tumor Treg genes such as *TNFRSF8* (encoding CD30), *HAVCR2* (TIM-3), *PDCD1LG2* (PD-L2), *LGALS9* (galectin-9) and *TFRC* (encoding transferrin receptor CD71). Together with flow cytometric analysis of proteins on Tregs, this study has pin-pointed a novel set of tumor Treg markers: CD30, IL1R2, IL21R, TIM-3, PD-L1, PD-L2⁹⁶. Further studies of Tregs from both human and mouse tumors have confirmed relevance of molecules such as CCR8, CD39, IL21R, 4-1BB, CCR4, TIGIT, ICOS and IL1R2 as drivers of Treg function in tumors¹⁰¹. Finally, a study by Alvisi *et al.*¹⁰² has brought even more dimensionality into research on Tregs in tumors. Application of 27-parameter flow cytometry has enabled identification of two distinct subsets of Tregs in lung cancer samples. These subsets could be distinguished by expression of IRF4 transcription factor, as well as high expression of CCR8 and ICOS by the IRF4+ subset. IRF4+ Tregs exhibited an effector phenotype, amplified suppressive activity and deletion of IRF4 in Tregs *in vivo* slowed down tumor growth in mouse model of MC38 colon cancer. IRF4 and its partner BATF directly regulated expression of immunosuppressive genes in Treg¹⁰². Collectively, Tregs in cancer acquire an effector, highly immunosuppressive phenotype, which may be determined by expression of various functional markers. As single cell studies have revealed, Tregs can consist of distinct subsets which signifies the need for use of advanced single cell technologies and clustering methods to analyze these cells in a tumor setting.

Another feature of Treg cells in the tumor microenvironment is their metabolic adaptation. Cancer cells rely on glucose metabolism (Warburg effect) and thus the tumor microenvironment is generally poor in glucose. Interestingly, effector T cells with anti-tumor function also employ aerobic glycolysis as main catabolic pathway, which is unfavorable in low-glucose tumors and one of mechanisms of immunosuppression. Curiously, regulatory T cells have lower dependency on glucose and rely on different bioenergetic processes to efficiently perform their immunosuppressive, tumorigenic function. Tregs in the tumor microenvironment rely on expression of scavenger receptor CD36 (responsible for lipid uptake)¹⁰³, uptake of free fatty acids¹⁰⁴ and fatty acid oxidation to perform suppressive function¹⁰⁵. Tumors which synthesize and release fatty acid into the microenvironment facilitate Treg function¹⁰⁴. Interestingly, Tregs can also utilize lactate as an energy source. Lactate is an abundant metabolite in the hypoxic, acidic tumor microenvironment. Deletion of lactate transporter MCT1 in Tregs has attenuated their immunosuppressive activity and inhibited tumor growth in mouse models of melanoma, colon and oral cancers¹⁰⁶. Similar effect was observed in mouse model of breast cancer. Knock-down of lactate dehydrogenase and therefore lactate release in tumor cells led to loss of Treg functional stability and amplified anti-tumor effects of anti-CTLA-4 immunotherapy¹⁰⁷. Altogether, Tregs rely on specific metabolic adaptation to promote cancer growth. Importantly, attenuated mTOR signaling in Tregs not only promotes differentiation and activity of these cells (as mentioned in one of the previous chapters), but also facilitates their metabolic adaptation. mTOR-S6 activity drives glycolysis in effector (non-Treg) T cells, so its inhibition contributes to metabolic program that promotes Treg function in tumors. Opposite to mTOR signaling, Treg cells usually maintain activated AMPK signaling, which promotes reliance on fatty acid oxidation¹⁰⁸.

Overall, as regulatory T cells expand and acquire an immunosuppressive, effector phenotype in tumors, they constitute an attractive therapeutic target in cancer. As already mentioned, experimental Treg depletion in animal models of cancer yielded very promising results⁸⁸⁻⁹¹, but such approach is far more challenging in humans. Early approaches included targeting Tregs by anti-CCR4 or anti-CD25 antibodies. Though Treg depletion was successful, these antibodies also targeted activated, anti-tumor effector (non-Treg) T cells, which can express these receptors following activation^{109,110}. Moreover, markers of tumor, effector Tregs are also expressed (though at lower level) on Tregs in blood of healthy people and tissue Tregs. Thus depletion of Tregs may lead to autoimmune events, as Treg subsets that maintain self-tolerance could be depleted⁹². Thus, therapeutic Treg depletion requires thorough studies into Treg phenotypes depending on tissues and tumor, as well as insight into specificity and mode of action of Treg-depleting antibodies. As direct Treg targeting proves challenging, an attractive option is to target tumor-derived mechanisms and factors that promote effector Tregs in tumors. Such approach may not elicit autoimmunity, as

well as affect other tumorigenic cell subsets, not only Tregs. This signifies the need to study mechanisms that drive Treg in cancer.

1.2.5 Regulatory T cells in myeloid leukemias

Similarly to solid tumors, immunosuppressive Tregs have also been implicated in myeloid neoplasms, in both chronic and acute myeloid leukemia (Figure 1.5). Amount of regulatory T cells is increased in peripheral blood of both AML and CML patients^{111–113}. Tregs from blood of AML patients exhibited increased suppressive activity in an *in vitro* suppression assay, as well as increased expression of GITR, CTLA-4 and granzyme B¹¹³. Another study has demonstrated that AML Tregs were predominantly more suppressive towards CD4+ effector cells, rather than CD8+ T cells. AML Tregs potently inhibited release of IFN- γ by effector cells¹¹⁴. Tregs from AML patients potently produce IL-35, which can directly protect AML blast from cell death induced by chemotherapy¹¹⁵. In CML, Tregs exhibited suppressive activity towards effector T cells that were specific for leukemic antigens, such as HLA-A3 restricted BCR-ABL peptide¹¹⁶. This provides evidence that Tregs in CML can perform a pro-leukemic function by specifically targeting anti-tumor immune cells.

Recent studies have also shown increased Treg numbers in the bone marrow (BM) of AML and CML patients, both by flow cytometry^{114,117} and histological analyses of BM biopsies^{21,118}. Cells in the leukemic bone marrow secrete factors that induce chemotaxis of Tregs into the bone marrow niche. Studies using MLL-AF9 mouse model of AML have revealed that this process is dependent on the CCL3/CCR1/CCR5 and CXCL12/CXCR4 axes. Blockade of this interaction has reduced Treg migration into the BM and resulted in slower development of leukemia-like disease¹¹⁹.

Relevance of Treg cells for development and progression of myeloid leukemias has been signified by several clinical observations. In CML, Treg amount correlated with *BCR-ABL1* transcript level and blast counts. Tregs were elevated in patients in blast crisis (compared to chronic phase) and in patients with high Sokal score¹²⁰. Treg amount in the AML bone marrow correlated with shorter survival²¹. Treg levels may predict response to chemotherapy in AML, as patients with high Treg levels in blood generally fail to respond to chemotherapy^{113,121,122} and patients who relapsed after therapy had higher Treg amount than patients at diagnosis^{117,123}. In fact, patients who responded to chemotherapy in AML had decreased level of Tregs in both peripheral blood and bone marrow aspirates^{124,125}. In CML, successful treatment with tyrosine kinase inhibitors (imatinib, dasatinib) also led to lower Treg numbers and weaker suppressive phenotype (expression of CTLA-4, GITR, IL-10)^{126,127}. Patients that achieved treatment-free remission had the same Treg levels as healthy, non-leukemic control patients¹²⁸. Interestingly, imatinib, a BCR-ABL1 inhibitor, has been shown to directly target Tregs and induce their apoptosis, due to its off-target activity towards kinases required for Treg activation^{129,130}. Direct evidence of Tregs relevance for development of myeloid

leukemias was obtained using mouse models of AML-like disease. In MLL-AF9 model of AML developed in *Foxp3^{DTR}* animals (DTR - diphtheria toxin receptor) - administration of DT and therefore Treg depletion resulted in longer survival of animals¹¹⁹. In an *in vivo* AML model generated by C1498 cells, depletion of Tregs by CD25-targeting antibody or IL-2DT (diphtheria toxin conjugated to IL-2, which binds CD25 and Tregs) has augmented effect of adoptive immunotherapies and slowed down disease progression^{131,132}. Only recently, similar studies have been carried out in an *in vivo* model of CML, using *Foxp3^{DTR}* animals, and led to similar observations. Depletion of Tregs by DT injections led to prolonged survival of animals with BCR-ABL1-positive CML¹³³.

Finally, mechanisms that drive regulatory T cells in myeloid neoplasms have not been extensively studied and, so far, have only been described for acute myeloid leukemia. Enzyme IDO (engaged in tryptophan metabolism) can be produced by AML blasts and mesenchymal stem cells in the AML bone marrow. IDO levels correlated with amount of CD4+CD25^{hi} Tregs in BM and blood of AML patients and led to expansion of suppressive Tregs in *in vitro* cultures of AML blasts with CD3+ T cells^{134,135}. Several *in vitro* and *in vivo* studies have also implicated costimulatory and coinhibitory pathways in Treg expansion, maintenance and suppressive function in AML (Figure 1.5). These pathways included ICOSL/ICOS¹³⁶, PD-L1/PD-1¹³⁷, Gal-9/TIM-3¹³⁸ and CD200/CD200R¹³⁹. Finally, Tregs could also be induced by regulatory B cells (CD19+CD25^{hi}CD38^{hi}) from AML bone marrow¹¹⁴.

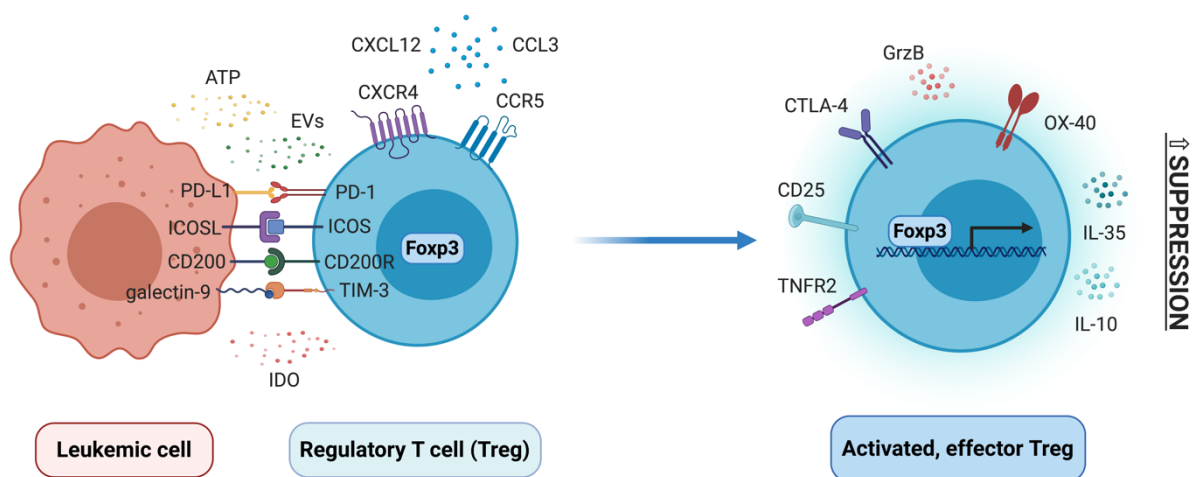


Figure 1.5. Treg cells are promoted in the leukemic microenvironment to exhibit effector phenotype and perform immunosuppressive, pro-leukemic function (figure from Swatler *et al.*, 2021¹⁸). Abbreviations: ATP–adenosine triphosphate; EVs–extracellular vesicles; PD-1–programmed cell death protein 1; PD-L1–programmed death ligand- 1; ICOS–inducible T-cell costimulator; ICOSL–ICOS ligand; TIM-3–T cell immunoglobulin and mucin domain 3; IDO–indoleamine 2,3-dioxygenase; Foxp3–forkhead box P3; CXCL12–C-X-C motif chemokine 12; CCL3–chemokine (C-C motif) ligand 3; CXCR4–C-X-C chemokine receptor type 4; CCR5–C-C chemokine receptor type 5; TNFR2–tumor necrosis factor receptor 2; CTLA-4–cytotoxic T lymphocyte-associated protein 4; GrzB–granzyme B; IL-35–interleukin 35; IL-10–interleukin 10.

Nevertheless, mechanism that drive Tregs in myeloid leukemias, especially in CML, are still largely unexplored. Moreover, despite several clinical studies have been performed (described above), Tregs from CML and AML patients remain poorly characterized. Finally, very few studies on CML and AML biology have been performed using immunocompetent mouse models. Therefore, the field is lacking information on immunity in tissues where myeloid neoplasms initially develop. Bone marrow and spleen are resident tissues for leukemic stem cells, thus dissecting function of immunosuppressive cells and their subsets in the tissues is of high relevance, for example in terms of therapy-resistance of quiescent LSCs. In the presented thesis, a new mechanism (extracellular vesicles) that promotes immunosuppressive Tregs in myeloid neoplasms is extensively studied and described. Moreover, studies using mouse model of CML-like disease provide further insight into Treg biology *in vivo* in the tissues that establish myeloid leukemia microenvironment.

1.3 Extracellular vesicles (EVs)

1.3.1 Characteristics, composition and biogenesis of EVs

Extracellular vesicles (EVs) have only recently become well recognized mediators of intercellular communication. They are small particles with a lipid bilayer that are released by all types of cells. EVs mediate indirect communication between cells and, potentially faraway, tissues. EVs can contain variety of different cargo, including proteins, nucleic acids (DNA and different kinds of RNA) and lipids (Figure 1.6)¹⁴⁰. EVs cargo, such as their proteome, may be similar to the composition of parental cell type, but may as well be significantly different, due to a specific function¹⁴¹. Moreover, function and cargo may vary in different subtypes of extracellular vesicles released by the same type of cells. Traditionally, EVs have been divided into small exosomes (50-150 nm in diameter) and medium/large microvesicles (50-500 nm). Large apoptotic bodies or oncosomes are also classified as extracellular vesicles. However, the main difference between exosomes and microvesicles, rather than size, is their origin and biogenesis. Microvesicles are formed due to budding from the plasma membrane, whereas exosomes are derived from endocytic recycling pathways and multivesicular bodies^{141,142}. However, current methods of EVs isolation do not enable clear distinction of these populations, when large amounts of EVs are analyzed. Origin of a specific EV/group of EVs can be determined by imaging methods, such as electron or high-resolution fluorescent microscopy, by observing biogenesis processes as they occurred. On the other hand, current methods of sequential high-speed ultracentrifugation and density gradient ultracentrifugation enable isolation of EVs of different size (small vs. large EVs) or density (light vs. dense EVs) and attribution of biological properties to these subsets of vesicles. Indeed, studies by group of Clotilde Théry identified specific protein content of different subsets of EVs¹⁴³, as well as different ability to stimulate T cells by small or large EVs released by dendritic cells¹⁴⁴. Independent on size or origin of EVs, some proteins have been established as general "EV-marker" proteins

(highly expressed in all EVs) and allow to assess purity of the isolated biological material. These EV-marker proteins include for example tetraspanins CD9 and CD63, membrane protein Flotillin-1, chaperones Hsp70 and Hsp90. Tetraspanin CD81 and biogenesis factors Alix and Tsg101 (endocytic proteins) are rather specific for small EVs/exosomes¹⁴³.

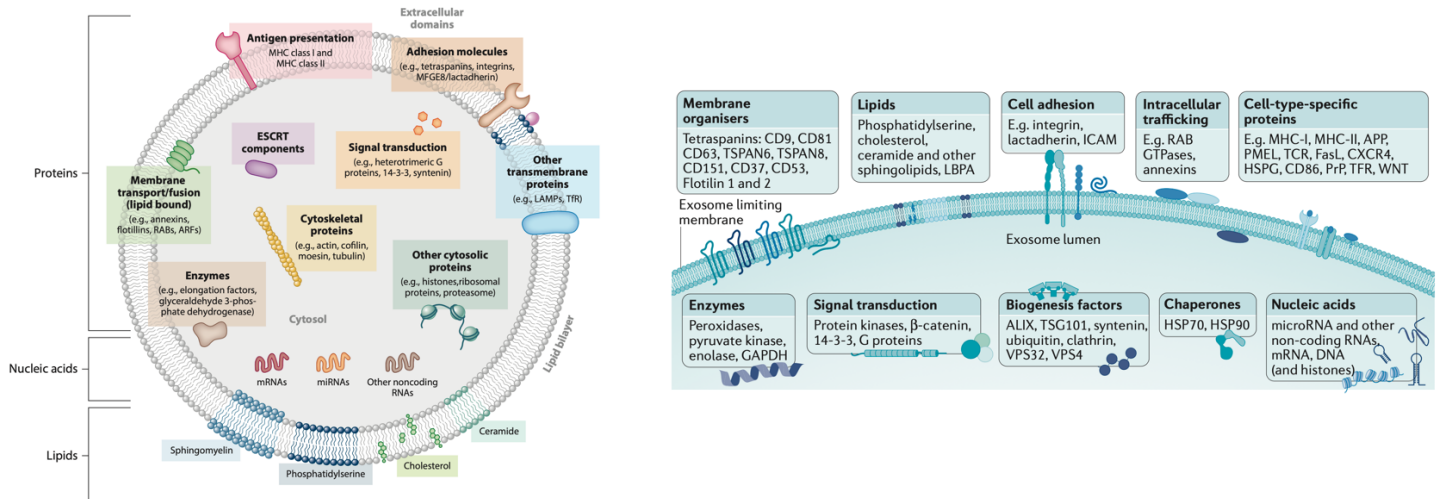


Figure 1.6. Extracellular vesicles may shuttle different sorts of cargo. General sorts of cargo that can be transported by all kinds of extracellular vesicles (left). Types of cargo and proteins enriched in small EVs/exosomes (right) (figures from Colombo *et al.*, 2014¹⁴⁰ and van Niel *et al.*, 2018¹⁴¹).

The scope of this thesis is focused on small leukemic EVs, thus mechanisms of small EVs/exosomes biogenesis will be briefly described below. Exosomes originate from multivesicular bodies (MVBs, a compartment of endocytic recycling) which contain intraluminal vesicles (ILVs). After MVBs fuse with plasma membrane, intraluminal vesicles can be released outside the cell as exosomes/small EVs. Formation of intraluminal vesicles and cargo targeting into the ILVs requires function of the ESCRT (endosomal sorting complex required for transport) and ESCRT-accessory molecules. Proteins from the ESCRT machinery, such as Tsg101, Alix and VPS4 are thus often considered as protein markers of exosomes. Additionally, ESCRT-mediated formation of the ILVs can be facilitated by syntenin-1/syndecan-1 binding and subsequent recruitment of ESCRT protein Alix¹⁴⁵. Budding of ILVs requires ceramide - a lipid generated by sphingomyelinases, such as nSMase2. Targeting of nSMase2 by RNA interference or inhibitor GW4869 affects secretion of small EVs¹⁴⁶. Release of ILVs (thus exosomes/small EVs) requires fusion of MVBs with the plasma membrane. This process engages small GTPases such as Rab27a, Rab27b or Rab7, as well as SNARE complexes¹⁴⁵. Indeed, silencing (by shRNA) of Rab27a and Rab27b, but not of other Rab GTPases (such as Rab6a, Rab7, Rab11a) led to diminished secretion of EVs¹⁴⁷. On the contrary, overexpression of Rab27b increases amount of released EVs¹⁴⁸. Such genetic manipulations thus constitute useful tools in studies of extracellular vesicles. Nevertheless, they should be used with caution, as Rab GTPases are not only engaged in biogenesis of EVs, but also for example secretion of soluble factors via the Golgi apparatus¹⁴⁵.

Once extracellular vesicles are released, they can reach their target cells. Currently, it is not clear whether these processes are generic or programmed in any way (that is if EVs of specific origin have specific target cells). *In vivo* studies that tracked labelled-EVs injected into mice have demonstrated that EVs first localize in the liver and lungs, due to highly phagocytic activity of tissue-resident macrophages¹⁴⁹. On the other hand, when EVs isolated from different cell types were injected into animals, their distribution across tissues was different, though still majority of particles localized in the liver¹⁵⁰. Indeed, as EVs have different molecules on their surface, it may predispose them to bind different cells or avoid certain cells. For example, as dendritic cell-derived EVs express MHC molecules, it increases the likelihood of binding T cells via MHC-TCR interaction. EVs from certain cell types, such as tumor cells, express CD47 molecules, which specifically prevents endocytosis by phagocytic cells¹⁵¹. The interaction between an EV and recipient cell may also not be cell type specific and depend on interaction between adhesion molecules and integrins or extracellular matrix components^{141,145}. Once EVs bind the target cell, they may activate intracellular signaling cascades without internalization (by receptor-ligand interactions, e.g. antigen presentation¹⁵²) or may be internalized by the cell. Internalization may occur through several types of endocytosis - macropinocytosis, phagocytosis, clathrin-dependent endocytosis or via caveolae. Membrane of EV may also fuse with membrane of target cell and release content of an EV into the cytoplasm. When EVs undergo endocytosis, their fate inside the cell may include lysosomal degradation, release of vesicle contents, but also secondary release outside the cell. If cargo of extracellular vesicles is released inside the target cell, it can influence intracellular signaling or gene expression, e.g. by miRNAs or mRNAs released from EVs¹⁵³.

1.3.2 Isolation and methods in extracellular vesicles research

Extracellular vesicles were first discovered in the 1980's as a way of elimination of redundant proteins by reticulocytes¹⁵⁴. Initial studies, that have provided invaluable insight into biogenesis, morphology and size of EVs have been mainly based on ultrastructural methods, such as transmission electron microscopy (TEM). Electron microscopy enables imaging of structures inside the cell with great detail and thus image EVs "in the flesh", though at a fixed point in time. It has been used to this day as a reliable method for studies on EVs structure, trafficking and biogenesis. Only recently, methods based on fluorescent, high-resolution microscopy have been introduced and, combined with electron microscopy (in methods such as CLEM - combined light electron microscopy) have enabled studies on dynamics of EVs release and trafficking in 3D and live in time¹⁵⁵, also *in vivo* in the zebrafish model¹⁵⁶.

Assessment of composition or functional significance of extracellular vesicles requires isolation of these structures from medium conditioned by cells of interest. This still constitutes one of the biggest issues in the field. As EVs are very small structures, their isolation may be biased by

contamination with other components of similar size which is impossible to validate by rapid methods, as it is possible in case of isolation of cells or DNA/RNA. Several methods of EVs isolation have been developed at the frontier of 20th and 21st century and have been further developed and perfected until now¹⁵⁷. The most traditional method is differential ultracentrifugation, which enables pelleting of EVs based on sequential high-speed ultracentrifugation steps¹⁵⁸. Moreover, EVs can be isolated by density gradient centrifugation using sucrose or iodixanol (Optiprep™), which allows isolation based on different density of particles. Additionally, methods based on size exclusion chromatography, immunocapture by antibodies or commercial precipitation-based kits (such as Exo-Quick™), have been developed. Each of these methods has its advantages and drawbacks and provides different yield (quantity), but also different purity of EVs, which is an important consideration before functional studies. Several methods have been elegantly compared in a study by the group of An Hendrix¹⁴⁸. While density gradient is a method that provides best purity of EVs preparations, it is also the most time-consuming and most-challenging technically. On the other hand, differential ultracentrifugation delivers decent purity and high yield, whereas it is much easier and cheaper^{142,148}. Indeed, differential ultracentrifugation and density gradient are (in that order) two most widely used methods for EVs isolation¹⁵⁹. Nevertheless, isolation method should be based on aim of the experiment and research question. Importantly, several other aspects should be taken into consideration, such as culture conditions of cells that release of EVs of interest. For example, use of serum, which contains large amount of bovine EVs, constitutes a challenging aspect. Serum may be purified of EVs before such culture (e.g. by overnight ultracentrifugation), some cells may also be cultured without serum, though it may induce cellular stress response^{142,160}. Another aspect is isolation of extracellular vesicles from biofluids, such as urine, milk or, in the scope of this thesis, blood plasma/serum¹⁶¹. Challenges and good practices in functional studies of EVs have been described in detail in a Swatler *et al.* (2020) protocol article in *Current Protocols in Immunology*¹⁴².

Overall, huge dispersion in methods of EVs isolation has caused an unordered and somewhat confusing state of the field. With simultaneously increasing interest in EV research, this has encouraged leaders in the field to establish International Society of Extracellular Vesicles (ISEV) in 2011 and, in 2012, a society peer-reviewed *Journal of Extracellular Vesicles* (JEV). One of the crucial tasks of the Society has been to introduce guidelines, good practices and standardization in research on extracellular vesicles. The first aim is to increase reproducibility of EVs research, by providing, in research papers, detailed methodology of EVs isolation, especially culture conditions for conditioned medium generation and parameters of differential ultracentrifugation (including rotor type, ultracentrifugation speed and time etc.). The second aim of these standardization and guidelines efforts has been introduction of requirements to provide evidence that the isolated, analyzed material is indeed EVs. Isolation protocols are not straightforward, often challenging and may require adaptation to different cell types. Taking "shortcuts" or inappropriate protocol

adaptations may lead to severe contamination or low yield of EVs. In such case providing data on "influence of EVs released by ..." is inappropriate and may spread false scientific conclusions. To enable realization of both aims, ISEV has published a position paper on "Minimal experimental requirements for definition of extracellular vesicles and their functions" in 2014¹⁶² and a largely update version on "Minimal information for studies of extracellular vesicles" (shortly: MISEV) in 2018¹⁶³. Moreover, ISEV has also issued several position papers on specific areas of EVs analyses, such as analysis of RNA composition of EVs¹⁶⁴, analysis of EVs by flow cytometry¹⁶⁵ or clinical applications of EVs¹⁶⁶. The main postulates of MISEV 2018 include appropriate nomenclature of EVs, thorough reporting, experimental controls and extensive characterization of isolated EVs preparations. To characterize and validate EVs, several experiments need to be conducted - such as electron microscopy imaging of EVs, quantification and size measurement of EVs by nanoparticle tracking and analysis of EV-markers proteins and proteins absent in EVs (such as mitochondrial or ER proteins and lipoproteins, for example by western blot)^{162,163}. A large effort by group of An Hendrix has facilitated observing of these standardization and characterization guidelines by creating a platform that collects information if a certain study has fulfilled the recommendations. The created platform - EV-TRACK - collects information on EVs characterization and analysis and generates an EV-metric, that allows to assess the extent of thoroughness of a certain EV study¹⁶⁷. In the presented thesis, both MISEV 2018 and EV-TRACK guidelines have been followed and will be thoroughly presented in the Methods and Results sections.

1.3.3 Extracellular vesicles in immunity and cancer

Initial evidence that EVs can be engaged in immunity has come from studies on antigen presenting cells, such as dendritic cells (DCs) and B cells. First experiments have revealed that EVs from these cells can contain MHC (major histocompatibility complex) molecules and thus stimulate T cells^{158,168}. Further analyses have also identified costimulatory B7 proteins and functional antigen peptide-MHC complexed in EVs derived from antigen presenting cells^{169,170}. Stimulation of T cells by antigen-loaded EVs can lead to formation of anti-tumor immunity¹⁶⁹. Interestingly, composition of EVs of dendritic cells can vary depending on the stimuli and polarization (pro- versus anti-inflammatory) and they can thus induce different kinds of T cell responses, including proinflammatory Th1 or more tolerogenic Th2 or Treg^{171,172}. T cells themselves are also capable of releasing EVs, for further cross-talk with dendritic cells¹⁷³, but also to perform their own function, such as immune suppression by regulatory T cells. Tregs have been shown to inhibit proinflammatory response of type Th1 helper T cells, as well as secretion of proinflammatory cytokines by DCs, via miRNAs shuttled in extracellular vesicles^{174,175}. EVs are engaged in immunity not only via communication between immune cells, but may also involve interaction with non-immune cells. Induction of immune tolerance has been widely attributed to EVs secreted by mesenchymal stem cells (MSCs). EVs from MSCs contain regulatory miRNAs and proteins such

as IDO, TGF- β and IL-10, which potentiate anti-inflammatory and regenerative arms of the immune system¹⁷⁶. Indeed, significant progress has been achieved in studies on MSC-derived EVs and they have already been tested in first clinical trials for treatment of graft-versus-host disease following transplantation¹⁷⁷. Also EVs derived from cancer cells can have an immunosuppressive influence¹⁶⁹. Tumor EVs contain variety of mRNAs, non-coding RNAs and proteins that facilitate immune evasion by promoting either dysfunction of effector cells or amplified activity of suppressive immune cell subsets. EVs can for example carry an immune checkpoint molecule PD-L1¹⁷⁸ or induce PD-L1 expression by myeloid cells (such as monocytes), via shuttled Y-RNAs^{179,180} - to attenuate effector T cell function (influence of tumor EVs on T cells and Tregs will be described in detail in the next chapter). Moreover, cancer EVs can impair activating signals of antigen presenting DCs¹⁸¹, induce immunosuppressive M2-polarized macrophages¹⁸² and decrease cytotoxicity (expression of CD107a, NKG2D) of natural killer cells¹⁸³. In some cases, such as following chemotherapeutic treatment, EVs released by cancer cells can elicit anti-tumor immunity, though this occurs less often than the immunosuppressive influence¹⁶⁹.

Extracellular vesicles establish important players in the tumor milieu also by influencing non-immune cells and processes (or at least processes where immune cells are not the sole players). EVs in cancer can contain proteins or nucleic acids specific or upregulated by cancer cells, which determines their tumorigenic function, but also enables their use for cancer diagnostics by liquid biopsy, such as EGFRvIII mRNA in glioblastoma¹⁸⁴ or miR-21 in esophageal cancer¹⁸⁵. EVs can also contain DNA fragments, including mutated oncogenes or pathogenic oncoproteins themselves¹⁸⁶. Most importantly, tumor EVs can regulate several types of cells in the cancer microenvironment, such as endothelial and stromal cells. Extracellular vesicles have been well documented in stimulation of angiogenesis by modifying endothelial cells, especially when EVs were released by tumor cells in hypoxic conditions¹⁸⁷. Influence on vessels also includes downregulation of tight junction proteins and increased vascular "leakiness" - a process which facilitates metastases^{188,189}. Moreover, EVs released by cancer cells promote activation of fibroblasts and differentiation into cancer-associated fibroblasts (CAFs)^{190,191}. In turn, CAFs further support tumor growth, by for example attenuating the immune response and increasing migratory capacity and chemoresistance of tumor cells. In part, CAFs modulate these processes by releasing pro-tumorigenic EVs themselves^{190,192,193}. Cancer EVs can also facilitate epithelial to mesenchymal transition, as well as remodeling of the extracellular matrix¹⁹⁴. EVs-derived proteinases remodel the extracellular matrix to facilitate formation of invadopodia and thus invasiveness/migration of tumor cells^{195,196}. Finally, as extracellular vesicles can modulate faraway cells, they can establish a premetastatic niche in distant tissues. For example, EVs can form premetastatic niche in the lung by influencing the secretome of lung epithelial cells, as well as recruitment of immunosuppressive

monocytes/macrophages and neutrophils. Interestingly, expression of organ-specific integrins on EVs can predispose them to formation of premetastatic niche in a specified tissue¹⁹⁷.

Collectively, extracellular vesicles may be engaged in both effector immunity, immunosuppression, as well as modulate cancer microenvironment by non-immune mechanisms. The outcome of EVs influence may differ depending on other cues in the microenvironment and type of disease studied. This provides the rationale to study these particles in new experimental and tissue settings to dissect their relevance to previously uninvestigated biological processes.

1.3.4 Extracellular vesicles as modulators of T cells and Tregs in cancer

Cancer extracellular vesicles can contain variety of immunosuppressive protein cargo, such as TGF- β /LAP, cyclooxygenase-2, ectonucleosidases CD39/CD73, PD-L1 or arginase-1^{198–203}. These proteins are well recognized for attenuation of effector activity of CD4⁺ and cytotoxic CD8⁺ T cells, as well as upregulation of Treg function. *Ex vivo* studies of T cells treated with purified extracellular vesicles have demonstrated that EVs from several solid tumors induced apoptosis and decreased proliferation of both CD4⁺ and cytotoxic CD8⁺ T cells^{199,200,204}, as well as remodeled gene expression of T cell subsets²⁰⁵. Also functionality of T cells was affected, as they have secreted less IL-2 and TNF- α (due to adenosine generated by CD39/CD73 shuttled in tumor EVs)¹⁹⁸ and expressed lower levels of CD3 ζ (due to activity of arginase-1 shuttled in ovarian cancer EVs)¹⁹⁹. PD-L1-expressing glioblastoma EVs have inhibited proliferation and activation (expression of CD25 and CD69) of T cells via PD-1/PD-L1 signaling²⁰⁶. Strong evidence of immunosuppressive influence of EVs towards effector T cells has come from *in vivo* studies on prostate cancer (TRAMP-C2 model) by Poggio *et al.*²⁰². The authors have observed PD-L1 presence in tumor EVs and generated cell lines deficient in PD-L1 or Rab27a (that secreted lower amounts of EVs) and injected these cell lines (and wt counterparts) into animals. Deficiency of PD-L1 and Rab27a led to a more proliferative (Ki67⁺), cytotoxic (granzyme B⁺) and less exhausted (TIM-3⁺) phenotype of CD4⁺ and CD8⁺ T cells in tumor draining lymph nodes of animals, demonstrating that PD-L1-containing EVs induce T cell dysfunction *in vivo*. Importantly, PD-L1 and Rab27a knock-outs have slowed down cancer progression in tumor-bearing animals in a syngeneic model, but not in immunodeficient (T cell and B cell deficient) mice. This proves that the effect on disease progression depended on T cell modulation by tumor cells and EVs²⁰².

Moreover, EVs from some solid tumors have been shown to upregulate Foxp3⁺ regulatory T cells. Interestingly, tracking of fluorescently labelled EVs has demonstrated that EVs modulate Tregs via interactions and signaling on cell surface, rather than following uptake/internalization²⁰¹. First studies revealed that oral carcinoma and ovarian cancer EVs promoted expansion of human regulatory T cells cultured *ex vivo*^{207,208}. However, these early studies (published in 2009-10) were not conclusive in terms of influence on Treg suppressive activity, phenotype and Foxp3 induction.

Experiments on EVs released by nasopharyngeal carcinoma have shown their engagement in Foxp3 induction in non-regulatory T cells, via microRNA miR-24-3p^{209,210}. Another study has revealed that nasopharyngeal carcinoma EVs can contain chemokine CCL20, which mediates migration of Tregs into the tumor²¹¹. Finally, EVs released by Lewis lung carcinoma cells have also induced Foxp3 expression and upregulated expression of IL-10 by Tregs via miR-214 shuttled in extracellular vesicles. Treg modulation by extracellular miR-214 has facilitated *in vivo* lung tumor growth²¹². Altogether, EVs released by solid tumors can promote regulatory T cell differentiation and function, although experimental data in this topic is limited. Interaction between cancer and Tregs via EVs is in the scope of this thesis, in the context of hematological malignancies (myeloid leukemias) which has not been evaluated to date. Moreover, precise signaling and transcriptomic changes, as well as suppressive phenotype and heterogeneity of Treg subsets have not been addressed in the literature so far and thus constitute one of significant areas explored in the presented dissertation.

1.3.5 Extracellular vesicles in myeloid leukemias

Similarly to solid tumors, also extracellular vesicles released by myeloid leukemia (CML, AML) cells have been shown to have a beneficial role for disease development and spreading. This includes strictly autocrine influence of leukemic EVs, as CML EVs led to activation of anti-apoptotic signaling in CML cells, as well as increased clonogenicity and *in vivo* growth in a xenograft model²¹³. EVs released by therapy-resistant cells (TKI-resistant CML cells and chemotherapy-resistant AML cells) can shuttle specific cargo (such as miRNAs) that induces resistance to drug in previously therapy-sensitive cells^{214–216}. CML-derived EVs can contain BCR-ABL1 protein and DNA^{217,218}. Injection of CML EVs with *BCR-ABL1* DNA has led to the development of leukemia-like disease in mice and rats, as EVs led to malignant transformation of granulocytes/neutrophils²¹⁷.

Leukemic EVs can also modify cells in the bone marrow microenvironment. AML EVs led to dysregulation of normal osteogenesis and bone formation, as well as inhibited normal hematopoiesis, by downregulation of factors such as IGF1, CXCL12 and KITL²¹⁹. This leads to decreased clonogenic potential and lower expression of stem factors by HSCs²²⁰. On the other hand, leukemic EVs modify stromal cells/mesenchymal stem cells in the BM into leukemia-supportive cells²²¹. CML EVs modified stroma in a way that increased expression of IL-8, which promoted adhesion between stromal and leukemic cells and increased clonogenic potential of leukemic cells²²². Both AML and CML EVs have promoted expression of proangiogenic VEGF by bone marrow cells, which led to increased tube formation and vascularization^{220,223}.

AML EVs can contain proteins relevant to immunosuppression, such as TGF- β , ectonucleosidases CD73/CD39, PD-L1 and CD47 (an anti-phagocytic molecule - "don't eat me" signal)²²⁴. Leukemic EVs have been shown to modulate several subsets of myeloid cells, such as dendritic cells,

macrophages and myeloid-derived suppressor cells (MDSCs)^{225–229}. This includes induction of suppressive MDSCs by both CML and AML EVs, in mechanisms dependent on TLR2 signaling or MUC1 glycoprotein^{228,229}. Moreover, CML EVs can induce regulatory polarization of macrophages, by increasing expression of IL-10 and decreasing expression of inducible nitric oxide synthase²²⁶. TGF- β in AML EVs is capable of decreasing cytotoxic activity and NKG2D expression in NK cells²³⁰. By far, influence on T cells has been described only for AML-derived extracellular vesicles, though by far the only observed effect was induction of apoptosis of CD8+ cytotoxic T cells^{231,232}.

Influence of leukemic EVs on subsets of CD4+ T cells, including Tregs, has not been studied and described. Data from solid tumors shows that such interaction may be relevant to immunity in cancer and progression of the disease. Therefore, the aim of work presented in this thesis has been to dissect its relevance for myeloid leukemias.

2 AIMS

Previous studies of our group have demonstrated that the bone marrow microenvironment (especially stromal cells) constitutes a relevant factor supporting development of myeloid leukemias^{64,233–235}. Other groups have also implicated immunosuppressive cell subsets, including Foxp3+ regulatory T cells, in progression of myeloid neoplasms¹⁸. However, mechanisms that drive Foxp3+ regulatory T cells in chronic and acute myeloid leukemia have been poorly understood.

The general aim of this thesis was to verify if extracellular vesicles (EVs), released by myeloid leukemia cells, may be a factor that promotes immunosuppressive Foxp3+ regulatory T cells in chronic and acute myeloid leukemia. The specific goals to evaluate the general aim were:

1. To study the influence of mouse leukemic extracellular vesicles on suppressive activity and Foxp3 level in mouse thymic regulatory T cells.
2. To study the influence of human leukemic extracellular vesicles on Foxp3 induction and suppressive phenotype and activity of human regulatory T cells.
3. To identify signaling pathways responsible for modulation of human regulatory T cells and Foxp3 by leukemic extracellular vesicles.
4. To characterize human regulatory T cells driven by leukemic extracellular vesicles by high-throughput RNA sequencing and 23-color spectral flow cytometry.
5. To study the proteome of leukemic EVs and pinpoint proteins that may be responsible for driving regulatory T cells by leukemic EVs.
6. To verify to role of leukemic EVs in modulation of regulatory T cells *in vivo* - by studying regulatory T cells and leukemic engraftment in mouse model of leukemia like disease, either wild-type or Rab27a-deficient (with diminished secretion of EVs).

Identifying a new mechanism that drives regulatory T cells in myeloid leukemias would contribute to the knowledge of the leukemic microenvironment, as well as identify novel factors, that could be potentially targeted therapeutically in myeloid neoplasms.

3 MATERIALS AND METHODS

3.1 Cell lines and cell culture

Cells in the presented studies were cultured in a CO₂ cell culture incubator HERAcell 150i (Thermo Fisher), in a humidified atmosphere (95%), at a constant concentration of CO₂ (5%), oxygen (21%) and temperature of 37°C.

Cell lines used in the studies were regularly screened for mycoplasma infection (by nested PCR test). All commercial cell lines used in this thesis were authenticated by ATTC cell line authentication service.

3.1.1 Mouse cell lines 32D, 32D BCR-ABL1+ and modifications

For *in vitro* studies on mouse cells, 32D and 32D BCR-ABL1+ cells were used. 32D cells constitute an established cell line of mouse, non-transformed myeloid progenitor cells (ATCC CRL-11346). 32D BCR-ABL1+ cells constitute CML-like, malignant counterparts of 32D cells. 32D BCR-ABL1+ cells were obtained at University College Cork, Ireland and were a generous gift from Dr SL McKenna²³⁶. Both cell lines (growing in suspension) were cultured in RPMI-1640 media (Biowest, #L07490-500), supplemented with 10% heat-inactivated fetal bovine serum (FBS, Biowest, #S181H-500), antibiotics (penicillin [100 IU/ml] and streptomycin [100 µg/ml], Biowest, #L0022100) and L-glutamine (2 mM, Biowest, #X0550-100). 32D cells, as IL-3 (interleukin-3) dependent, were additionally supplemented with 10% WEHI-conditioned medium, rich in IL-3. 32D BCR-ABL1+ were additionally cultured with 0.2 µg/ml puromycin, to maintain stable expression of the pBABE plasmid overexpressing BCR-ABL1. Both cell lines were maintained in culture at 0.2-1x10⁶ cells/ml. As both cell lines exhibit identical genetic background, they constitute an appropriate model to study effects of solely BCR-ABL1 expression in myeloid progenitor cells.

Moreover, modifications of the 32D BCR-ABL1+ cell line were used for *in vivo* studies. 32D BCR-ABL1+GFP+ cells with overexpression of fluorescent protein GFP (pEGFP-C1 vector) were previously obtained at Laboratory of Cytometry. 32D BCR-ABL1+GFP+ Rab27a^{-/-} (without expression of Rab27a and thus releasing lower amounts of extracellular vesicles) were obtained as part of studies in this thesis by CRISPR/Cas9 methodology (Chapter 3.1.3). 32D BCR-ABL1+GFP+luc+ cells with stable expression of enzyme luciferase ("luc", type firefly, for *in vivo* bioluminescent analyses) were obtained as part of studies in this thesis, by lentiviral transduction with a p.Lenti6.3 plasmid (with generous help of Dr Agata Klejman, Laboratory of Animal Models, Nencki Institute). The modified cell lines were cultured as the original 32D BCR-ABL1+ cell lines, as described above.

WEHI cells (ATCC CRL-1702) are mouse B-cell lymphoma cells that naturally secrete high amounts of interleukin-3 (IL-3). They are thus used to generate conditioned medium used for culture of 32D cells. To obtain conditioned medium, WEHI cells (growing as adherent cells) were cultured until full confluence in RPMI-1640 media (supplemented as described above), kept at full confluence for 24 hours, followed by conditioned media collection. Media was centrifuged at 160 xg for 5 minutes (to get rid of residual cells and debris), filtered through a 0.22 µm filter and stored at -20°C until use (stored no longer than 12 months).

3.1.2 Human cell lines K562, MOLM-14 and modifications

For *in vitro* studies on human cells and EVs, K562 and MOLM-14 cell lines were used. K562 cells (ATCC CCL-243) were used as a model of chronic myeloid leukemia. K562 is the first and most commonly used CML cell line, obtained already in 1970 from a 53-year old female patient in CML blast crisis²³⁷. K562 cells are characterized by presence of the Philadelphia chromosome and expression of the BCR-ABL1 oncoprotein. K562 cells were cultured in IMDM media (Biowest, #L0190, containing stable glutamine), supplemented with antibiotics (penicillin [100 IU/ml] and streptomycin [100 µg/ml]) and 10% EVs-depleted, heat-inactivated fetal bovine serum (FBS, Gibco, #10500-064). EVs-depleted FBS was obtained by overnight ultracentrifugation (18 hours) at 35.000 xg. EVs-depleted FBS was used to culture human cells during the entire culture, as (in the process of conducting research for this thesis) I have observed it enables adaptation to culture conditions required for isolation of extracellular vesicles (described in detail in Chapter 3.3.1). K562 cells were maintained in culture at 0.15-1x10⁶ cells/ml. K562 4-1BBL^{-/-} cells (without expression of 4-1BBL/CD137/TNFSF9 protein) were obtained as part of studies in this thesis by CRISPR/Cas9 methodology (Chapter 3.1.3).

MOLM-14 (DSMZ ACC 777) were used as a model of acute myeloid leukemia. MOLM-14 cell line was established in 1995 from a 20-year old male patient at relapse of acute monocytic leukemia²³⁸. MOLM-14 cells exhibit *MLL-AF9* fusion, as well as expression of FLT3-ITD²³⁹, the latter being most common genetic abnormality in AML. MOLM-14 cells were cultured in RPMI-1640 media (Biowest), supplemented with antibiotics (penicillin [100 IU/ml] and streptomycin [100 µg/ml], Biowest), L-glutamine (2 mM, Biowest) and 10% EVs-depleted, heat-inactivated fetal bovine serum (FBS, Gibco). MOLM-14 cells were maintained in culture at 0.2-1x10⁶ cells/ml. MOLM-14 have been widely employed in studies on AML extracellular vesicles^{215,220}, therefore they were used in this thesis as well.

3.1.3 Cell line modification by CRISPR/Cas9-mediated genome editing

To obtain leukemic cells without expression of specified proteins, CRISPR/Cas9 methodology was used. Rab27a protein was silenced in mouse 32D BCR-ABL1+GFP+ cells, whereas 4-1BBL protein (encoded by *TNFSF9* gene) was silenced in human K562 cells.

The general pipeline of CRISPR/Cas9 methodology used in this thesis is presented on Figure 3.1A. Specifically, "all-in-one" plasmids, encoding Cas9, gRNAs (guide RNAs) and RFP, were used (Merck-Sigma-Aldrich). Cell lines were transfected by electroporation (Amaxa Nucleofector, Lonza). For each cell line and gene, two plasmids were simultaneously used - each encoding different gRNA towards gene of interest. Use of two plasmids has increased the efficiency of obtaining cells with full knock-out of selected protein. After overnight culture, cells were washed and sorted by flow cytometry activated sorting (BD FACS Aria IIu sorter, using 100 micron nozzle), based on RFP fluorescence (Figure 3.1B). For 32D BCR-ABL1+GFP+, single cells were sorted into 96-well plates to obtain Rab27a-deficient clones. For K562 cells, cell with high expression of RFP (RFP^{hi}) were sorted to obtain a polyclonal 4-1BBL-deficient cell line.

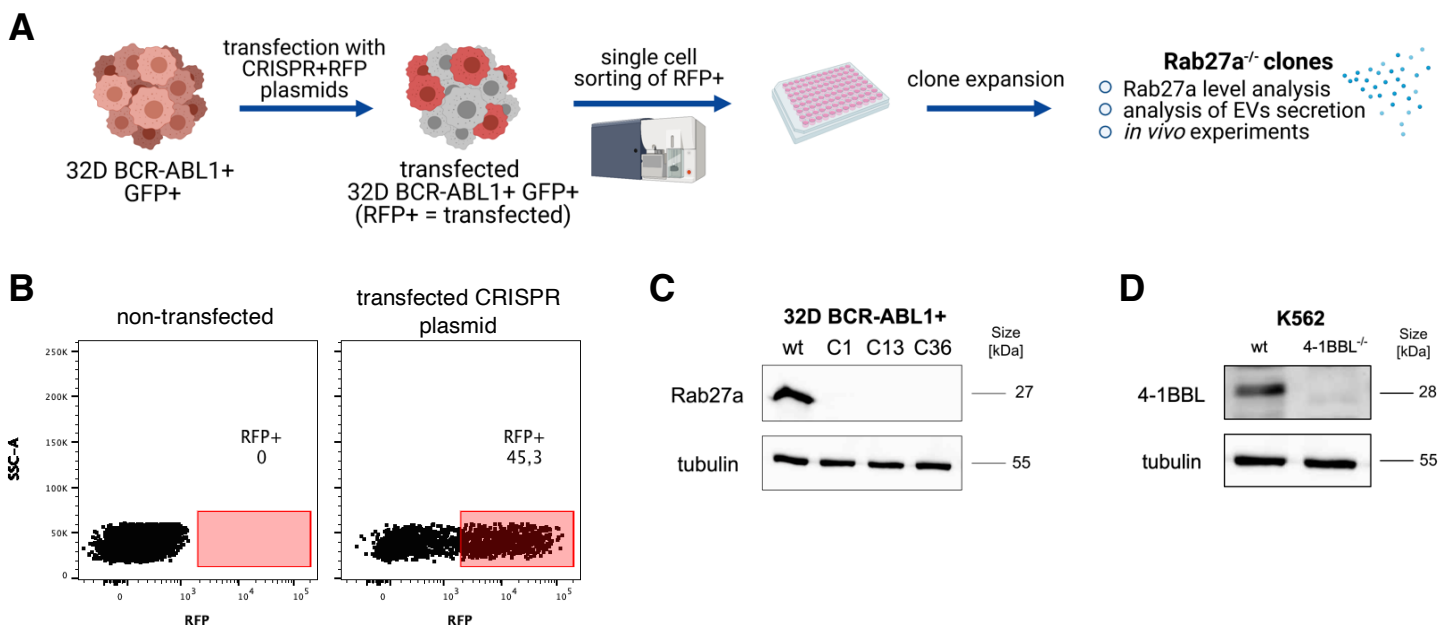


Figure 3.1 Obtaining of knock-out cell lines by CRISPR/Cas9 methodology. (A) Schematic pipeline of CRISPR/Cas9 methodology used in this thesis, on the example of obtaining Rab27a-deficient 32D BCR-ABL1+GFP+ cells. Figure created with BioRender.com. **(B)** Representative dot plot of RFP expression by cells transfected with CRISPR plasmids. **(C)** Representative western blot analysis Rab27a protein level in wt (Parental) and Rab27a-deficient clones (C1, C13, C36) of 32D BCR-ABL1+GFP+ cells. **(D)** Representative western blot analysis of 4-1BBL protein level in wt (Parental) and 4-1BBL-deficient K562 cells.

Sorted cells were further cultured and expression of proteins of interest was validated by western blotting (Figure 3.1C-D). To select Rab27a-deficient clones of 32D BCR-ABL1+GFP+ cells, clones obtained from single cells were first validated for complete Rab27a-deficiency (by western blotting),

followed by analysis of GFP expression and cell cycle, to exclude clones that might have lost GFP expression or represented abnormal growth. Finally, chosen clones (11 clones) were screened by nanoparticle tracking analysis for diminished secretion of extracellular vesicles. Finally, 3 clones were chosen and clone 1 (C1) was used for *in vivo* studies (data shown in Results Chapter 4.3.2). "Parental" cells were cultured simultaneously with knock-out cells, to obtain wild-type counterparts for further experiments. gRNA sequences used to target specific genes were as following (5'-3'):

- *Rab27a*: GTACGCGTGCATCTGTAGC, GAACTTGCCATCAGTGTAC;
- *4-1BBL*: TTTCGCCCGACGATCCCGC, TAGCTCAGGCCCCCGTCA;

3.2 Cell cycle and population doubling time analysis, clonogenic assay

To assess basic growth parameters of 32D BCR-ABL1+GFP+ cells and their Rab27a-deficient counterparts, parameters such as population doubling time, cell cycle and clonogenicity were measured.

To quantify cell growth as population doubling time, cells were seeded at density of 0.15×10^6 cells/ml ("I") and cultured for a time of 48 hours ("t"). Following 48 hours, cells were counted to assess final density ("F"). Population doubling time ("PD") was calculated according to the formula: $[PD = t * (\log 2 / \log E - \log I)]$. To precisely count the cells (for all the other applications as well), Muse Cell Analyzer (Merck Millipore) was used to assess cell number and viability.

To assess cell cycle of leukemic cells, flow cytometric analysis of DNA by propidium iodide staining of cells was performed, as described previously²³⁵. In brief, cells were washed and fixed in 70% ethanol, at -20°C. Cells were washed and incubated for 5 minutes, RT in extraction buffer (8 mM citric acid in 0.2 M Na₂HPO₄). DNA was then stained for 30 minutes, RT using 50 µg/ml propidium iodide and 50 µg/ml RNase A, in a staining buffer (3.8 mM sodium citrate). DNA content in cells was analyzed using BD LSR Fortessa cytometer. Data was analyzed in FlowJo, percentage of cells in G1, S, G2/M phases was analyzed by manual gating.

To measure colony forming capacity, 4×10^4 32D BCR-ABL1+GFP+ cells were seeded in MethoCult H4230 (STEMCELL, #04230) medium, in 35x10 mm plates with grid (Sarstedt, #83.3900.002), for 72 hours. Formed colonies were then manually counted under an inverted microscope.

3.3 Extracellular vesicles isolation and characterization

3.3.1 Isolation by differential ultracentrifugation

The main method used for isolation of extracellular vesicles (EVs) in the presented thesis was differential ultracentrifugation. It has been the most common and recognized method for EVs isolation¹⁵⁹, as it enables isolation of EVs with both high yield and very good purity. The principle of the method is to simply pellet EVs from cell cultured conditioned medium by high-speed

ultracentrifugation. Potential contaminants, such as cellular debris or larger particles, are first depleted by centrifugation/ultracentrifugation steps at lower speeds. To obtain EVs released by leukemic cells, human or mouse leukemic cells were first seeded for 24 hours, to generate EVs-containing conditioned medium. Conditioned medium was then subjected to several centrifugation steps and EVs were pelleted during the final two ultracentrifugation steps (Table 3.1).

Mouse cell lines 32D and 32D BCR-ABL1+ were first cultured for 2 weeks (to establish stable growth, signaling etc.) and then seeded at 0.4×10^6 cells/ml in T175 flasks in 35 ml of media (6 flasks each, 210 ml of media in total each), for 24 hours, to generate conditioned medium for EVs isolation. Media used were as described above (Chapter 3.1.1), only 32D BCR-ABL1+ were cultured without puromycin. Serum used for EVs-conditioned medium was first depleted of bovine EVs by ultracentrifugation (2 hours) at 35.000 xg. FBS needs to be depleted of bovine EVs and other serum components by high-speed ultracentrifugation. FBS ultracentrifugation limits contamination of conditioned medium with these components, as they would co-isolate with EVs of interest (here, leukemic EVs). Therefore, FBS would usually be ultracentrifuged overnight (for 18 hours) to deplete bovine EVs, lipoproteins and other components¹⁴². For preparation of medium conditioned by 32D/32D BCR-ABL1+ cells, only 2 hours of ultracentrifugation (to purify FBS) was used instead of 18 hours, as use of FBS ultracentrifuged for 18 hours led to apoptosis, abnormal growth and induction of unfolded protein response in 32D BCR-ABL1+ cells (observed during studies for this thesis, data not shown).

Human cell lines K562 (CML) and MOLM-14 (AML) were first cultured for 2 weeks (to establish stable growth, signaling etc.) and then seeded at 0.4×10^6 cells/ml in T175 flasks in 35 ml of media (11 flasks each, 385 ml of media in total each), for 24 hours, to generate conditioned medium for EVs isolation. Media used were as described above (Chapter 3.1.2). Serum used for EVs-conditioned medium was first depleted of bovine EVs by ultracentrifugation (18 hours) at 35.000 xg. In case of human cell lines, FBS ultracentrifuged for 18 hours did not interfere with cell growth (like in case of mouse cell lines, described above). Moreover, human cell lines were cultured in EVs-depleted FBS the entire time since thawing, for additional adaptation.

Cell culture conditioned medium was used for isolation of extracellular vesicles, by differential ultracentrifugation protocol, as described previously^{142,157}. For each isolation, viability of cells was checked and has always exceeded 95%. Entire procedure was carried out at 4°C, to preserve biological activity of EVs. Cell culture conditioned medium was first collected into 50 ml conical tubes and centrifuged at 160 xg, 5 minutes, at 4°C, to pellet cells. Supernatants were then moved into fresh tubes and centrifuged at 320 xg, 5 minutes, at 4°C, to pellet residual and apoptotic cells. Supernatants were collected again and centrifuged at 1.300 xg, 20 minutes, at 4°C, to pellet cellular debris. Obtained supernatants were then subjected to three ultracentrifugation steps. Ultracentrifugation steps were performed using 70-ml polycarbonate bottles (Beckman Coulter,

#355622), type 45Ti fixed-angle rotor (Beckman Coulter, #339160) and Beckman Coulter Optima XPN-100 ultracentrifuge. Firstly, supernatants were ultracentrifuged at either 15.000 xg (mouse cell lines EVs) or 10.000 xg (human cell lines EVs), for 40 minutes. Obtained supernatants were then ultracentrifuged again at either 140.000 xg, 100 minutes (mouse cell lines EVs) or 100.000 xg, 90 minutes (human cell lines EVs), to pellet small EVs. EVs pellets were resuspended in fresh PBS and subjected to one final ultracentrifugation step - a wash in PBS - at either 140.000 xg, 100 minutes (mouse cell lines EVs) or 100.000 xg, 90 minutes (human cell lines EVs). Final obtained pellets of EVs were then resuspended in 100 μ l of PBS (for EVs characterization), non-supplemented RPMI media (functional assays using mouse cells) or non-supplemented AIM V media (functional assays using human cells) and moved into fresh 1.5-ml tubes. Centrifugation and ultracentrifugation steps used in the protocol are summed up in Table 3.1 below.

Table 3.1 Sequential centrifugation and ultracentrifugation steps used to obtain final pellets of extracellular vesicles by differential ultracentrifugation method.

	Aim	Speed	Time	Speed	Time
		Mouse cell lines		Human cell lines	
Centrifugation steps	Pellet cells	160xg, 5 minutes			
	Pellet residual/apoptotic cells	320xg, 5 minutes			
	Pellet debris	1.300xg, 20 minutes			
Ultracentrifugation steps	Pellet debris/large vesicles	15.000xg	40 minutes	10.000xg	40 minutes
	Pellet EVs	140.000xg	100 minutes	100.000xg	90 minutes
	Wash EVs in PBS	140.000xg	100 minutes	100.000xg	90 minutes

Following isolation, EVs were immediately used for downstream applications. To quantify amount of EVs for downstream applications, measurements of either protein by Bradford assay (for mouse EVs) or nanoparticles tracking analysis (NTA, for human EVs), were used. For *ex vivo* studies using mouse cells, amount (protein) of EVs is specified in each figure in the Results section. For *ex vivo* studies using human cells, unless specified otherwise, human lymphocytes were treated with either 3×10^9 CML (K562) EVs (number of particles) or 5×10^9 AML (MOLM-14) EVs (number of particles). These amounts of particles/EVs are equivalent of EVs released by 1×10^8 cells. In dose-dependent analyses with CML EVs, lymphocytes were treated with 3×10^9 - 3×10^7 CML (K562) EVs/particles (doses are specified on relevant figures).

3.3.2 Isolation by density gradient ultracentrifugation

To obtain extracellular vesicles with even higher purity, other methods, such as density gradient ultracentrifugation, may be additionally applied. This method enables full elimination of (eventual) contaminants, such as Argonaute proteins (e.g. for miRNA studies) or fluorescent dye following EVs labelling. In this method, EVs are isolated based on their density, following ultracentrifugation of EVs on a gradient of sucrose, OptiPrep (iodixanol) medium or others. In the presented thesis, density gradient ultracentrifugation, using OptiPrep (STEMCELL, #07820) was applied to human,

K562-derived EVs after fluorescent labelling with CFSE (Chapter 3.3.7). This has enabled isolation of extremely pure EVs and separation from residual CFSE dye, for further use in a culture to assess EVs uptake/binding by human lymphocytes.

Density gradient ultracentrifugation was performed as previously described^{142,148}. EVs obtained by differential ultracentrifugation were layered on top of a discontinuous OptiPrep (iodixanol) gradient. Entire procedure was carried out at 4°C, to preserve biological activity of EVs. Sequential layers of OptiPrep were first layered in 13.2 ml thin-wall ultra-clear tubes (Beckman Coulter, #344059) - 2.9 ml of 40% solution was layered on the bottom, followed by 2.9 ml of 20% solution, 2.9 ml of 10% solution and 2.5 ml of 5% solution. Finally, EVs in a volume of 0.73 ml were layered on top of the gradient. Tubes were then placed in a SW 41Ti swinging-bucket rotor (Beckman Coulter, #331362) and ultracentrifuged at 100.000 xg, for 18 hours, using Beckman Coulter Optima XPN-100 ultracentrifuge. To not disturb the generated gradient, deceleration speed was set to minimum. Following ultracentrifugation, twelve 1 ml fractions (from top to bottom) were collected, moved into fresh 13.2 ml tubes, topped up with PBS and washed, by ultracentrifugation at 100.000 xg, for 3 hours, also using 41Ti rotor. Supernatants from this ultracentrifugation step were carefully aspirated and pellets resuspended in either PBS (for western blotting) or AIM V medium (for functional assay).

Material from each of 12 fractions was analyzed by western blot for expression of CD63 protein (an EV marker) - representative of EVs presence in each fraction. This has revealed that EVs were present predominantly in fraction 7, but also in fractions 8 and 9, collected from OptiPrep density gradient (Figure 3.2). Therefore, material isolated from these three fractions was further considered as pure EVs preparations and used for EVs uptake/binding assay (Chapter 3.3.7, Figure 4.9).

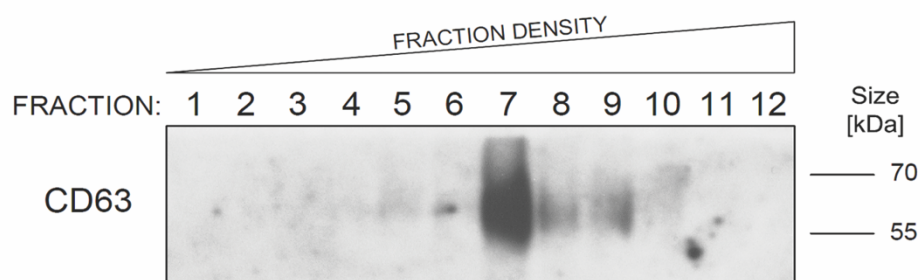


Figure 3.2 Analysis CD63 expression (representative of EVs presence) in fractions obtained by density gradient ultracentrifugation. EVs released by K562 (CML) cells were firstly pelleted using differential ultracentrifugation protocol (figure from Swatler *et al.*, 2020, Curr Protoc Immunol¹⁴²).

3.3.3 Primary EVs from plasma of CML/AML patients and isolation by size exclusion chromatography

To study EVs of leukemic origin in a primary, patient setting, EVs were isolated from plasma of patients suffering from chronic or acute myeloid leukemia and healthy counterparts. Material from 7 CML and 3 AML patients at diagnosis was obtained from Medical University of Warsaw (in collaboration with prof. G. Basak and prof. U. Wojda). Material from 10 healthy donors (age-matched) was drawn from 10 healthy volunteers by a licensed nurse. Proper informed consent was obtained from patients and all procedures were approved by Bioethics Committee of the Medical University of Warsaw (KB/107/2018) and Ethics and Bioethics Committee of the Cardinal Stanislaw Wyszyński University in Warsaw (KEiB-19/2017), in accordance with Declaration of Helsinki and Polish regulations.

Blood was collected using 9 ml EDTA tubes (Greiner Bio-one, #455036) and centrifuged at 1.000 xg, 10 minutes, RT to obtain plasma. Plasma was once again centrifuged at 1.000 xg, 10 minutes, RT, divided into 1 ml aliquots and stored at -80°C until further use.

Extracellular vesicles (EVs) from plasma were isolated by size exclusion chromatography (SEC). Plasma constitutes a complex biofluid and methods such as differential ultracentrifugation or density gradient ultracentrifugation have proven insufficient to purify plasma EVs from contaminants, such as lipoproteins²⁴⁰. Size exclusion chromatography has been proposed to be a more effective alternative²⁴¹ and has been the most common method used for isolation of plasma EVs. In this thesis, size exclusion chromatography qEVoriginal/35nm columns from Izon (#ICO-35) were used. The isolation procedure was carried out according to manufacturer's instructions. Plasma was first centrifuged for 10 minutes, at 10.000 xg, RT, to deplete debris. 700 µl of plasma was loaded onto a SEC column and elution was immediately started (PBS at RT was used as an eluate). First 6 fractions of 0.5 ml each were discarded. The following fractions 7-9 were collected (total volume of 1.5 ml), as EVs containing fractions, as per manufacturer's instructions. Content of fractions was validated by western blotting and, indeed, fractions 7-9 contained EVs, as exhibited by presence of Tsg101 (EV marker). Fractions 7-9 contained significantly less APOA1 (lipoprotein marker) than the following fractions 10 and 11, proving efficient elimination of majority of lipoproteins. SEC fractions did not contain GM130 (Golgi marker), excluding contamination with whole cell fragments (Figure 4.29A). Following isolation, pooled fractions 7-9 (total volume of 1.5 ml) were concentrated using Amicon Ultra-2 10 kDa concentration columns (Merck, #UFC201024) down to the volume of approximately 130 µl. 5 µl of plasma EVs was used for downstream applications (functional assays with T cells). Volume of 5 µl was chosen based on preliminary experiments. As single experiments with plasma EVs were performed on different batches of primary T cells, plasma of patients and healthy donors for each experiment were matched by age.

3.3.4 Transmission electron microscopy

To perform imaging of extracellular vesicles "in the flesh", transmission electron microscopy (TEM) was used. To image EVs by TEM, negative staining of particles deposited on electron microscopy grids was performed, as described previously¹⁴². EVs were isolated by differential ultracentrifugation, as described above (Chapter 3.3.1) and resuspended in 100 μ l of PBS. 10 μ l of EVs was then deposited onto a formvar/carbon-coated copper grid (Cell Microscopy Core, UMC Utrecht, #CU 100 mesh) for 20 minutes. The liquid was then drained on filter paper and the grid was fixed for 15 minutes, by placing it on a drop of 2% paraformaldehyde. The liquid was then again drained and the grid was placed onto a drop of 4% uranyl acetate, for 10 minutes, for sample contrasting. Residual uranyl acetate was drained on filter paper and prepared sample was stored until TEM imaging. Obtained samples were imaged at the Laboratory of Electron Microscopy (Nencki Institute), using JEM 1400 (JEOL Co., Japan, 2008) electron microscope, Morada G2 camera and iTEM software. Both close-up and wide-field images of EVs released by each cell line were obtained, magnifications are specified under each image in the Results section. Close-up images were obtained to observe morphology and size of single EVs, whereas wide-field images aimed to demonstrate even distribution and presence of EVs on the grid. EVs were identified based on their typical round, cup-shaped morphology, characteristic for such TEM preparations.

3.3.5 Western blot analysis of proteins

Proteomic studies performed by several groups have revealed proteins significantly enriched in extracellular vesicles, that have been therefore considered "EV markers"^{140,143}. On the other hand, several proteins have been established as absent in EVs ("negative EV markers"). Proteins most commonly used as EV markers have been collected in position papers by ISEV (International Society of Extracellular Vesicles)^{162,163}. To verify expression of such proteins, I have opted to perform analysis by western blotting. Western blot analysis was also used for protein level analysis in whole cell lysates, to verify silencing of certain proteins (Rab27a, 4-1BBL) in cell lines.

To obtain proteins lysates of EVs, EVs were isolated by differential ultracentrifugation, resuspended in 50 μ l of PBS, mixed with 100 μ l of protein extraction buffer (50 mM Tris-HCl, pH 6.8, 10% glycerol, 2% SDS), incubated at 95°C for 10 minutes and further stored at -20°C until use. For analysis of tetraspanins (CD63, CD81), EVs were resuspended in 50 μ l of PBS and stored at -80°C until use (no direct protein extraction). To obtain whole cell protein lysates, 1×10^7 cells were washed and resuspended in 300 μ l of protein extraction buffer, followed by 5 minutes at 95°C, 5-time shearing through a 0.33 mm needle and final 3-minute incubation at 95°C. Lysates were then stored at -20°C until use.

To prepare samples for western blot gels, protein lysates were mixed with 5x loading buffer (62.5 mM Tris·HCl, pH 6.8, 2% SDS, 10% glycerol, 0.01% bromophenol blue) supplemented with 0.25 M DTT. For analysis of proteins in EVs, 48 µl of EVs lysate was mixed with 12 µl of 5x loading buffer and incubated at 95°C for 5 minutes. For analysis of CD63 and CD81 tetraspanins, 24 µl of frozen EVs were mixed with 6 µl of 5x loading buffer (without DTT) and incubated at 95°C for 10 minutes. Samples were then run on polyacrylamide gels in denaturing conditions (SDS-PAGE). Polyacrylamide gels were prepared with either 8, 10, 12 or 15% acrylamide, also containing Tris (pH 8.8), SDS, APS, and TEMED. Gels used were 1.5 mm thick and contained 10 wells. Gels were run in electrophoresis buffer (25 mM Tris·HCl, 250 mM glycine, 0.1% SDS) using Mini-PROTEAN Tetra System (Bio-Rad).

Proteins separated on polyacrylamide gels were then transferred onto nitrocellulose membranes (GE Healthcare Life Sciences, #10600002) in a transfer buffer (25 mM Tris·HCl, 192 mM glycine, 0.05% SDS, 20% methanol). Transfer was carried out at 4°C, 75 minutes, 400 mA, using Mini-Trans-Blot Electrophoretic Transfer Cell (Bio-Rad).

Membranes following transfer were rapidly washed in TBTS buffer (20 mM Tris·HCl, pH 7.6, 136 mM NaCl, 0.1% Tween-20) and blocked (to avoid non-specific antibody binding) for 1 hour, RT, in a blocking solution (either 5% BSA or 5% milk in TBST). Membranes were then incubated overnight, at 4°C, with primary antibodies in a specified blocking solution. Primary antibody specifics and staining conditions are listed in Table 3.2. The next day, membranes were washed (3x10 minutes, in TBST buffer), stained with secondary antibodies, conjugated with horseradish peroxidase (1 hour at RT, 1:2000, antibodies from Dako, goat anti-mouse, #P0447, and goat anti-rabbit, #P0448) and again washed 3 times for 10 minutes in TBST buffer. Membranes were developed using Super Signal West Pico ECL (Thermo Fisher Scientific, #34579) reagent, using either X-ray films (Amersham Hyperfilm ECL, #28-9068-36) or ChemiDoc Imaging System (Bio-Rad).

Table 3.2 Antibodies used for western blotting.

Protein	Dilution	Staining conditions	Antibody (origin, clonality, clone)	Source	Catalog no
4-1BBL	1:1000	5% milk	Anti-human mouse monoclonal (1B4B1)	Proteintech	66450-1-Ig
Alix	1:500	5% BSA	Anti-human/mouse mouse monoclonal (3A9)	Abcam	ab117600
APOA1	1:1000	5% milk	Anti-human/mouse rabbit polyclonal	Proteintech	14427-1-AP
CD63	1:1000	5% BSA	Anti-human mouse monoclonal (TS63)	Abcam	ab59479
CD81	1:500	5% BSA	Anti-human mouse monoclonal (M38)	Abcam	ab79559
Flotilin-1	1:500	5% milk	Anti-human/mouse mouse monoclonal (18/Flotillin-1)	BD	610820
GM130	1:1000	5% milk	Anti-human rabbit monoclonal (D6B1)	Cell Signaling	12480
Grp78	1:2000	5% milk	Anti-human/mouse mouse monoclonal (40/BiP)	BD	610978
Hsp70	1:500	5% BSA	Anti-human/mouse mouse monoclonal (5A5)	Abcam	ab2798
Rab27a	1:1000	5% BSA	Anti-mouse rabbit monoclonal (D7Z9Q)	Cell Signaling	69295S
TOM20	1:2000	5% milk	Anti-human/mouse rabbit polyclonal (FL-145)	Santa Cruz	sc-11415
TSG101	1:1000	5% BSA	Anti-human/mouse rabbit monoclonal (EPR7130(B))	Abcam	ab125011
tubulin	1:4000	5% milk	Anti-human/mouse mouse monoclonal (DM1A)	Merck	CP06
β -actin-HRP	1:10000	2.5% milk	Anti-human/mouse mouse monoclonal (AC-15)	Sigma-Aldrich	A3854

3.3.6 Nanoparticle tracking analysis

Nanoparticle tracking analysis (NTA) is a light-scattering based technique that enables measurement and quantification of nanoparticles (10-1000 nm in diameter), based on their Brownian motions in a liquid. In the presented thesis, it was used to measure the average size, as well as number of extracellular vesicles isolated from several sources (conditioned medium and plasma). NTA measurements for this thesis were performed using Malvern Nanosight NS300 device.

EVs isolated from conditioned medium (by differential ultracentrifugation) or plasma (by size exclusion chromatography) were diluted in PBS at either 1:1.000 (conditioned medium) or 1:10.000 (plasma), to obtain particle density optimal for measurements. Before dilution, PBS alone was run through NTA device to make sure it does not contain any residual particles, that could interfere with measurements. Diluted EVs were aspirated by a 1 ml syringe (BD, #309628) and all residual air bubbles were removed. Syringe was inserted into the device port and EVs were loaded for measurements. Camera focus, gain and measurement threshold were adjusted appropriately for each sample. The syringe was then placed into an automatic autosampler to maintain constant flow rate and stability of measurements. For each sample, 5 measurements of 30 seconds were performed and used for analysis. The obtained reports included mean/median particle size, as well as particle concentration, that could be re-calculated to assess number of particles released by an average number of cells.

Nanoparticle tracking analysis was also used to screen Rab27a-deficient clones of 32D BCR-ABL1+GFP+ cells for diminished secretion of EVs. Medium conditioned by wt and Rab27a-deficient cells was subjected to first four steps of differential ultracentrifugation protocol

(3 regular centrifugations and ultracentrifugation at 15.000 xg for 40 minutes). The obtained supernatant was therefore depleted of cells, debris and large particles and was measured (undiluted) by NTA. The obtained particle numbers were re-calculated to assess number of EVs released per cell, to choose Rab27a-deficient clones with significantly diminished secretion of EVs.

3.3.7 Uptake of extracellular vesicles by mouse and human T lymphocytes

To provide evidence for potential leukemic EVs-Treg/T cell interaction, EVs were fluorescently labelled with a CFSE dye, which becomes fluorescent following cleavage by esterases, which are also present in EVs. CFSE-labelled EVs were added to *ex vivo* cultures of murine or human lymphocytes and (following incubation) cells were analyzed by flow cytometry for CFSE signal. CFSE fluorescence by T cells should therefore correspond to EVs and prove interaction between cells and particles. However, analysis by flow cytometry cannot discriminate whether EVs were internalized or have bound the plasma membrane (both of which are established modes of interaction between EVs and cells, as described in Introduction Chapter 1.3.1). Therefore, I refer to the interaction analyzed in this assay as uptake/binding.

For EVs uptake/binding by murine T cells, thymocytes were isolated and cultured as described further in Chapter 3.4.1. EVs released by 32D BCR-ABL1+ cells were isolated as described in Chapter 3.3.1. EVs were stained with 10 μ M CFSE by adding CFSE to the conditioned medium before 2nd ultracentrifugation step (140.000xg for 100 minutes). Residual CFSE was additionally washed out during PBS wash of EVs. Thymocytes were seeded in 48-well plates in 200 μ l of media, at density of 1×10^6 cells/ml and specified amounts of EVs were added (10, 50 or 100 μ g/ml). Uptake/binding was analyzed after 2, 4, 6 and 24 hours of culture in the entire population of viable thymocytes. For analysis in specific subsets of T cells, analysis was performed only at the 2-hour time-point. T cells were stained for viability and with antibodies against CD4, CD8 and CD25 (Table 3.3). Cells were acquired on BD LSR Fortessa cytometer and analyzed in FlowJo as presented in Figure 3.3.

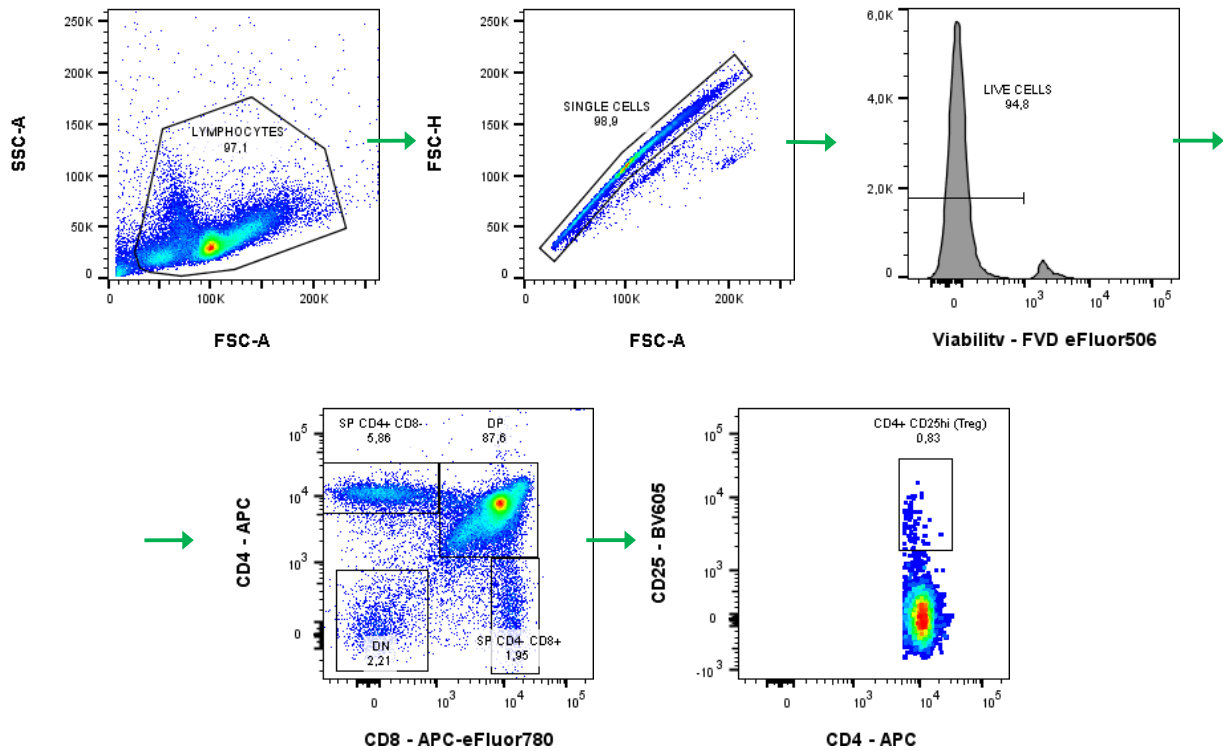


Figure 3.3 Analysis of mouse T cells cultured with CFSE-labelled leukemic EVs. Representative gating strategy to analyze T cells and Tregs (from the thymus). In identified cell populations, CFSE signal (corresponding to EVs) was analyzed and quantified. Different subsets of maturing thymocytes were identified based on expression of CD4 and CD8 among viable, single cells. Among SP CD4+CD8- thymocytes, Tregs were identified as CD25^{hi} (figure from Swatler *et al.*, 2020, Eur J Immunol²⁴²).

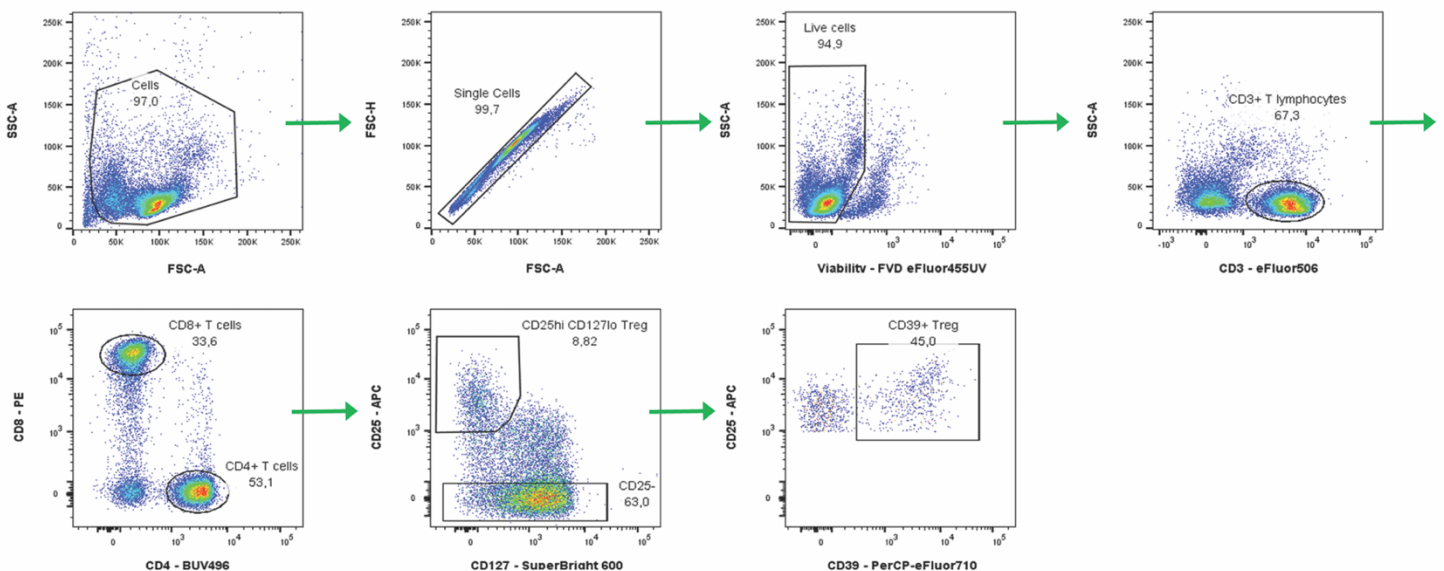


Figure 3.4 Analysis of human T cells cultured with CFSE-labelled leukemic EVs. Representative gating strategy to analyze T cells and Tregs (from human peripheral blood). In identified cell populations, CFSE signal (corresponding to EVs) was analyzed and quantified. Tregs were identified as CD3+CD4+CD8-CD25^{hi}CD127^{lo} cells among live, single cells. CD39+ cells among Tregs were considered as subset of highly suppressive, effector Tregs (figure from Swatler *et al.*, 2020, Curr Protoc Immunol¹⁴²).

For EVs uptake/binding by human T cells, non-adherent PBMCs were isolated as described further in Chapter 3.4.2.1. EVs released by K562 (CML) cells were isolated as described in Chapter 3.3.1-2. The EVs uptake/binding by human T cells was performed as described previously¹⁴². EVs isolated by differential ultracentrifugation were labelled with 20 μ M CFSE for 60 minutes, at 37°C. They were then layered onto an OptiPrep gradient and further purified by density gradient ultracentrifugation. EVs from fraction 7 and pooled fractions 8+9 were resuspended in 50 μ l of AIM V medium. As fraction 7 should contain significantly more EVs than fractions 8+9 (Figure 3.2), material from these 2 samples was compared to study dose-dependent uptake/binding of EVs. Non-adherent PBMCs were seeded in 48-well plates in 200 μ l of media (AIM V supplemented with 50 IU/ml IL-2), at density of 2×10^6 cells/ml, and 25 μ l of each EVs sample was added to culture of human T cells. Uptake/binding was analyzed after 2 and 24 hours of culture. T cells were stained for viability and with antibodies against CD3, CD4, CD8, CD25, CD127 and CD39 (Table 3.4). Cells were acquired on BD LSR Fortessa cytometer and analyzed in FlowJo as presented in Figure 3.4.

3.4 Primary cells and cell culture

3.4.1 Primary mouse lymphocytes

3.4.1.1 Mouse strains used as source of primary cells

For *ex vivo* cultures using mouse lymphocytes, cells were isolated from either wild-type C57BL/6 animals (for *in vitro* suppression assays, due to higher endogenous suppressive function of Tregs from this strain than from Foxp3-GFP mice) or transgenic B6.Cg-Foxp3^{tm2Tch} mice (referred to as "Foxp3-GFP", for analysis of Foxp3 level in Tregs). Mice 8-12 weeks of age were used. Mice were bred and maintained in the Animal Facility at the Faculty of Biology, University of Warsaw, with a 12/12 light-dark photoperiod and *ad libitum* access to food and water. Mice were maintained in individually ventilated cage system, under specific pathogen-free conditions. All procedures were performed according to the guidelines of the Poland's National Ethics Committee for Animal Experimentation.

3.4.1.2 Cell isolation and sorting

To obtain tissues and cells, mice were sacrificed, followed by isolation of thymi (as a source of tTregs) and axillary lymph nodes (as a source of responder T cells in the *in vitro* suppression assay). Tissues were immediately homogenized (using manual glass homogenizers) in cold PBS and passed through a 100 μ m strainer (Falcon, #352360). Thymic cells were counted and stained (as described further in Chapter 3.5.2) with antibodies against CD4, CD8 and CD25 (Table 3.3, Figure 3.5), in PBS, at 4°C, for 30 minutes, followed by 2 washes in PBS. Tregs were sorted using BD FACS Aria IIu cell sorter (70 micron nozzle, with sorting speed not exceeding 6.000 events/second), as shown in Figure 3.5. Tregs were sorted as CD4+CD8-CD25^{hi} (C57BL/6 mice)

or CD4+CD8-CD25^{hi}Foxp3⁺ (Foxp3-GFP mice). Among CD4+CD8-CD25^{hi} cells, approximately 88% expressed Foxp3.

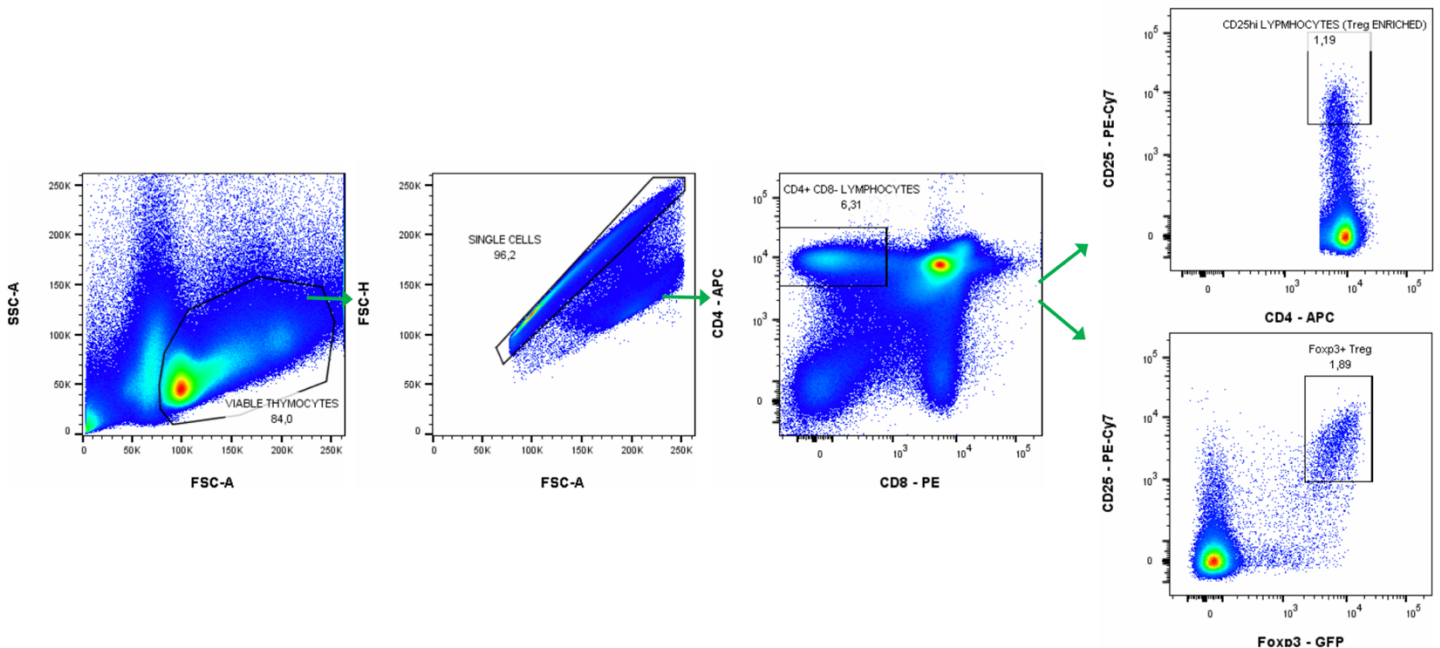


Figure 3.5 Sorting of mouse tTregs. Representative gating strategy used to sort mouse tTregs from murine thymi, based on expression of CD4, CD8, CD25 and Foxp3-GFP (figure from Swatler *et al.*, 2020, Eur J Immunol^[242]).

3.4.1.3 Primary cell culture

Mouse lymphocytes were cultured in RPMI-1640 media (Gibco, #61870-010, containing GlutaMAX), supplemented with antibiotics (penicillin [50 IU/ml] and streptomycin [50 µg/ml], Gibco, #15140122), 0.2 mM 2-mercaptoethanol (Gibco, #31350-010), 50 IU/ml IL-2 (Peprotech, #212-12) and 10% EVs-depleted, heat-inactivated fetal bovine serum (FBS, Gibco, #10500-064). Cultures were performed with EVs depleted FBS, so that bovine EVs would not interfere with effects of added EVs of leukemic origin. For cell cultures (*in vitro* suppression assays and Foxp3 level analysis), T cells were stimulated with 0.5 µg/ml soluble anti-CD3 (BD, #553057) and 0.05 µg/ml soluble anti-CD28 (BD, #553294) antibodies. Specific details of culture in each experiment are provided in Chapters with methodology of each experimental assay (Chapter 3.6).

3.4.2 Primary human lymphocytes

3.4.2.1 Cell isolation and sorting

Primary human cells were isolated from buffy coats of healthy donors (different donor for each experiment). Buffy coats were obtained from Regional Center for Blood Donation and Blood Care in Warsaw, Poland (in accordance with Declaration of Helsinki and Polish regulations). Peripheral blood mononuclear cells (PBMCs) were obtained using either Biocoll (Merck, #L6113-BC) or Lymphoprep (STEMCELL, #07851), by density gradient centrifugation for 20 minutes, at 1.200 xg, RT. PBMCs were washed in sodium chloride and depleted of monocytes by plating for 35 minutes on highly adherent plates (Nunc, #150350). Non-adherent cells were then collected and left for overnight resting in AIM V serum-free medium (Gibco, #12055083). Overnight resting did not affect T cell parameters, such as apoptosis, distribution of CD4⁺/CD8⁺ subsets, amount of Tregs or expression of activation markers CD69 and CD25 (validated during studies for this thesis, data not shown). Following overnight resting, non-adherent PBMCs were collected, counted and stained (as described further in Chapter 3.5.2) with antibodies against CD4, CD8, CD25, CD127 (Table 3.4, Figure 3.6A), in PBS, at 4°C, for 30 minutes, followed by 2 washes in PBS. Tregs were sorted using BD FACS Aria IIu cell sorter (70 micron nozzle, with sorting speed not exceeding 6.000 events/second), as shown in Figure 3.6A. Tregs were sorted as CD4⁺CD25^{hi}CD127^{lo} and conventional T cells as CD4⁺CD25⁻. CD3 (T cell marker) expression on sorted CD4⁺ cells was confirmed by backgating flow cytometry analysis (Figure 3.6B). Treg identity of CD4⁺CD25^{hi}CD127^{lo} cells was confirmed by intracellular staining of Foxp3 on sorted cells (Figure 3.6C).

3.4.2.2 Primary cell culture

Human T lymphocytes were cultured in AIM V serum-free media (Gibco, #12055083), supplemented with either 50 or 100 IU/ml IL-2 (Peprotech, #200-02). For all experiments except human *in vitro* suppression assay, T cells were stimulated with antibodies anti-CD3 (coated wells, 5 µg/ml, Biolegend, #317326) and anti-CD28 (soluble, 1 µg/ml, Biolegend, #302934). Specific details of culture in each experiment are provided in Chapters with methodology of each experimental assay (Chapter 3.6).

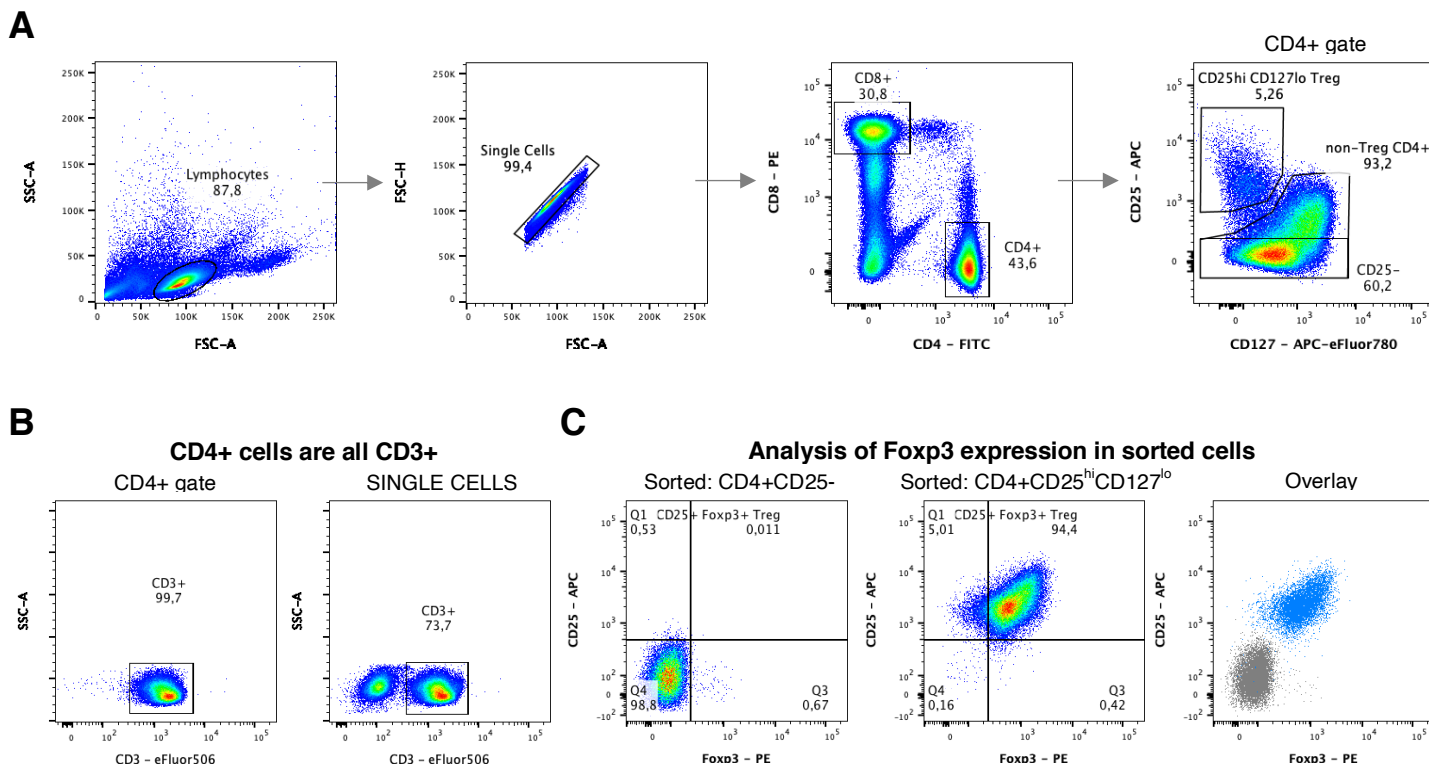


Figure 3.6 Sorting of human T cells. (A) Representative gating strategy used to sort human Tregs from peripheral blood, based on expression of CD4, CD8, CD25 and CD127. **(B)** Verification of CD3 expression (T cell identity) of CD4+ cells. **(C)** Verification of Foxp3 expression in sorted Tconv and Tregs.

3.5 Flow cytometry

3.5.1 Antibodies and dyes used for flow cytometry

Antibodies used for flow cytometry experiments and flow cytometric cell sorting are listed in the Tables 3.3 (staining of mouse cells) and 3.4 (staining of human cells) below. The antibodies have been grouped according to application, which is listed in the first column of the Table. It also references the appropriate Figure with gating strategy to a given application.

Fluorescent dyes used for flow cytometric applications (such as analysis of viability, proliferation or fluorescent labelling of extracellular vesicles) are listed in the Table 3.5 below.

Table 3.3 Antibodies used for flow cytometric staining of mouse cells. In terms of amount of antibody used, both amount of μg , as well as volume are listed. Test is defined as cells (no more than 1×10^7 cells) in a total volume of 100 microliters.

Application	Antigen	Fluorochrome	Amount/test $[\mu\text{g}](\text{volume})$	Antibody (clonality, origin, clone)	Source	Catalog no
Mouse Treg sorting and <i>ex vivo</i> cultures (gating: Figure 3.5, 3.9, 3.10)	CD4	APC	0,05 (0.25 μl)	rat monoclonal (RM4-5)	BD Pharmingen	553051
	CD8	PE	0,1 (0.5 μl)	rat monoclonal (53-6.7)	BD Pharmingen	553033
	CD8	APC-eFluor780	0,1 (0.5 μl)	rat monoclonal (53-6.7)	eBioscience/Invitrogen	47-0081-82
	CD8	PerCP	0,2 (1 μl)	rat monoclonal (53-6.7)	BD Pharmingen	553036
	CD25	PE-Cy7	0,2 (1 μl)	rat monoclonal (PC61)	BD Pharmingen	552880
	CD25	BV605	0,2 (1 μl)	rat monoclonal (PC61)	BD Horizon	563061
	Helios	PerCP-eFluor710	0,00375 (5 μl)	armenian hamster monoclonal (22F6)	eBioscience/Invitrogen	46-9883-42
Mouse T cell & Treg phenotyping in <i>in vivo</i> experiments (gating: Figure 3.18)	CD3	BUV496	0,2 (1 μl)	hamster monoclonal (145-2C11)	BD Horizon	612955
	CD4	Alexa Fluor 700	0,05 (0.25 μl)	rat monoclonal (RM4-5)	eBioscience/Invitrogen	56-0042-82
	CD8	PE-eFluor610	0,1 (0.5 μl)	rat monoclonal (53-6.7)	eBioscience/Invitrogen	61-0081-82
	CD25	PE-Cy7	0,2 (1 μl)	rat monoclonal (PC61)	BD Pharmingen	552880
	Foxp3	eFluor450	0,1 (0.5 μl)	rat monoclonal (FJK-16s)	eBioscience/Invitrogen	48-5773-82
	CD44	APC-eFluor780	0,1 (0.5 μl)	rat monoclonal (IM7)	eBioscience/Invitrogen	47-0441-82
	CD62L	APC	0,05 (0.25 μl)	rat monoclonal (MEL-14)	eBioscience/Invitrogen	17-0621-82
	CD39	Super Bright 600	1 (5 μl)	rat monoclonal (24DMS1)	eBioscience/Invitrogen	63-0391-82
	CD73	PE	0,05 (0.25 μl)	rat monoclonal (TY/11.8)	Biolegend	127206
Helios	PerCP-eFluor710	0,00375 (5 μl)	armenian hamster monoclonal (22F6)	eBioscience/Invitrogen	46-9883-42	
Intracellular cytokine staining in mouse splenocytes in <i>in vivo</i> experiments (gating: Figure 3.20)	CD3	BUV496	0,2 (1 μl)	hamster monoclonal (145-2C11)	BD Horizon	612955
	CD4	Alexa Fluor 700	0,05 (0.25 μl)	rat monoclonal (RM4-5)	eBioscience/Invitrogen	56-0042-82
	CD8	PE-eFluor610	0,1 (0.5 μl)	rat monoclonal (53-6.7)	eBioscience/Invitrogen	61-0081-82
	Foxp3	eFluor450	0,1 (0.5 μl)	rat monoclonal (FJK-16s)	eBioscience/Invitrogen	48-5773-82
	B220	APC-eFluor780	0,2 (1 μl)	rat monoclonal (RA3-6B2)	eBioscience/Invitrogen	47-0452-82
	CD11b	PE-Cy7	0,05 (0.25 μl)	rat monoclonal (M1/70)	eBioscience/Invitrogen	25-0112-82
	IL-10	PE	0,25 (1.25 μl)	rat monoclonal (JES5-16E3)	eBioscience/Invitrogen	12-7101-82
	Arg1	APC	0,25 (1.25 μl)	rat monoclonal (A1exF5)	eBioscience/Invitrogen	17-3697-82
Mouse myeloid cell phenotyping in <i>in vivo</i> experiments (gating: Figure 3.19)	CD11b	Alexa Fluor 700	0,05 (0.25 μl)	rat monoclonal (M1/70)	eBioscience/Invitrogen	56-0112-80
	PD-L1	Super Bright 600	0,2 (1 μl)	rat monoclonal (MIH5)	eBioscience/Invitrogen	63-5982-82
	SIRP	PE	0,2 (1 μl)	rat monoclonal (P84)	eBioscience/Invitrogen	12-1721-80
	Ly6C	eFluor450	0,05 (0.25 μl)	rat monoclonal (HK1.4)	eBioscience/Invitrogen	48-5932-80
	Ly6G	PerCP-eFluor710	0,05 (0.25 μl)	rat monoclonal (1A8-Ly6g)	eBioscience/Invitrogen	46-9668-80
	F4/80	PE-eFluor610	0,4 (2 μl)	rat monoclonal (BM8)	eBioscience/Invitrogen	61-4801-80
	Arg1	APC	0,25 (1.25 μl)	rat monoclonal (A1exF5)	eBioscience/Invitrogen	17-3697-82

Table 3.4 Antibodies used for flow cytometric staining of human cells. In terms of amount of antibody used, both amount of μg , as well as volume are listed (unless antibody concentration was not listed by manufacturer, in which case only volume is listed). Test is defined as cells (no more than 1×10^7 cells) in a total volume of 100 microliters.

Application	Antigen	Fluorochrome	Amount/test $[\mu\text{g}](\text{volume})$	Antibody (clonality, origin, clone)	Source	Catalog no
Human T cell & Treg sorting (gating: Figure 3.6)	CD4	FITC	0,0625 (1.25 μl)	mouse monoclonal (OKT-4)	eBioscience/Invitrogen	11-0048-42
	CD8	PE	0,03125 (1.25 μl)	mouse monoclonal (RPA-T8)	eBioscience/Invitrogen	12-0088-42
	CD25	APC	0,06 (5 μl)	mouse monoclonal (CD25-4E3)	eBioscience/Invitrogen	17-0257-42
	CD127	APC-eFluor780	0,125 (5 μl)	mouse monoclonal (eBioRDR5)	eBioscience/Invitrogen	47-1278-42
	CD3	eFluor506	0,5 (5 μl)	mouse monoclonal (UCHT1)	eBioscience/Invitrogen	69-0038-42
Human Treg and T cell analysis and phenotyping (gating: Figure 3.12, 3.14)	CD4	FITC	0,0625 (1.25 μl)	mouse monoclonal (OKT-4)	eBioscience/Invitrogen	11-0048-42
	CD25	APC	0,03 (2.5 μl)	mouse monoclonal (CD25-4E3)	eBioscience/Invitrogen	17-0257-42
	Foxp3	PE	0,125 (2.5 μl)	rat monoclonal (PCH101)	eBioscience/Invitrogen	12-4776-42
	CD127	Super Bright 600	0,5 (5 μl)	mouse monoclonal (eBioRDR5)	eBioscience/Invitrogen	63-1278-42
	CD39	PerCP-eFluor710	0,06 (5 μl)	mouse monoclonal (eBioA1 (A1))	eBioscience/Invitrogen	46-0399-42
	PD-1	BV605	5 μl	mouse monoclonal (EH12.1)	BD Horizon	563245
	LAG-3	BV421	5 μl	mouse monoclonal (T47-530)	BD Horizon	565720
	CTLA-4	PE-Cy7	0,06 (5 μl)	mouse monoclonal (14D3)	eBioscience/Invitrogen	25-1529-42
Analysis of phosphorylated signaling proteins in human T cells and Treg (gating: Figure 3.12, 3.14)	CD4	FITC	0,0625 (1.25 μl)	mouse monoclonal (OKT-4)	eBioscience/Invitrogen	11-0048-42
	CD25	PE-Cy7	0,03125 (1.25 μl)	mouse monoclonal (CD25-4E3)	eBioscience/Invitrogen	25-0257-42
	Foxp3	APC	0,25 (2.5 μl)	rat monoclonal (PCH101)	eBioscience/Invitrogen	17-4776-42
	Foxp3	eFluor450	0,125 (1.25 μl)	rat monoclonal (PCH101)	eBioscience/Invitrogen	48-4776-42
	Foxp3	PE	0,125 (2.5 μl)	rat monoclonal (PCH101)	eBioscience/Invitrogen	12-4776-42
	p-mTOR	eFluor660	0,5 (5 μl)	mouse monoclonal (MRRBY)	eBioscience/Invitrogen	50-9718-41
	p-S6	eFluor450	0,125 (5 μl)	mouse monoclonal (cupk43k)	eBioscience/Invitrogen	48-9007-42
	p-STAT5	PE	0,25 (5 μl)	mouse monoclonal (SRBCZX)	eBioscience/Invitrogen	12-9010-42
	p-p38	APC	0,125 (5 μl)	mouse monoclonal (4NIT4KK)	eBioscience/Invitrogen	17-9078-42
	p-ReIA/p65	PE	0,06 (5 μl)	mouse monoclonal (B33B4WP)	eBioscience/Invitrogen	12-9863-42
	p-SMAD2/3	Alexa Fluor 647	5 μl	mouse monoclonal (O72-670)	BD Phosflow	562696
	23-color human Treg phenotyping (gating: Figure 3.7)	CD4	BUV496	1.25 μl	mouse monoclonal (SK3)	BD Horizon
CCR8		BV421	0.625 μl	mouse monoclonal (433H)	BD Horizon	566379
CD25		Alexa Fluor 700	2.5 μl	mouse monoclonal (M-A251)	BD Pharmingen	561398
Foxp3		PE-Cy5	0,125 (1.25 μl)	rat monoclonal (PCH101)	eBioscience/Invitrogen	15-4776-42
CD127		Alexa Fluor 532	0,0625 (2.5 μl)	mouse monoclonal (eBioRDR5)	eBioscience/Invitrogen	58-1278-42
IRF4		PE-eFluor610	0,125 (1.25 μl)	rat monoclonal (3E4)	eBioscience/Invitrogen	61-9858-82
BATF		PerCP-eFluor710	0,0625 (2.5 μl)	mouse monoclonal (MBM7C7)	eBioscience/Invitrogen	46-9860-42
Helios		FITC	0,125 (0.25 μl)	armenian hamster monoclonal (22F6)	eBioscience/Invitrogen	11-9883-82
ICOS		APC-eFluor780	0,0625 (2.5 μl)	mouse monoclonal (ISA-3)	eBioscience/Invitrogen	47-9948-42
CD73		BV605	5 μl	mouse monoclonal (AD2)	BD Horizon	563199
CD39		Super Bright 702	0,5 (5 μl)	mouse monoclonal (eBioA1 (A1))	eBioscience/Invitrogen	67-0399-42
CCR4		BUV615	5 μl	mouse monoclonal (1G1)	BD Horizon	613000
CD71		BV786	5 μl	mouse monoclonal (M-A712)	BD Horizon	563768
4-1BB		BUV661	0,1 (2.5 μl)	mouse monoclonal (4B4-1)	BD OptiBuild	741642
TIGIT		BV650	0,1 (2.5 μl)	mouse monoclonal (741182)	BD OptiBuild	747840
TNFR2		PE-Cy7	0,125 (1.25 μl)	rat monoclonal (3G7A02)	Biolegend	358412
CD30		BUV395	0,05 (1.25 μl)	mouse monoclonal (BerH8)	BD OptiBuild	744412
OX-40		BUV805	0,1 (2.5 μl)	mouse monoclonal (ACT35)	BD OptiBuild	749285
TIM-3		BUV737	0,1 (2.5 μl)	mouse monoclonal (7D3)	BD OptiBuild	748820
LAG-3		BV480	0,1 (2.5 μl)	mouse monoclonal (T47-530)	BD OptiBuild	746609
IL1R2		PE	10 μl	mouse monoclonal (34141)	Invitrogen	MA5-23543
IL21R		APC	0,375 (1.25 μl)	mouse monoclonal (2G1-K12)	Biolegend	347808

Table 3.5 Fluorescent dyes used for staining and analysis by flow cytometry.

Fluorescent dye	Amount/test (volume) or Concentration	Source	Catalog no
Annexin-V-BV421	5 μ l	BD Horizon	563973
7-AAD	5 μ l	BD Pharmingen	559925
Fixable Viability Dye eFluor™ 455UV	1 μ l	eBioscience/Invitrogen	65-0868-14
Fixable Viability Dye eFluor™ 506	1 μ l	eBioscience/Invitrogen	65-0866-14
Fixable Viability Dye eFluor™ 450	1 μ l	eBioscience/Invitrogen	65-0863-18
CFSE	10-20 μ M	Sigma-Aldrich	21888-25MG-F
Cell Proliferation Dye eFluor™ 450	10 μ M	eBioscience/Invitrogen	65-0842-85

3.5.2 Staining and analysis of surface and intracellular proteins

To analyze protein level by flow cytometry, proteins were stained with antibodies conjugated to fluorochromes (Table 3.3, 3.4). To stain proteins expressed on cell surface, lymphocytes collected from *in vitro* cultures or mice were first washed with PBS and centrifuged at 500 xg, 8 minutes, at 4°C. Depending on application, up to 1x10⁷ cells were used in a single staining sample (1 test). Surface proteins were stained with a cocktail of antibodies, in a total volume of 100 μ l, for 30 minutes, at 4°C. Antibody cocktails were prepared in PBS or in Brilliant Stain Buffer Plus (BD, #566385), in case two or more antibodies conjugated to Brilliant Violet/Brilliant Ultraviolet/Super Bright type of fluorochrome were used. Simultaneously with surface protein staining, viability dye (to discriminate dead cells) was added to cells (Table 3.5). For analysis of intracellular targets, fixable viability dyes were used, to discriminate which cells were dead prior to fixation. Following surface protein staining, cells were either washed twice with PBS and subjected to analysis by flow cytometry or subjected to staining of intracellular targets. Intracellular proteins were stained using eBioscience Foxp3/Transcription Factor Staining Buffer Set (Invitrogen, #00-5523-00), according to manufacturer's protocol. In brief, cells washed after surface staining were first fixed and permeabilized, followed by staining of intracellular proteins (such as Foxp3, Helios, intracellular cytokines, arginase-1 and others), for 30 minutes, at 4°C. Cell were then washed twice, resuspended in PBS and analyzed by flow cytometry. Following fixation, all washes were carried out in permeabilization buffer and cells were centrifuged at 500 xg, 10 minutes, at 4°C.

Flow cytometry and data analysis were performed according to the guidelines of the International Society for Advancement of Cytometry (ISAC)²⁴³. Gating strategies for analysis by flow cytometry are shown in proper Material and Methods Chapters and are referenced in the Results section figure with corresponding data. Antibody specifics and used concentration have been listed in Table 3.3 (anti-mouse) and 3.4 (anti-human) in Chapter 3.5.1. For all flow cytometry applications, antibody titration was done to choose optimal antibody concentration for highest resolution of data. Unless specified otherwise, BD LSR Fortessa cytometer was used for analysis. For single

experiments (mouse *in vitro* suppression assay, mouse EVs uptake/binding assay) BD FACS Verse cytometer was used. For 23-color phenotyping of human Tregs, Cytex Aurora spectral flow cytometer was used. Data analysis was performed using FlowJo software (BD).

3.5.3 Analysis of phosphorylated signaling proteins

To analyze phosphorylation of proteins by flow cytometry, Transcription Factor Phospho Buffer Set (BD, #563239) was used, according to manufacturer's instructions. Staining was performed in 96-well, deep-well, V-bottom plates (Abgene, Thermo Fisher, #AB0932), to enable staining of low number of cells. Either human Tregs or CD4⁺CD25⁻ cells (differentiating into iTregs), treated with leukemic EVs for 18 hours (Chapter 3.6.2 and 3.6.3), were collected, washed with PBS and stained for viability. They were then processed using the Transcription Factor Phospho Buffer Set. First, cells were fixed and permeabilized, followed by treatment with buffer containing methanol, to enable staining of phosphorylated epitopes. Following the treatment, cells were washed with permeabilization buffer and stained with antibodies against both surface markers (CD4, CD25) and intracellular targets (Foxp3 and phosphorylated proteins, STAT5, mTOR, S6, p38, RelA, SMAD2/3) (Table 3.4). Surface antigens were stained in this step due to interference of buffers in used in earlier steps with several fluorochromes. Following staining, cells were washed twice with permeabilization buffer and analyzed on BD LSR Fortessa cytometer. All washing steps were performed at 500 xg, 10 minutes, at 4°C. Samples not stained with antibodies against phosphorylated epitopes were used as negative (background) control for flow cytometry. Samples were analyzed using BD LSR Fortessa cytometer and data were analyzed in FlowJo software (BD).

3.5.4 Phenotyping of human Tregs by 23-color spectral flow cytometry

To design a 23-color panel for high resolution spectral flow cytometry analysis, guidelines and protocols were followed^{243,244}. Markers for analysis were chosen based on RNA sequencing data obtained in this thesis (Chapter 4.2.8) and novel tumor Treg markers described in literature, in studies of solid tumors (described in Introduction Chapter 1.2.4 and Results Chapter 4.2.9). Some of desired proteins were not included due to lack of antibodies for flow cytometry. The 23-color panel was composed to enable sensitive detection of markers with lower expression, by using antibodies conjugated to brightest fluorochromes. Moreover, fluorochromes close to each other on the emission spectrum were avoided for markers that were likely to be co-expressed. This has enabled avoiding issues with data compensation or spreading error. Nevertheless, avoiding of these issues was facilitated by using spectral flow cytometry approach. Spectral cytometry allows more sensitive detection of fluorescent signal, as well as well distinguishing of similar fluorochromes, due to detection of whole fluorescent spectra, rather than narrow signal in detect filters (as in conventional flow cytometry). Moreover, fluorochromes were chosen also based on

market availability, as antibodies for some of the less common protein markers (such as IL1R2, IL21R or BATF) were only available with few fluorochromes.

For analysis, cells from *in vitro* cultures of Tregs with leukemic EVs (described further in Chapter 3.6.3) were stained as described in Chapter 3.5.2. In brief, cells were first stained with surface antibody cocktail (18 antibodies in Brilliant Stain Buffer Plus, Table 3.4) and viability dye, followed by intracellular staining (Foxp3, Helios, IRF4, BATF) using eBioscience Foxp3/Transcription Factor Staining Buffer Set. Data were acquired on Cytex Aurora spectral flow cytometer. Spectral unmixing and compensation were set up using unstained cells and single-stained beads (UltraComp Compensation Beads, Thermo Fisher, #01-2222-41). Based on single-stained controls and visualizing each marker versus each marker (also in multicolor samples), compensation was verified in FlowJo software. In every experiment (for each experimental condition), samples without phenotype staining (only stained for viability, CD4, CD25, CD127, Foxp3) were prepared to facilitate setting up gates in manual analysis of phenotypic markers. Following data acquisition and quality control (as described above), data was analyzed by either traditional manual gating or computational analysis methods (tSNE, FlowSOM), as shown on Figure 3.7.

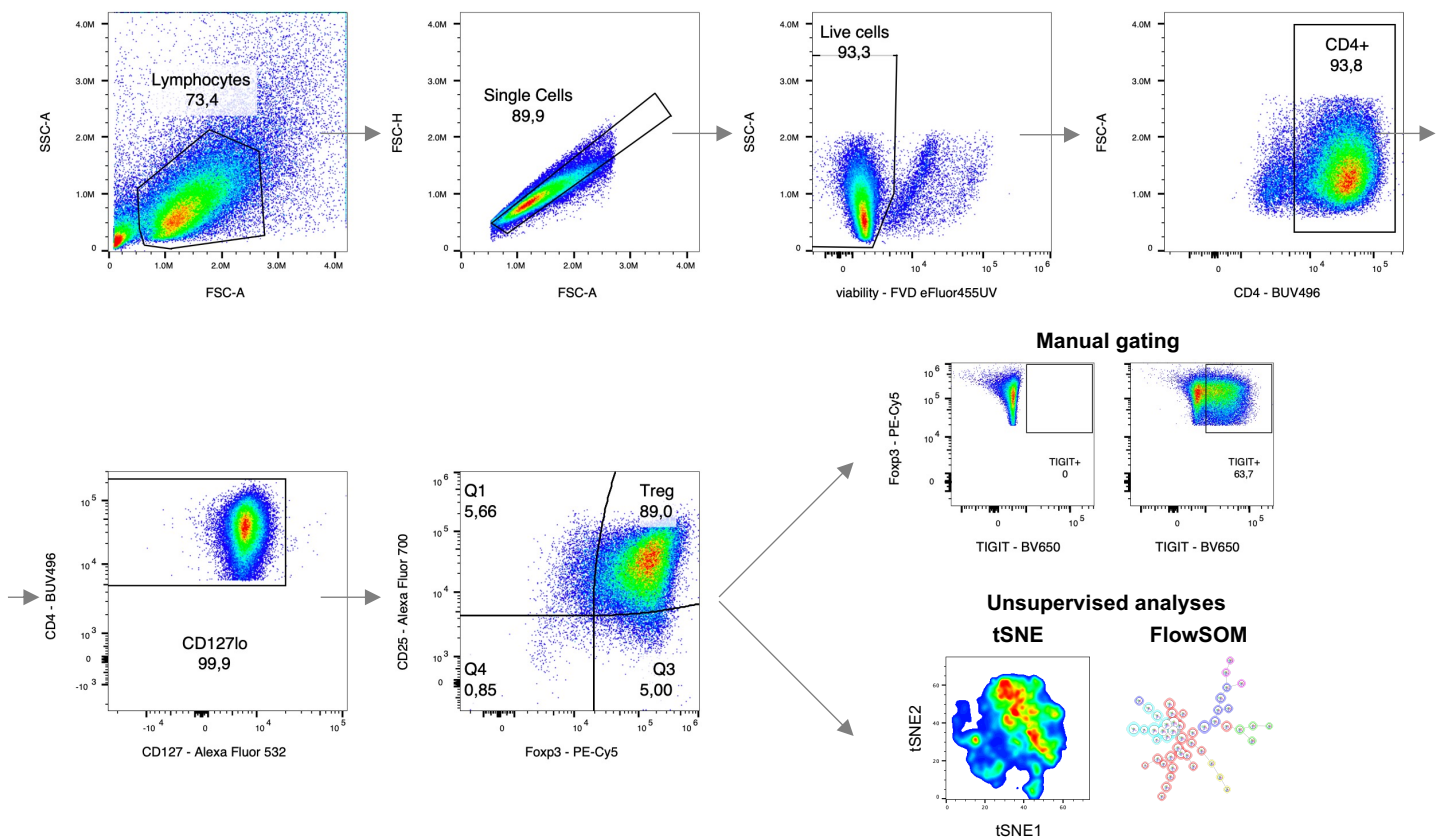


Figure 3.7 23-color analysis of Treg phenotype in human Tregs cultured with EVs. Representative gating strategy to analyze Treg phenotype by 23-color spectral flow cytometry. CD25^{hi}CD127^{lo}Foxp3⁺ cells were identified among single, viable CD4⁺ T cells. Then, expression of phenotypic markers was analyzed in the CD25^{hi}CD127^{lo}Foxp3⁺ population by manual gating or CD25^{hi}CD127^{lo}Foxp3⁺ cells were analyzed in an unsupervised manner by tSNE or FlowSOM.

3.5.5 Computational analysis of flow cytometry data

To analyze obtained data in an unsupervised manner, two methods were used. tSNE was used to visualize high-dimensional data, whereas FlowSOM algorithm was used to cluster cells into subpopulations, that could be later quantified and compared between experimental conditions. For both methods, cells of interest were first gated by manual gating (to filter out aggregates and dead cells) - viable CD3+ cells from mice (Results Chapter 4.3.3), CD4+ or Tregs from human *ex vivo* cultures (Results Chapters 4.2.4 and 4.2.9). As computational analyses are time- and power-consuming, they are limited in terms of cells/events they can process. Therefore, cells of interest were downsampled, by using Downsample plugin in FlowJo, which means that a smaller group of cells, but representative of the sample, was exported as a new FCS file. Downsampled files were then concatenated (merged into a single sample) and analyzed by tSNE or FlowSOM, to first generate a joint analysis/clustering scheme for each entire dataset. For each parameter analyzed, biexponential transformation of data for each fluorescence channel was adjusted to maximize resolution of the data. Number of cells obtained by downsampling and total number of cells used for analysis/clustering are specified in the legends of figures presenting the data.

To visualize flow cytometry data based on more than 2 parameters, but in 2D space, tSNE (t-distributed stochastic neighbor embedding) method was used²⁴⁵. In general, tSNE groups cells that are similar in a high-dimensional space (based on many parameters) into islands on a 2D graph. The generated islands represent populations of cells with a similar phenotype. In presented study, tSNE maps were generated using tSNE plugin in FlowJo v10, based on specified number of parameters (parameters used are indicated in the appropriate legends of figures in the Results section), using default settings in FlowJo. The generated tSNE map was representative of the entire dataset for each experiment. Cells from each experimental condition were then separately visualized on the same tSNE map, to visually observe differences in T cell/Treg biology between experimental conditions.

To cluster cells into subsets, based on many parameters simultaneously, FlowSOM algorithm was used²⁴⁶. FlowSOM benefits from self-organizing maps to cluster cells and reduce dimensionality. It therefore identifies and quantifies cell subsets and usually visualizes them using a minimal spanning tree. Identified populations may also be visualized on tSNE plots. FlowSOM was performed using FlowSOM plugin in FlowJo v10. For first FlowSOM analysis of human Treg cells cultured with EVs (Results Chapter 4.2.4, Figure 4.12), cells were clustered into 6 populations, 25 nodes, based on 4 parameters. For FlowSOM analysis of human Treg cells phenotyped by 23-color spectral cytometry (Results Chapter 4.2.9, Figure 4.27), cells were clustered into 6 populations, 49 nodes, based on 15 parameters. Clustering determined on concatenated samples was then applied

to individual samples from different experimental conditions and identified populations were quantified.

Computational analysis of flow cytometry data has been carried out in collaboration with Professor Andrea Cossarizza and Dr Sara de Biasi (Department of Medical and Surgical Sciences for Children & Adults, University of Modena and Reggio Emilia).

3.6 Treg/T cell assays with extracellular vesicles

3.6.1 Mouse *in vitro* suppression assay and analysis of Foxp3 level

To analyze influence of EVs released by mouse 32D/32D BCR-ABL1+ cells, a well-established *in vitro* suppression assay by mouse Tregs was used²⁴⁷. The assay was modified to adapt to low numbers of Tregs that were obtained from the murine thymus (thymic Tregs, tTregs), as well as adapted to study effect of EVs. The main principle of suppression assay is to track proliferation of responder T cells (such as non-regulatory, effector CD4+ and CD8+ T cells), based on dilutions of a proliferation tracking dye, such as CFSE or violet Cell Proliferation Dye eFluor450 (Table 3.5). Differences in proliferation rate between responder cells cultured without Tregs and with Tregs (or differently treated Tregs) enable measurement of Treg suppressive activity, that is how significantly have Tregs inhibited proliferation of responder T cells. The general schematic of the assay used in this thesis is presented on Figure 3.8.



MOUSE *IN VITRO* SUPPRESSION ASSAY

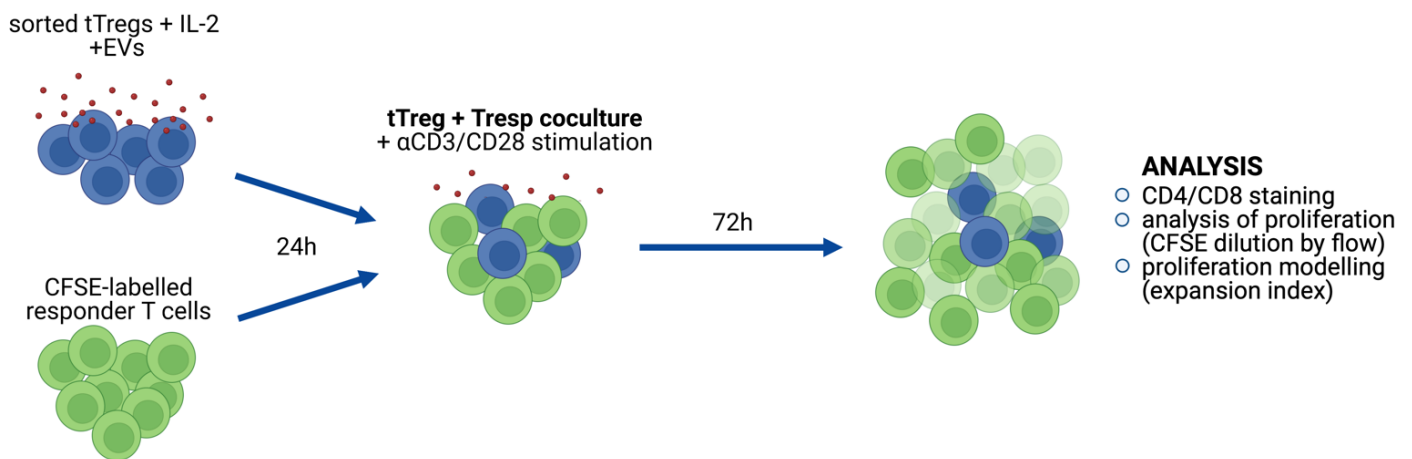


Figure 3.8 Experimental pipeline of mouse *in vitro* suppression assay used in the thesis. Figure created with BioRender.com.

To study effects of EVs on suppressive activity, 1.25×10^4 sorted CD4+CD8-CD25^{hi} tTregs (from C57BL/6 mice) were first preincubated for 24 hours with isolated EVs (specified amounts of protein) and IL-2 (50 IU/ml), in 100 μ l of media, in 96-well U-bottom plates. Simultaneously with Treg sorting,

lymphocytes from axillary lymph nodes (used as responder T cells, Tresp) were labelled with 10 μ M CFSE, thoroughly washed and seeded (2.5×10^4 cells) in 100 μ l of media, in 96-well U-bottom plates, for 24 hours. Following 24 hours, tTregs and Tresp were mixed at 1:2 ratio and stimulated with 0.5 μ g/ml anti-CD3 and 0.05 μ g/ml anti-CD28 soluble antibodies, to induce proliferation of responder T cells. Due to low numbers of tTregs, washing out of EVs was not possible, therefore tTregs were first preincubated with EVs for 24 hours, to maximize effect of EVs on Tregs, and only then added to responder T cells. Appropriate control experiments without tTregs were performed to exclude bystander effects. The culture of Tregs and Tresp was carried out for 72 hours, followed by analysis of proliferation by flow cytometry. To distinguish between CD4+ and CD8+ responder T cells, cultures were stained with anti-CD4 and anti-CD8 antibodies. Flow cytometry was performed using BD FACS Verse cytometer and data were analyzed using BD FACS Diva and FlowJo software, as shown in Figure 3.9. To assess suppressive activity of Tregs, either percentage (%) of inhibition was calculated ($\% \text{ inhibition} = 100 - (\% \text{ of proliferated cells in co-culture with tTreg}) / (\% \text{ of proliferated cell in control culture without tTreg}) \times 100$) or expansion index of Tresp was calculated using proliferation modelling tool in FlowJo. Decrease in expansion index corresponded to increase in Treg suppressive activity.

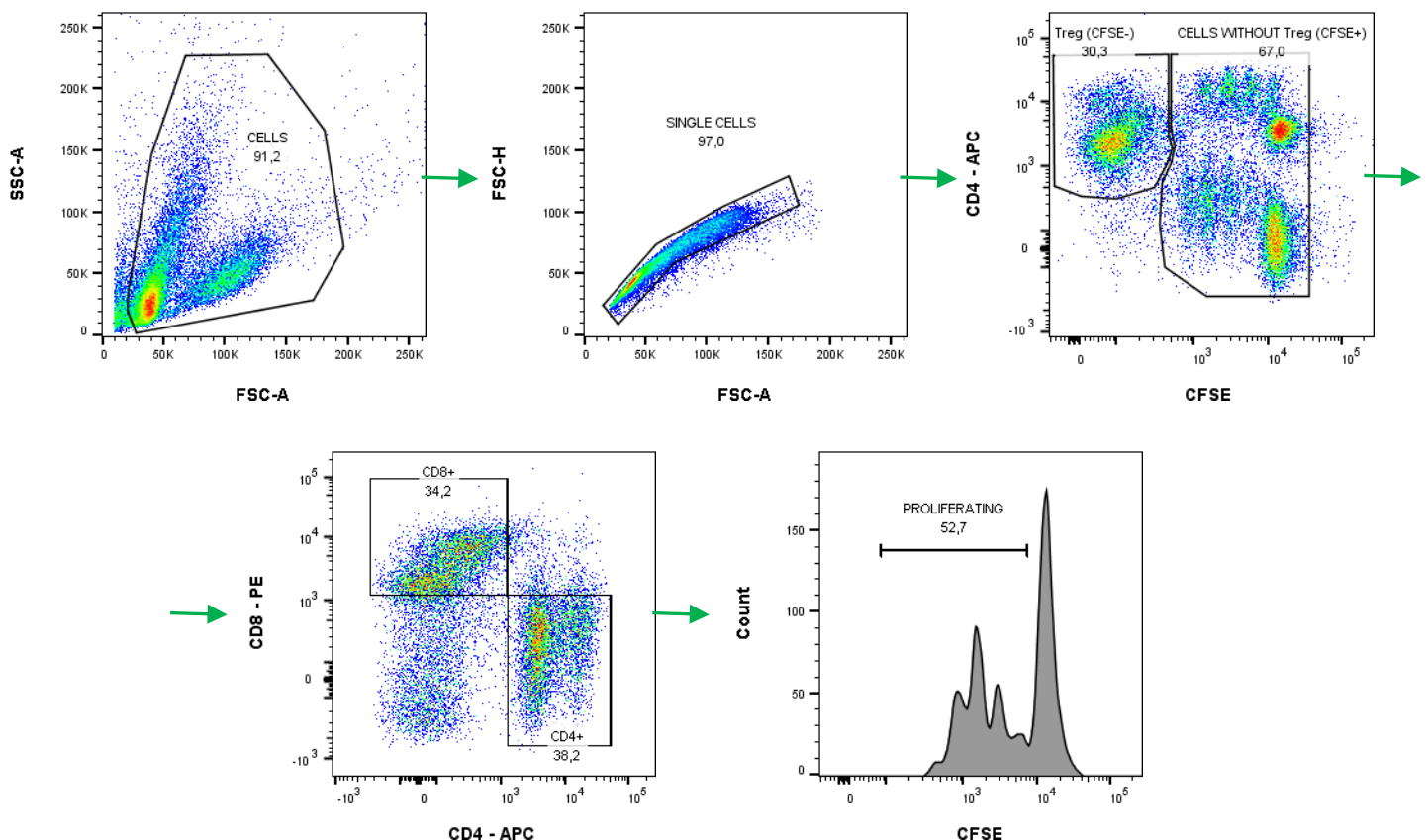


Figure 3.9 Analysis of mouse *in vitro* suppression assay cultures. Representative gating strategy to analyze proliferation of responder T cells. Among single cells, Tregs were first excluded based on lack of CFSE fluorescence, followed by identification of CD4 and CD8 responder cells. In identified cell populations, cell divisions by CFSE dilution were analyzed (figure from Swatler *et al.*, 2020, Eur J Immunol^[242]).

As mentioned, even though in the suppression assay EVs were first added to tTregs alone for 24 hours, some bystander effects via interaction with Tresp could not be excluded. To exclude potential interference of this in the final suppression assay results, control experiments without tTregs, only with Tresp and EVs were performed. In this type of experiment, the culture was performed exactly as described above and presented in Figure 3.8, only without tTregs. EVs and responder T cells were first kept in culture separately for 24 hours, followed by adding Tresp to EVs and stimulation with anti-CD3 and anti-CD28 antibodies. Following 72 hours, proliferation of Tresp was measured, as previously described. Percentage (%) of proliferating cells and expansion index were calculated to measure proliferation.

Finally, to assess influence of EVs on the level of Foxp3 in Tregs, tTregs from Foxp3-GFP mice were cultured with EVs. Again, this culture was performed exactly as in the *in vitro* suppression assay, only without responder T cells. Sorted tTregs were first incubated with EVs (and IL-2) for 24 hours. They were then stimulated with anti-CD3 and anti-CD28 antibodies and further cultured, though in this case for 48 hours. Foxp3 level (GFP fluorescence) was analyzed at the beginning of culture (0-hour timepoint) and at 24-, 48- and 72-hour timepoints. At each timepoint, cultures were stained with anti-CD4, anti-CD8 and anti-CD25 antibodies and viability dye (7-AAD). Flow cytometry was performed using BD LSR Fortessa cytometer and data were analyzed using BD FACS Diva and FlowJo software, as shown in Figure 3.10.

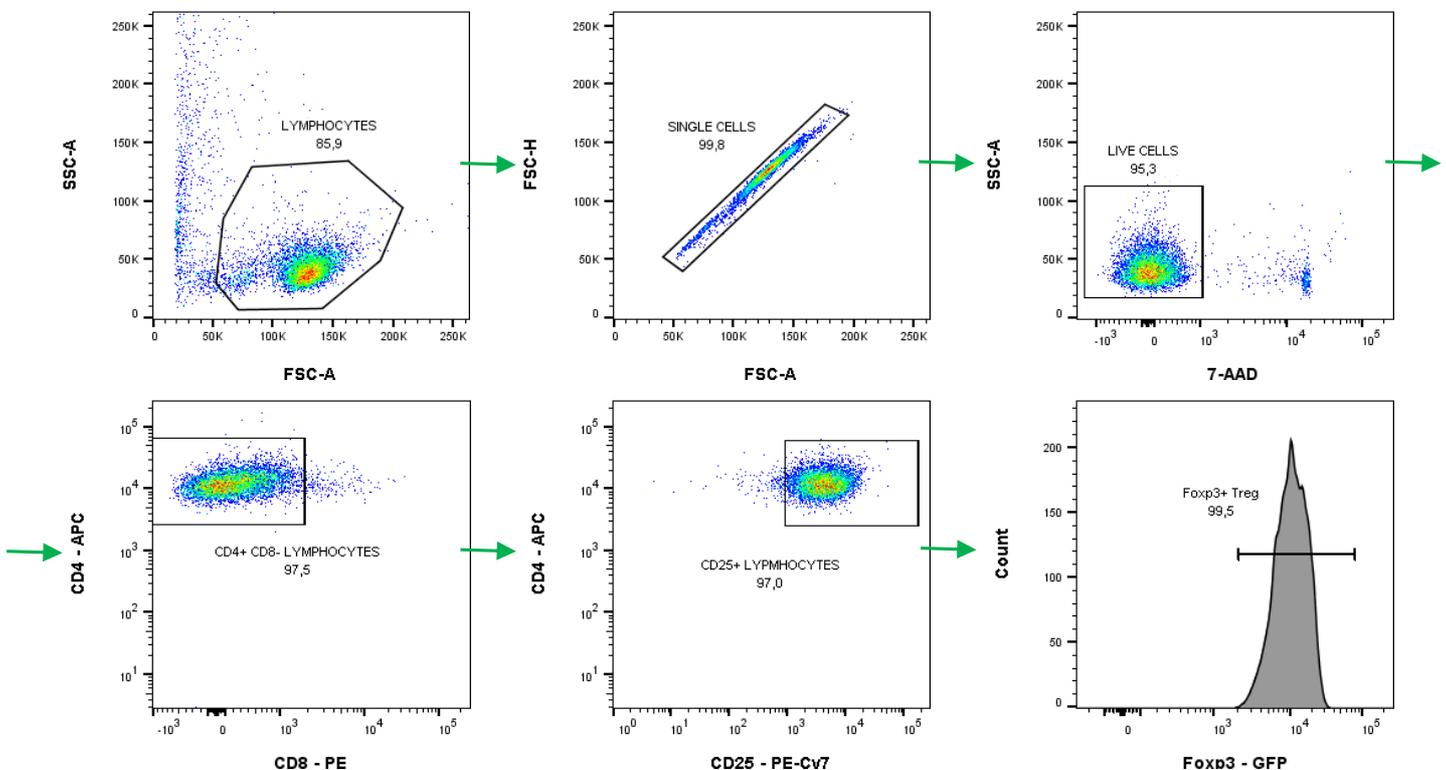


Figure 3.10 Analysis of Foxp3 level in mouse tTregs. Representative gating strategy to analyze Foxp3-GFP level in tTregs cultured with EVs. Among viable, single cells, Tregs were identified as CD4+CD8-CD25+. In identified cell populations, GFP (Foxp3) level was analyzed, measured as geometric mean, gMFI (figure from Swatler *et al.*, 2020, Eur J Immunol²⁴²).

3.6.2 Human iTreg inducing culture

To study influence of leukemic EVs on generation of *in vitro* induced regulatory T cells (iTregs) from non-regulatory T cells, CD4+CD25- conventional T cells were cultured in Foxp3-inducing conditions, as previously described²⁴⁸. The experimental pipeline of experiments performed in this thesis is presented graphically on Figure 3.11.

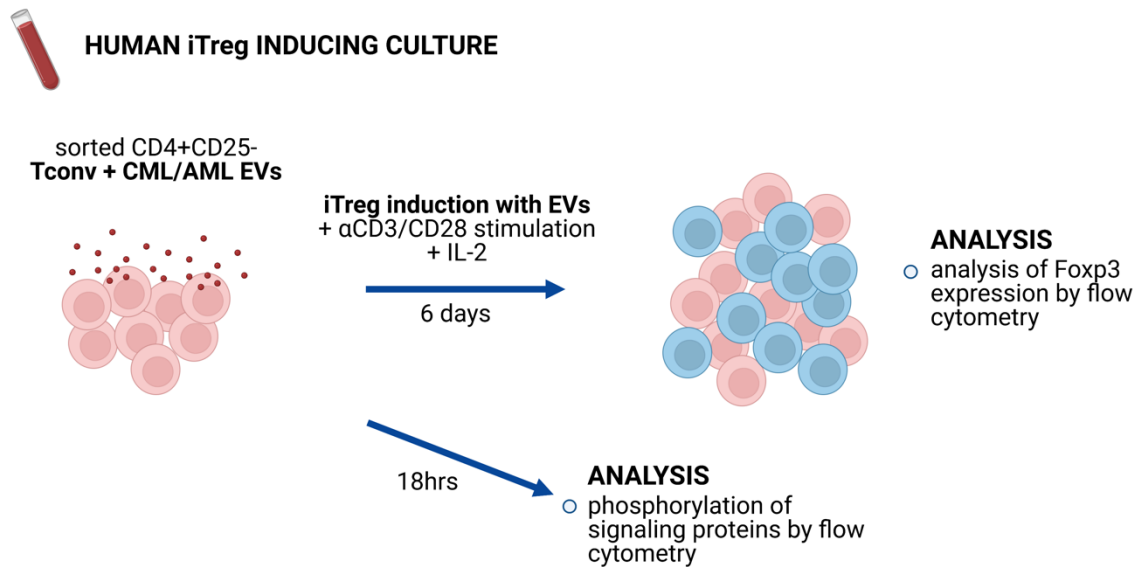


Figure 3.11 Experimental pipeline of human iTreg/Foxp3 inducing cultures. Figure created with BioRender.com.

To study Foxp3 induction in non-regulatory cells, sorted CD4+CD25- conventional T cells were cultured with leukemic EVs (either released by K562 or MOLM-14 cells or from plasma of patients). 1.3×10^5 CD4+CD25- cells were cultured in 200 μ l of AIM V media, in 96-well U-bottom plates. To facilitate iTreg generation, cells were stimulated with antibodies anti-CD3 (coated wells, 5 μ g/ml), anti-CD28 (soluble, 1 μ g/ml) and recombinant IL-2 (100 IU/ml). CD4+CD25- were treated with either 3×10^9 - 3×10^7 CML (K562) EVs (number of particles, in a dose-dependent study) or 5×10^9 AML (MOLM-14) EVs (number of particles). Top doses of EVs (number of particles) are equivalent of EVs released by 1×10^8 cells. As positive control of Foxp3/iTreg induction, CD4+CD25- cells were also cultured with recombinant human TGF- β (20 ng/ml, Peprotech #100-21). Foxp3/iTreg inducing cultures were carried out for 6 days. To study early signaling events in CD4+CD25- cells in Foxp3-inducing conditions, phosphorylation of signaling proteins was analyzed 18 hours after treatment with EVs (methodology described in detail in Chapter 3.5.3). To analyze Foxp3 induction in CD4+CD25- cells, after 6 days of culture, cells were stained with a cocktail of surface antibodies and viability dye (Table 3.4, 3.5), followed by intracellular detection of Foxp3, using eBioscience Foxp3/Transcription Factor Staining Buffer Set, as described in Chapter 3.5.2. Cells were analyzed

using BD LSR Fortessa cytometer. Analysis was performed in FlowJo software and cells were gated as shown in Figure 3.12.

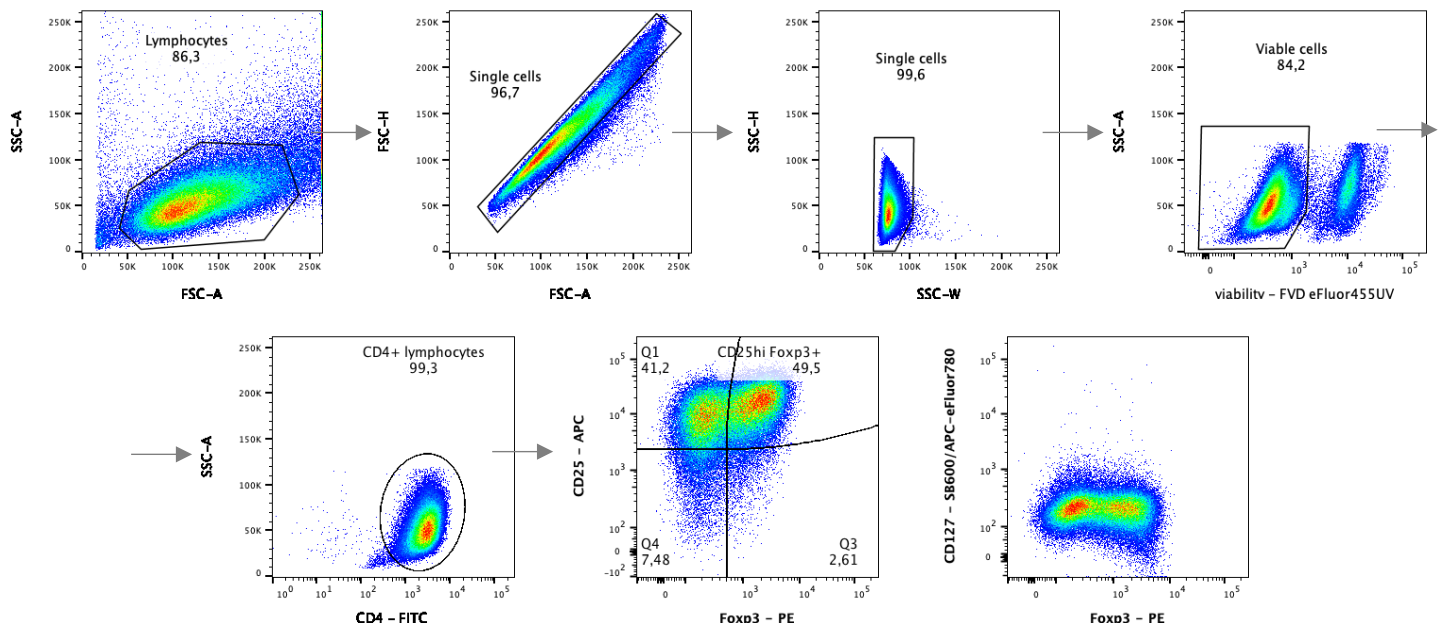


Figure 3.12 Analysis of Foxp3 induction in CD4+CD25⁻ Tconv, cultured in iTreg inducing conditions. Representative gating strategy to analyze Foxp3 induction in non-regulatory cells. CD25^{hi}Foxp3⁺ cells (considered iTregs) were identified among single, viable CD4⁺ T cells. Independent on Foxp3 expression, all cells following *ex vivo* culture have become CD127^{lo}.

3.6.3 Human Treg/T cell expansion culture

To study influence of leukemic EVs on different aspects of human Treg biology, sorted CD4⁺CD25^{hi}CD127^{lo} Treg cells were activated and cultured with EVs. The experimental pipeline of experiments performed in this thesis is presented graphically on Figure 3.13.

Sorted CD4⁺CD25^{hi}CD127^{lo} Treg cells were cultured with leukemic EVs (either released by K562 or MOLM-14 cells or from plasma of patients). 5x10⁴ Treg cells were cultured in 200 μ l of AIM V media, in 96-well U-bottom plates. Tregs were stimulated with antibodies anti-CD3 (coated wells, 5 μ g/ml), anti-CD28 (soluble, 1 μ g/ml) and recombinant IL-2 (50 IU/ml). Tregs were treated with either 3x10⁹-3x10⁷ CML (K562) EVs (number of particles, in a dose-dependent study) or 5x10⁹ AML (MOLM-14) EVs (number of particles). In studies using CML (K562) EVs without dose-dependency analysis, 3x10⁹ CML EVs/particles were used. Top doses of EVs are equivalent of EVs released by 1x10⁸ cells. In specified experiments, CD4⁺CD25⁻ cells were cultured simultaneously with Tregs, as biological negative control for expression of Treg-specific proteins or RNAs. For majority of experiments, Treg cultures were carried out for 5 days. To study early signaling events in Tregs following treatment with EVs, phosphorylation of signaling proteins was analyzed 18 hours after treatment with EVs (methodology described in detail in Chapter 3.5.3). To analyze basic changes in Treg phenotype after 5 days of culture, cells were stained with a cocktail

of surface antibodies and viability dye (Table 3.4, 3.5), followed by intracellular detection of Foxp3, using eBioscience Foxp3/Transcription Factor Staining Buffer Set, as described in Chapter 3.5.2. Cells were analyzed using BD LSR Fortessa cytometer. Analysis was performed in FlowJo software and cells were gated as shown in Figure 3.14. Tregs cultured with EVs for 5 days, as described above, were also used for several other applications, such as *in vitro* suppression assay (methodology described in detail in Chapter 3.6.4), RNA-sequencing (methodology described in detail in Chapter 3.8), analysis of methylation of TSDR region in the *FOXP3* gene by methylation-specific PCR (methodology described in detail in Chapter 3.8) and analysis of released cytokines (conditioned medium was collected and stored at -80°C until use for cytokine analysis, methodology described in detail in Chapter 3.7).

To study influence of EVs on human non-regulatory cells (CD8+ T cells and non-Treg CD4+ T cells), sorted CD8+ and non-Treg CD4+ cells (Figure 3.6A) were cultured in the same conditions as Tregs. Following 5 days of culture, cells were stained for surface markers of T cell exhaustion/dysfunction (PD-1, CTLA-4, LAG-3, CD39, Table 3.4) and conditioned medium was collected and stored at -80°C until use for cytokine analysis (methodology described in detail in Chapter 3.7).

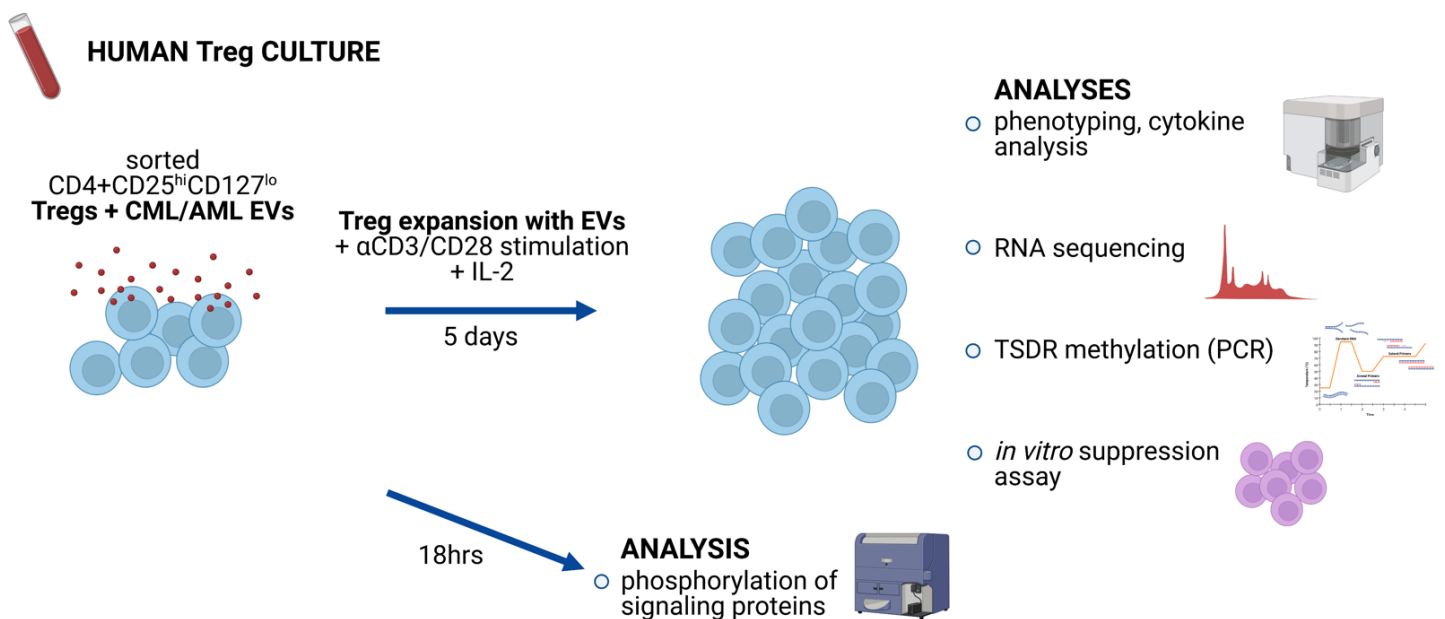


Figure 3.13 Experimental pipeline of human Treg cultures with EVs. Human CD4+CD25^{hi}CD127^{lo} Tregs were cultured with EVs and used for several applications, to study several aspects of Treg biology: signaling, phenotype, transcriptome and gene methylation. Figure created with BioRender.com.

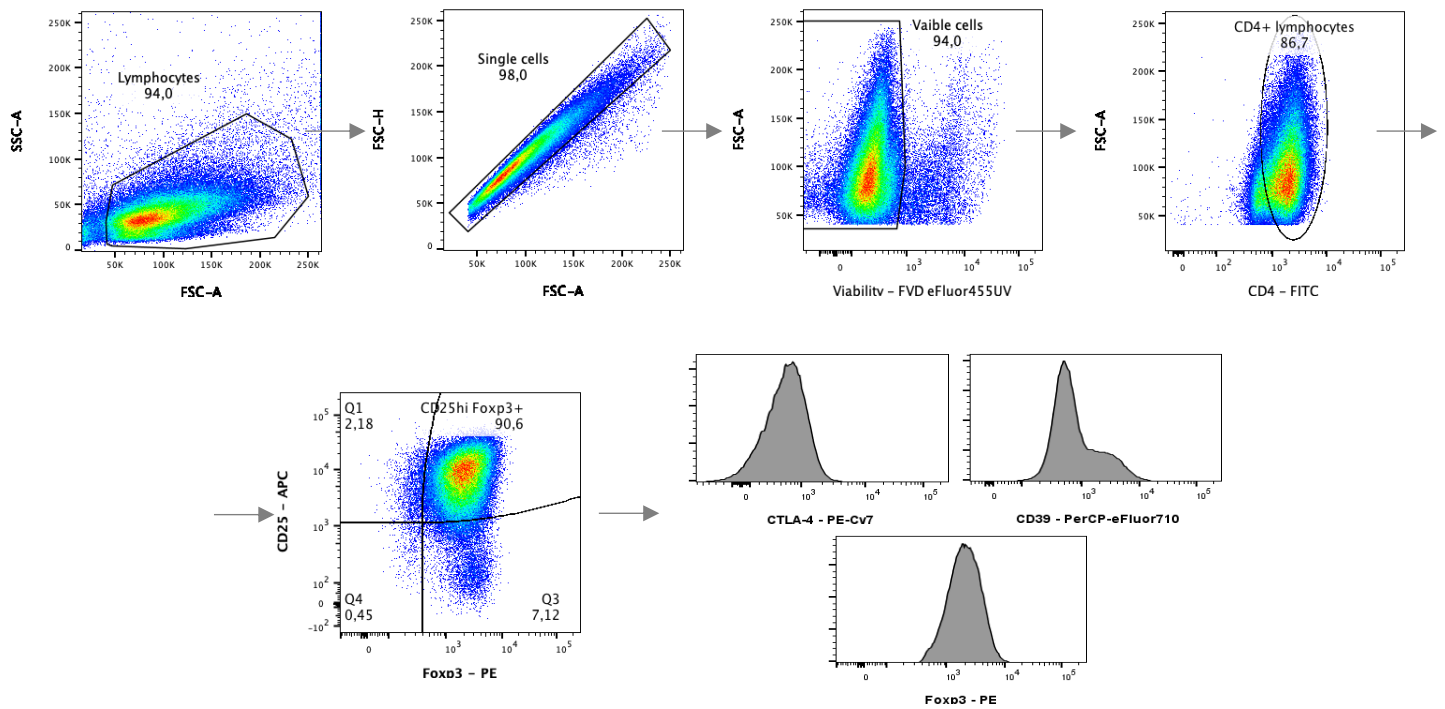


Figure 3.14 Analysis of basic Treg phenotype in human Tregs cultured with EVs. Representative gating strategy to analyze Treg phenotype. CD25^{hi}Foxp3⁺ cells were identified among single, viable CD4⁺ T cells. Then, expression of CTLA-4, CD39 and Foxp3 was analyzed in the CD25^{hi}Foxp3⁺ population.

3.6.4 Human *in vitro* suppression assay

To assess functionality (suppressive activity) of human Tregs treated with leukemic EVs (as described in Chapter 3.6.3), human version of the *in vitro* suppression assay was performed. The general experimental pipeline of human *in vitro* suppression assay is presented on Figure 3.15.

Tregs (CD4⁺CD25^{hi}CD127^{lo}) were first sorted and cultured with EVs for 5 days, as described above (Chapter 3.6.3). As the *in vitro* suppression should be performed using autologous (from the same blood donor as Tregs) responder T cells (Tresp), CD4⁺CD25⁻ and CD8⁺CD25⁻ T cells (used as Tresp) were sorted simultaneously with Tregs and frozen (in AIM V media with 45% FBS and 10% DMSO), until suppression assay cultures. The freezing procedure did not influence viability (over 95% following thawing) or ability to proliferate of CD4⁺ and CD8⁺ Tresp.

After 5 days of Tregs expansion with EVs, suppression assay cultures were set up. Firstly, Tresp were thawed into AIM V medium with IL-2 (10 IU/ml) and immediately stimulated with anti-CD2/CD3/CD28 beads (Miltenyi Biotec, #130-091-441), at 1:2 bead:cell ratio, for 5 hours, to recover following freezing. Activating beads remained in the culture until the end of suppression assay. Tresp were then labelled with 10 μ m eBioscience Cell Proliferation Dye eFluor450 (shortly: CPD eFluor450, Table 3.5), to track their proliferation in the suppression assay. Tregs were collected from cultures with EVs, stained with antibodies anti-CD4, CD25, CD127 and viability dye

and once again sorted, to obtain only pure, viable and activated Tregs for suppression assay cultures. Following sorting, Tregs were also stimulated with anti-CD2/CD3/CD28 beads, at 1:2 bead:cell ratio.

Suppression assay cultures were then established in 96 flat-bottom plates, using AIM V medium with IL-2 (10 IU/ml). Tresp (either CD4+ or CD8+), labelled with proliferation dye, were first seeded in 100 μ l of media, 5×10^4 Tresp per well. Tregs were then added to cultures, at either 1:4 or 1:2 Treg:Tresp ratio. Tresp without Tregs were cultured as controls. As additional controls for flow cytometry, Tresp not labelled with proliferation dye and unstimulated Tresp were also cultured. Suppression assay cultures were carried out for 4 days. Following culture, cells were additionally stained with anti-CD4 and anti-CD8 antibodies and 7-AAD viability dye. Analysis of Tresp proliferation was performed by flow cytometry (BD LSR Fortessa) and analysis in FlowJo software. Proliferation of viable (7-AAD negative) responder T cells (either CD4+ or CD8+) was analyzed as expansion index, using proliferation modelling tool in FlowJo. Decrease in expansion index corresponded to increase in suppressive activity of Tregs.

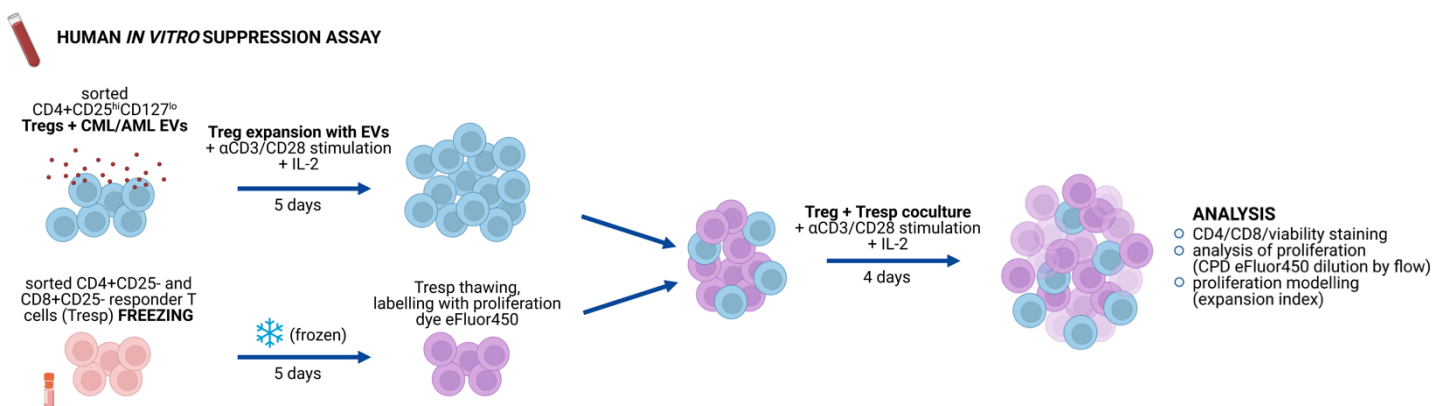


Figure 3.15 Experimental pipeline of human *in vitro* suppression assay. Human CD4+CD25^{hi}CD127^{lo} Tregs, treated with EVs, were cultured with responder T cells (Tresp), labelled with Cell Proliferation Dye eFluor450 (CPD eFluor450). This was followed by flow cytometric analysis of Tresp proliferation, to assess suppressive influence of Tregs. Figure created with BioRender.com.

3.7 Soluble cytokine analysis

Secretion of cytokines by Tregs, non-Treg CD4+ and CD8+ cells (cultured as described in Chapter 3.6.3) was measured by analysis of soluble cytokines in medium conditioned by cells (cell culture supernatants), by a bead-based cytometric array. Supernatants were collected from cultures by first pelleting the cells at 500 xg, 8 minutes, at 4°C. Supernatants were then centrifuged again to remove residual cells and debris, aliquoted and frozen at -80°C until use. As negative controls, non-conditioned medium (cultured without any cells) and medium cultured with CML EVs (but without cells) were collected. For cytokines presented in this thesis, no background signal was observed in these negative controls. For each experiment, prior to collection of supernatants,

cytokine producing cells were checked for viability and counted, to enable quantification of cytokines produced by 1×10^5 cells.

Measurement of cytokines was performed using LEGENDplex technology and Human Essential Immune Response Panel (13-plex) (Biolegend, #740930). The array is based on binding of cytokines to beads coated with antibodies against specific cytokines. As beads in the assay are of different sizes and internal fluorescence, 13 types of beads (and therefore cytokines) can be detected by flow cytometry at once. In brief, supernatants were first incubated with antibody-coated beads, to bind specific cytokines to beads. This was followed by incubation with biotinylated antibodies against cytokines and streptavidin (conjugated to fluorescent PE fluorochrome), to generate quantifiable fluorescent signal of each cytokine. Beads were then acquired on BD LSR Fortessa cytometer. Simultaneously with samples, standard curves for cytokines were run, in duplicate. Data were analyzed using LEGENDplex Analysis Software. Cytokine concentration was calculated per 1×10^5 viable cells.

3.8 RNA sequencing, RT-qPCR, methylation-specific PCR

For analyses of RNA (by sequencing or RT-qPCR) and DNA methylation, human Tregs from *ex vivo* cultures were first stained with antibodies anti-CD4, CD25, CD127 and viability dye and once again sorted, to obtain only pure, viable and activated Tregs. In initial studies, viability of sorted cells was validated with 7-AAD dye, to make sure that cells of high purity and viability were used for downstream applications (Figure 3.16). For RNA extraction, sorted cells were centrifuged and resuspended in 1 ml of TRI Reagent (Sigma, #T9424). RNA was isolated using Total RNA Mini columns (A&A Biotechnology, #031-100), according to manufacturer's protocol.

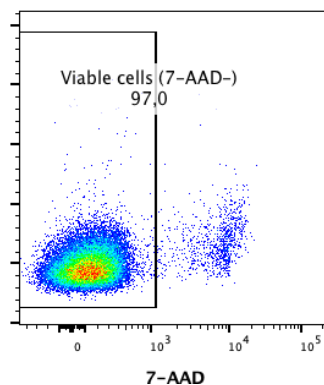


Figure 3.16 Viability of Tregs cultured for 5 days with EVs and sorted again to obtain pure, viable and activated Tregs for molecular analyses.

For reverse transcription for RT-qPCR, 0.25 μg of RNA was used to further obtain cDNA. First, RNA was incubated with 1 μM universal oligo(dT)₁₈ and 1 μM "random hexamers" primers (Bioline, #BIO-38029, #BIO-38028), for 5 minutes at 70°C. Next, 4 U/ μl M-MLV reverse transcriptase (Promega, #M1705), 1.25 mM dNTPs (Blirt, #RP65), 0.32 U/ μl ribonuclease inhibitor

RIBOPROTECT (Blirt, #RT36) and buffer for M-MLV enzyme (Promega, #1705) were added. Reverse transcription was run for 60 minutes at 37°C and 5 minutes at 95°C. For real-time PCR reaction, SensiFAST SYBR Green Hi-ROX (Bioline, #BIO-92020) kit was used. For reactions, 2 µl of cDNA was used, mixed with 5 µl of SYBR Green, 0.25 µl of each forward and reverse primers (500nM final concentration) and 2.5 µl of water. qPCR reaction was run using StepOnePlus Real-Time PCR System (Thermo Fisher). Initial denaturation was run for 20 seconds at 95°C, followed by 40 amplification cycles (3 seconds at 95°C and 30 seconds at 60°C) and melting curve generation. Analysis was performed using StepOne Plus software, using $2^{-\Delta\Delta C_t}$ comparative method to compare mRNA levels. 18SrRNA was used for data normalization. Primers were used as following:

Table 3.6 Primers used for detection of gene expression by RT-qPCR.

Primers sequences for RT-qPCR		
Gene	Forward	Reverse
<i>18srRNA</i>	5' GTAACCCGTTGAACCCC 3'	5' CCATCCAATCGGTAGTAGCG 3'
<i>FOXP3</i>	5' GCACCTTCCCAAATCCCAGT 3'	5' GGCCACTTGCAGACACCAT 3'
<i>ENTPD1 (CD39)</i>	5' AGGTGCCTATGGCTGGATTAC 3'	5' CCAAAGCTCCAAAGGTTTCCT 3'
<i>CCR8</i>	5' GTGTGACAACAGTGACCGACT 3'	5' CTTCTTGCAGACCACAAGGAC 3'

RNA sequencing was performed at Genomics Core Facility (GeneCore) at EMBL, Heidelberg. First, isolated RNA was used to prepare sequencing libraries, using NEB Next Ultra II Directional RNA library prep kit for Illumina (New England Biolabs, #E7765), according to manufacturer's protocol. Sequencing was run using Illumina NextSeq 500. Sequencing was run at 75-bp single-end reads. Obtained sequencing datasets were then subjected to bioinformatic analysis. Reads from sequencing were aligned to hg38 genome using Hisat2 (version 2.1.0), with default settings. Python HTSeq script (version 0.11.2) and Bioconductor package DESeq2 (version 1.28.1) were used to compute numbers of reads aligned to each gene and the differential expression, respectively. Genes were considered differentially expressed once they had had significant (adj. p-value < 0.05) changes in their expression levels (log-fold-change > 1). Bioconductor package ClusterProfiler (version 3.16.1) was used to perform Gene Ontology analysis. To analyze transcription factor binding motifs (TFBM), PSCAN software was used, by referencing -950 to +50 bp regions of DEGs to JASPAR 2018_NR database.

Bioinformatic analysis of RNA sequencing data has been carried out in collaboration with Dr Jakub Mieczkowski and Elyas Mohammadi (3P-Medicine Laboratory, Medical University of Gdansk).

Methylation-specific PCR analysis of TSDR region (Treg-specific demethylation region) in the human *FOXP3* gene was performed as described previously²⁴⁹. In brief, DNA was isolated from sorted Tregs (2.5x10⁴ cells, snap frozen in liquid nitrogen following sorting) using EZ DNA Methylation-Direct kit (Zymo Research, #D5020), according to manufacturer's protocol.

Simultaneously with DNA isolation, bisulfite conversion of unmethylated cytosines to uracil was performed, using the same kit. Methylated cytosines remained unaffected, therefore changes in methylation of specific regions can be further detected by using starters towards methylated and demethylated sequences. DNA was eluted in 10 µl of elution buffer and 2 µl were used for each PCR reaction. PCR reactions were run in total volume of 8 µl, including 2 µl of DNA, 2 µl of SensiFast SYBR Green Hi-ROX and 2 µl of each primer. Primers were used either towards methylated or demethylated sequences (separate reactions) and were as following:

Table 3.7 Primers used to quantify TSDR methylation by methylation-specific PCR.

Primers sequences for MS-PCR		
Sequence	Forward	Reverse
methylation specific	5' CGATAGGGTAGTTAGTTTTCGGAAC 3'	5' CATTAAACGTCATAACGACCGAA 3'
demethylation specific	5' TAGGGTAGTTAGTTTTTGAATGA 3'	5' CCATTAACATCATAACAACCAAA 3'

PCR reaction was run using StepOnePlus Real-Time PCR System (Thermo Fisher). Initial denaturation was run for 10 minutes at 98°C, followed by 40 amplification cycles (15 seconds at 98°C and 60 seconds at 60°C) and melting curve generation. Methylation was calculated using the following formula: [% methylation = 100/(1+2^{ΔCt(met)-Ct(demet)})]. CD4+CD25- conventional T cells, cultured simultaneously with Tregs, were used as positive control of TSDR methylation, as they have fully methylated TSDR.

3.9 Proteomics

To perform analysis of proteins in CML (K562-derived) EVs, extracellular vesicles were isolated using differential ultracentrifugation (4 separate isolations) and subjected to analysis by mass spectrometry. In each isolation, approximately 9x10⁹ EVs/particles were isolated, which corresponded to particles released by approximately 3x10⁸ K562 cells. Pelleted EVs were resuspended in 300 µl of buffer containing 0.5% SDS, 6 M urea, 100 mM Tris and sonicated for 30 cycles 30 on /60 off at "high" (Bioruptor, Diagenode). Obtained material was filtered on Vivacon-500 30k filters, followed by wash with 6 M urea. Obtained samples were reduced with TCEP and digested with LysC/trypsin, followed by fractionation in an increasing acetonitrile gradient (in buffer containing 10 mM NH₄CHO₂, pH=10), using Oasis HLB Waters 10 mg cartridges. The obtained solution was evaporated and resuspended in buffer containing 0.1% TFA, 2% MeCN. The final proteomic analysis was performed by LC-MS (liquid chromatography-mass spectrometry), using NanoAcquity UPLC System (Waters), coupled to a QExative Orbitrap (Thermo Scientific) mass spectrometer. Analysis was performed at the Laboratory of Mass Spectrometry (IBB PAS, Warsaw). Data analysis was performed using MaxQuant 1.6.3.4, referenced to human proteome from UniProt database, downloaded on 27.01.2020, 75776 entries. The analysis has enabled identification of 2036 proteins in CML EVs (FDR/false discovery rate 1%). Identified targets were

referenced to ExoCarta (<http://www.exocarta.org/>) database²⁵⁰ (which contains proteins identified in extracellular vesicles). Functional annotation of proteins was performed using David Bioinformatics Resources 6.8.

Analysis of proteomic data has been carried out in collaboration with Dominik Cysewski (Laboratory of Mass Spectrometry, Institute of Biochemistry and Biophysics).

3.10 *In vivo* mouse model of CML-like disease

3.10.1 Development of CML-like disease

To induce chronic myeloid leukemia-like disease in immunocompetent animals, C3H/HeJ strain of mice was used, as 32D BCR-ABL1+GFP+ cells used for the studies originate from bone marrow cells of this mouse strain. Animals were purchased from the Maria Skłodowska-Curie National Research Institute of Oncology in Warsaw and were further maintained in the Animal Facility at the Faculty of Biology, University of Warsaw, with a 12/12 light-dark photoperiod and *ad libitum* access to food and water. Mice were maintained in microisolator cages. All procedures were performed according to the guidelines of the Poland's National Ethics Committee for Animal Experimentation and approved by the by the First Local Ethics Committee for Animal Experimentation in Warsaw (permission numbers: 567/2018, 835/2019, 1059/2020).

To induce leukemia-like disease, animals 8-10 weeks of age were injected intraperitoneally with 1×10^6 cells, suspended in 300 microliters of sodium chloride. The following cell lines were used for experiments:

- 32D BCR-ABL1+GFP+luc (with expression of luciferase ["luc"], for full body bioluminescent imaging)
- 32D BCR-ABL1+GFP+ (to induce wild-type CML-like disease)
- 32D BCR-ABL1+GFP+ Rab27a^{-/-} (to induce CML-like disease with diminished secretion of EVs)

Control, non-leukemic animals were injected with sodium chloride alone. Mice were sacrificed using carbon dioxide after 2 months of development of leukemia-like disease, followed by isolation of tissues (blood, bone marrow, spleen) and analysis of immune cells and engraftment of GFP+ leukemic cells. The 2-month time-point was chosen based of bioluminescent tracking of leukemic cell growth *in vivo*, as well as based on the observation that animals entered terminal stage of leukemia-like disease following the 2-month mark. The general pipeline of *in vivo* experiments using mice is shown on Figure 3.17.

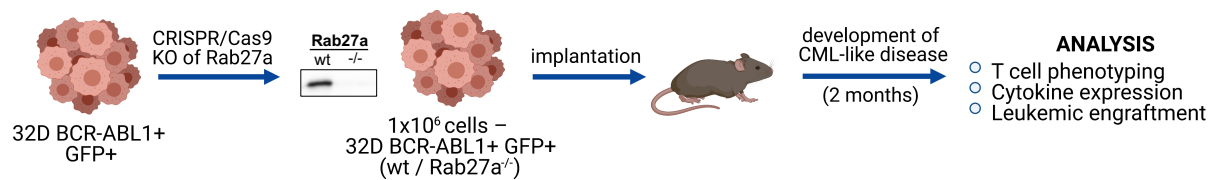


Figure 3.17 Development of leukemia (CML)-like disease in mice. Figure created with BioRender.com.

3.10.2 Bioluminescent imaging of entire animals

To help validate the *in vivo* experimental model, as well as establish a time-point for analysis of animals, experiments were performed using 32D BCR-ABL1+GFP+luc cells, with stable expression of enzyme luciferase. This has enabled bioluminescent imaging of leukemic cells in entire animals, quantification of bioluminescent signal corresponding to amount of leukemic cells and assessment of disease progression, without sacrificing animals. Initially, animals were planned to be analyzed 1, 2 and 4 months following leukemic cell implantation, but following a 2-month mark, animals started dying due to leukemia-like disease.

To generate bioluminescent signal, animals were intraperitoneally injected with luciferase substrate - D-luciferin salt (Synchem, #BC218, resuspended in sodium chloride) - 150 mg/kg of body mass, approximately 200 μ l per animal. Mice were anesthetized with 4% isoflurane, following by transfer to In-Vivo XTreme Imaging System (Bruker) and kept under constant anesthesia. 10 minutes post luciferin injection, mice were scanned for 1 minute and the signal on generated images was eventually quantified as photon/sec/mm². In the end, bioluminescent signal was quantified for the same animals 1 and 2 month following leukemic cell implantation and compared, to assess if CML-like disease has progressed.

Bioluminescent imaging and analysis using XTreme Imaging System has been carried out in collaboration with Paulina Pilanc (Laboratory of Molecular Neurobiology, Nencki Institute).

3.10.3 Isolation of tissues, engraftment analysis

Mice were sacrificed using carbon dioxide, followed by isolation of tissues (blood, bone marrow, spleen) and analysis of immune cells and engraftment of GFP-expressing leukemic cells.

Blood was isolated from the heart onto heparin, to avoid clotting. Blood was first centrifuged at 500 xg, 8 minutes, RT, to separate plasma. Plasma was centrifuged once again to deplete residual blood cells and further stored at -80°C. Red blood cells were further lysed using ACK lysing buffer (Gibco, #A1049201) and cells were washed twice with PBS. Cells were then counted using Muse Cell Analyzer and 5x10⁵ cells were used for engraftment analysis.

Spleen was first homogenized (using manual glass homogenizers) in cold PBS and passed through a 100 μm strainer. Following centrifugation, red blood cells were further lysed using ACK lysing buffer and splenocytes were washed twice with cold PBS. Cells were then counted and 1×10^6 cells were used for engraftment analysis, 5×10^6 cells were used for each T cell and myeloid cell phenotyping and 4×10^6 cells (for two wells) were used for *ex vivo* cell cultures for intracellular cytokine staining.

Bone marrow cells were isolated from femur and tibia of mice, by flushing the bones with cold PBS. Obtained suspensions were passed through a 100 μm strainer. Cells were washed twice with PBS and counted. 1×10^6 cells were used for engraftment analysis, 5×10^6 cells were used for each T cell and myeloid cell phenotyping.

For engraftment analysis, specified number of cells from each tissue were stained for viability by adding 5 μl of 7-AAD viability dye, 15 minutes before flow cytometry analysis. Cells were then acquired on BD LSR Fortessa cytometer to detect GFP-expressing CML cells. GFP+ cells were gated among viable (7-AAD-), single cells. 32D BCR-ABL1+GFP+ cells cultured *in vitro* were used as a positive control of GFP expression and were used to establish gates for flow cytometric analysis. Tissues from control, non-leukemic mice have served as negative controls.

3.10.4 Cell phenotyping

Cell isolated from spleens (5×10^6 per sample) and bone marrow (5×10^6 per sample) were used for two cell phenotyping panels: T cell/Treg phenotyping and phenotyping of myeloid cells. For myeloid cell phenotyping, cells were incubated with 0.2 μg of Fc block (anti CD16/CD32 antibodies, BD, #553142), for 5 minutes, prior to antibody staining. Cells were first stained with a cocktail of surface antibodies (Table 3.3) and viability dye (Table 3.5), followed by intracellular staining (Foxp3 and Helios in T cell/Treg panel, arginase-1 in myeloid panel) using eBioscience Foxp3/Transcription Factor Staining Buffer Set, as described in Chapter 3.5.2. Cells were analyzed using BD LSR Fortessa cytometer. Analysis was performed in FlowJo software and cells were gated as shown in Figure 3.18 (T cell/Treg phenotyping) and Figure 3.19 (myeloid cell phenotyping). Gates for positive populations of cells were set based on FMO (fluorescence minus one) controls.

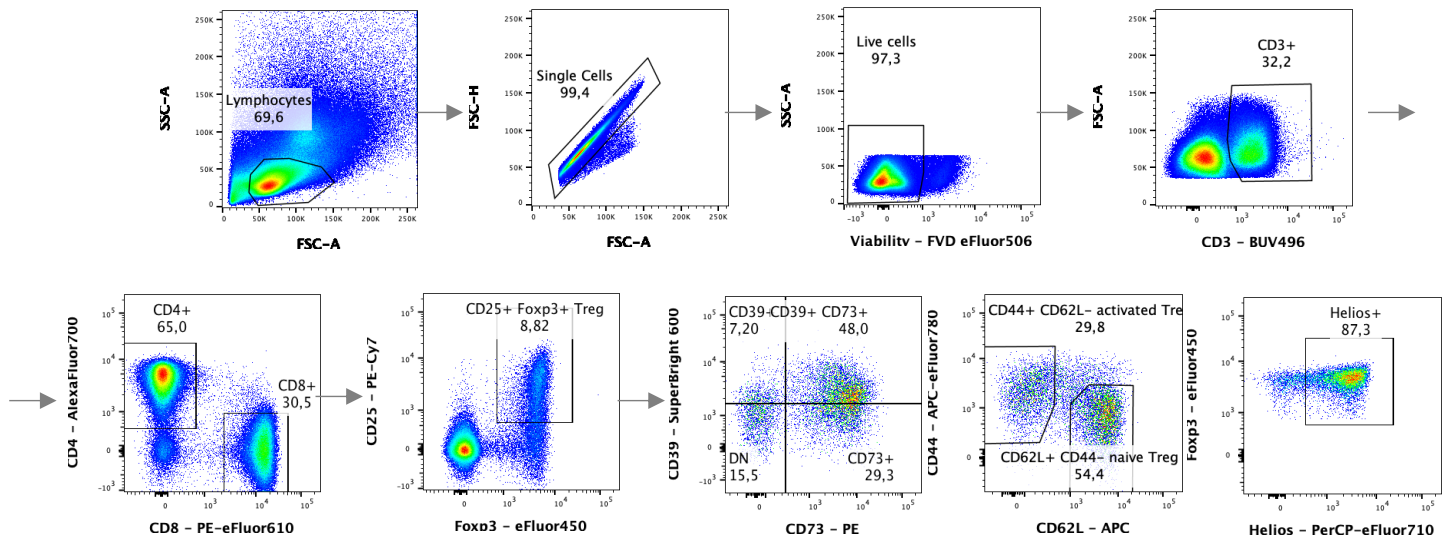


Figure 3.18 Analysis of T cells/Tregs in spleen and bone marrow of mice with CML-like disease. Representative gating strategy to analyze T cells and Tregs, presented on a spleen sample. Treg cells were first identified as viable CD3+CD4+CD8-CD25+Foxp3+ cells. Expression of CD39, CD73, CD44, CD62L and Helios was then analyzed on Tregs.

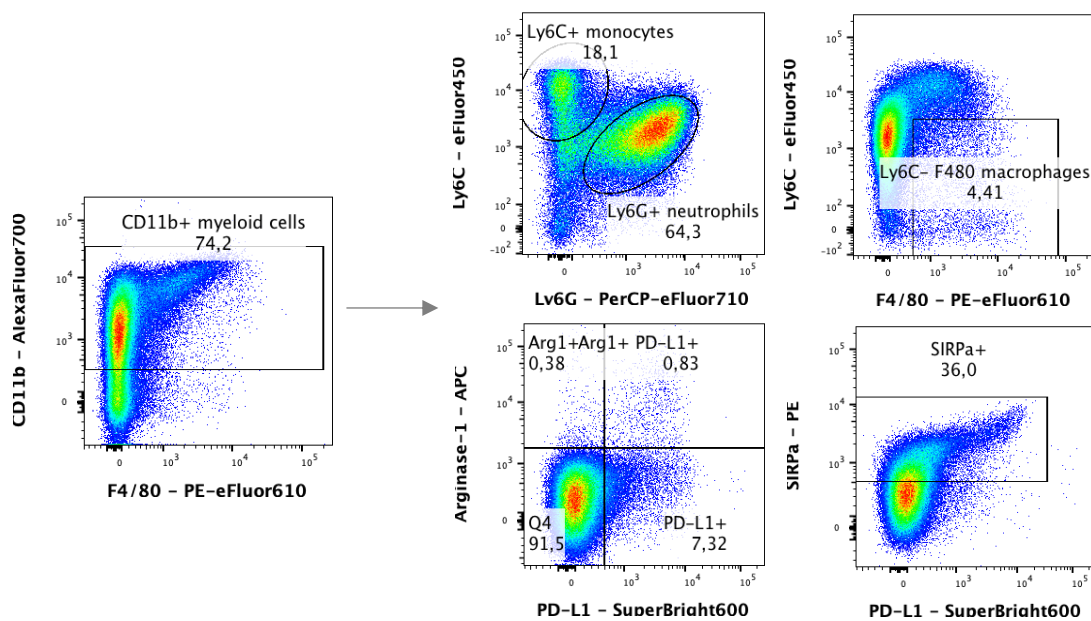


Figure 3.19 Analysis of myeloid cells in spleen and bone marrow of mice with CML-like disease. Representative gating strategy to analyze CD11b+ myeloid cells, presented on a bone marrow sample. Amongst live, single cells (gated as in Figure 3.18), pan-myeloid cells were first gated as CD11b+. Monocytes, neutrophils and tissue-resident macrophages were then identified based on expression of Ly6C, Ly6G and F4/80. Regulatory/suppressive phenotype of CD11b+ myeloid cells was assessed based on expression of arginase-1 (Arg1), PD-L1 and SIRP α .

Phenotyping of myeloid cells has been carried out in collaboration with Salvador Cyranowski (Laboratory of Molecular Neurobiology, Nencki Institute).

3.10.5 *Ex vivo* culture of splenocytes and intracellular cytokine staining

To further assess functionality of immune cells in animals with CML-like disease, expression of suppressive cytokines (interleukin-10 and arginase-1) was analyzed in different subsets of immune cells. As spleen exhibits high abundance of T cells, B cells and myeloid cells (bone marrow has few T cells), splenocytes were used for this experiment. To detect cytokines produced by immune cells, intracellular cytokine staining was performed. To enable that, splenocytes were cultured with stimuli and secretion inhibitors. Splenocytes were seeded in 24-well plates, 2×10^6 cells in 1 ml of media (for culture of T cells, Chapter 3.4.1.3). To stimulate all immune cells, splenocytes were treated with Cell Stimulation Cocktail (eBioscience/Invitrogen, #00-4970-93, containing PMA [final concentration 50 ng/ml] and ionomycin [$1 \mu\text{g/ml}$]). To inhibit secretion, splenocytes were treated with Protein Transport Inhibitor Cocktail (eBioscience/Invitrogen, #00-4980-03, containing brefeldin A and monensin). Cells were cultured for 4 hours, washed and stained with a cocktail of surface antibodies and viability dye (Table 3.3, 3.5), followed by intracellular staining (Foxp3, IL-10 and arginase-1) using eBioscience Foxp3/Transcription Factor Staining Buffer Set, as described in Chapter 3.5.2. Cells were analyzed using BD LSR Fortessa cytometer. Analysis was performed in FlowJo software and cells were gated as shown in Figure 3.20. Samples not treated with PMA/ionomycin were used as negative controls and used to set gates for analysis (Figure 3.20).

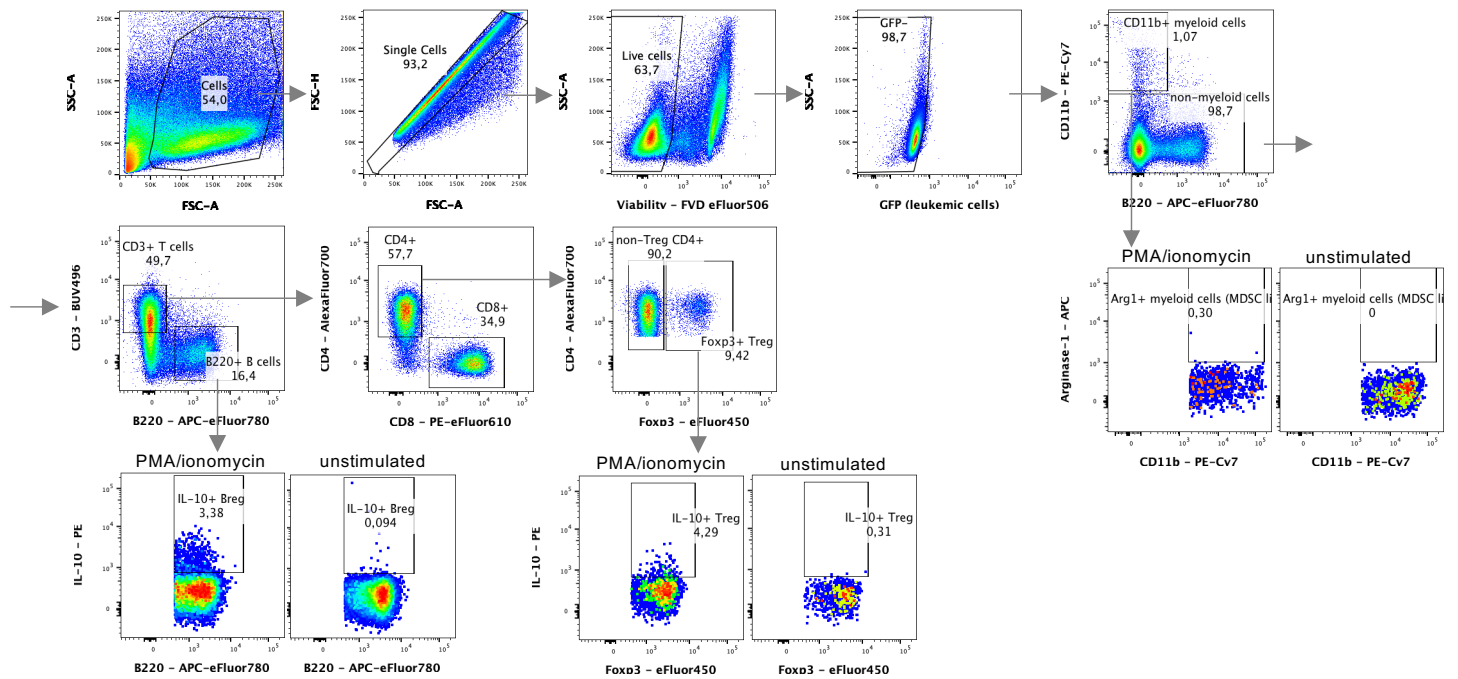


Figure 3.20 Intracellular cytokine staining in splenocytes from animals with CML-like disease. Representative gating strategy to study interleukin-10 (IL-10) and arginase-1 (Arg1) expression in cells. Amongst live, single, GFP-negative cells, myeloid cells were identified as CD11b+, B cells were identified as CD11b-CD3-B220+ and T cells were identified as CD11b-B220-CD3+. Amongst T cells, Tregs were identified as CD4+Foxp3+. IL-10 was analyzed in B220+ B cells to identify regulatory B cells (Breg). IL-10 was also analyzed in Tregs. Arginase-1 was analyzed in CD11b+ myeloid cells to identify myeloid-derived suppressor cell-like (MDSC-like) cells.

3.11 Statistics

Experimental data were visualized and statistics calculated using GraphPad Prism v9 software. Statistical tests used for each experiment are listed in the figure legends (unless statistics was not performed), together with number of experiments (indicating biological replicates) and total number of technical replicates (n). In case of data normalization, data from each experiment were normalized to average value of CTRL samples of that experiment, which is indicated in appropriate figure legends as well. If not specified otherwise, statistics were performed in comparison to control (CTRL) samples. Statistical significance ($p < 0.05$) is marked on graphs with asterisks (* $p < 0.05$, ** $p < 0.01$, *** $p < 0.001$, **** $p < 0.0001$).

4 RESULTS

4.1 Chronic myeloid leukemia-derived extracellular vesicles upregulate suppressive activity and Foxp3 level in mouse thymic regulatory T cells

In the first part of performed research, the aim was to assess whether chronic myeloid leukemia derived extracellular vesicles (CML EVs) have any influence on the biology of regulatory T cells, such as suppressive activity. To evaluate this initial question in a stable experimental setting, mouse *ex vivo* models were used for experiments. The source of EVs were mouse progenitor 32D cells and their CML-like counterparts - 32D cells with stable expression of BCR-ABL1 oncoprotein (32D BCR-ABL1+). 32D BCR-ABL1+ cells were established previously²³⁶ and constitute a model to study effects of solely BCR-ABL1 expression in progenitor cells, without molecular and phenotypic changes that might have occurred in leukemic patients (from whom human CML cell lines were established). Moreover, a non-malignant control cell line (32D) serves as a perfect source of non-leukemic, control EVs for experiments. Such perfectly-matched control does not exist for human leukemic cell lines. For mouse *ex vivo* studies, regulatory T cells from the thymus were used as a source of self-tolerant, thymic Tregs (tTregs), which are of high relevance in CML.

4.1.1 Characterization of 32D and 32D BCR-ABL1+ extracellular vesicles

Firstly, extracellular vesicles, isolated by differential ultracentrifugation (as described in Chapter 3.3.1) from conditioned medium of 32D and 32D BCR-ABL1+ cells, were characterized and validated, according to the guidelines of the International Society for Extracellular Vesicles (ISEV) and the EV-TRACK consortium^{163,167}. Wide-field (60kx magnification) and close-up (150kx magnification) transmission electron microscopy images demonstrated that isolated samples contained small EVs that had typical cup-shaped morphology and were approximately 100 nm in diameter (Figure 4.1A). Analysis of protein composition of isolated EVs has identified proteins typically present in EVs - CD81, Alix, Tsg101, flotilin-1, Hsp70 and β -actin (Figure 4.1B). Compared to whole cell protein lysates (same amount of protein was loaded on the gel), especially Alix, Tsg101 and flotilin-1 were enriched in the EVs samples. Alix and Tsg101 are proteins associated with multivesicular bodies, thus EVs used in experiments are most probably EVs of endocytic origin (exosomes). Importantly, protein analysis showed absence of ER protein Grp78 and mitochondrial protein TOM20 which proves that EVs samples have not been contaminated with cellular organelles (Figure 4.1B). The size of isolated EVs was measured using nanoparticle tracking analysis (NTA) which revealed that they were between 100-110 nm in diameter. NTA did not reveal any differences in size, as well as amount of EVs released by non-malignant 32D and leukemic 32D BCR-ABL1+ cells (Figure 4.1C). Size assessment by NTA confirmed that analyzed EVs were small EVs/exosomes. Overall, initial characterization has confirmed that isolated samples were

indeed extracellular vesicles, which sized approximately 100 nm in diameter and were mostly of endocytic origin - they can thus be considered small EVs/exosomes.

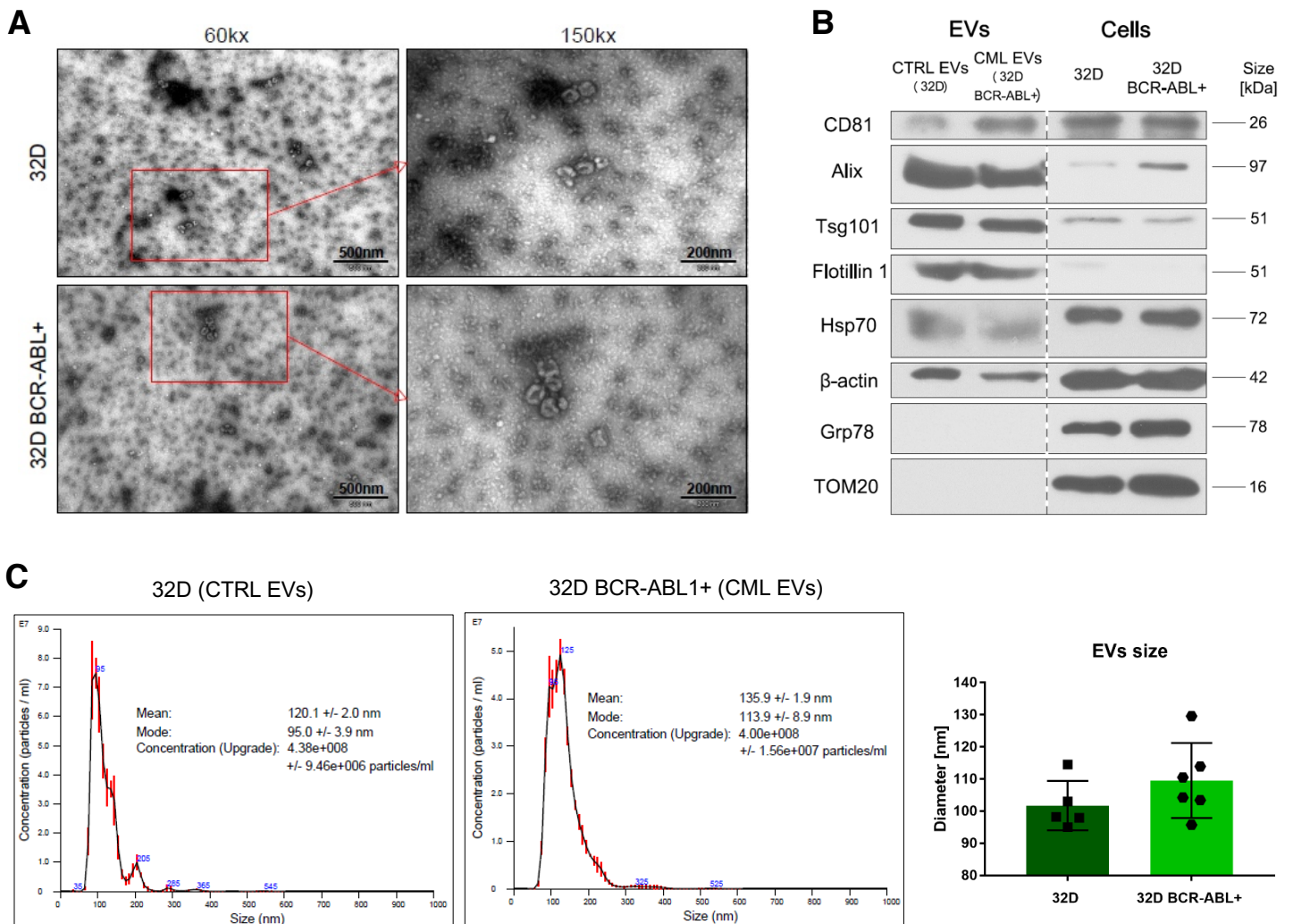


Figure 4.1 Characterization of extracellular vesicles released by mouse cell lines 32D and 32D BCR-ABL1+. (A) Transmission electron microscopy imaging of EVs - wide-field (magnification 60kx) and close-up (150kx) images are shown (representative of 2 experiments). (B) Western blot analysis of proteins enriched (CD81, Alix, Tsg101, flotilin-1), present (Hsp70, β-actin) and absent (Grp78, TOM20) in EVs (representative of 1-2 western blots for each protein). Equal amount of cellular and EVs' protein was loaded on the gel. Dashed line marks that all samples were run on the same gel. (C) Nanoparticle tracking analysis - quantification and size measurement of EVs. Size measurements from 5-6 replicates have been collected and shown on a graph bar with single data points (modified figures from Swatler *et al.*, 2020, Eur J Immunol²⁴²).

4.1.2 Mouse thymocytes take up/bind CML EVs

To provide a proof-of-concept that leukemic EVs could influence murine T cells and Treg cells, isolated CML EVs (released by 32D BCR-ABL1+ CML-like cells) were labelled with a CFSE dye, which becomes fluorescent following cleavage by esterases, which are also present in EVs. As in functional studies using mouse *ex vivo* models the interest was focused on thymic Tregs (tTregs),

analysis of fluorescent EVs uptake/binding was performed on thymic T cells (thymocytes). Firstly, thymocytes was treated with different doses and amounts of CFSE-labelled EVs, followed by analysis of entire thymocytes population by flow cytometry. As already mentioned, flow cytometric approach allows quantitative detection of EVs' CFSE signal, though it does not distinguish between "uptake" (inside the cell) or "binding" (to the plasma membrane) of EVs. Indeed, murine thymocytes took up/bound fluorescently labelled EVs, in a dose- and time-dependent manner (Figure 4.2A-B). EVs' fluorescent signal has decreased over time, meaning that following relatively quick uptake, vesicles were gradually metabolized (or detached) by T cells (Figure 4.2B). To observe whether there is a difference in leukemic EVs uptake/binding by different subsets of T cells in the thymus (double negative [DN] CD4-CD8-, double positive [DP] CD4+CD8+, single positive [SP] CD4+CD8- or CD4-CD8+ and CD4+CD25^{hi} Tregs), the experiment was repeated and different subsets of T cells were stained for flow cytometric analysis. Importantly, CD4+CD25^{hi} Tregs potently took up/bound CML EVs, in a dose-dependent manner. Interestingly, double positive CD4+CD8+ thymocytes took up/bound EVs less efficiently (Figure 4.2C). Collectively, mouse thymic Treg cells can interact with CML-derived extracellular vesicles, which provides a proof-of-concept that this interaction may affect Tregs in myeloid neoplasms.

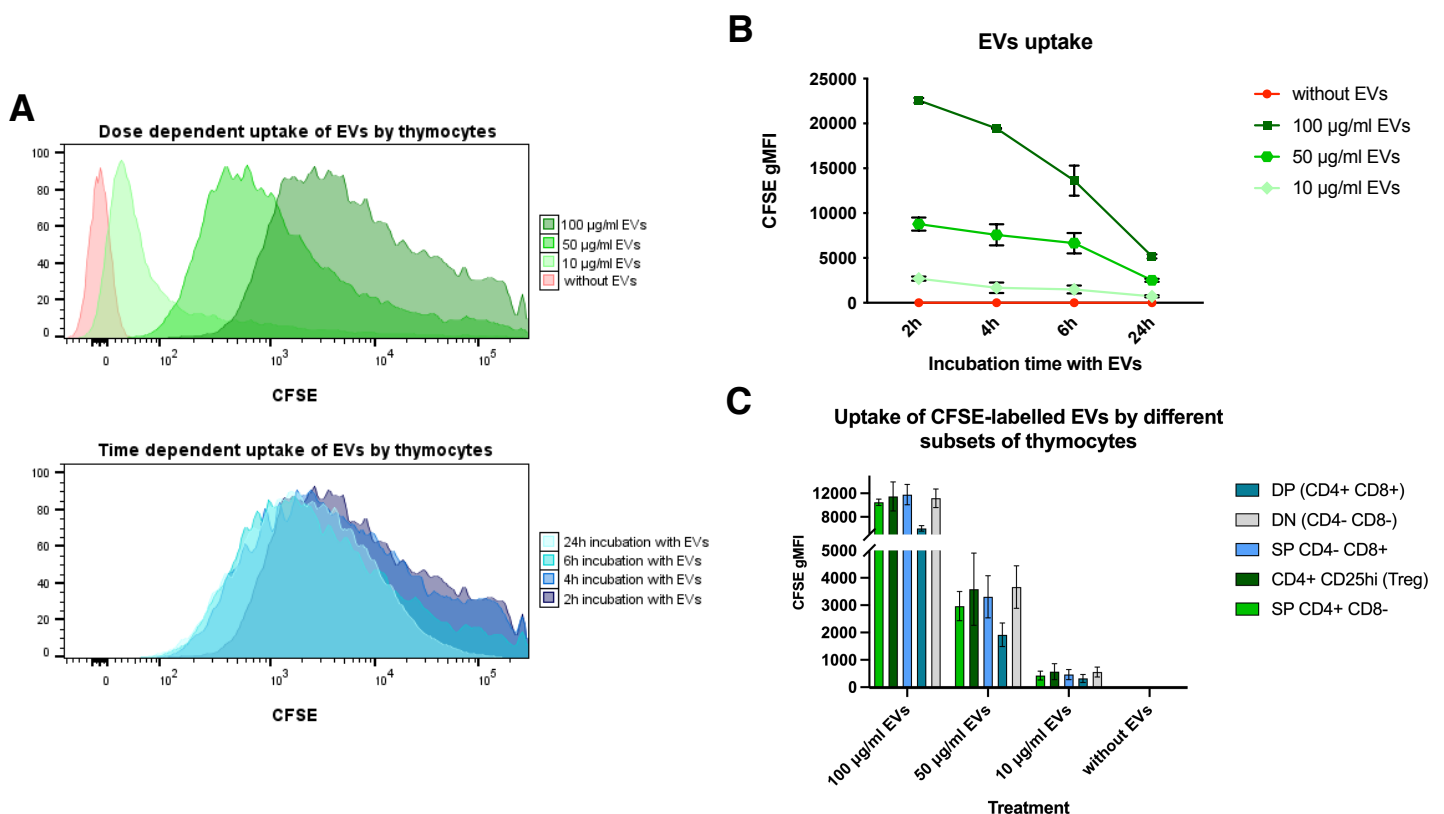


Figure 4.2 Mouse thymocytes, including tTregs, interact with fluorescently labelled CML EVs. (A) Representative histograms of CFSE fluorescence showing dose- (upper panel) and time-dependent (lower panel) uptake of CML EVs by thymocytes. **(B)** Dose- and time-dependent uptake of CML EVs by thymocytes. For (A) and (B), data are from 2 experiments, 1-2 replicates each. **(C)** Uptake of CFSE-labelled CML EVs by different subsets of thymocytes, following 2 hours of incubation with EVs. Data are from 2 experiments (n=4-5). Gating strategy is shown in Figure 3.3 (modified figures from Swatler *et al.*, 2020, Eur J Immunol²⁴²).

4.1.3 CML EVs amplify suppressive activity of mouse tTregs

As mentioned above, regulatory T cells from the thymus were used, as a source of self-tolerant thymic Tregs (tTregs), which are of high relevance in CML. CML cells have a relatively low mutational load and many leukemia associated antigens are self-antigens (PR3, WT1, PRAME), thus self-tolerant tTregs are of high importance^{25,251}. Of course, CML neoantigens are also present (such as BCR-ABL-derived peptides), though only 4% of antigens identified in primary CML samples are truly CML exclusive²⁵². To additionally verify this, expression of Helios protein - a marker of thymic, self-tolerant tTregs, was analyzed in Tregs in an *in vivo* mouse model of CML-like disease developed in this thesis (described in detail in Chapter 4.3/4.3.1). Tregs were analyzed in main tissues of leukemic development - spleen and bone marrow. In both spleen and bone marrow of leukemic animals - Helios+ tTregs were more abundant than in control, non-leukemic animals (Figure 4.3A). This further demonstrates high relevance of thymic Tregs (expressing Helios) in CML and strengthens rationale to use tTregs for *ex vivo* experiments studying influence of CML EVs on Tregs. For *ex vivo* assays with EVs, tTregs were obtained by cell sorting from murine thymus of either C57BL/6 mice (for suppression assays) or Foxp3-GFP [B6.Cg-Foxp3^{tm2Tch}] transgenic mice (for analysis of Foxp3 level). True tTreg identity of cells sorted from the thymus was confirmed by exclusive expression of Helios (Figure 4.3B).

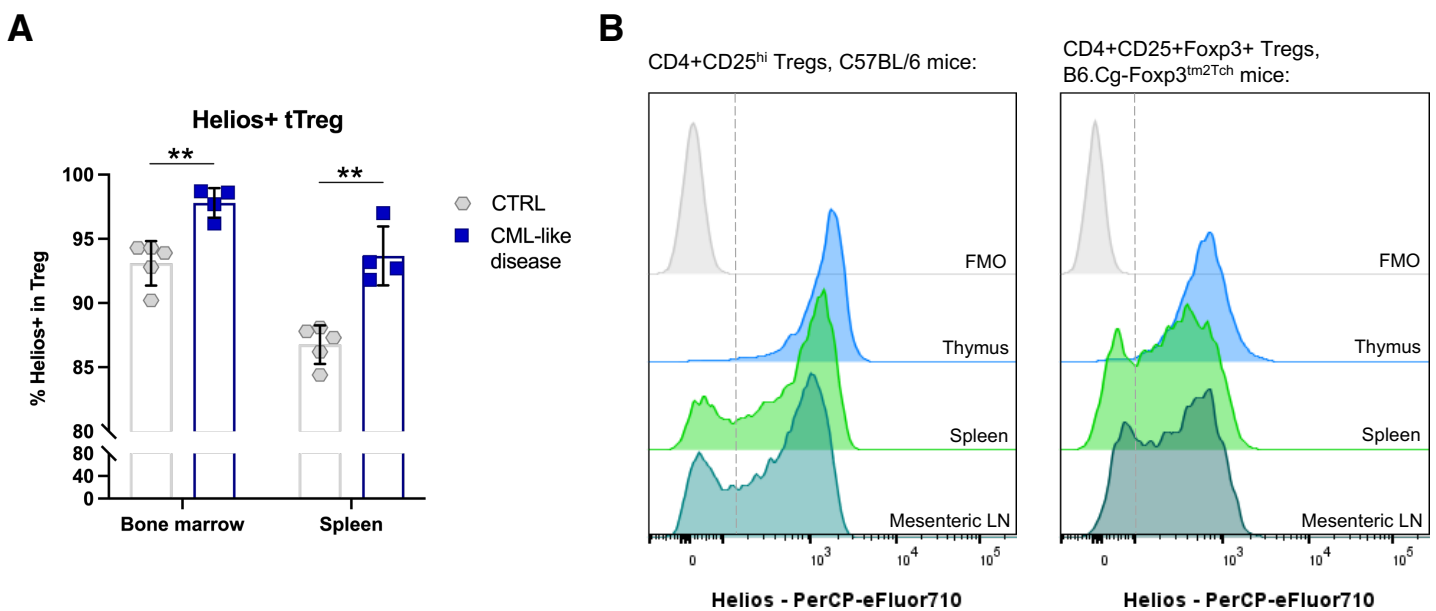


Figure 4.3 Analysis of Helios expression in Tregs. (A) Analysis of Helios expression in Tregs in spleen and bone marrow of healthy mice and mice with CML-like disease. Data are from 2 experiments (n=4-5). Unpaired t-test with Welch's correction, single data points and mean \pm SD are shown. Gating strategy is shown in Figure 3.18. **(B)** Analysis of Helios expression in Tregs of healthy animals (two strains - C57BL/6 and Foxp3-GFP [B6.Cg-Foxp3^{tm2Tch}]), isolated from thymus, spleen and mesenteric lymph nodes (MLN). Treg from the thymus are exclusively tTregs, whereas Tregs from spleen and MLN are a mixture of tTregs and Helios-negative pTregs (data are representative of 2 experiments, n=2).

To study influence of CML EVs on mouse tTregs functionality, EVs from non-malignant 32D and CML-like 32D BCR-ABL1+ cells were isolated by differential ultracentrifugation and used to treat tTregs. To study tTregs' suppressive function, a well-established *in vitro* suppression assay was used²⁴⁷. Due to technical limitations of work with low numbers of murine tTregs and to study effect of EVs, the suppression assay was modified, as described in Materials and Methods (Chapter 3.6.1). In brief, tTregs were first preincubated with IL-2 (interleukin-2) and EVs. Next, CFSE-labelled responder T cells (Tresp, lymphocytes from lymph nodes) were added to tTregs and cultures were stimulated with anti-CD3/CD28 antibodies, to induce proliferation of Tresp (tracked by analysis of CFSE dilution). Suppressive activity of Tregs was measured by analysis of inhibition of proliferation of Tresp (based on CFSE read-out), separately towards CD4+ and CD8+ responder cells (for clarity of the followed experimental pipeline, critical steps of the *in vitro* suppression assay used are presented on Figure 4.4, detailed description in Materials and Methods Chapter 3.6.1).

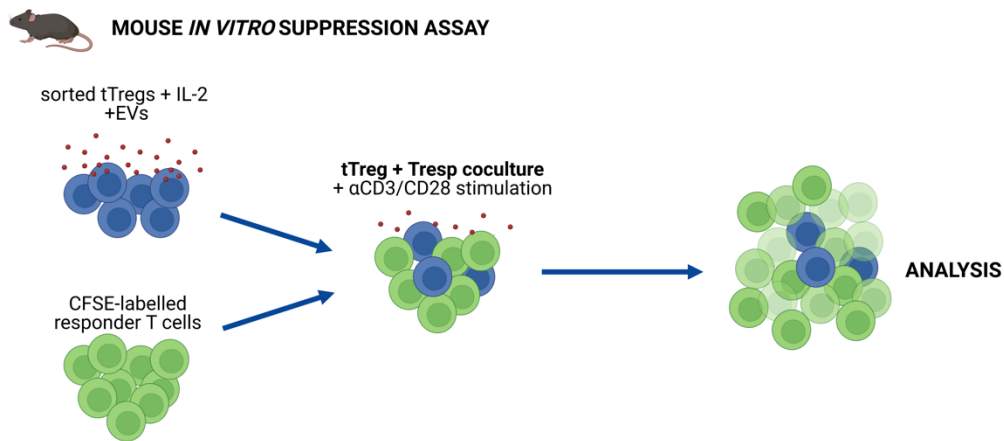


Figure 4.4 Experimental pipeline of mouse *in vitro* suppression assay used in the thesis (based on the schematic shown in Figure 3.8). Figure created with BioRender.com.

Analysis of responder T cells proliferation has revealed that CML EVs-treated tTregs had amplified suppressive activity towards CD8+ T cells. This was observed by 2 separate parameters - amplified percentage of inhibition by Tregs, as well as decreased expansion index of CD8+ Tresp (Figure 4.5A). The effect can also be clearly observed on representative proliferation profiles (histograms) of CD8+ Tresp. In samples with tTregs+CTRL EVs (compared to CML EVs), peaks with low CFSE signal (left part of the axis) are higher, which corresponds to increased number of proliferating responder cells and, therefore, lower suppressive activity of Tregs (Figure 4.5B). Interestingly, the effect did not seem to depend on the amount of EVs used to treat the cells. Surprisingly, in the same suppression assay cultures, there was no influence of CML EVs on suppressive activity of tTregs towards CD4+ Tresp (Figure 4.5C).

Altogether, performed studies demonstrated increased suppressive potential of thymic regulatory T cells, following treatment with chronic myeloid leukemia derived EVs.

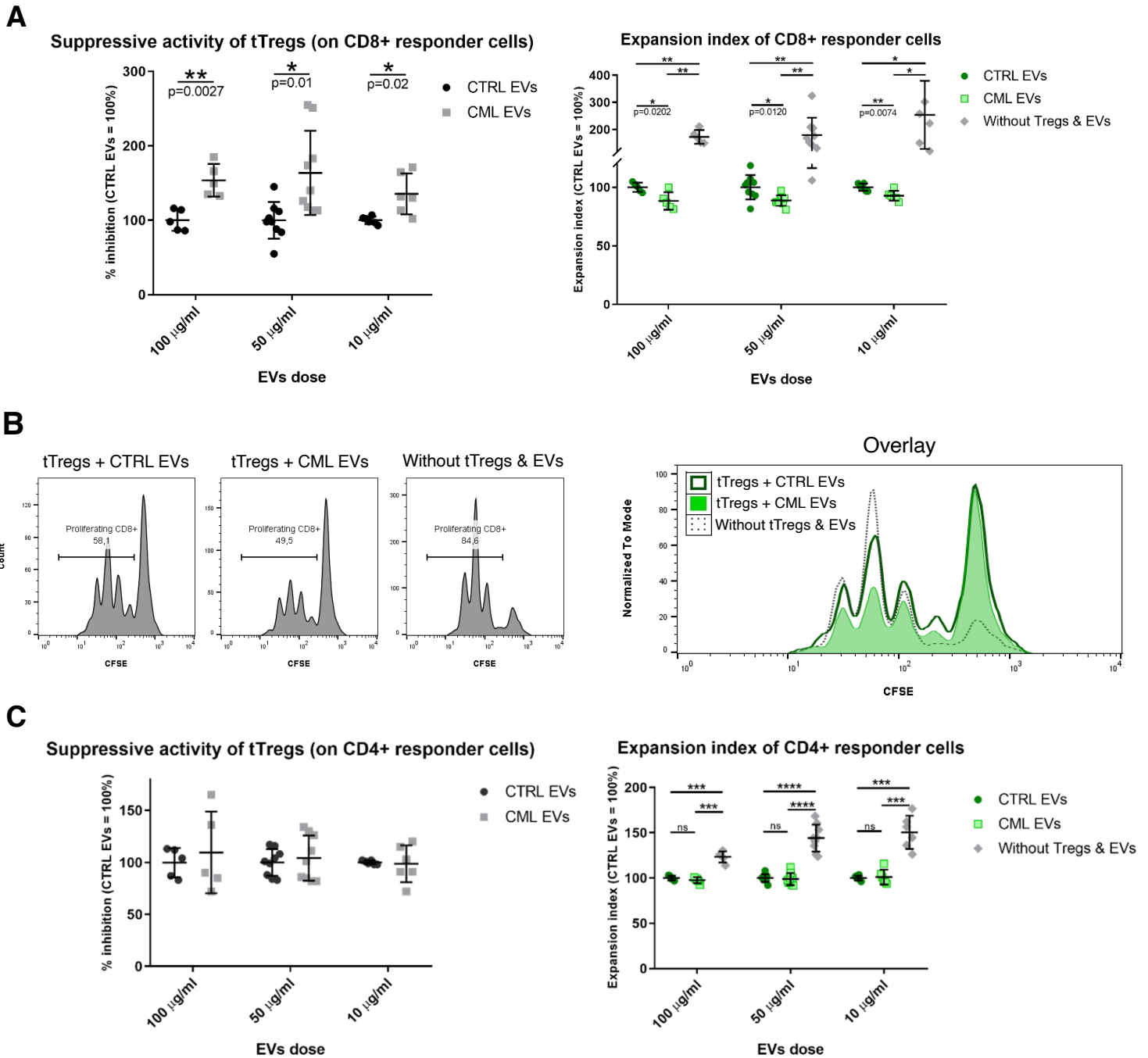


Figure 4.5 tTregs treated with CML EVs more potently suppress CD8+ T cells, but not CD4+ T cells. (A) Suppressive activity (% of inhibition) towards CD8+ Tresp (left) and expansion index of CD8+ Tresp (right) in *in vitro* suppression assay cultures with tTregs treated with EVs. Decreased expansion index corresponds to increased % of inhibition. (B) Representative histograms (separately for each condition on the left and overlay on the right) for CD8+ Tresp proliferation in suppression assay cultures with tTregs treated with EVs (50 µg/ml). (C) Suppressive activity (% of inhibition) towards CD4+ Tresp (left) and expansion index of CD4+ Tresp (right) in *in vitro* suppression assay cultures with tTregs treated with EVs. Decreased expansion index corresponds to increased % of inhibition. Data are from 3 experiments (n=6-9). Unpaired t-test with Welch's correction, single data points with mean ± SD are presented, data were normalized to average value of CTRL EVs in each experiment. Gating strategy is shown in Figure 3.9 (figures from Swatler *et al.*, 2020, *Eur J Immunol*²⁴²).

4.1.4 CML EVs do not inhibit proliferation of effector CD8+ and CD4+ T cells

Although the suppression assay cultures in Chapter 4.1.3 were modified to study effect of EVs on Tregs rather than Tresp (Figure 4.4), such bystander effect could not be entirely excluded. Therefore, control experiments were performed - without tTregs, only with Tresp and CTRL/CML-derived EVs. Proliferation of Tresp was measured as both expansion index and total percentage of dividing cells (% proliferating cells), again based on CFSE dilution analysis. CML-derived EVs upregulated proliferation of both CD4+ and CD8+ T cells in cultures (Figure 4.6A-B). In this experiment, effect of CML-derived EVs on Tresp proliferation was dose dependent and statistically significant differences were not observed when lowest amount of EVs (10 µg/ml) was used. Importantly, CML EVs have promoted proliferation of responder T cells in these experiments, contrary to suppression assay cultures described above. This means the diminished proliferation of Tresp in suppression assay cultures is due to upregulated suppressive activity of tTregs, following treatment with CML EVs. Moreover, based on analysis of % of proliferating cells, it seems like CML-derived EVs exert stronger effect on CD4+ Tresp (Figure 4.6A).

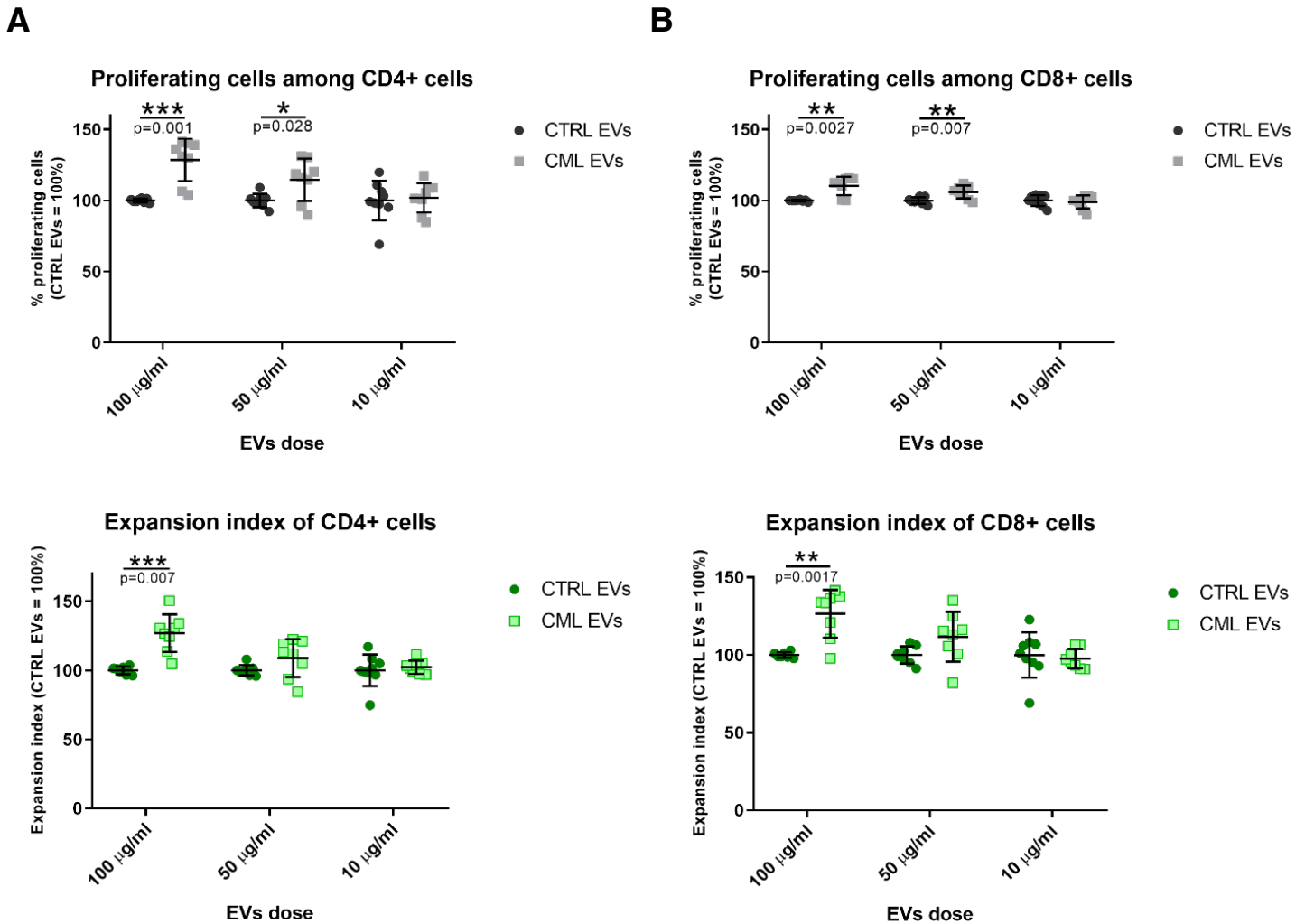


Figure 4.6 Treatment with CML EVs amplifies proliferation of effector CD8+ and CD4+ T cells (in cultures without tTregs). (A) Percentage of proliferating cells (upper panel) and expansion index (bottom panel) of CD4+ T cells, following treatment with EVs. (B) Percentage of proliferating cells (upper panel) and expansion index (bottom panel) of CD8+ T cells, following treatment with EVs. Data are from 3 experiments (n=6-9). Unpaired t-test with Welch's correction, single data points with mean \pm SD are presented, data were normalized to average value of CTRL EVs in each experiment. Gating strategy is shown in Figure 3.9 (figures from Swatler *et al.*, 2020, Eur J Immunol²⁴²).

4.1.5 CML EVs increase Foxp3 expression in mouse tTregs

Data presented above have demonstrated that leukemic EVs amplify suppressive activity of mouse tTregs in an *in vitro* suppression assay. Finally, only tTregs alone were treated with control and CML-derived extracellular vesicles. This experiment aimed to analyze expression of Foxp3 transcription factor in tTregs, to obtain preliminary data about molecular mechanisms, by which CML EVs modulate Tregs. As mentioned in the Introduction to this thesis, Tregs can exert their suppressive effect via several mechanisms, which in majority are either directly or indirectly regulated by Foxp3 transcription factor, thus analysis of Foxp3 level is crucial to understand molecular mechanisms of Treg-CML EVs interaction. To precisely analyze Foxp3 amount in tTregs

treated with EVs, Treg cells were sorted from Foxp3-GFP [B6.Cg-Foxp3^{tm2Tch}] mice, which express GFP under the *Foxp3* gene promoter^{253,254}. Therefore, GFP signal analyzed quantitatively by flow cytometry and presented on histograms (as in Figure 4.7A) corresponds to Foxp3 protein level. Upon culture with CML EVs, Foxp3 level in tTregs has significantly increased, as compared to tTregs treated with control, 32D-derived EVs and tTregs not treated with any EVs (Figure 4.7A-B). Slight difference was visible 48 hours after beginning of *ex vivo* culture and was significantly more pronounced at 72 hours (Figure 4.7B). As tTregs were cultured with IL-2 and anti-CD3/CD28 stimulation, Foxp3 level has in general gradually increased with culture time. Therefore, CML-derived EVs regulate tTregs by controlling central transcription factor of these cells - Foxp3, which most likely contributes to expression of suppressive molecules and increased suppressive activity of these cells, as evidenced above.

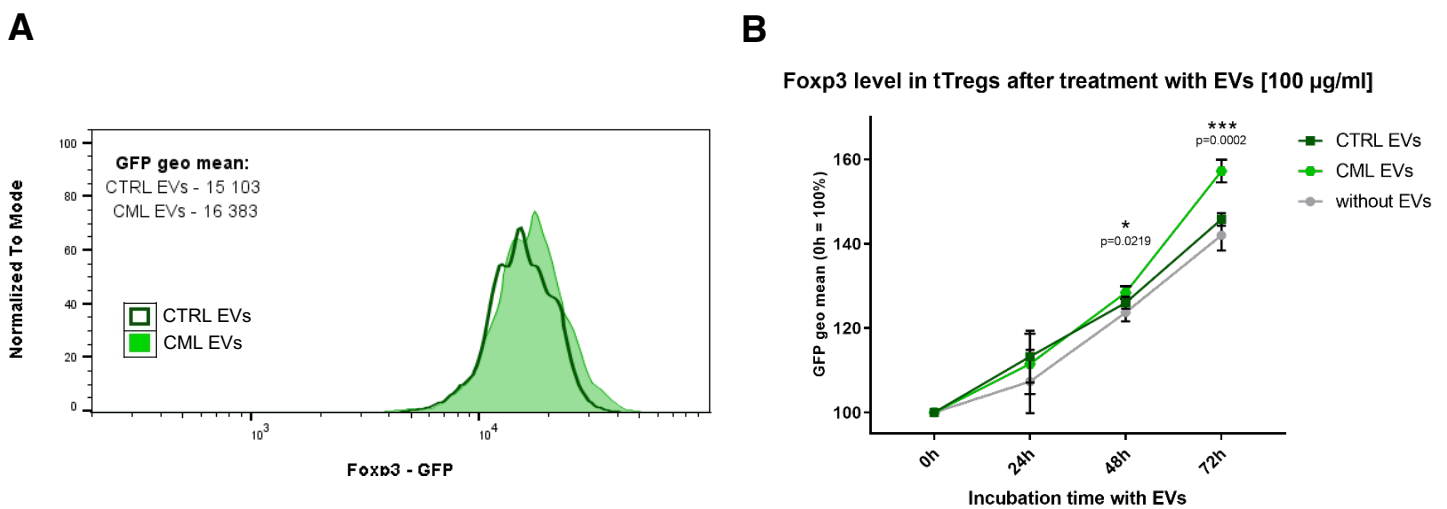


Figure 4.7 Treatment with CML EVs upregulates Foxp3 level in tTregs. (A) Representative histograms of Foxp3-GFP level in tTregs treated with either CTRL or CML EVs (100 µg/ml, 72-hour time point). (B) Foxp3 level (pronounced as GFP geometric mean) in tTregs - either non treated or treated with CTRL/CML EVs, at different time points. Data are from 3 experiments (n=3-6). Unpaired t-test with Welch's correction, mean ± SD is shown, data was normalized to Foxp3 level at the beginning (0h) of each experiment. Statistical significance shown is for comparison of CTRL and CML EVs. Gating strategy is shown in Figure 3.10 (figures from Swatler *et al.*, 2020, Eur J Immunol²⁴²).

Altogether, data from *ex vivo* studies using murine thymic regulatory T cells demonstrated that leukemic (chronic myeloid leukemia-derived) extracellular vesicles can amplify suppressive function of Tregs, as well as increase Foxp3 expression. This data have provided first rationale and proof that leukemic EVs-Treg interaction may be relevant to significant polarization and phenotypic changes of Tregs in CML, as well as may support disease progression. Following that, we have decided to pursue further studies using human *ex vivo* settings, as well as *in vivo* model of CML.

4.2 Chronic and acute myeloid leukemia extracellular vesicles, containing 4-1BBL protein, promote human immunosuppressive regulatory T cells

As mentioned in the previous chapter, mouse models of Tregs and BCR-ABL1-expressing progenitor cells have several advantages. On the other hand, use of human immune and leukemic cells has its own significant benefits, despite some drawbacks. The main drawback of human leukemic cell lines is lack of healthy counterparts, as well as possible variability between cell lines. However, initial experiments on mouse BCR-ABL1-expressing cells (Chapter 4.1) have clearly shown that EVs derived from control, normal myeloid progenitors do not upregulate Foxp3 or suppressive function of Tregs (Figure 4.5, 4.7). The main (and obvious) advantage of experimental settings based on human cells is that they deliver data closer to human physiology. Also, human immune cells isolated from peripheral blood are much more viable *ex vivo* than mouse counterparts. Moreover, use of human peripheral blood/buffy coats as a source of cells allows to obtain higher cell numbers. These two factors enable more robust experiments and analyses by techniques that would be limited by low amount of viable mouse cells. Therefore, further *ex vivo* studies on direct Treg-leukemic EVs interactions have been performed using human cells. For these studies, regulatory T cells (and other T cell subsets) sorted from buffy coats (peripheral blood) of healthy donors were used. As a source of leukemic EVs, two well established cell lines were used: chronic myeloid leukemia cell line K562 and acute myeloid leukemia cell line MOLM-14. Finally, primary EVs were isolated from plasma of chronic and acute myeloid leukemia patients, to validate most crucial data obtained in experiments with EVs from cell lines.

4.2.1 Characterization of K562 and MOLM-14 extracellular vesicles

Similarly to mouse cell lines, extracellular vesicles isolated (by differential ultracentrifugation) from conditioned medium of K562 (CML) and MOLM-14 (AML) cells were first characterized and validated, according to guidelines of ISEV and the EV-TRACK consortium^{163,167}. As the differential ultracentrifugation protocol was identical for both cell lines, western blot analysis of marker proteins was only performed for K562 cells. Transmission electron microscopy demonstrated presence of numerous cup-shaped vesicles, which were approximately 100 nm in diameter (Figure 4.8A). Western blot analysis of proteins in obtained preparations has shown high abundance of EV-enriched proteins, such as CD63, CD81, Tsg101 and Alix (Figure 4.8B). CD63 protein signal on western blot has demonstrated a classical "smear", due to presence of multiple glycosylated forms of CD63 in EVs. Obtained EVs preparations did not contain GM130 protein, which is specific for the Golgi apparatus which demonstrates purity and lack of contamination with cellular organelles (Figure 4.8B). Moreover, EVs samples did not contain lipoprotein APOA1 (Figure 4.8B). Presence of this protein would suggest contamination with serum components, which is therefore not the case. Analysis of serum specific components (such as APOA1) has been added as a new

requirement in MISEV 2018 guidelines, to control purity of EVs isolated from cell line conditioned medium. As cell line culture typically requires addition of bovine/calf serum (which contains large amounts of bovine EVs) to the culture media, this constitutes a significant factor that needs to be accounted for, when isolating EVs for functional or molecular analyses. As mentioned in the Materials and Methods Chapter 3.3.1, for experiments in this thesis FBS was depleted of bovine EVs by ultracentrifugation. Finally, quantitative analysis of K562- and MOLM-14-derived EVs was performed using nanoparticle tracking analysis (NTA). Both CML and AML EVs were approximately 90-100 nm in size. Interestingly, MOLM-14 AML cells released over 50% more EVs than K562 CML cells (Figure 4.8C). Altogether, EVs isolated from conditioned medium of human leukemic cell lines, K562 (CML EVs) and MOLM-14 (AML EVs), can be described as small EVs (due to their size) and are probably of endocytic origin, especially based on high abundance of Tsg101 and Alix in the obtained preparations. These EVs could thus be considered exosomes.

4.2.2 Human T cells take up/bind leukemic EVs

As in the mouse *ex vivo* studies described above (Chapter 4.1.2), I set out to perform a proof-of-concept experiment that human T cells are capable of interaction with leukemic extracellular vesicles, either by active uptake (internalization) or binding to the plasma membrane. Again, EVs released by chronic myeloid leukemia K562 cells were labelled with a fluorescent dye CFSE. However, for these experiments I have used a more advanced experimental set up, that enabled isolation of even higher purity EVs and more efficient elimination of residual CFSE in the EVs preparation. K562-derived EVs were first isolated by differential ultracentrifugation and were labelled with CFSE, as described in Material and Methods Chapters 3.3.1-2, 3.3.7. CFSE-labelled EVs were then loaded on a sequential gradient of Optiprep™ and further purified by density gradient centrifugation. This has enabled isolation of fractions of different density which contained EVs of different density. As exhibited by western blot analysis of EV marker CD63, fraction 7 was most enriched in EVs, whereas fraction 8 and 9 also contained EVs, though in lesser amount (Figure 4.9A). To assess if uptake/binding of EVs is dose dependent, non-adherent PBMCs were treated with either EVs from fraction 7 or EVs from pooled fractions 8+9. Uptake/binding was analyzed at either 2 hours or 24 hours after adding EVs, by flow cytometric analysis, which enabled quantification of CFSE (EVs) signal. CFSE signal was detected in several subsets of CD3+ T cells, distinguished based on expression of CD4, CD8, CD25, CD127 and CD39. Most importantly (at least for the scope of this thesis), CD4+CD25^{hi}CD127^{lo} Tregs took up/bound leukemic EVs, which occurred in a dose-dependent manner, as the strongest CFSE fluorescent signal was detected in culture with Fraction 7 obtained from density gradient centrifugation of EVs (Figure 4.9B). CD39+ subset of Tregs, which represent highly suppressive effector Tregs, did not seem to take up/bind more EVs than the whole Treg population (Figure 4.9C-D).

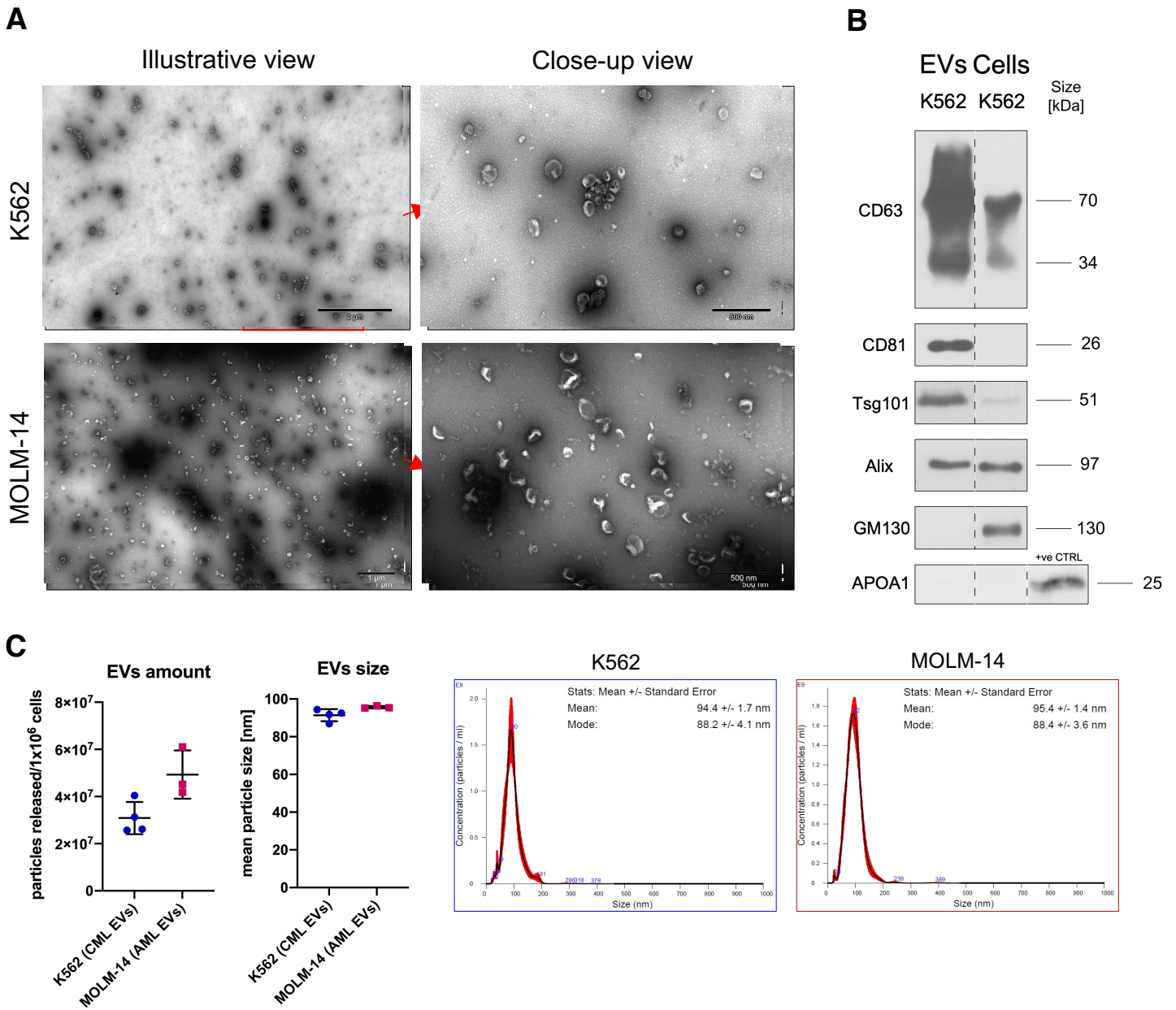


Figure 4.8 Characterization of extracellular vesicles released by human cell lines K562 and MOLM-14. (A) Transmission electron microscopy imaging of EVs - wide-field (magnification 20kx) and close-up (60kx) images are shown (representative of 2 experiments). **(B)** Western blot analysis of proteins enriched (CD63, CD81, Tsg101, Alix) and absent (GM130, APOA1) in EVs (representative of 1-3 western blots for each protein). Equal amount of cellular and EVs' protein was loaded on the gel. Dashed line marks that all samples were run on the same gel. Positive control for APOA1 was lysate from fractions 10+11 from size exclusion chromatography (described in Material and Methods Chapter 3.3.3, Figure 4.29A) that are enriched in lipoproteins. **(C)** Nanoparticle tracking analysis quantification and size measurement of K562- and MOLM-14-derived EVs. Size measurements from 3-4 replicates have been collected and shown on a graph bar with single data points (left). Representative plots from NTA are shown on the right.

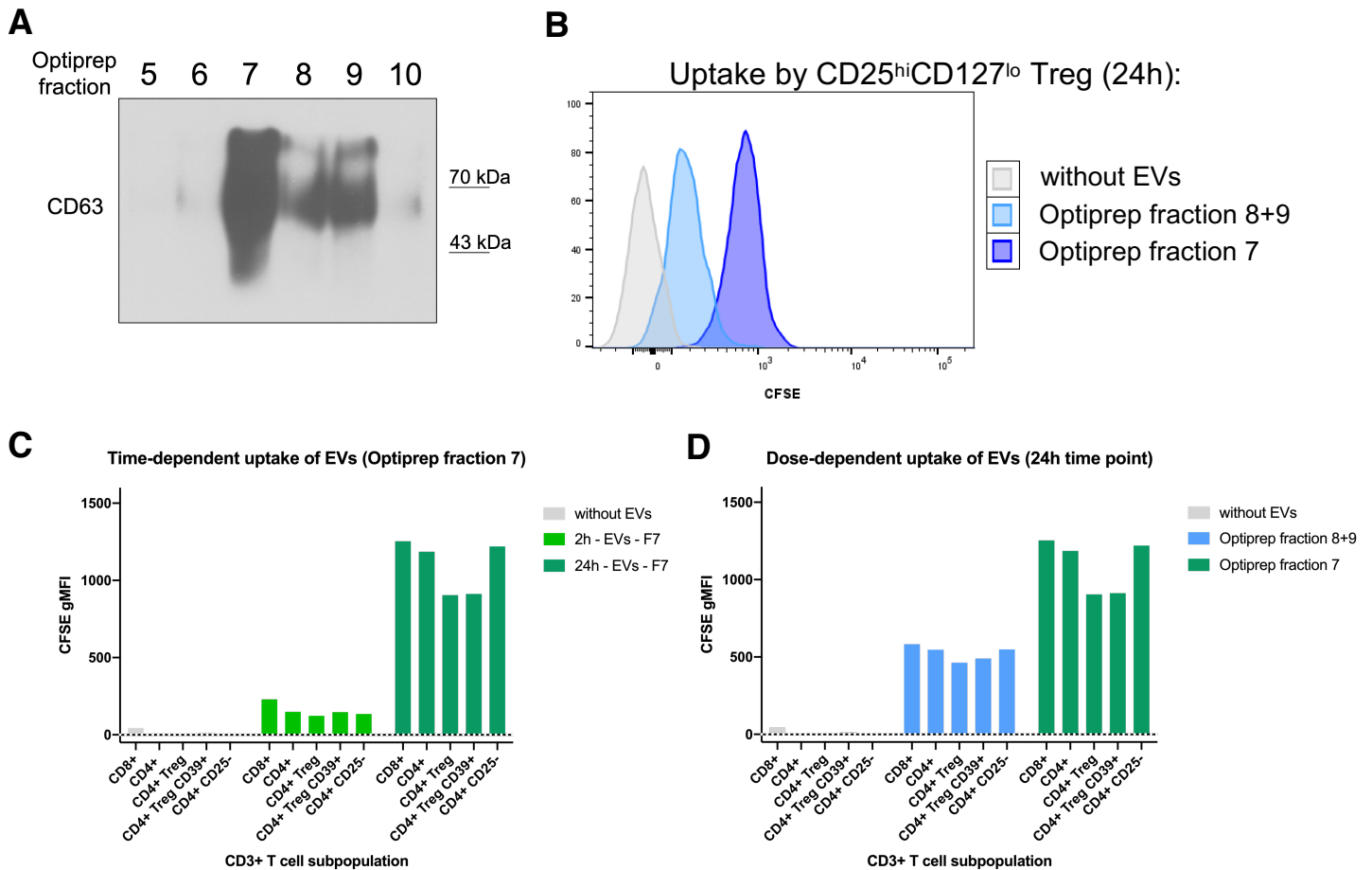


Figure 4.9 Human T cells, including Tregs, interact with fluorescently labelled CML EVs. (A) Western blot analysis of CD63 (EV marker) in fractions obtained by Optiprep™ density gradient centrifugation. CD63 is representative of EVs presence in specified fraction (representative of 3 experiments). **(B)** Representative histogram of CFSE fluorescence showing dose-dependent uptake/binding of CML EVs by Tregs (representative of 2 experiments). **(C)** Time- and **(D)** dose-dependent uptake/binding of CFSE-labelled CML (K562) EVs by different subsets of CD3+ T cells. Data are from 2 experiments (n=2). Mean value is shown. Gating strategy is shown in Figure 3.4.

In general, interaction of leukemic EVs with T cells was not only dose-dependent (Figure 4.9D), but also time-dependent, as the CFSE signal (representative of EVs) was stronger after 24 hours of culture, as compared to 2 hours of incubation (Figure 4.9C). Intriguingly, this represents a different kinetics/trend to cultures of murine thymocytes with leukemic EVs (Figure 4.2A-B). Moreover, non-Treg subsets (CD8+ T cells and CD4+CD25- T cells) seemed to take up/bind more EVs than CD4+ regulatory T cells. However, as the experiment was performed only twice (to simply prove that T cells are capable of interaction with CML EVs), this observation cannot be supported by statistical analysis and concluded. Altogether, tracking of fluorescently labelled leukemic EVs (K562-derived) in culture with human T cells proves that leukemic EVs can interact with human lymphocytes and thus may potentially influence the biology of human Foxp3+ regulatory T cells.

4.2.3 Leukemic extracellular vesicles induce Foxp3 and iTregs from non-regulatory cells

The immunosuppressive milieu of tumors can induce expression of Foxp3 (a Treg-specific transcription factor) in non-regulatory conventional T cells, leading to generation of CD25^{hi}Foxp3⁺ induced Tregs (iTregs) (also known as peripheral Tregs, pTregs)⁴⁸. I aimed at checking whether leukemic EVs can induce Foxp3 expression and iTregs. Sorted CD4⁺CD25⁻ conventional T cells were cultured in iTreg inducing conditions and treated with either CML (K562) EVs or AML (MOLM-14) EVs. Cultures were then analyzed for expression of CD25 and Foxp3 by flow cytometry, to detect CD25^{hi}Foxp3⁺ iTregs.

Both CML and AML EVs have induced expression of Foxp3 and thus generation of CD25^{hi}Foxp3⁺ iTregs (Figure 4.10A-B). As visible on representative dot plots and histograms, the Foxp3-expressing cells have constituted a clearly distinguished population of iTreg cells, rather than non-regulatory T cells with transient, low expression of Foxp3 (Figure 4.10A). The percentage of induced Foxp3-expressing cells (in a culture with 3x10⁹ CML EVs) was almost as high as in positive control cultures - cells treated with TGF- β , which is the strongest known inducer of Foxp3 in non-regulatory T cells. The amount of induced Foxp3⁺ cells depended on amount of CML EVs added to the culture of CD4⁺CD25⁻ T cells (Figure 4.10B). To control that the effect is specific to leukemic EVs, rather than potential contaminants in samples obtained by differential ultracentrifugation (though several contaminants were already excluded, Chapter 4.2.1, Figure 4.8) I have performed a "non-conditioned medium" control (NC medium), as advised by ISEV¹⁶³. This means that cell culture medium (used for generation of conditioned medium) was "cultured" for 24 hours without any cells and subjected to differential ultracentrifugation protocol, to pellet potential serum components/contaminants, such as e.g. bovine EVs. Transmission electron microscopy has revealed that no EVs were present in such a preparation (Figure 4.10C). More importantly, sample isolated from non-conditioned medium did not induce Foxp3 expression in non-regulatory CD4⁺CD25⁻ cells, as compared to CML EVs and TGF- β (Figure 4.10D). Altogether, human leukemic extracellular vesicles can induce Foxp3 and generation of iTregs/pTregs, therefore contributing to increased number of Tregs in myeloid leukemias.

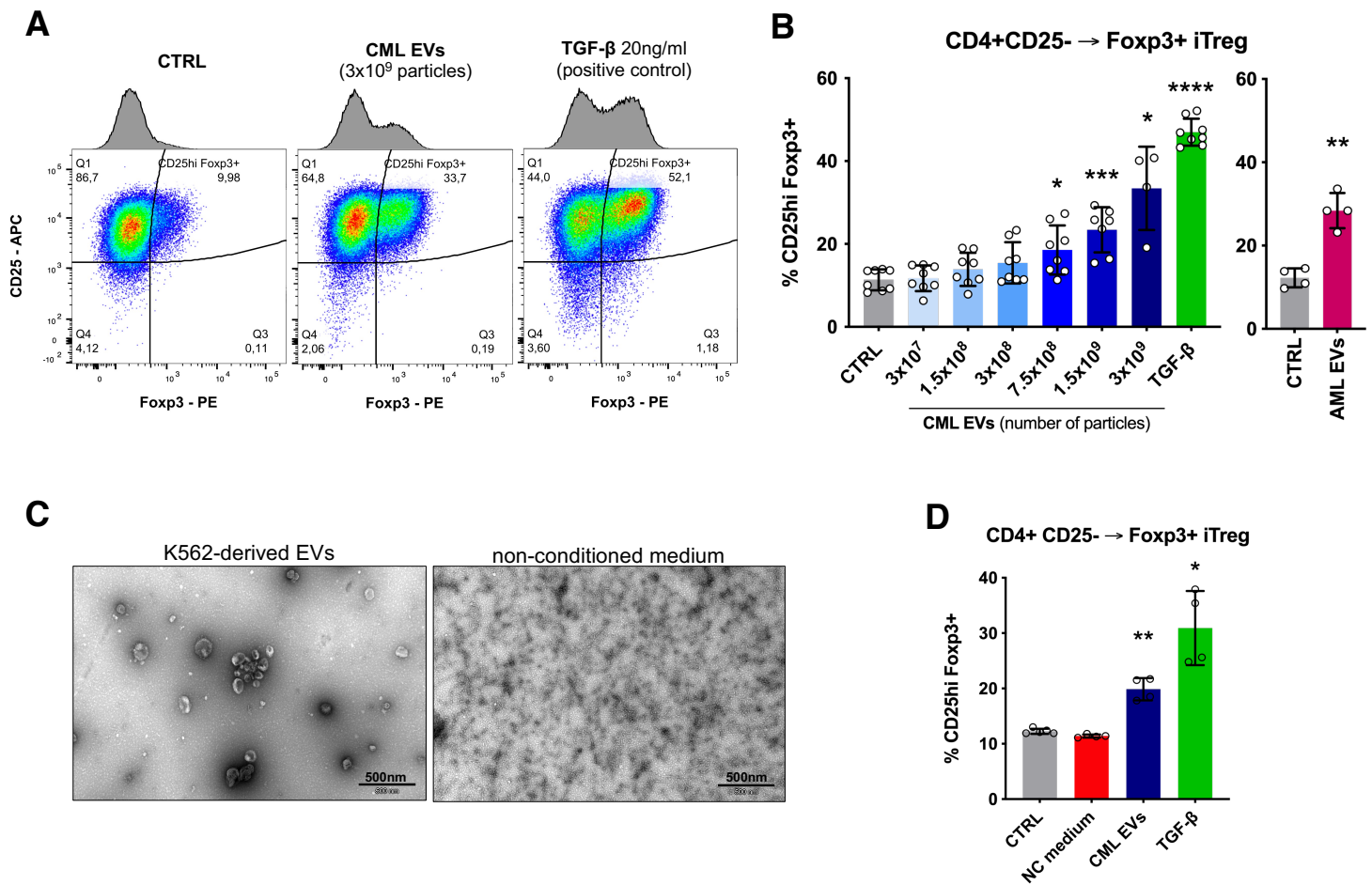


Figure 4.10 Leukemic EVs induce Foxp3 and Tregs from non-regulatory conventional T cells. (A) Representative dot plots and histograms of CD25^{hi}Foxp3⁺ iTreg induction from CD4⁺CD25⁻conventional T cells in control conditions or following treatment with CML EVs or TGF-β. **(B)** Induction of CD25^{hi}Foxp3⁺ iTregs after treatment with different doses of CML (K562) EVs and AML (MOLM-14) EVs (5x10⁹ particles). Data are from 4 experiments (n=8, except n=4 for 3x10⁹ CML EVs/particles, AML EVs). Unpaired t-test with Welch's correction, single data points and mean ± SD are shown. **(C)** Transmission electron microscopy imaging of EVs - CML (K562) EVs and non-conditioned medium sample. Close-up (60kx) images are shown (representative of 2 experiments). **(D)** Induction of CD25^{hi}Foxp3⁺ iTregs after treatment with CML (K562) EVs and non-conditioned (NC) medium samples. Data are from 2 experiments (n=4-5). Unpaired t-test with Welch's correction, single data points and mean ± SD are shown. Gating strategy is shown in Figure 3.12.

4.2.4 Leukemic extracellular vesicles upregulate suppressive phenotype and activity of human regulatory T cells

The effect on Tregs induction/generation was followed by analysis of influence of human leukemic EVs on Treg functionality. Specific molecules that mediate Treg suppressive activity were investigated, to gain more insight into functionality of these cells. The aim of this experiment was also to validate and strengthen data from mouse *ex vivo* models and to establish an experimental setting based on human Tregs. The effect on Treg suppressive capability was first evaluated by flow cytometric phenotyping of landmark molecules connected to suppressive function - CD39,

CTLA-4 and Foxp3. Indeed, expression of all of them was elevated following treatment of sorted human CD4+CD25^{hi}CD127^{lo} Tregs with CML (K562) EVs (Figure 4.11A). The differences in expression pattern are visible on representative histograms as stronger fluorescent signal, also in comparison with conventional, non-regulatory T cells (Tconv, sorted as CD4+CD25⁻), that established a negative biological control. As described in Chapter 4.2.3, non-conditioned medium control is necessary to exclude influence of potential contaminants and was thus also performed for Treg phenotyping experiment. Non-conditioned medium preparations did not upregulate expression of suppressive markers CD39, CCR8 and Foxp3, contrary to CML EVs (Figure 4.11B).

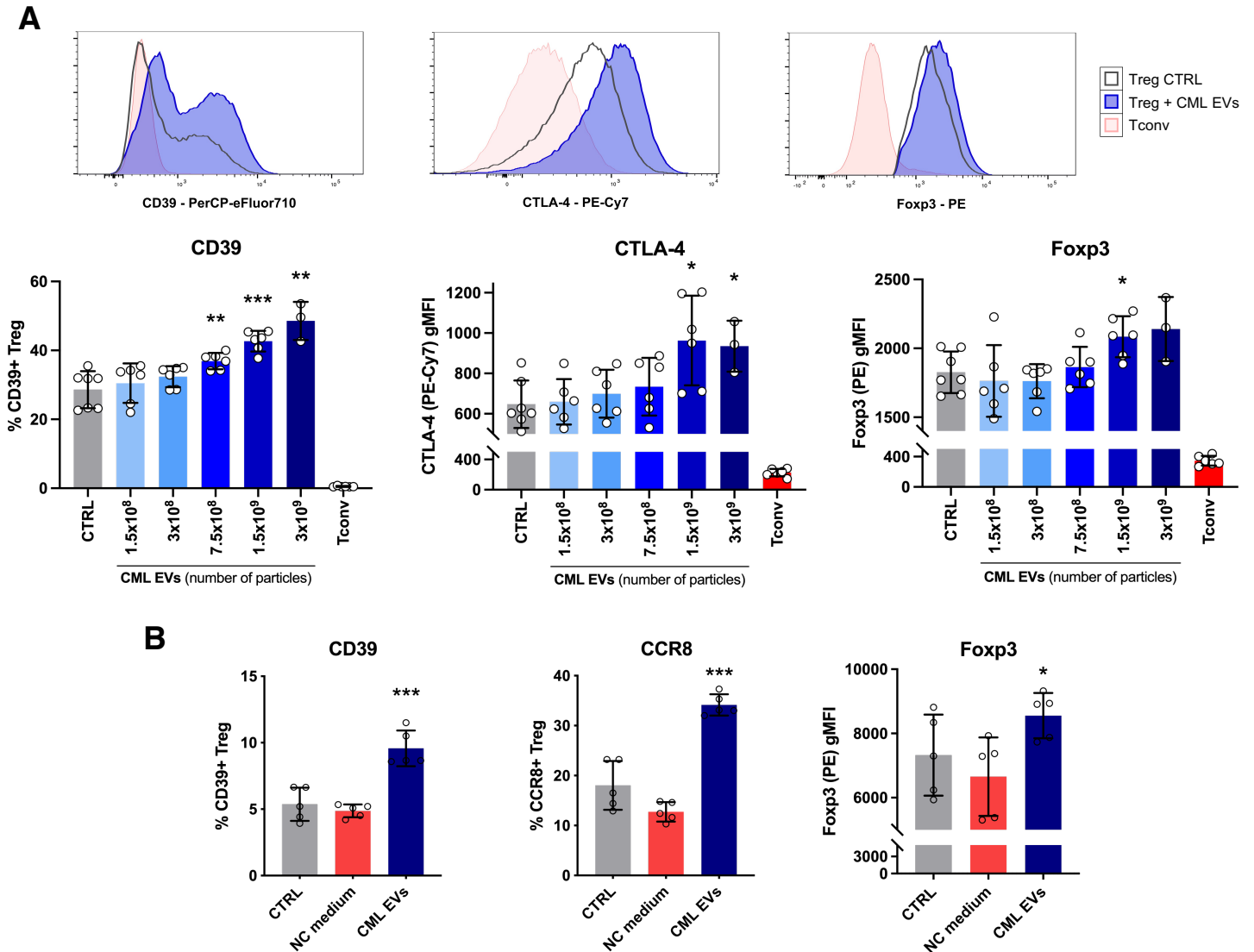


Figure 4.11 Leukemic EVs upregulate suppressive phenotype of human regulatory T cells. (A) Expression of CD39, CTLA-4 and Foxp3 in Tregs treated with different doses of CML (K562) EVs. Tconv (sorted as CD4+CD25⁻) cells were used as negative biological control of expression of molecules typical for Tregs. Representative histograms are shown (for CD39 – 3x10⁹ particles, for CTLA-4, Foxp3 - 1.5x10⁸ particles). Data are from 3 experiments (n=6, n=3 for 3x10⁹ particles). Unpaired t-test with Welch's correction, single data points and mean ± SD are shown. **(B)** Non-conditioned medium (NC) samples do not upregulate expression of suppressive molecules (CD39, CCR8, Foxp3) by Tregs, contrary to CML EVs. Data are from 2 experiments (n=5). Unpaired t-test with Welch's correction, single data points and mean ± SD are shown. Gating strategy is shown in Figure 3.14.

To gain information based not only on analysis of single parameters, but several parameters at once, CD4⁺ T cells in this experiment were re-analyzed in an unsupervised manner, using tSNE and FlowSOM algorithms^{245,246,255}. Use of unsupervised tools enables visualization of cells in a 2D space, but based on several (more than 2) parameters. This enables detection of populations that could have been missed by traditional manual gating, when only 2 parameters are analyzed simultaneously on flow cytometry plots. Moreover, unsupervised tools enable quantification of cell subsets identified based on several parameters, providing a reproducible and sensitive tool for detection of cell states and subsets, not detectable by manual analysis. Both algorithms (tSNE and FlowSOM) were performed based on expression of 4 markers: already mentioned CD39, CTLA-4 and Foxp3, as well as CD25 (T cell activation marker and IL-2 receptor chain α , which exhibits highest expression of Tregs, as they highly depend on IL-2). Even though only 4 parameters were used in this analysis, tSNE clustering has already revealed that CTRL and CML EVs-treated Tregs are significantly different in terms of their phenotype, as cells exhibit different cell density (seen as change in color - red corresponds to highest cell density) in different regions of the tSNE map. Moreover, CML EVs-treated Tregs formed two separate clusters of cells, suggesting that leukemic EVs drive Treg heterogeneity and specialized subsets (Figure 4.12A). On tSNE plots, Tregs treated with CML EVs localized in zones of high expression of CD39, CTLA-4, CD25 and Foxp3 (Figure 4.12B, expression/MFI is visible as change in color - orange/yellow corresponds to high expression of a given protein), confirming results from manual gating analysis (Figure 4.11A).

Another algorithm - FlowSOM - enables clustering of cells into specific subsets and quantification of these subsets. Data from FlowSOM is often visualized as a "minimal spanning tree" (Figure 4.12C). The tree is created by nodes (in form of pie charts, where each piece represents expression of a given protein) and nodes create populations/subsets, visualized as different color backgrounds of the nodes (for example, on Figure 4.12C, nodes with red background represent one population/subset of Treg cells). Size of the nodes corresponds to abundance of a given population in the sample. Using FlowSOM, CD4⁺ T cells from Treg phenotyping experiments were clustered into 6 subsets (represented by 6 different colors of background on the minimal spanning tree in Figure 4.12C). Based on nodes/pie charts (Figure 4.12C), it is visible that Population 1 ("Pop1", with yellow background, additionally circled in yellow) constitutes a subset with highest expression of all 4 markers used - CD39, CTLA-4, Foxp3 and CD25. It thus constitutes the most suppressive, effector subset of Tregs in performed experiments, which is clearly underlined by entire absence of this population in Tconv samples (Figure 4.12C). When percentage of Pop1 was quantified for each separate sample and experimental condition, it was twice as abundant after treatment with CML EVs (1.5×10^9 particles, Figure 4.12D).

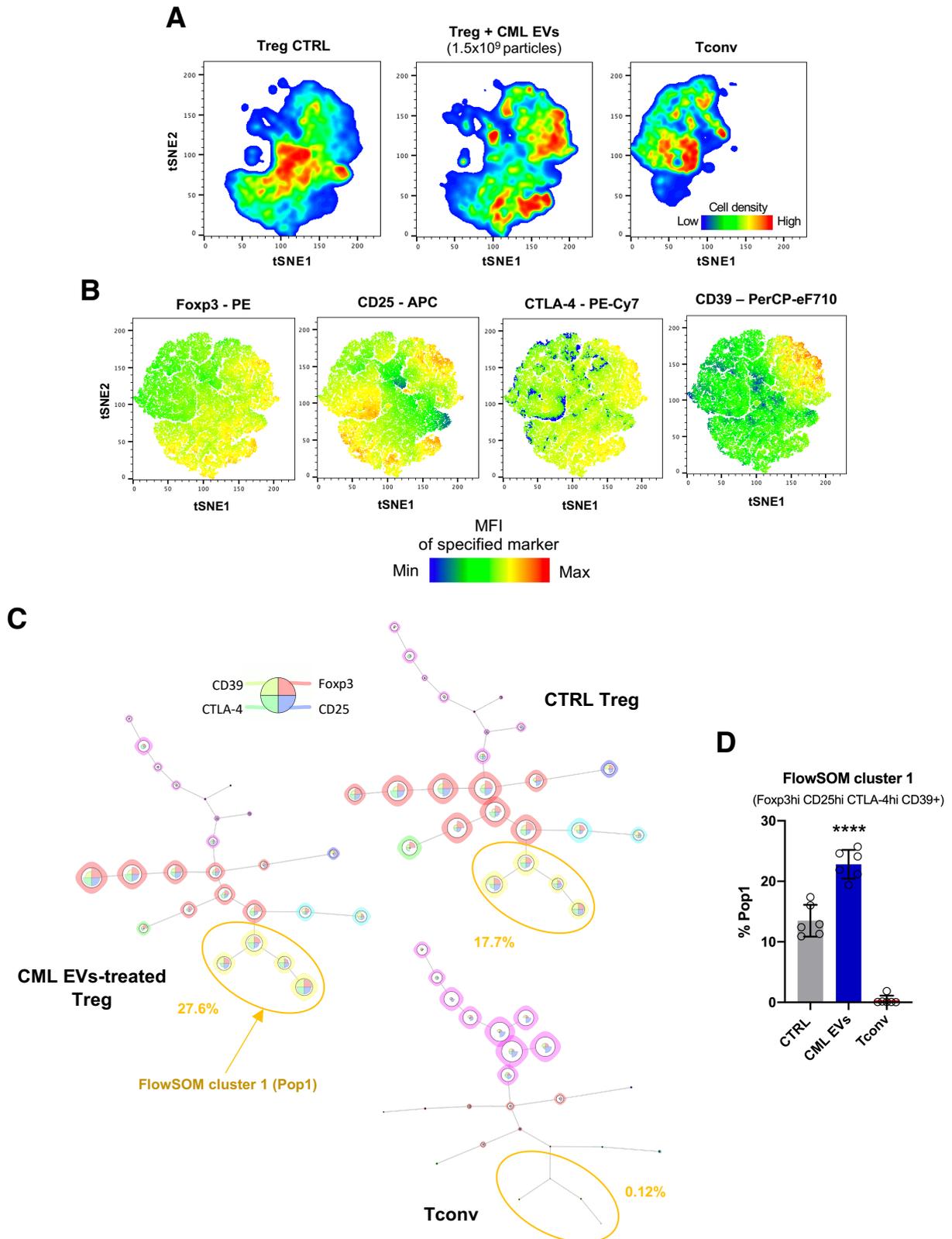


Figure 4.12 Unsupervised analyses reveal heterogeneity and expansion of an effector Treg subset. (A) tSNE clustering of CTRL Tregs, Tregs treated with CML EVs (1.5x10⁹ particles) and Tconv. Each analyzed sample was downsampled in FlowJo to 10,000 viable CD4⁺ T cells, followed by concatenation (to total 60,000 events per condition, 180,000 events in total) and tSNE analysis. (B) Density plots of Foxp3, CD25, CTLA-4 and CD39 expression on a tSNE map obtained in (A). (Legend continued on the next page)

(C) FlowSOM analysis (minimal spanning trees) of CTRL Tregs, Tregs treated with CML EVs (1.5×10^9 particles) and Tconv. Downsampling and concatenation were performed as for tSNE (same samples). Cluster with yellow background (FlowSOM cluster - Pop1) represents cluster with high expression of all 4 markers analyzed. Indicated percentage constitutes an average percentage that Pop1 constitutes of all viable CD4+ T cells analyzed in each experimental condition. **(D)** Percentage of cells in FlowSOM cluster Pop1 in each experimental conditions quantified for each sample (same samples as in Figure 4.11A). Data are from 3 experiments ($n=6$). Unpaired t-test with Welch's correction, single data points and mean \pm SD are shown.

Altogether, leukemic (CML) extracellular vesicles lead to upregulation of suppressive molecules on human regulatory T cells. Moreover, as discovered by FlowSOM, CML EVs lead to polarization of a specific effector subset of Tregs, that is characterized by high expression of suppressive molecules and high Foxp3 expression.

To validate these data functionally, human *in vitro* suppression assay was performed. Tregs were first cultured in control conditions or with CML (K562) EVs, followed by suppression assay culture with sorted CD4+CD25- or CD8+ responder T cells (Tresp). Tresp were labelled with a violet (eFluor450) proliferation dye, to track their proliferation rate and therefore assess suppressive activity of Tregs. Expansion index of Tresp, calculated by proliferation modelling tool in FlowJo, was used as a measure of Tresp proliferation. Both CD4+ and CD8+ responder T cells have exhibited lower expansion index in cultures with Tregs, which means that Tregs exerted suppressive effect. Crucially, Tregs treated with CML EVs have exhibited stronger suppressive function, as observed by diminished proliferation (lower expansion index), towards both CD4+ and CD8+ Tresp (Figure 4.13A-B). This is consistent with results of Treg phenotyping and amplified suppressive phenotype of Tregs.

In conclusion, data from experiments on human regulatory T cells demonstrate that leukemic EVs lead to amplified suppressive phenotype and function of Tregs.

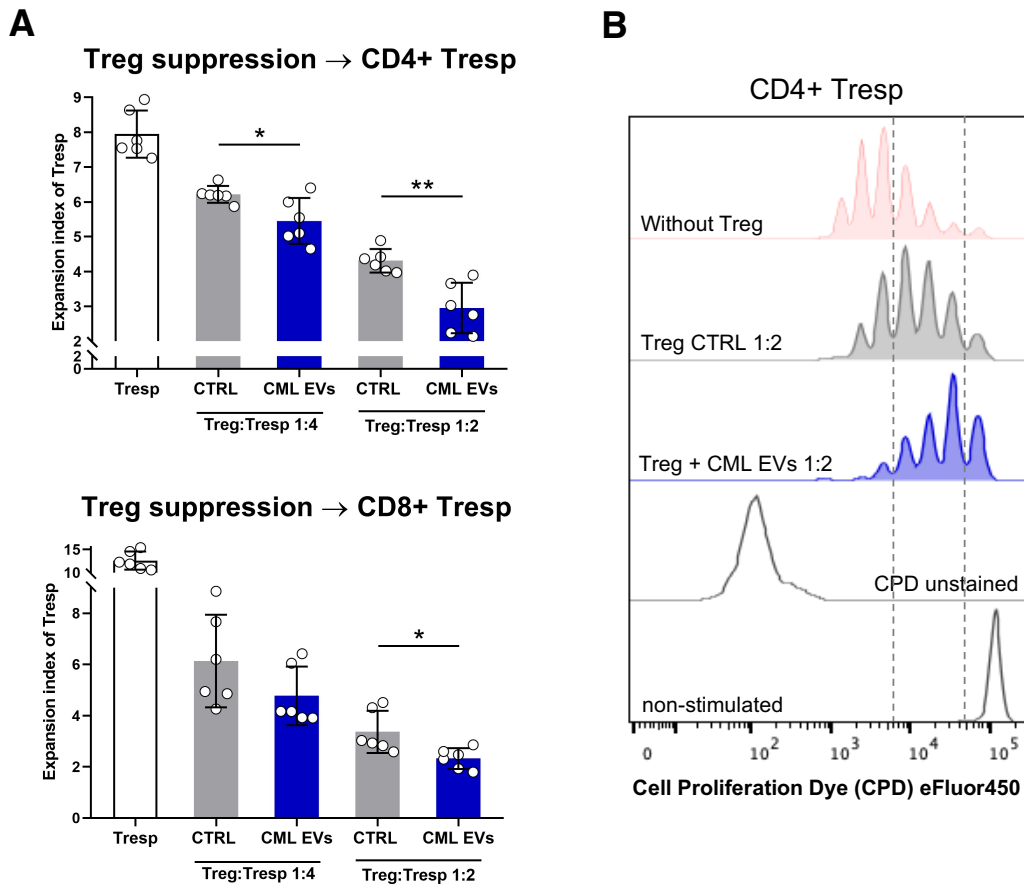


Figure 4.13 Human Tregs treated with CML EVs are more suppressive in a functional *in vitro* suppression assay. (A) Expansion index of CD4+ and CD8+ responder T cells in an *in vitro* suppression assay. Decrease in expansion index corresponds to increased suppressive activity of Tregs. Ratio of Treg to Tresp (Treg:Tresp) is indicated on the bottom of each graph. Data are from 3 experiments (n=6). Unpaired t-test with Welch's correction, single data points and mean \pm SD are shown. (B) Representative histograms of CD4+ Tresp proliferation in the *in vitro* suppression assay.

4.2.5 Leukemic extracellular vesicles induce exhausted phenotype and attenuate secretion of inflammatory cytokines in effector, non-regulatory T cells

Analysis of EVs' uptake/binding by human T cells has revealed that not only Tregs could be influenced by CML EVs. Therefore, influence of CML (K562) EVs on non-regulatory CD4+ (non-Treg) and CD8+ T cells was verified. To assess functionality of these cells, secretion of proinflammatory mediators (cytokines and chemokines) was analyzed, by analyzing these molecules in cell culture supernatants from cultures of effector T cells with EVs. Secretion of proinflammatory cytokines IL-6 (interleukin 6), TNF- α and IFN- γ (interferon γ) was downregulated in effector T cells (Figure 4.14), although in case of IFN- γ the difference did not reach statistical significance (due to variability in the scale of response by T cells from different blood donors). Importantly, both non-regulatory CD4+ (non-Treg) and CD8+ secreted significantly less of CCL2 - a chemokine that attracts myeloid cells in the microenvironment (Figure 4.14).

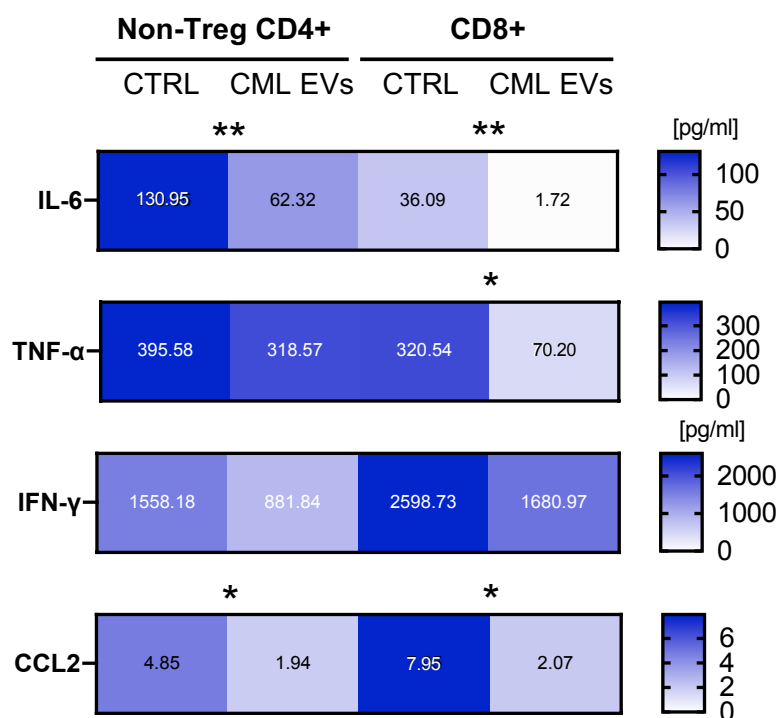


Figure 4.14 Effector T cells treated with leukemic EVs have diminished secretion of proinflammatory mediators. Secretion (pg/ml, calculated per 1×10^5 cells) of IL-6, TNF- α , IFN- γ and CCL2 by non-regulatory CD4+ (non-Treg) T cells and CD8+ T cells in *ex vivo* cultures with CML (K562) EVs, measured in cell culture supernatants by cytometric bead-based array. Data are from 4 experiments (n=4). Two-tailed paired t-test.

Moreover, to assess activation state of effector, non-regulatory CD4+ (non-Treg) and CD8+ T cells, expression of molecules associated with T cell exhaustion was measured. Exhausted phenotype was especially pronounced by non-regulatory CD4+ (non-Treg) T cells, as they have exhibited increased expression of PD-1, CD39, LAG-3 and CTLA-4 following treatment with CML EVs. CD8+ T cells treated with leukemic EVs exhibited increased expression of CD39, CTLA-4 and PD-1, although in case of PD-1 the difference did not reach statistical significance (Figure 4.15A-D).

Altogether, leukemic EVs can also negatively affect the effector function of non-regulatory CD4+ T cells and CD8+, by downregulating secretion of proinflammatory, anti-tumor cytokines/chemokines, as well as by inducing T cell exhaustion. Therefore, leukemic EVs can drive the immunosuppressive milieu by driving differentiation of Tregs, amplifying function of Tregs, as well as inhibiting anti-leukemic function of effector cells.

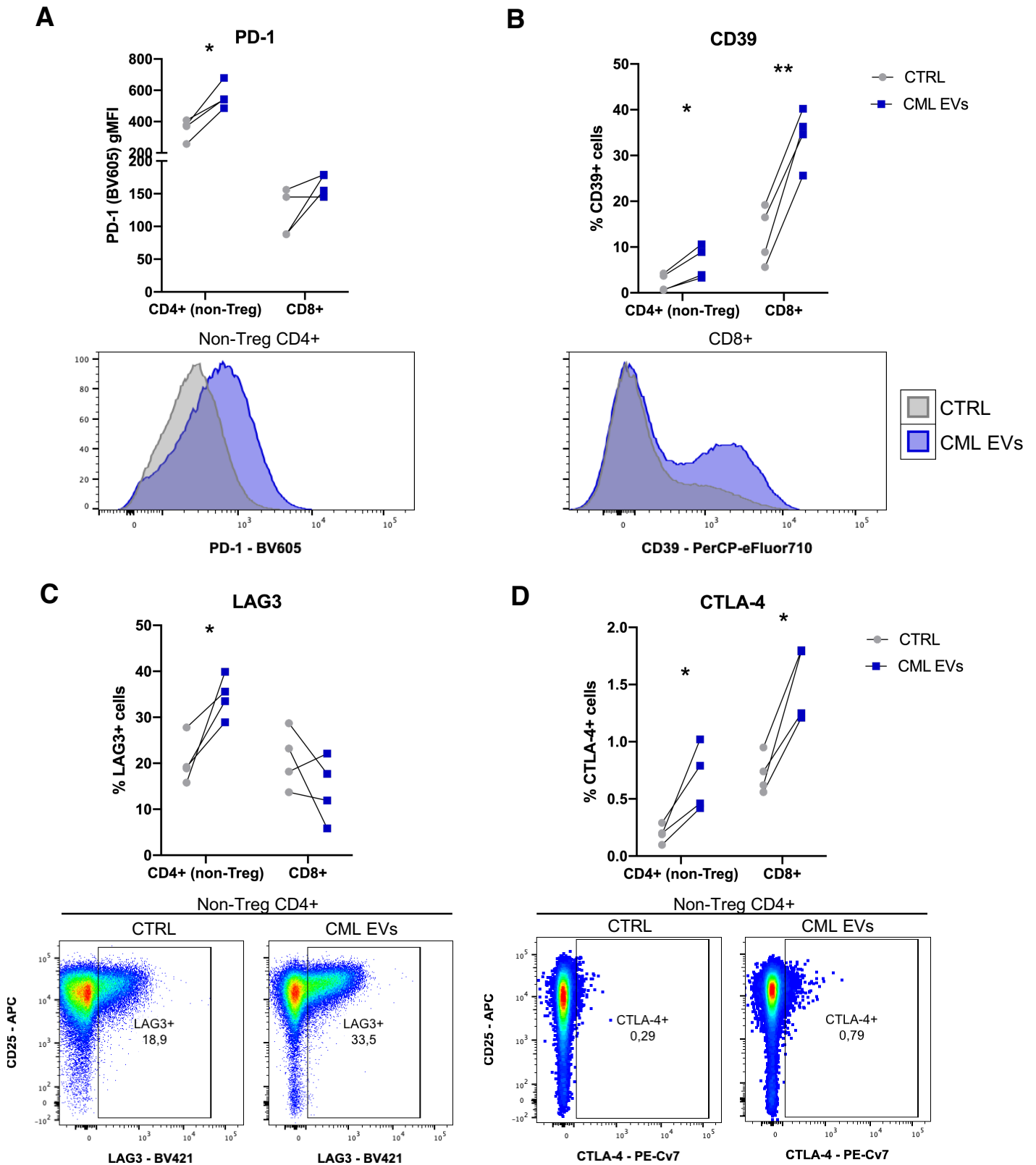


Figure 4.15 Effector T cells treated with leukemic EVs upregulate expression of T cell exhaustion markers. Expression of PD-1 (A), CD39 (B), LAG-3 (C) and CTLA-4 (D) by non-regulatory CD4+ T cells and CD8+ T cells, following treatment with CML (K562) EVs. Representative histograms or pseudocolor plots for specified populations are shown. Data are from 4 experiments (n=4). Two-tailed paired t-test, single data points, connected for each experiment, are shown.

4.2.6 Leukemic extracellular vesicles modulate STAT5 and mTOR signaling to induce Foxp3 and upregulate suppressive Tregs

Experiments described above have well documented influence of leukemic (CML, AML) extracellular vesicles on T cells and, specifically, Foxp3⁺ positive regulatory T cells. In the next steps I wanted to elucidate molecular events that may drive these phenomena, such as amplified suppressive activity and Foxp3 induction. Data from both mouse (Figure 4.7) and human (Figure 4.10-4.11) studies showed that Foxp3 level is upregulated by leukemic EVs. Therefore, I have decided to analyze molecular events both upstream of Foxp3 (that regulate Foxp3 expression), as well as downstream, such as potential engagement of other transcription factors. To study these processes, I have first employed flow cytometric measurement of phosphorylated signaling proteins. Based on literature (Chapter 1.2.3) and availability of fluorescently conjugated antibodies, several signaling pathways relevant to Foxp3 signaling and Tregs were chosen for analysis - STAT5, mTOR, S6 (mTOR downstream effector protein), p38, p65-NF κ B (RelA), SMAD2/3. While mTOR-S6 is a negative regulator of Foxp3 and Treg function, the remaining pathways positively regulate Foxp3 and Treg activity. Importantly, phosphorylation of these proteins is a relatively early signaling event. Therefore, phosphorylation of these signaling proteins was analyzed only 18 hours following treatment with leukemic EVs, when the process of EVs uptake/binding was still actively ongoing (Figure 4.9C).

Firstly, phosphorylated proteins were analyzed in CD4⁺CD25⁻ cells upon Foxp3 induction (Chapter 4.2.3, Figure 4.10). Already after 18 hours of treatment with CML EVs, as well as TGF- β , there was a significant increase in the number of Foxp3-expressing cells, despite their amount in culture has only established 2-4% of all CD4⁺ cells (Figure 4.16A). Among analyzed pathways, CML EVs have influenced two of them - the mTOR-S6 phosphorylation was attenuated, whereas STAT5 phosphorylation was upregulated. Interestingly, these pathways were not influenced by TGF- β (Figure 4.16B), which has induced phosphorylation of SMAD2/3. On the other hand, SMAD2/3 phosphorylation was not affected by CML EVs. CML EVs did not influence remaining signaling molecules, such as p38 and RelA (Figure 4.16C). This data demonstrates that leukemic EVs drive Foxp3 expression in CD25⁻ conventional T cells in a different mechanism than TGF- β . Moreover, I have looked in more detail at the small population of Foxp3⁺ cells that have already been induced in this short-term culture. Similarly to Tregs, they have exhibited high expression of pSTAT5 and low expression of pS6 (Figure 4.17), independently on culture conditions, contrary to Foxp3⁻ cells. However, in CML EVs treated samples, amount of pSTAT5^{hi} cells was even higher (Figure 4.17A) and amount pS6^{lo} cells even lower (Figure 4.17B) than in CTRL and TGF- β treated cells, which signified that these signaling pathways are relevant to induction of Foxp3 by leukemic extracellular vesicles.

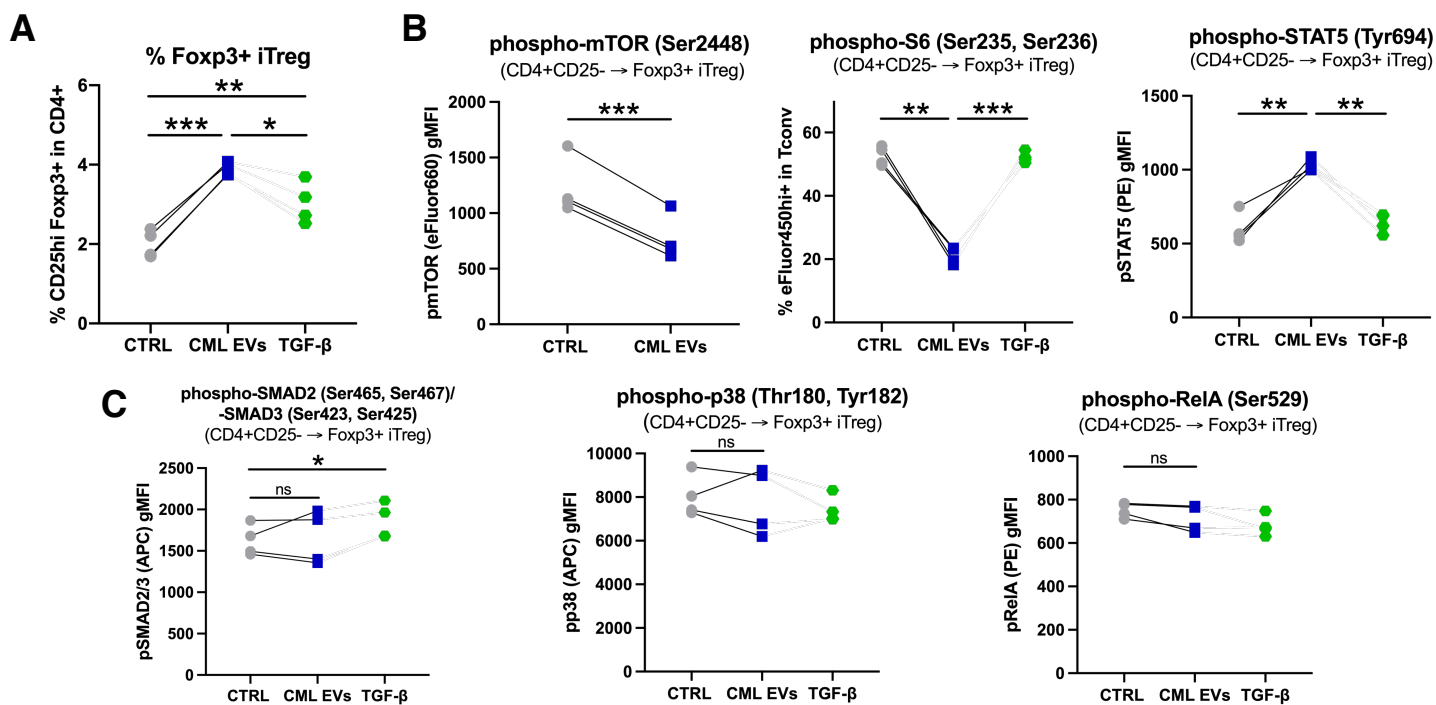


Figure 4.16 Leukemic EVs downregulate mTOR-S6 and upregulate STAT5 phosphorylation in CD4+CD25- Tconv upon Foxp3 induction. (A) Induction of Foxp3 in CD4+CD25- Tconv 18 hours after treatment with CML (K562) EVs. **(B)** Level of phospho-mTOR, phospho-S6 and phospho-STAT5 in CD4+CD25- Tconv 18 hours after treatment with CML (K562) EVs. **(C)** Level of phospho-SMAD2/3, phospho-p38 and phospho-RelA in CD4+CD25- Tconv 18 hours after treatment with CML (K562) EVs. In all experiments, TGF- β treatment was used as positive control of Foxp3 induction. Data are from 4 experiments (n=4). Two-tailed paired t-test, single data points, connected for each experiment, are shown. Gating strategy is shown in Figure 3.12.

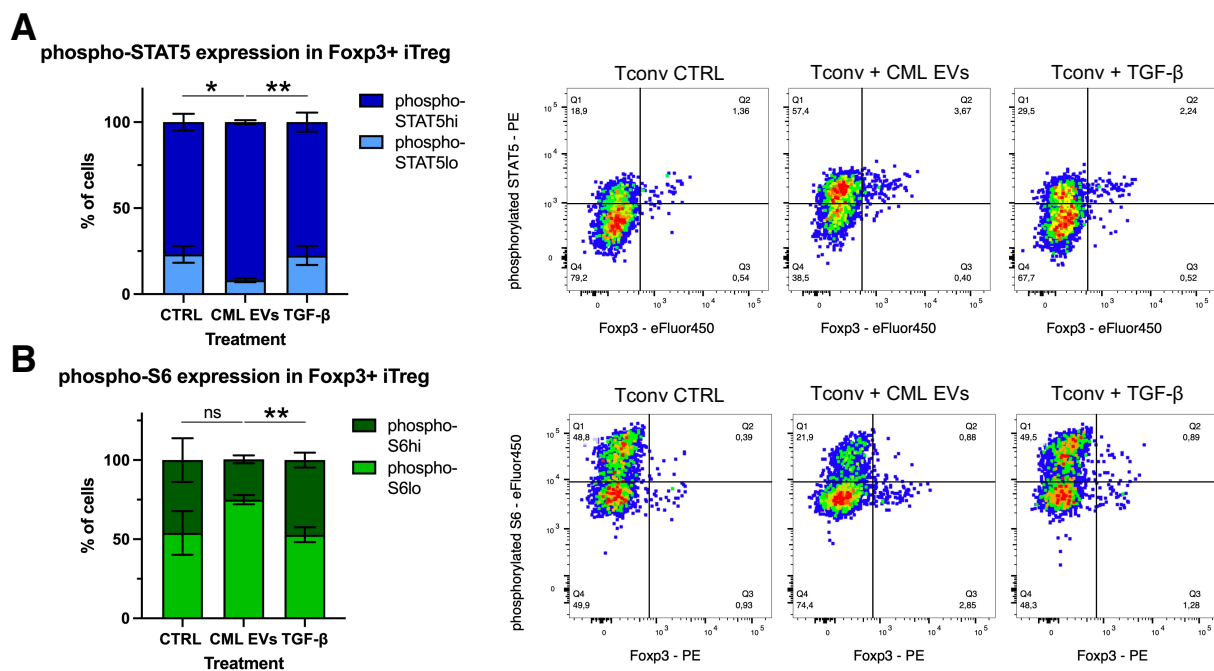


Figure 4.17 Phosphorylated STAT5 is upregulated and phosphorylated S6 is downregulated in Foxp3+ iTregs induced with CML EVs. (A) Percentage of pSTAT5^{hi} and pSTAT5^{lo} cells among induced Foxp3⁺ cells (left). Representative pseudocolor plots of pSTAT5 and Foxp3 in Tconv in short-term cultures leading to Foxp3 induction (right). (Legend continued on the next page)

(B) Percentage of pS6^{hi} and pS6^{lo} cells among induced Foxp3⁺ cells (left). Representative pseudocolor plots of pS6 and Foxp3 in Tconv in short-term cultures leading to Foxp3 induction (right). Data are from 4 experiments (n=4). Two-tailed paired t-test, single data points, connected for each experiment, are shown.

Phosphorylation of signaling molecules was also analyzed in short-term (18 hours) cultures of Tregs (sorted as CD4⁺CD25^{hi}CD127^{lo}), to assess which pathways may be responsible for modulation of suppressive phenotype and activity in these cells by EVs. Also in Tregs, treatment with CML EVs led to attenuated activity of the mTOR-S6 pathway, simultaneously with increased phosphorylation of STAT5 (Figure 4.18A). On the other hand, SMAD2/3, RelA and p38 were not influenced (Figure 4.18B).

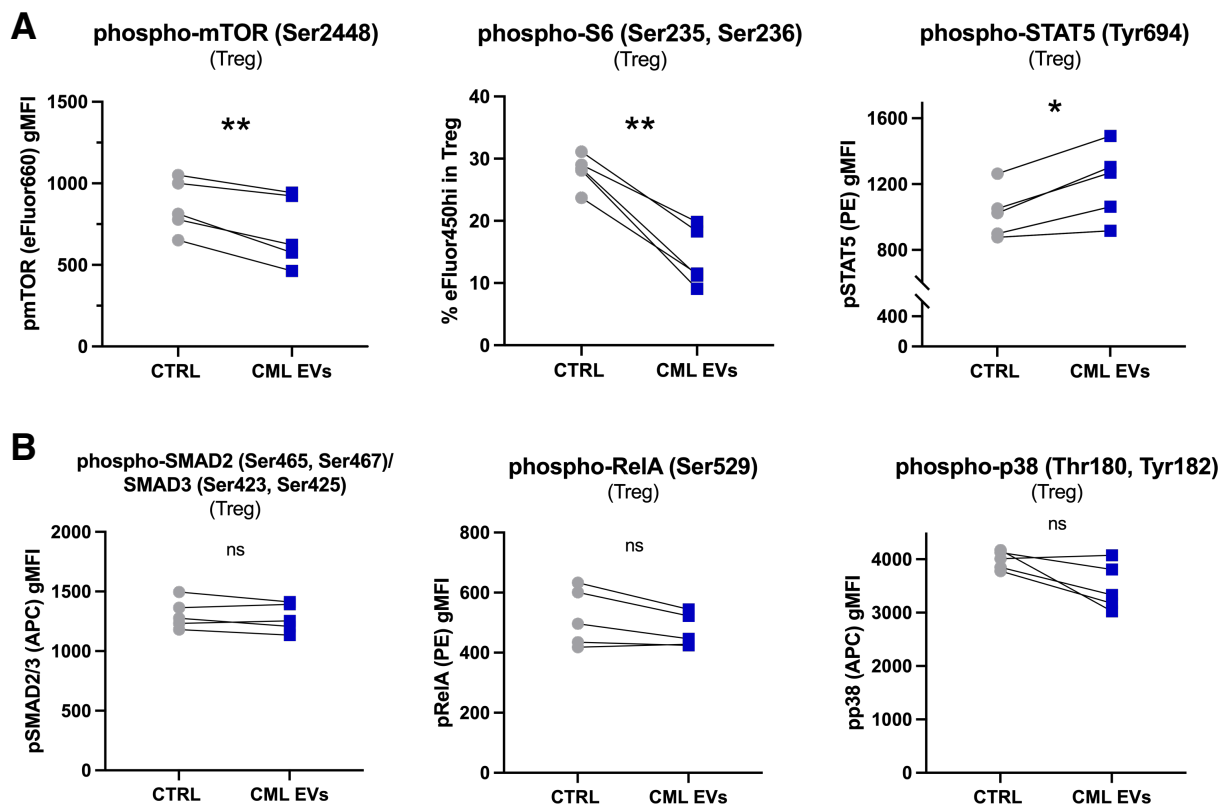


Figure 4.18 Leukemic EVs downregulate mTOR-S6 and upregulate STAT5 phosphorylation in Tregs. (A) Level of phospho-mTOR, phospho-S6 and phospho-STAT5 in Tregs 18 hours after treatment with CML (K562) EVs. **(B)** Level of phospho-SMAD2/3, phospho-p38 and phospho-RelA in Tregs 18 hours after treatment with CML (K562) EVs. Data are from 5 experiments (n=5). Two-tailed paired t-test, single data points, connected for each experiment, are shown. Gating strategy is shown in Figure 3.14.

Altogether, analysis of phosphorylation of several signaling pathways, crucial for regulatory T cells biology, has revealed that leukemic extracellular vesicles exert their effect on Foxp3 and Tregs via modulation of mTOR-S6 and STAT5 signaling. Performed experiments have excluded modulation of p38, SMAD2/3 and RelA phosphorylation, as crucial for Treg-leukemic EVs interaction.

4.2.7 Leukemic EVs maintain genetic and functional stability of Tregs *ex vivo*

Changes in STAT5 and mTOR pathways in Tregs have been described previously as involved not only in suppressive function and differentiation, but also Treg stability, which may be affected for example in the inflammatory milieu. STAT5 binds the *Foxp3* gene to maintain its expression, whereas expression of *Foxp3* is inhibited by mTOR and its downstream components^{69,80}. Therefore, to validate link between STAT5 upregulation and mTOR downregulation with Treg stability, I set out to check features that may be dysregulated when Tregs become unstable - demethylation of the TSDR region in the human *FOXP3* gene, as well as secretion of non-Treg specific cytokines⁷⁴. Although *in vitro* culture conditions used in presented studies maintain high percentage of CD25^{hi}Foxp3⁺ cells (Figure 3.14) and suppressive activity (Figure 4.13), some instability features usually appear in Treg cultures *in vitro*. Therefore, I expected that in the used experimental setting, effect of leukemic EVs on Treg stability should be visible. Firstly, DNA was isolated from cultured Tregs and, by methylation-specific PCR, demethylation of TSDR region in the human *FOXP3* gene was analyzed. As Tconv (sorted CD4⁺CD25⁻) have fully methylated TSDR, they were used as a positive control in the experiment. Both control and CML EVs treated Tregs have maintained demethylated TSDR after 5 days of culture, showing stability at the genetic level (Figure 4.19A). On the other hand, secretion of non-Treg specific cytokines has demonstrated that some Tregs may lose their stability. Secretion of IFN- γ , IL-6 and IL-17A suggests that upon *in vitro* culture some Tregs acquire features of the Th1 or Th17 lineage. However, Tregs treated with leukemic EVs secreted significantly less IL-17A and IFN- γ and practically did not secrete IL-6, which means that CML EVs help maintain Treg stability (Figure 4.19B). These results demonstrate that leukemic EVs, apart from upregulating Foxp3 and suppressive activity of Tregs, also help maintain genetic and functional stability of these cells and prevent de-differentiation into other T cells lineages. This is most probably facilitated by modulation of STAT5 and mTOR-S6 signaling.

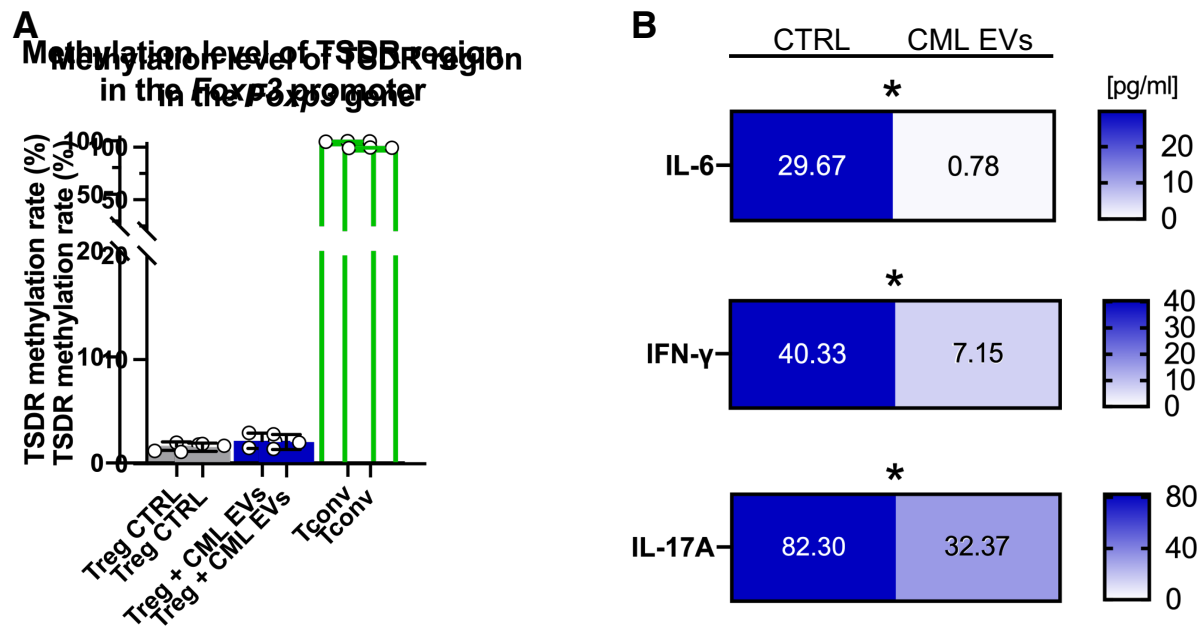


Figure 4.19 Leukemic EVs maintain stability of Tregs *ex vivo*. (A) Methylation level of the TSDR region in the *FOXP3* gene, measured by methylation-specific PCR. Data are from 3 experiments (n=3). Single data points and mean \pm SD are shown. (B) Secretion (pg/ml, calculated per 1×10^5 cells) of IL-6, IFN- γ and IL-17A by regulatory T cells in *ex vivo* cultures with CML (K562) EVs, measured in cell culture supernatants by cytometric bead-based array. Data are from 6 experiments (n=6). Two-tailed paired t-test.

4.2.8 Treg transcriptome is globally affected by leukemic EVs

To gain much broader insight into changes in the biology of Tregs due to leukemic EVs, RNA sequencing was performed. Transcriptomics enables identification of possibly unexpected, modulated genes, screening of changes in many genes of interest, identification of biological processes modulated (based on differentially expressed genes), as well as (by bioinformatic tools) further prediction of molecular drivers (such as transcription factors) of observed biological effects. On the other hand, one needs to remember that changes in RNA do not necessarily have to reflect changes in the level of functional protein. Moreover, in experimental setting used for human Tregs in this thesis, Tregs were treated with EVs and cultured together for five days. This means that differences at RNA level could arise much earlier than differences in the level of proteins described above (Figure 4.11) and could potentially no longer be visible at day five of the culture. Therefore, to first pick up a time point for RNA sequencing analysis, RT-qPCR analysis of selected genes (*ENTPD1* [encoding CD39], *CCR8*, *FOXP3*) was performed two, three, four and five days following treatment with EVs.

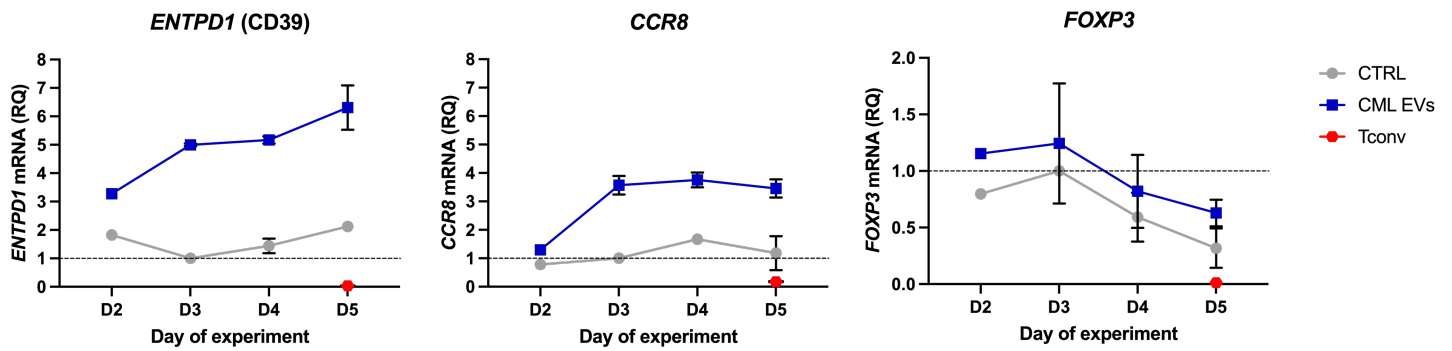


Figure 4.20 Level of *ENTPD1* (CD39), *CCR8*, *FOXP3* mRNA in Tregs cultured with leukemic EVs. RNA level was analyzed at different time points of cell cultures (days specified). Relative values were first normalized to *18srRNA* expression and then normalized to values for D3 CTRL. Data is representative of 2 biological replicates for D3-5 and one replicate for D2. Activated Tconv at D5 have been used as negative control of expression of genes specific for Tregs.

RT-qPCR analysis revealed that differences for analyzed genes, especially *ENTPD1* and *CCR8*, have first appeared three days after beginning of cultures. The differences were well maintained until day five of culture, which was the day of analysis of proteins and functional assays. Differences in *FOXP3* expression were not clearly visible, though it seems like difference between CTRL Tregs and CML EVs-treated Tregs was most pronounced at day five (however, statistical analysis with only 2 biological replicates was not performed) (Figure 4.20). Nevertheless, this simplified analysis by RT-qPCR delivered information on RNA expression dynamics. As the differences on RNA level (especially for *ENTPD1* and *CCR8*) were maintained on each third, fourth and fifth day, the fifth day has been selected for analysis by RNA sequencing. As Tregs in performed experiments were stimulated to proliferate, on day five largest number of cells was available, which enabled highest RNA yield for sequencing.

Therefore, control and CML (K562) EVs-treated Tregs, following 5 days in culture, have been sorted (to sort viable and activated Tregs), used for RNA isolation and RNA sequencing, followed by bioinformatic analysis. Principal component analysis of entire RNA sequencing datasets has revealed that Tregs treated with leukemic EVs ("TregEVs") visibly separate alongside PC1 (Figure 4.21A), which indicated strong biological differences after treatment. Analysis of single genes has revealed statistically significant upregulation of 356 and downregulation of 566 genes in Tregs treated with CML EVs, altogether yielding 922 differentially expressed genes (DEGs) (Figure 4.21B). These two types of analysis already show that leukemic EVs significantly remodel the transcriptome of Tregs, possibly influencing several biological and molecular processes in these cells.

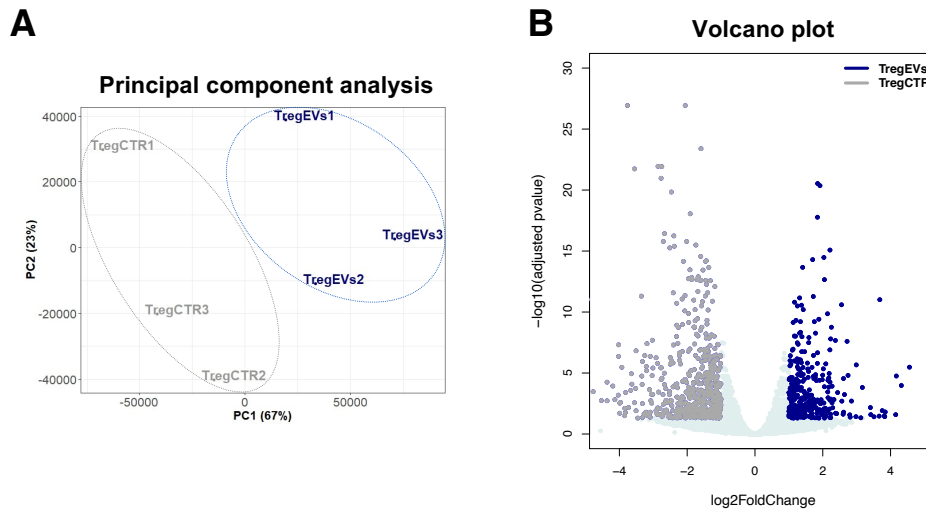


Figure 4.21 Leukemic EVs significantly remodel the transcriptome of Tregs. (A) Principal component analysis (PCA) of entire RNA sequencing datasets of control ("TregCTR") and CML (K562) EVs-treated Tregs ("TregEVs"). (B) Volcano plot of differentially expressed genes (DEGs) between control ("TregCTR") and CML (K562) EVs-treated Tregs ("TregEVs"). Genes were considered as differentially expressed when $-\log_{10}(\text{adjusted P-value}) < 0.05$ and $|\log \text{ fold change(LFC)}| > 1$. For RNA sequencing, 3 experiments were performed, each on Tregs from a different healthy donor.

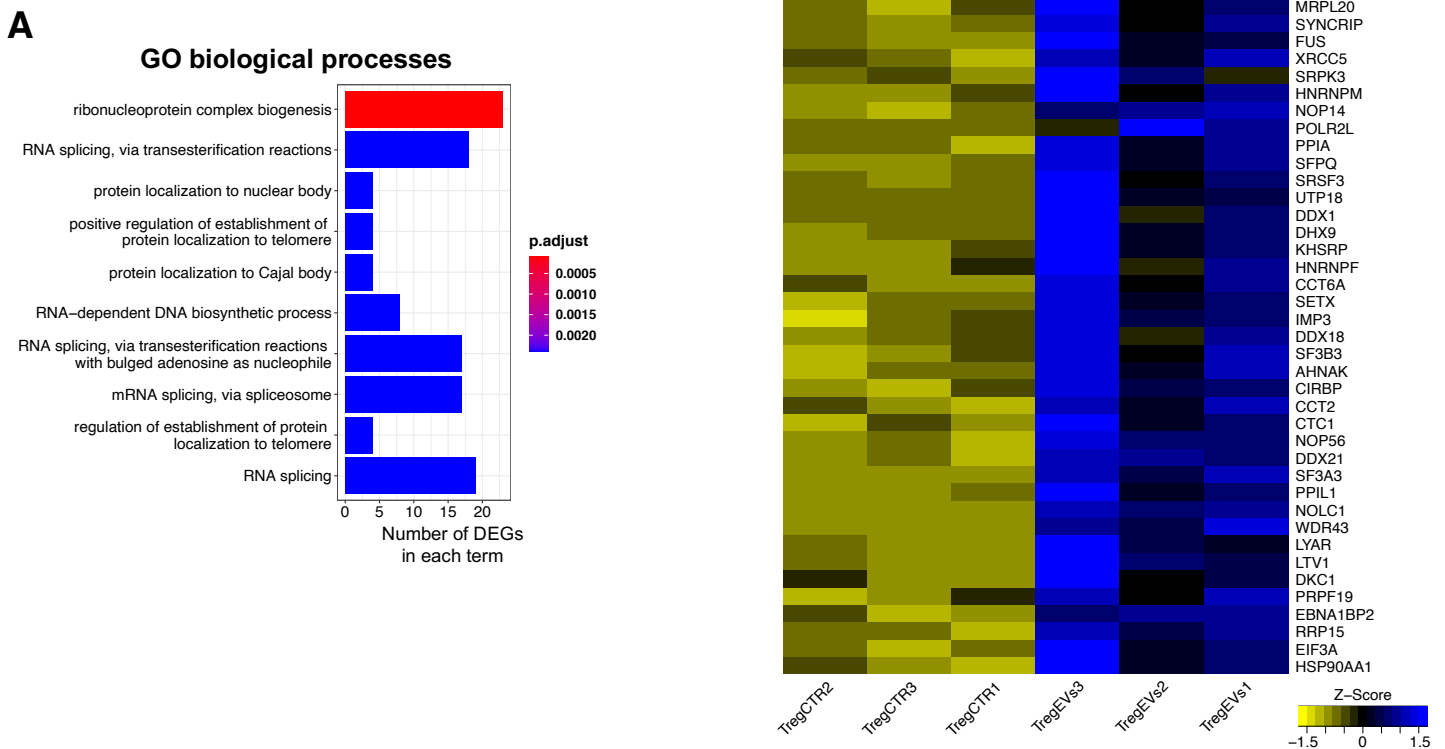


Figure 4.22 Expression of genes related to RNA processing and metabolism in Tregs is modified by leukemic EVs. (A) Biological processes (Gene Ontology, top 10 GO terms) influenced by CML EVs, identified based on differentially expressed genes (DEGs, $|\text{LFC}| > 1$) upregulated by CML EVs. (B) Heatmap showing DEGs that constitute biological processes, such as RNA processing and alternative splicing, identified by Gene Ontology analysis in (A). For RNA sequencing, 3 experiments were performed, each on Tregs from a different healthy donor.

To investigate changes in entire biological processes, either functional or molecular, gene ontology (GO) analysis was performed based on differentially expressed genes with a log fold change over 1 (ILFC>1). Amongst top 10 influenced GO processes, most were connected to RNA processing and metabolism and processes such as formation of ribonucleoprotein complexes or different forms of RNA splicing (Figure 4.22A). The influenced genes have included genes such as *HNRNPF*, *HNRNPN*, *FUS*, *SF3A3*, *SF3B3*, *SRSF3*, involved in regulation of these processes (Figure 4.22B). Identification of processes such as RNA splicing, as well as processes connected to protein localization to nuclear bodies and Cajal bodies (Figure 4.22A), suggests that leukemic EVs profoundly influence gene expression in regulatory T cells at different stages of gene expression.

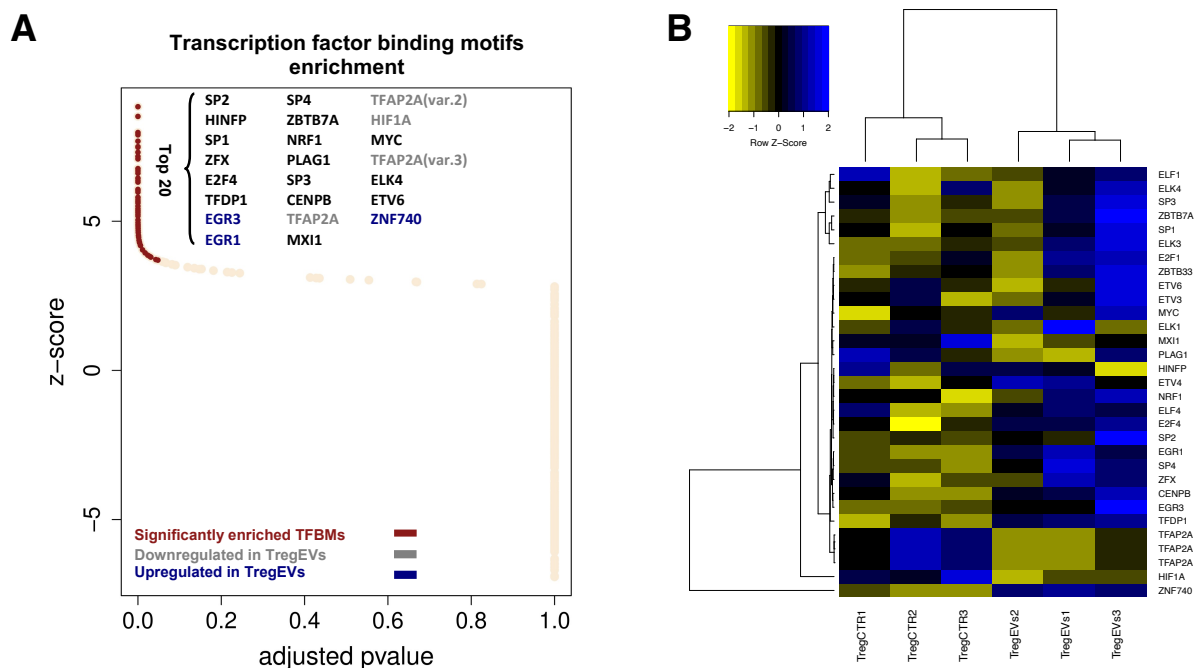


Figure 4.23 Transcription factors potentially engaged in molecular control of Tregs by CML EVs. (A) Identification of transcription factor binding motifs (TFBMs) enriched in differentially expressed genes (DEGs, ILFCI>1), analyzed by PSCAN software. Top 20 identified TFBMs/transcription factors are listed. Transcription factors, which were differentially expressed at RNA level, are marked in either navy blue (upregulated by CML EVs) or grey (downregulated by CML EVs). (B) Heatmap comparing RNA expression of transcription factors identified in (A). For RNA sequencing, 3 experiments were performed, each on Tregs from a different healthy donor.

To gain more insight into molecular mechanisms responsible for modulation of regulatory T cells by leukemic EVs, bioinformatic analysis of transcription factor binding motifs was performed. Based on analysis of sequences of differentially expressed genes by PSCAN software and referencing them to a database of transcription factor binding profiles (JASPAR 2018_NR database), transcription factors that potentially regulate highest number of genes were detected. Based on this analysis, 31 transcription factors (TFs) were identified and top 20 are shown on Figure 4.23A. They include TFs such as EGR1, EGR3, ZBTB7A(LRF), E2F4 or TFDP1, which have been previously

described in literature as engaged in Tregs development or function, also in tumors^{101,102,256,257}. On the other hand, out of TFs detected in the analysis, RNA level of only 3 of them was significantly upregulated by CML EVs - EGR1, EGR3, ZNF740 (Figure 4.23A-B). While this result increases the probability that these 3 TFs are engaged in Treg regulation by CML EVs, it does not exclude that the remaining TFs are also involved.

Finally, I decided to directly look at expression of genes that are involved in Treg activity, as well as have been previously described in literature as upregulated in tumor Tregs. Based on several papers that have analyzed Tregs from solid tumors, either by bulk RNA sequencing, single-cell RNA sequencing or high-resolution flow cytometry^{96,98,100-102}, I have comprised a list of genes of interest, that were plotted onto a heatmap (Figure 4.24). Only 3 genes were differentially expressed (upregulated by CML EVs: *TFRC*, encoding transferrin receptor 1/CD71 and *CCR4*; downregulated: *IKZF2*, encoding Helios). However, for remaining genes a visible trend of upregulation was observed, though this observation was affected by generally lower expression of all genes in the TregCTR2/TregEVs2 samples. Amongst genes with most visible trend of upregulation were *TNFRSF1B* (encoding TNFR2), *IL2RA* (encoding CD25), *ENTPD1* (encoding CD39), *TNFRSF8* (encoding CD30), *IL1R1*, *HAVCR2* (encoding TIM-3), *TGFB1* (encoding TGF- β), *IRF4* and *CXCR5* (Figure 4.24). Most of these are responsible for suppressive, effector phenotype of Tregs in tumors. Lack of statistically significant differences for the mentioned genes may be due to well-described disproportion between RNA and protein expression (reported also for Treg cells²⁵⁸) and indicates relevance of differences in RNA processing detected above. Nevertheless, to obtain final evidence (or lack thereof), majority of proteins encoded by these genes were included in large flow cytometric Treg phenotypic studies, described further (Chapter 4.2.9) in this thesis.

Altogether, RNA sequencing of Tregs treated with leukemic EVs has revealed significant remodeling of the Tregs' transcriptomic profile, confirming the significance and scope of the CML EVs' influence. Moreover, this analysis has revealed the influence on RNA processing/metabolism, as well as specific transcription factors that may be significant drivers of functional and phenotypic changes in Tregs modulated by leukemic EVs. Analysis of specific tumor Treg genes, though it did not allow final conclusions in terms of driving a tumor Treg signature, has hinted several genes (and proteins encoded by them) as crucial in the functional, phenotypic outcome of the Treg-leukemic EVs interaction.

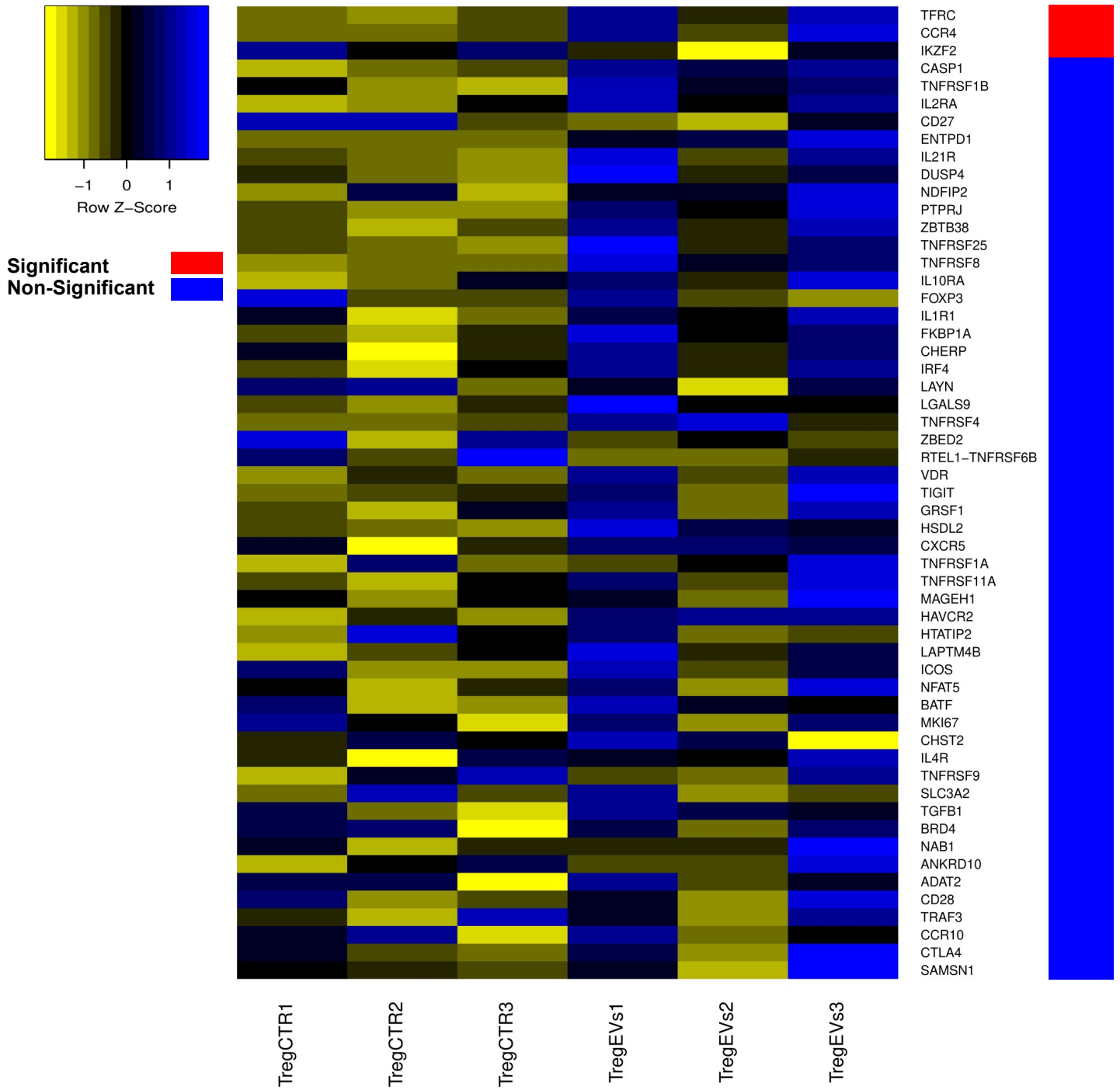


Figure 4.24 Heatmap showing expression of tumor Treg genes by Tregs treated with CML (K562) EVs. Statistical significance of each gene is indicated (genes were statistically significant when $-\log_{10}(\text{adjusted P-value}) < 0.05$ and $|\log \text{fold change (LFC)}| > 1$).

4.2.9 Leukemic EVs drive specific signature of human Tregs, including two effector subsets - CD30+CCR8^{hi}TNFR2^{hi} eTreg1 and CD39+TIGIT^{hi} eTreg2

The final step of Treg characterization, to assess influence of leukemic extracellular vesicles, was their extensive phenotypic analysis, on a single-cell, protein level. The aim was to validate molecules revealed by RNA sequencing, as well as dissect heterogeneity (such as existence of specialized subsets) of Tregs driven by leukemic EVs, in high resolution. To accomplish that, I have used spectral flow cytometry and a 23-color panel of fluorescent antibodies for different markers (described in Materials and Methods Chapter 3.5.4). The panel was constructed based on genes revealed by RNA sequencing, but also on the literature^{96,98,100-102}, to also include novel, most recently described markers of effector, tumor Tregs (Chapter 4.2.8).

Firstly, classical manual gating analysis was performed for each of the phenotypic markers included in the panel. Tregs were cultured in control conditions, as well as with EVs released by CML (K562) and AML (MOLM-14) cells. Majority of analyzed proteins were upregulated by leukemic EVs (Figure 4.25A-B). The upregulated proteins included ectonucleosidases CD73 and CD39, chemokine receptors CCR8 and CCR4, TNF receptor superfamily members CD30 and TNFR2, Foxp3, IL21R (though the difference was insignificant for AML EVs) and inhibitory molecules LAG-3, TIGIT and TIM-3 (the last one only due to AML EVs). What needs mentioning, while upregulation of LAG-3 and CD73 was significant, expression of these receptors was limited to only less than 1% of Tregs (as these molecules are rather expressed by Tregs in tissues than blood, whereas blood was the source of cells used in experiments). Nevertheless, it points out that CD73 and LAG-3 become upregulated by leukemic EVs, although this result needs further confirmation using another model. The remaining markers were either not affected by leukemic EVs or slightly downregulated (Figure 4.25A-B). Intriguingly, CD71 was one of the downregulated receptors, contrary to data from RNA sequencing, where CD71 encoding gene (*TFRC*) was significantly upregulated. On the other hand, downregulated expression of Helios was consistent with lower expression of *IKZF2* gene (Figure 4.24, 4.25). Altogether, several functional phenotypic proteins on Tregs were significantly upregulated by leukemic (both CML and AML) extracellular vesicles. Due to high expression on Tregs and consistent upregulation due to both CML and AML EVs - expression of CD39, CCR8, CD30, Foxp3, TNFR2, CCR4, TIGIT and IL21R - can be considered as a "signature" of effector Tregs driven by leukemic EVs.

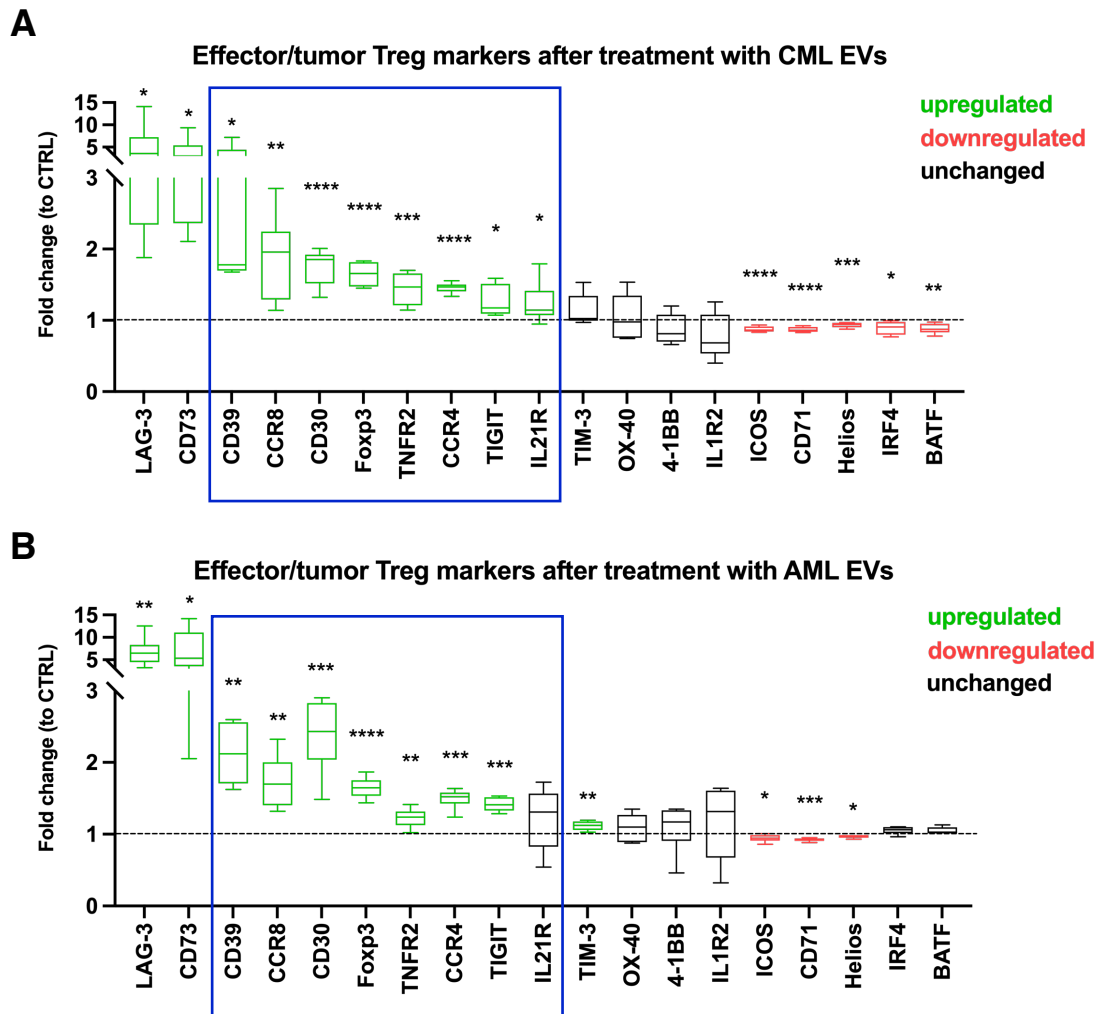


Figure 4.25 Leukemic EVs drive expression of several phenotypic molecules on Tregs. Expression (fold change to control samples) of phenotypic markers and transcription factors (Foxp3, IRF4, BATF, Helios) by regulatory T cells treated with CML (K562) EVs (**A**) and AML (MOLM-14) EVs (**B**). Significantly upregulated molecules are indicated in green, significantly downregulated in red. For Foxp3, IRF4, BATF and TNFR2 - gMFI was analyzed, for remaining molecules - % of positive cells. Values were normalized to average values of CTRL samples in each experiment and plotted as fold change. Data are from 4 experiments (n=8) for CML EVs and 4 experiments (n=6) for AML EVs. Unpaired t-test with Welch's correction. Box and whiskers are shown, whiskers represent minimal to maximal value for each group, box 25th to 75th percentiles. Gating strategy is shown in Figure 3.7.

Following traditional, manual gating analysis, two types of computational analyses were performed on datasets from 23-color phenotyping of Treg (described in detail in Material and Methods Chapter 3.5.5). For these analyses, firstly with CML EVs, live Tregs from each sample were downsampled in FlowJo to 7.500 events, followed by concatenation of both control and CML EVs samples and tSNE clustering (of total 120.000 cells). tSNE map was then applied to both control and CML EVs samples, allowing graphical distinction between samples (Figure 4.26). Firstly, it is already visible that control and CML EVs-treated Tregs constitute distinct subsets of cells. Moreover, control Tregs cluster rather as one big population, whereas Tregs treated with leukemic EVs are constituted by

several different subsets, which is visible by several high cell density regions on the tSNE map (Figure 4.26).

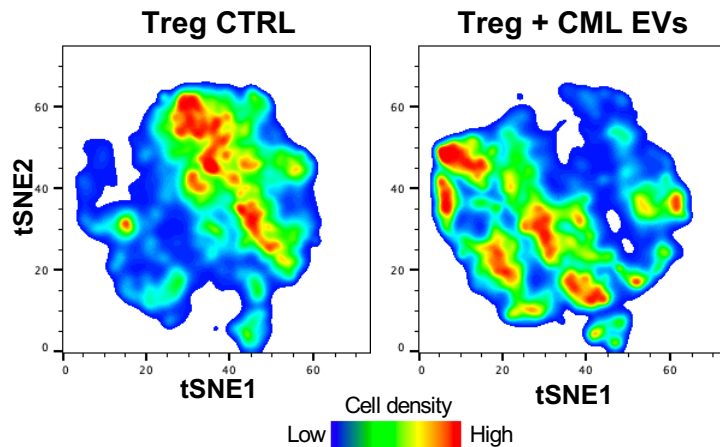


Figure 4.26 tSNE analysis of control Tregs and Tregs treated with leukemic EVs. Samples from 4 experiments (n=8 for each CTRL and CML EVs) were downsampled to 7.500 live Treg events, which were then concatenated (total of 120.000 cells) and used to create a tSNE map.

To dissect Treg heterogeneity and changes in effector, pro-leukemic Treg subsets, cells were further clustered cells using FlowSOM tool, based on 15 analyzed parameters (Figure 4.27B). FlowSOM clusters cells into specific subsets and allows precise quantification of these subsets (populations). Again, all samples from experiments with CML EVs were downsampled, concatenated into one big file (same file as for tSNE analysis above) and subjected to FlowSOM. FlowSOM has clustered Tregs into 6 populations (called Pop0, Pop1, Pop2, Pop3, Pop4, Pop5) (Figure 4.27A-B). The overlay of FlowSOM populations onto tSNE map generated above shows that both tools have identified similar clusters of cells (Figure 4.26, 4.27A). The heatmap in Figure 4.27B demonstrates expression pattern of molecules used for clustering. As Pop0 and Pop3 have expressed similar pattern of analyzed molecules (and established one cluster on tSNE, Figure 4.27A), we decided to merge these populations into merged subset Pop0+Pop3 and further quantify it as one. Amongst identified populations, Pop0+Pop3, Pop2 and Pop4 have established the largest ones and were thus investigated in more detail. Analysis of molecules expressed by these subsets has revealed that Pop2 and Pop4 have generally exhibited higher expression of receptors and factors connected to effector, tumorigenic Treg function (Figure 4.27C). Pop2 has expressed high levels of CCR8, CD30, TNFR2, CCR4, 4-1BB, TIM-3, OX-40, CD71, IL1R2, IL21R, ICOS, Foxp3, BATF, IRF4, whereas Pop4 has expressed high levels of TIGIT, CD39, CCR8, TNFR2, TIM-3, IL21R, ICOS and Foxp3. On the other hand, Pop0+Pop3 subset has exhibited rather low expression of effector markers, such as CD25, CCR4 and Foxp3 (Figure 4.27C). Based on expression patterns described, I can conclude that Pop2 and Pop4 constitute effector subsets of Tregs and can be described as CD30+CCR8^{hi}TNFR2^{hi} effector Treg1 (eTreg1, Pop2) and

CD39+TIGIT^{hi} eTreg2 (Pop4). Pop0+Pop3 constitute a less activated, non-effector CD25^{lo}Foxp3^{lo}CCR4^{lo} subset.

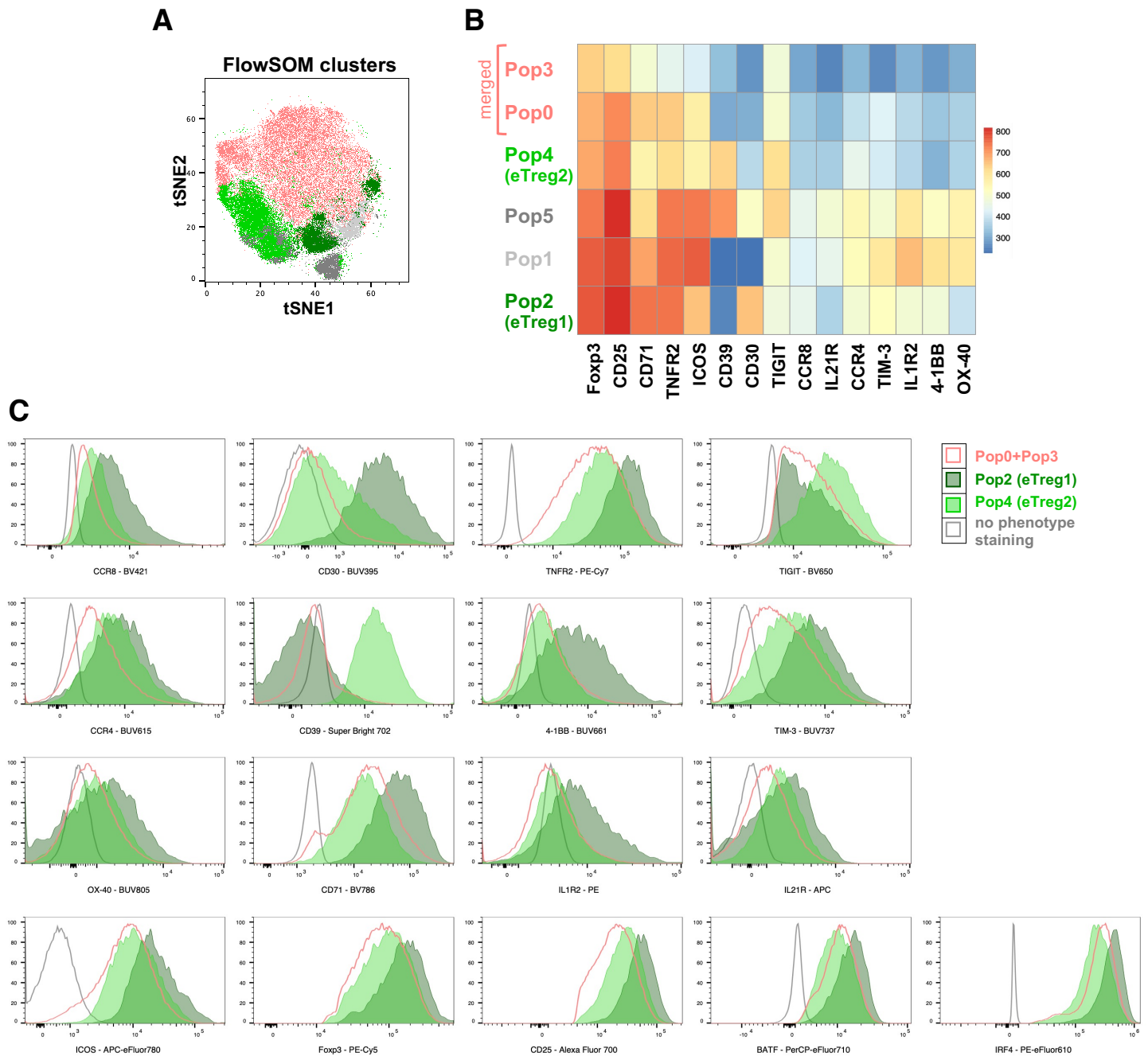


Figure 4.27 FlowSOM clustering of Tregs in *ex vivo* cultures. (A) Identified FlowSOM populations overlaid onto tSNE map generated in Figure 4.26. **(B)** Heatmap showing expression of 15 markers used for FlowSOM clustering in each of the identified Treg subsets/populations. For (A) and (B), downsampled (7.500 live Treg) events from each sample (16 samples in total, 8 per group) were used to create a FlowSOM clustering scheme. **(C)** Expression of phenotypic markers by different populations identified by FlowSOM clustering, shown on histograms.

The subsets identified by FlowSOM were then separately quantified for the control samples in comparison to Tregs treated with CML (K562) and AML (MOLM-14) extracellular vesicles, to see if

either effector or non-effector subsets expand following treatment. Both CML and AML leukemic EVs have led to significant expansion of both effector Treg subsets, eTreg1 and eTreg2. On the other hand, in leukemic EVs treated samples, the non-effector Pop0+Pop3 subset has significantly decreased (Figure 4.28A-B). Importantly, the non-effector Tregs (Pop0+Pop3) constitute practically all events in the control samples, whereas effector subsets expand and only become significant component of Tregs following treatment with leukemic EVs.

Altogether, the high-resolution spectral flow cytometric analysis has identified a specific signature of Tregs driven by leukemic EVs (expression of CD39, CCR8, CD30, Foxp3, TNFR2, CCR4, TIGIT and IL21R). These Tregs contain two effector, specialized subsets driven by leukemic EVs - CD30+CCR8^{hi}TNFR2^{hi} eTreg1 and CD39+TIGIT^{hi} eTreg2.

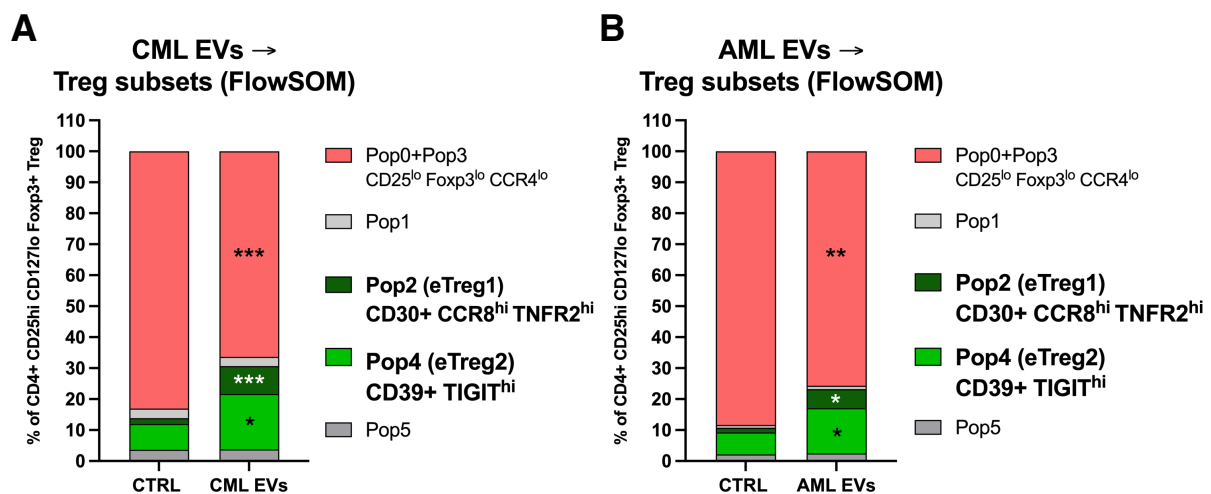


Figure 4.28 Effector Treg subsets are expanded by leukemic EVs. Distribution of human Treg subsets/populations identified by FlowSOM, in control conditions and after treatment with (A) CML (K562) or (B) AML (MOLM-14) EVs. Data are from 4 experiments (n=8) for CML EVs and 4 experiments (n=6) for AML EVs. Unpaired t-test with Welch's correction.

4.2.10 Leukemic EVs from plasma of CML and AML patients induce Foxp3 and promote effector signature of Tregs

While extracellular vesicles released by leukemic cell lines constitute a good model for *ex vivo* studies on influence of EVs, validation of findings using primary material is necessary to translate the findings into a clinical setting. To validate findings on CML and AML EVs, I have used plasma collected from peripheral blood of leukemic patients (7 CML patients and 3 AML patients) at diagnosis. Plasma of age-matched healthy donors was used as a source of control EVs.

Plasma is a much more complex biofluid than conditioned medium, thus it constitutes different challenges in terms of EVs isolation. The main challenge is high content of lipoprotein, which would co-isolate with EVs by differential ultracentrifugation or density gradient centrifugation. Therefore, EVs from patients' plasma were isolated by size exclusion chromatography (SEC), which allows to eliminate majority of lipoprotein from plasma and isolate fractions significantly enriched in extracellular vesicles. Isolation of plasma EVs by SEC was first validated. Protocol used was aimed at isolating three EVs-enriched fractions - collected fractions 7-9. Western blot analysis of protein lysates of concentrated SEC fractions 6-11 has revealed that fractions 7 to 9 were indeed enriched in EVs, as exhibited by presence of EV-marker protein Tsg101. Though lipoprotein marker APOA1 was partially present in fractions 8 and 9, it was significantly reduced compared to fractions 10 and 11 (and further fractions), so the SEC protocol has enabled to deplete most of this plasma component. GM130 (Golgi marker) was absent in all fractions, excluding contamination with cellular components/organelles (Figure 4.29A). Transmission electron microscopy imaging has demonstrated presence of extracellular vesicles in fraction 8 (most enriched in EVs as shown by Tsg101 analysis) obtained by size exclusion chromatography (Figure 4.29B). Finally, EVs isolated from plasma were quantified using nanoparticle tracking analysis. For this analysis, EVs isolated from leukemic patients and healthy donors (used in functional studies on Tregs), were measured during each experiment. The amount and size of primary plasma EVs did not differ between healthy donors and leukemic patients. Primary EVs were approximately 60nm in size, they were thus smaller than EVs isolated from leukemic cells lines (Figure 4.29C). However, these measurements may somehow be biased by presence of residual lipoprotein in the samples, as western blot analysis has still shown presence of APOA1 in fractions 8 and 9, which were used for experiments as EV-enriched (pooled fractions 7-9) (Figure 4.29A).

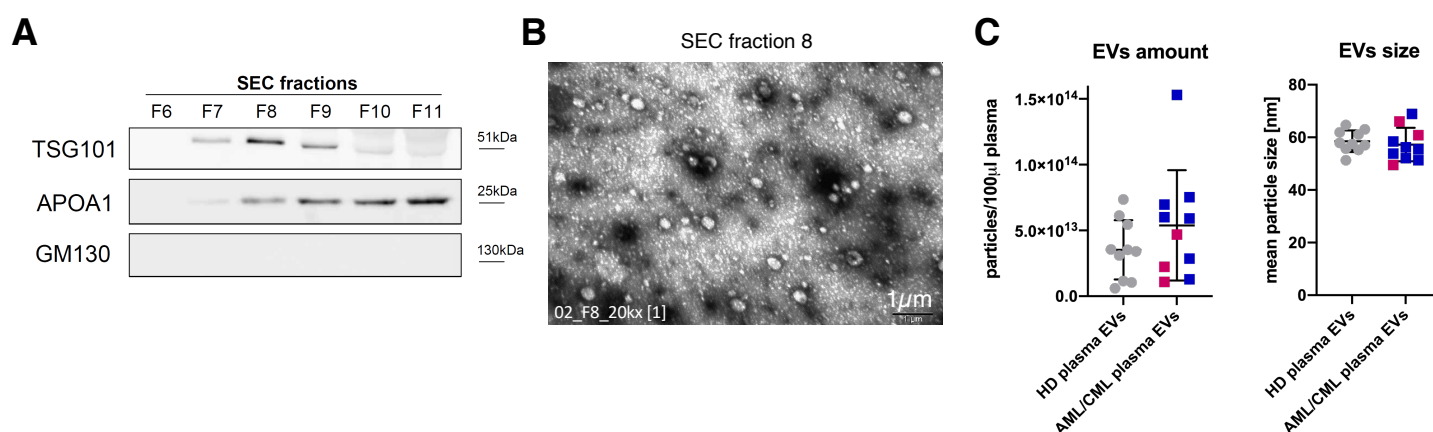


Figure 4.29 Characterization of extracellular vesicles isolated from plasma. (A) Western blot analysis of proteins enriched (Tsg101) and absent (APOA1, GM130) in EVs in fractions 6 to 11 from size exclusion chromatography EVs isolation from human plasma. Equal amount of each SEC fraction (concentrated) was loaded on the gel. **(B)** Transmission electron microscopy imaging of plasma EVs (SEC fraction 8, magnification 20kx) (representative of 2 experiments).

(Legend continued on the next page)

(C) Nanoparticle tracking analysis (quantification and size measurement) of healthy donor (HD) and AML/CML plasma EVs. Measurements of EVs from plasma of all 10 leukemic patients and healthy donors have been collected and shown on a graph bar with single data points (left). Blue dots indicate CML patients, whereas red dots AML patients.

EVs isolated from plasma of leukemic (CML, AML) patients and age-matched healthy donors were used for studies on Foxp3 induction in CD4+CD25- conventional T cells and analysis of effector phenotype of Tregs. EVs from CML and AML cell lines exerted similar effects on Tregs and immunosuppressive milieu in CML and AML described in literature are similar¹⁸. Therefore, effects of EVs from plasma of CML and AML patients were analyzed together (as leukemic EVs) and single data points from CML and AML were color-marked for information. Firstly, sorted CD4+CD25- conventional T cells (Tconv) were cultured with primary plasma EVs. Compared to EVs from healthy donors, plasma EVs of leukemic origin led to significant increase in the amount of CD25^{hi}Foxp3⁺ induced regulatory T cells (Figure 4.30). This confirms findings on EVs released by CML cell line K562 and AML cell line MOLM-14 (Figure 4.10). Moreover, this experiment confirms that the induction of Foxp3-expressing cells from CD25- Tconv is specific to leukemic EVs, as primary EVs from healthy donors have led to significantly lower amount of induced Foxp3⁺ Tregs.

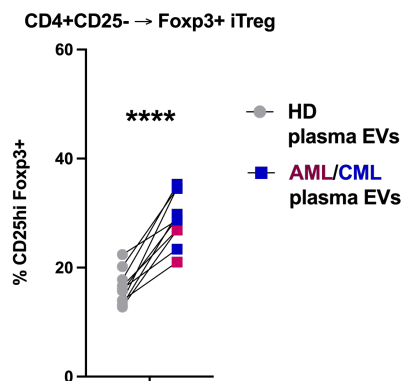


Figure 4.30 Leukemic EVs from patients' plasma induce Foxp3 and iTregs from non-regulatory conventional T cells. Induction of CD25^{hi}Foxp3⁺ iTregs after treatment with primary EVs from plasma of healthy donors and CML/AML patients. Data are from 10 experiments, each has compared one leukemic patient and one healthy donor. For leukemic group – plasma from 3 AML and 7 CML patients were used. Two-tailed paired t-test, single data points, connected for each experiment, are shown, pairing was done for EVs samples that were used to treat the same batch of (primary) CD4+CD25- T cells. Gating strategy is shown in Figure 3.12.

Furthermore, to verify influence on the Treg suppressive phenotype, primary plasma EVs were used to treat mature, sorted CD4+CD25^{hi}CD127^{lo} Tregs, in experiments analogical to those in Chapter 4.2.9. Tregs treated with plasma EVs were subjected to 23-color phenotyping, using spectral flow cytometry. Expression of several molecules was significantly upregulated by EVs from plasma of CML and AML patients. These have included CD39, CCR4, TNFR2, TIGIT, CCR8 and IL21R. In majority of experiments, also CD30 was upregulated, though the difference did not reach

statistical significance (Figure 4.31). The expression of remaining molecules, including the Foxp3 transcription factor, was not influenced by primary leukemic EVs (data not shown). Molecules upregulated by primary leukemic EVs were consistent with the effector Treg signature identified in Chapter 4.2.9, again confirming findings from EVs released by leukemic cell lines K562 and MOLM-14.

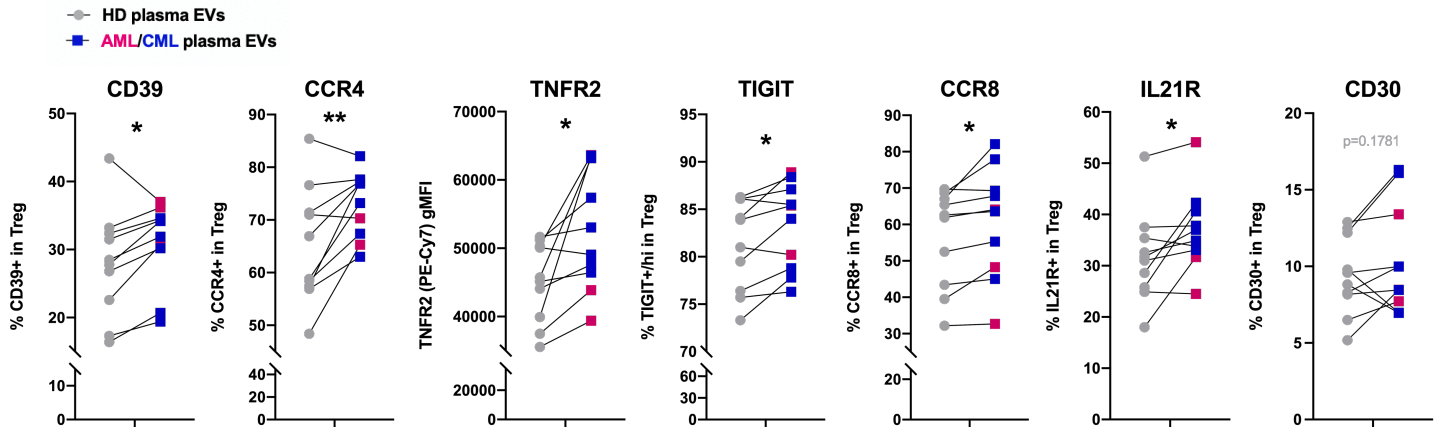


Figure 4.31 Leukemic EVs from patients' plasma upregulate expression of effector molecules on Tregs. Expression of CD39, CCR4, TNFR2, TIGIT, CCR8, IL21R, CD30 after treatment with primary EVs from plasma of healthy donors and CML/AML patients. For TNFR2 - gMFI was analyzed, for remaining molecules - % of positive cells. Data are from 10 experiments, each has compared one leukemic patient and one healthy donor. For leukemic group – plasma from 3 AML and 7 CML patients was used. Two-tailed paired t-test, single data points, connected for each experiment, are shown, pairing was done for EVs samples that were used to treat the same batch of (primary) Tregs. Gating strategy is shown in Figure 3.7.

Altogether, experiments performed using primary leukemic EVs from plasma of CML and AML patients have confirmed observations from experiments performed on K562- and MOLM-14-derived EVs. Primary leukemic EVs have led to induction of Foxp3 in CD4+CD25- conventional T cells, as well as upregulated effector signature of mature Tregs - expression of CD39, CCR4, TNFR2, TIGIT, CCR8 and IL21R.

4.2.11 Leukemic EVs contain 4-1BBL/CD137L protein

The final steps of experiments on human EVs and T cells aimed at identifying factors in EVs that may contribute to the expansion of effector Tregs. As mostly proteins have been implicated in control of Tregs cells, the proteome of leukemic EVs was investigated, in search of potential modulators of Tregs. EVs released by CML K562 cells, used for majority of experiments above, were also subjected to proteome analysis by mass spectrometry. CML (K562) EVs were isolated by differential ultracentrifugation, followed by protein extraction and analysis by liquid chromatography-mass spectrometry (LC-MS). Firstly, mass spectrometry has identified 2036 proteins in EVs preparations. Amongst identified proteins were EVs makers such as CD63, CD81, Tsg101, Alix, flotilin-1, flotilin-2 and others, confirming that protein preparations analyzed were

indeed preparations of EVs. To facilitate evaluation of a large protein dataset, identified proteins were functionally annotated using David Bioinformatic Resources tool. Functional clustering has identified 18 clusters of "functional categories" (Table 4.1).

Table 4.1. Annotations and functional groups of proteins identified in mass spectrometric profiling of CML extracellular vesicles (continued on two pages).

Annotation Cluster 1		Enrichment Score: 97.72	Count	P_Value	Benjamini
	GOTERM_MF_DIRECT	cadherin binding involved in cell-cell adhesion	182	1,20E-102	6,20E-100
	GOTERM_CC_DIRECT	cell-cell adherens junction	188	5,20E-102	1,20E-99
	GOTERM_BP_DIRECT	cell-cell adhesion	166	1,10E-90	5,10E-87
Annotation Cluster 2		Enrichment Score: 43.58	Count	P_Value	Benjamini
	GOTERM_BP_DIRECT	nuclear-transcribed mRNA catabolic process, nonsense-mediated decay	95	2,80E-68	4,50E-65
	GOTERM_BP_DIRECT	SRP-dependent cotranslational protein targeting to membrane	83	1,10E-66	1,40E-63
	GOTERM_BP_DIRECT	viral transcription	85	8,70E-58	7,00E-55
	UP_KEYWORDS	Ribosomal protein	83	4,90E-37	2,10E-35
	GOTERM_CC_DIRECT	ribosome	80	4,10E-35	3,70E-33
	GOTERM_BP_DIRECT	translation	102	4,40E-34	3,00E-31
	KEGG_PATHWAY	Ribosome	79	3,90E-30	1,10E-27
	GOTERM_MF_DIRECT	structural constituent of ribosome	83	2,50E-25	7,50E-23
Annotation Cluster 3		Enrichment Score: 22.08	Count	P_Value	Benjamini
	UP_SEQ_FEATURE	nucleotide phosphate-binding region:GTP	92	2,60E-24	5,70E-21
	UP_KEYWORDS	GTP-binding	94	1,00E-22	2,20E-21
	GOTERM_MF_DIRECT	GTP binding	108	2,30E-21	4,90E-19
Annotation Cluster 4		Enrichment Score: 19.79	Count	P_Value	Benjamini
	UP_KEYWORDS	Proteasome	42	1,10E-32	4,30E-31
	GOTERM_CC_DIRECT	proteasome complex	45	3,30E-31	2,50E-29
	GOTERM_BP_DIRECT	anaphase-promoting complex-dependent catabolic process	46	1,00E-23	4,40E-21
	GOTERM_BP_DIRECT	regulation of cellular amino acid metabolic process	36	1,20E-22	4,90E-20
	GOTERM_BP_DIRECT	negative regulation of ubiquitin-protein ligase activity involved in mitotic cell cycle	42	4,80E-22	1,80E-19
	GOTERM_BP_DIRECT	positive regulation of ubiquitin-protein ligase activity involved in regulation of mitotic cell cycle transition	43	1,60E-21	5,30E-19
	GOTERM_BP_DIRECT	Wnt signaling pathway, planar cell polarity pathway	46	3,80E-20	1,20E-17
	GOTERM_BP_DIRECT	antigen processing and presentation of exogenous peptide antigen via MHC class I, TAP-dependent	37	2,60E-19	7,70E-17
	KEGG_PATHWAY	Proteasome	34	1,10E-18	1,50E-16
	GOTERM_BP_DIRECT	NIK/NF-kappaB signaling	37	2,10E-18	5,50E-16
	GOTERM_BP_DIRECT	positive regulation of canonical Wnt signaling pathway	46	1,20E-14	2,50E-12
	GOTERM_BP_DIRECT	tumor necrosis factor-mediated signaling pathway	42	3,20E-12	5,30E-10
	GOTERM_BP_DIRECT	negative regulation of canonical Wnt signaling pathway	46	1,70E-09	1,90E-07
Annotation Cluster 5		Enrichment Score: 16.16	Count	P_Value	Benjamini
	UP_SEQ_FEATURE	short sequence motif:Effector region	45	8,30E-20	1,20E-16
	INTERPRO	Small GTP-binding protein domain	58	8,40E-18	1,10E-14
	UP_SEQ_FEATURE	lipid moiety-binding region:S-geranylgeranyl cysteine	42	6,40E-16	7,40E-13
	INTERPRO	Small GTPase superfamily	47	5,40E-14	4,90E-11
Annotation Cluster 6		Enrichment Score: 13.31	Count	P_Value	Benjamini
	GOTERM_BP_DIRECT	stimulatory C-type lectin receptor signaling pathway	47	3,70E-18	9,30E-16
	GOTERM_BP_DIRECT	T cell receptor signaling pathway	48	3,50E-12	5,60E-10
	GOTERM_BP_DIRECT	Fc-epsilon receptor signaling pathway	53	9,30E-12	1,40E-09
Annotation Cluster 7		Enrichment Score: 11.63	Count	P_Value	Benjamini
	GOTERM_CC_DIRECT	eukaryotic translation initiation factor 3 complex	16	1,30E-13	4,40E-12
	GOTERM_CC_DIRECT	eukaryotic 48S preinitiation complex	14	1,00E-11	2,90E-10
	GOTERM_CC_DIRECT	eukaryotic 43S preinitiation complex	14	1,00E-11	2,90E-10

Annotation Cluster 8		Enrichment Score: 10.88	Count	P_Value	Benjamini
	INTERPRO	Nucleotide-binding, alpha-beta plait	67	8,50E-13	5,80E-10
	SMART	RRM	58	1,80E-12	8,40E-10
	INTERPRO	RNA recognition motif domain	58	2,10E-11	9,50E-09
	GOTERM_MF_DIRECT	nucleotide binding	77	9,60E-10	8,20E-08
Annotation Cluster 9		Enrichment Score: 9.12	Count	P_Value	Benjamini
	UP_KEYWORDS	Viral nucleoprotein	18	1,50E-11	2,10E-10
	GOTERM_CC_DIRECT	viral nucleocapsid	18	8,50E-11	2,20E-09
	UP_KEYWORDS	Virion	18	3,50E-07	3,80E-06
Annotation Cluster 10		Enrichment Score: 8.43	Count	P_Value	Benjamini
	UP_SEQ_FEATURE	domain:PCI	14	5,60E-10	3,60E-07
	INTERPRO	Proteasome component (PCI) domain	13	3,30E-09	1,10E-06
	SMART	PINT	12	2,80E-08	6,60E-06
Annotation Cluster 11		Enrichment Score: 7.79	Count	P_Value	Benjamini
	UP_SEQ_FEATURE	repeat:HEAT 6	17	1,10E-09	6,30E-07
	UP_SEQ_FEATURE	repeat:HEAT 5	18	2,30E-09	1,10E-06
	UP_SEQ_FEATURE	repeat:HEAT 4	19	1,50E-08	6,60E-06
	UP_SEQ_FEATURE	repeat:HEAT 3	20	3,90E-08	1,60E-05
	UP_SEQ_FEATURE	repeat:HEAT 2	21	1,10E-07	4,20E-05
	UP_SEQ_FEATURE	repeat:HEAT 1	21	1,10E-07	4,20E-05
Annotation Cluster 12		Enrichment Score: 7.75	Count	P_Value	Benjamini
	GOTERM_BP_DIRECT	tRNA aminoacylation for protein translation	24	7,10E-13	1,30E-10
	UP_KEYWORDS	Aminoacyl-tRNA synthetase	19	9,20E-10	1,20E-08
	KEGG_PATHWAY	Aminoacyl-tRNA biosynthesis	19	8,70E-03	7,30E-02
Annotation Cluster 13		Enrichment Score: 7.73	Count	P_Value	Benjamini
	GOTERM_CC_DIRECT	proteasome core complex	15	6,80E-10	1,60E-08
	UP_KEYWORDS	Threonine protease	14	1,10E-09	1,40E-08
	INTERPRO	Proteasome, subunit alpha/beta	14	1,30E-09	5,00E-07
	GOTERM_MF_DIRECT	threonine-type endopeptidase activity	14	2,10E-08	1,60E-06
	GOTERM_BP_DIRECT	proteolysis involved in cellular protein catabolic process	16	1,00E-04	4,30E-03
Annotation Cluster 14		Enrichment Score: 5.53	Count	P_Value	Benjamini
	GOTERM_CC_DIRECT	SNARE complex	20	4,80E-07	7,50E-06
	GOTERM_MF_DIRECT	SNAP receptor activity	17	9,80E-07	4,50E-05
	KEGG_PATHWAY	SNARE interactions in vesicular transport	16	5,70E-05	9,40E-04
Annotation Cluster 15		Enrichment Score: 5.38	Count	P_Value	Benjamini
	INTERPRO	Chaperonin TCP-1, conserved site	9	7,50E-08	1,80E-05
	GOTERM_CC_DIRECT	chaperonin-containing T-complex	9	9,00E-08	1,50E-06
	INTERPRO	Chaperone tailless complex polypeptide 1 (TCP-1)	10	1,50E-07	3,10E-05
	GOTERM_BP_DIRECT	positive regulation of protein localization to Cajal body	8	1,20E-06	8,40E-05
	INTERPRO	GroEL-like equatorial domain	10	2,60E-06	4,40E-04
	INTERPRO	TCP-1-like chaperonin intermediate domain	9	3,10E-06	5,00E-04
	INTERPRO	Chaperonin Cpn60/TCP-1	10	5,40E-06	8,10E-04
	INTERPRO	GroEL-like apical domain	10	5,40E-06	8,10E-04
	GOTERM_CC_DIRECT	zona pellucida receptor complex	7	6,90E-05	6,70E-04
	GOTERM_BP_DIRECT	binding of sperm to zona pellucida	8	7,60E-02	7,00E-01
Annotation Cluster 16		Enrichment Score: 5.11	Count	P_Value	Benjamini
	GOTERM_BP_DIRECT	canonical glycolysis	14	6,80E-07	5,00E-05
	UP_KEYWORDS	Glycolysis	14	1,20E-06	1,20E-05
	GOTERM_BP_DIRECT	glycolytic process	12	6,00E-04	1,90E-02
Annotation Cluster 17		Enrichment Score: 5.06	Count	P_Value	Benjamini
	UP_SEQ_FEATURE	repeat:HEAT 8	11	1,90E-06	5,30E-04
	UP_SEQ_FEATURE	repeat:HEAT 9	9	1,90E-05	2,90E-03
	UP_SEQ_FEATURE	repeat:HEAT 10	9	1,90E-05	2,90E-03
Annotation Cluster 18		Enrichment Score: 5.01	Count	P_Value	Benjamini
	INTERPRO	Like-Sm (LSM) domain	12	6,40E-06	9,10E-04
	INTERPRO	Ribonucleoprotein LSM domain	11	1,10E-05	1,40E-03
	SMART	Sm	11	1,30E-05	1,50E-03

Annotation cluster 4 has included several groups of proteins connected to immune response, such as "GO:0033209~tumor necrosis factor-mediated signaling pathway", "GO:0038061~NIK/NF-kappaB signaling" and "GO:0002479~antigen processing and presentation of exogenous peptide antigen via MHC class I, TAP-dependent" (Figure 4.32A). Closer analysis of these categories has prompted investigation of molecules from the TNF and TNF receptor superfamilies. Indeed, mass spectrometry has identified presence of four proteins from these families - TNFSF9 (4-1BBL), TNFRSF8 (CD30), TNFRSF1B (TNFR2) and TNFRSF10A (DR4) (Figure 4.32B). As CD30, TNFR2 and DR4 themselves are also expressed by T cells (rather than constitute ligands for receptors on T cells), I hypothesized that TNFSF9/4-1BBL is most likely to modulate Tregs via interaction with 4-1BB receptor. Signaling via TNF superfamily molecules and ligands, including 4-1BBL/4-1BB, has been recently implicated in control of Treg biology, although predominantly in the intestine and during pathological states, such as colitis⁸¹⁻⁸³. Therefore, it may also be a potential modulator of Tregs in leukemia. Presence of 4-1BBL in leukemic EVs was validated by antibody-based technique (western blotting). Indeed, 4-1BBL was present in CML (K562) EVs and in AML EVs released by MOLM-14 cells (Figure 4.32C). Altogether, mass spectrometric profiling of leukemic EVs' proteome has revealed their immunomodulatory content, such as molecules from TNF/TNF receptor superfamilies, including 4-1BBL/TNFSF9 (also recognized as CD137L).

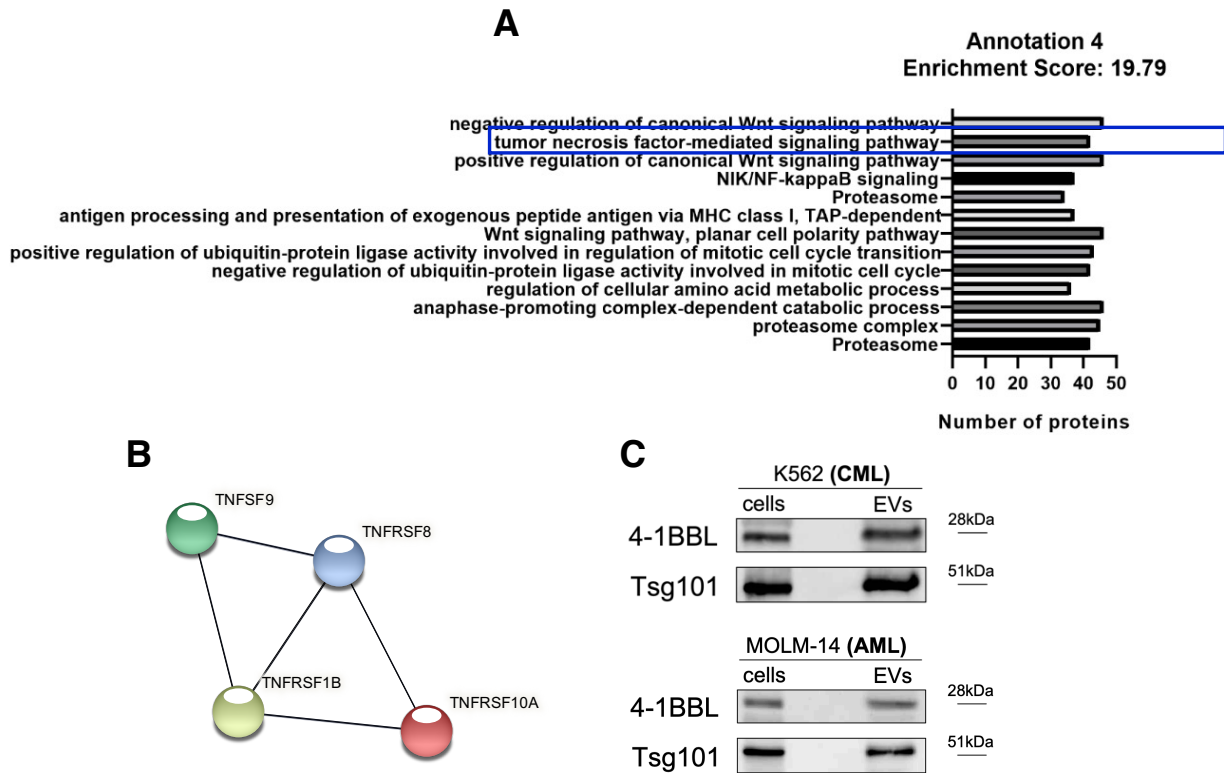


Figure 4.32 Leukemic EVs contain proteins from TNF/TNF receptor superfamilies, including 4-1BBL/TNFSF9/CD137L. (A) Protein groups identified in Annotation 4 (Table 4.1) of the functional analysis of mass spectrometric profiling of leukemic (K562) EVs. Number of proteins in each group is indicated. Data are from 4 experiments. (B) Members of TNF (TNFSF9/4-1BBL) and TNF receptor (TNFRSF1B/TNFR2, TNFRSF8/CD30, TNFRSF10A/DR4) superfamilies identified in the mass spectrometric profiling of CML EVs. (C) Western blot validation of 4-1BBL expression in EVs released by K562 (CML) and MOLM-14 (AML) cells. Equal amount of cellular and EVs' protein was loaded on the gel. Blots are representative of 4 experiments (CML EVs) and 2 experiments (AML EVs).

4.2.12 4-1BBL protein in leukemic EVs partially regulates effector Treg phenotype

To validate if 4-1BBL protein in leukemic EVs may be engaged in Treg functionality, a CML K562 cell line without expression of this protein was obtained by CRISPR/Cas9 methodology (Figure 4.33A). The knock-out of 4-1BBL in cells has also resulted in lack of 4-1BBL protein in K562-derived extracellular vesicles (Figure 4.33A). This proves that the established cellular model is an appropriate tool to study role of 4-1BBL, contained in leukemic EVs, in modulation of Tregs. For these experiments, EVs released by parental (CML wt) and 4-1BBL-deficient (CML 4-1BBL^{-/-}) K562 cells were isolated and simultaneously used to treat human Tregs. Following culture (as in the experiments above, Chapters 4.2.4 and 4.2.9), Tregs were subjected to the 23-color phenotyping by spectral flow cytometry. This aimed at identifying features of Tregs that were upregulated by leukemic EVs and could be influenced by 4-1BBL in CML EVs. Indeed, following treatment with 4-1BBL-deficient EVs, three effector receptors were no longer upregulated by Tregs treated with CML EVs - LAG-3, CD30 and TNFR2 (Figure 4.33B). CD30 and TNFR2 constitute receptors from the

TNF receptor family, suggesting modulation of TNF/TNFR superfamily members by each other (here, by 4-1BBL/4-1BB interaction).

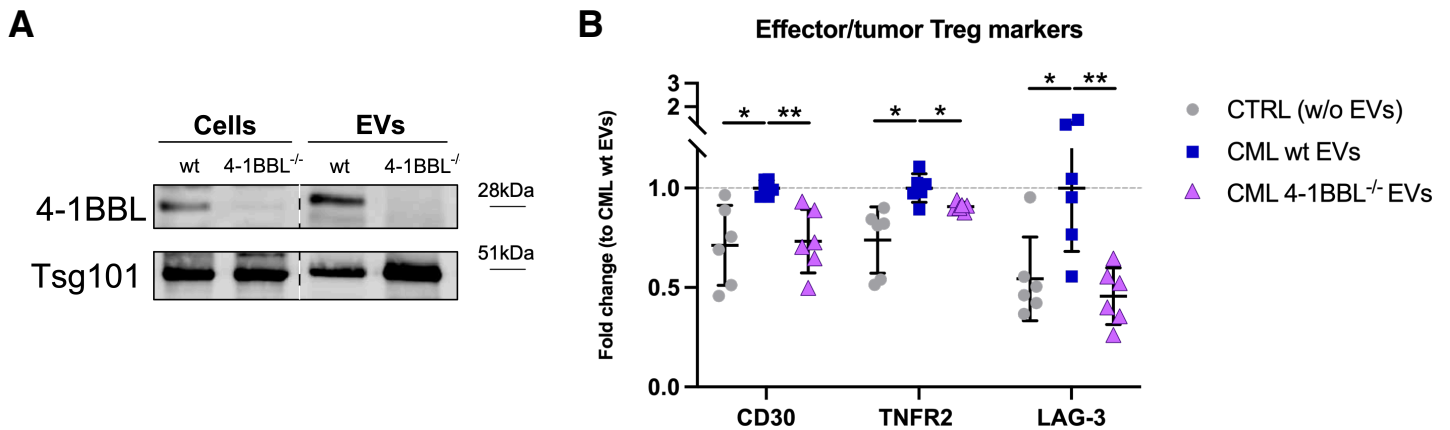


Figure 4.33 4-1BBL protein in EVs partially modulates effector Treg phenotype upregulated by leukemic EVs. (A) Western blot analysis of 4-1BBL in wild-type and 4-1BBL-deficient K562 cells and K562-derived EVs. Dashed line marks that all samples were run on the same gel. Equal amount of cellular and EVs' protein was loaded on the gel. (B) Expression of CD30, TNFR2 and LAG-3 on Tregs after treatment with wt or 4-1BBL-deficient CML (K562) EVs. For TNFR2 - gMFI was analyzed, for CD30 and LAG-3 - % of positive cells. Values were normalized to average values of CML wt EVs samples in each experiment and plotted as fold change. Data are from 3 experiments (n=6). Unpaired t-test with Welch's correction, single data points and mean \pm SD are shown. Gating strategy is shown in Figure 3.7.

Altogether, mass spectrometric analysis of the proteome of leukemic (CML, K562-derived) extracellular vesicles revealed presence of a TNF superfamily protein 4-1BBL (CD137L/TNFSF9). Deficiency of 4-1BBL protein in leukemic EVs has affected interaction between EVs and Tregs, revealing the role of 4-1BBL in driving expression of CD30, TNFR2 and LAG-3 on Treg cells.

4.3 Rab27a-dependent extracellular vesicles promote development of leukemia and expand immunosuppressive regulatory T cells *in vivo*

The experiments presented above, using mouse and human *ex vivo* cultures, have demonstrated direct interaction between leukemic extracellular vesicles and regulatory T cells. This interaction has resulted in an amplification of Treg suppressive function, induction and amplification of Foxp3 expression, as well as expansion of effector Treg subsets. While such experiments provide direct evidence towards a studied biological phenomenon, they lack a fully physiological context - a spatial setting in a tissue, presence of other immune/non-immune cells and physiological dosing of EVs. Considering the last aspect, it is challenging (at least at this moment) to exactly extrapolate which dose (number of particles) of EVs added to an *in vitro* culture may correspond to EVs constantly released by cells *in vivo*. To evaluate all the above aspects, I have decided to perform *in vivo* studies, using mouse model of chronic myeloid leukemia-like (CML-like) disease. To evaluate the effect of EVs in an *in vivo* setting, leukemic cells were genetically modified to lack expression of a small GTPase Rab27a, a well-established regulator of EVs biogenesis¹⁴⁷. Downregulation of Rab27a leads to diminished secretion of EVs and has been used to study effects of tumor derived EVs in mouse models of cancer²⁰². The use of *in vivo* model of CML-like disease would enable not only studies of leukemic EVs relevance for Treg biology in a physiological setting, but also link these observations to leukemic development, by analysis of leukemic cell engraftment.

4.3.1 Mouse model of CML-like disease

Until now, several mouse models of BCR-ABL1+ chronic myeloid leukemia have been employed²⁵⁹. However, they were either based on xenografts of human cells (cell lines or primary patients' CD34+ blasts) into immunodeficient animals or on adoptive transfer of murine cells into irradiated or immunodeficient mice. These models would not enable studies of the immune system, especially of T cells. On the other hand, a transgenic model of BCR-ABL1-expressing leukemia developed by Koschmieder *et al.*²⁶⁰, or models based on adoptive transfer of bone marrow cells transduced to overexpress BCR-ABL1 into immunocompetent animals, may allow studies of leukemic immunity *in vivo* in mice. However, they do not facilitate stable and reproducible silencing of genes in leukemic cells for genetic studies, to analyze relevance of functional proteins *in vivo*.

Therefore, I have decided to try and induce leukemia-like disease by adoptive transfer of 32D BCR-ABL1+GFP+ cells into immunocompetent animals of the C3H strain (same genetic background as 32D cells). This would enable induction of leukemia-like disease by cells with stable knock-out of Rab27a, as well as enable tracking of leukemic cells that express GFP. Initial attempts to inject 32D BCR-ABL1+GFP+ cells either intravenously or intraperitoneally have demonstrated that only intraperitoneal injection has enabled development of leukemia-like disease in animals (observed as presence of GFP+ leukemic cells in blood and bone marrow, by flow cytometry).

Previously, both routes of administration have been used in studies of different leukemias in mouse models²⁶¹. For initial set up and validation of the experimental model, 32D BCR-ABL1+GFP+luc+ cells were injected into animals. 32D BCR-ABL1+GFP+luc+ cells with stable expression of enzyme luciferase (luc), which enable whole-body imaging of leukemic cells, based on bioluminescent signal generated by luciferase activity, following injection of its substrate luciferin. Whole-body imaging of animals at different timepoints (1- and 2-months following injection of leukemic cells) has confirmed that leukemic cells engraft and gradually grow in animals (Figure 4.34A). Initial observations have also shown that animals injected with leukemic cells have started dying or have shown terminal symptoms (due to leukemia-like disease) following the 2-month timepoint. Therefore, an *in vivo* experimental model was used, where 1×10^6 32D BCR-ABL1+GFP+ cells (wt or Rab27a^{-/-}) were injected into C3H animals, followed by 2 months of CML-like disease development (before animal death or terminal symptoms) and analyses of immune cells and leukemic engraftment (Figure 4.34B).

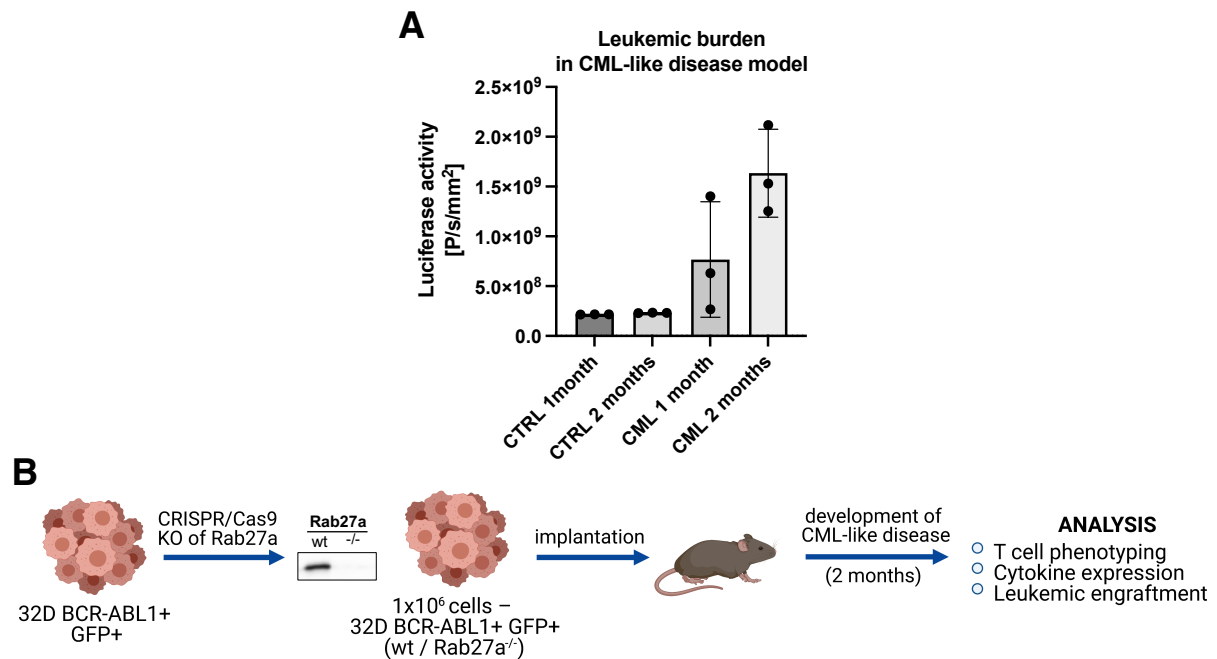


Figure 4.34 Development of leukemia/CML-like disease in mice. (A) Comparison of luciferase activity in a whole-body scan in control (CTRL) animals and specimens injected with leukemic cells with luciferase expression (32D BCR-ABL1+GFP+luc+), 1 and 2 months following implantation. n=3 animals, single data points correspond to single animals. **(B)** Schematics of experiments using mouse model of CML-like disease (the same schematic shown as in Material and Methods Figure 3.17, shown again for clarity of followed experimental process/pipeline). Figure created with BioRender.com.

Most importantly, the established mode of injection and disease trajectory lead to engraftment of GFP-expressing leukemic cells (32D BCR-ABL1+GFP+) into tissues typically engrafted by myeloid leukemias - bone marrow, spleen and blood (Figure 4.35). GFP-expressing leukemic cells were clearly visible as a separate population of GFP+ cells on dot plots from flow cytometry, compared to control animals injected with NaCl only. GFP fluorescence from cells after 2 months *in vivo* was rather unchanged compared to the same cells cultured *in vitro*.

Altogether, the developed model enables studies of CML immunity in immunocompetent mice, as well as monitoring of disease development by analysis of percentage of GFP-expressing cells in tissues. Therefore, mice injected with 32D BCR-ABL1+GFP+ cells and their Rab27a-deficient counterparts were used for further studies.

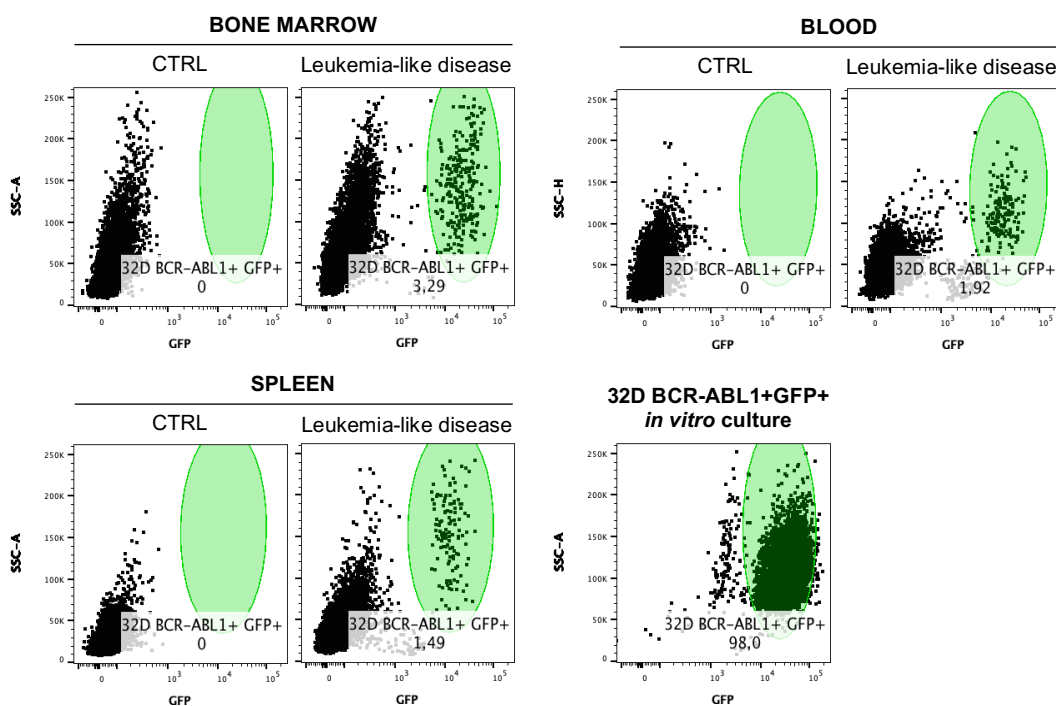


Figure 4.35 Engraftment of leukemic, GFP-expressing cells into bone marrow, blood and spleen of mice. Representative dot plots are shown, viable (7-AAD negative) cells were analyzed. GFP-expressing cells were detected by flow cytometry, as described in Chapter 3.10.3.

4.3.2 Rab27a-deficient 32D BCR-ABL1+ cells demonstrate unaffected cell growth and clonogenicity

As mentioned above, to study effect of continuous EVs release *in vivo*, in a model of leukemia-like disease, EVs secretion could be attenuated in leukemic cells by knock-out of Rab27a GTPase. Rab27a-deficient (Rab27a^{-/-}) 32D BCR-ABL1+GFP+ cells were obtained by CRISPR/Cas9 methodology. 32D BCR-ABL1+GFP+ cells were transfected with two plasmids encoding Cas9 nuclease, gRNAs towards Rab27a and RFP reporter. RFP positive cells were sorted into single wells and clones were obtained (Figure 4.36A).

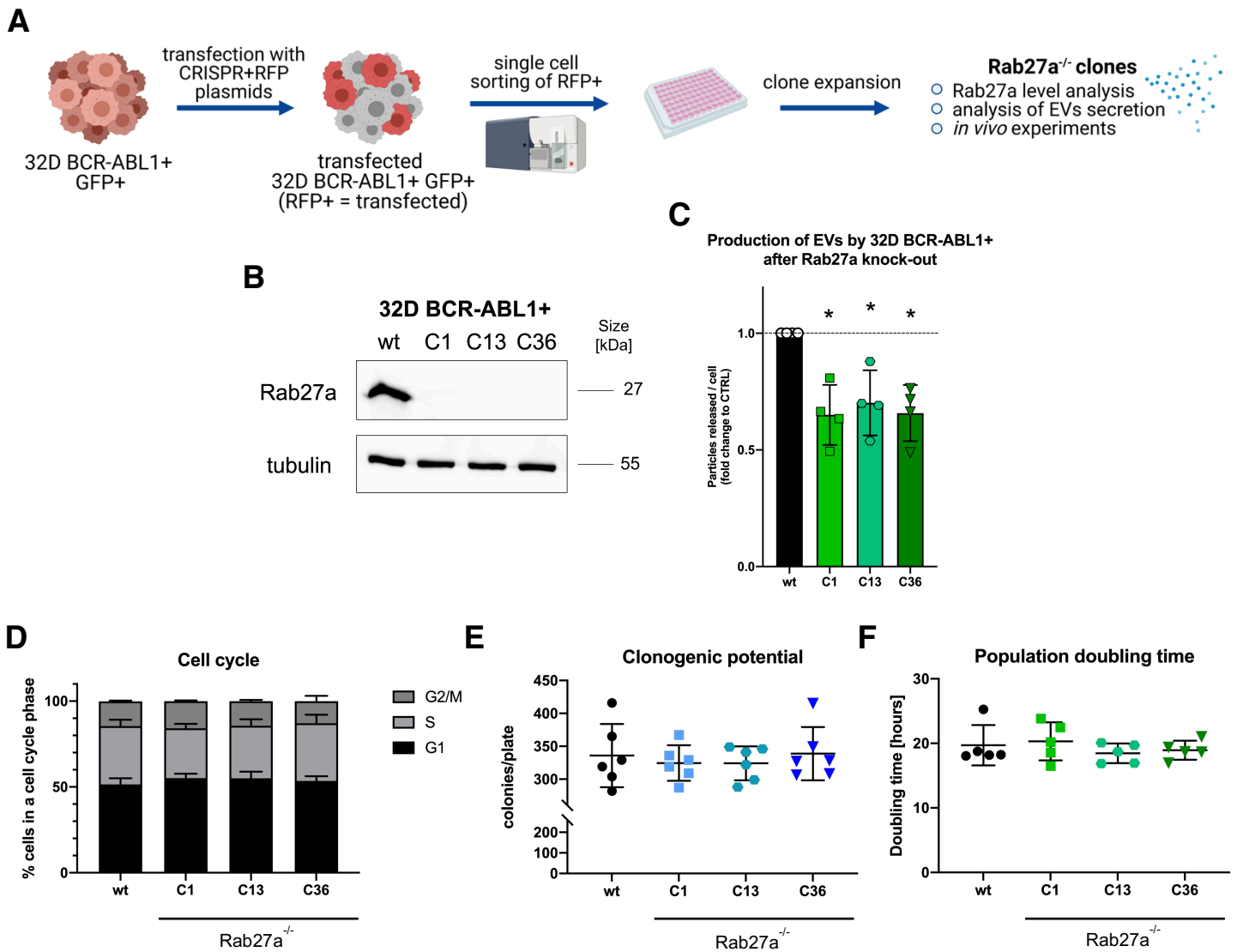


Figure 4.36 Obtaining and analysis of Rab27a-deficient CML-like cells. (A) Schematic of experimental pipeline used to obtain Rab27a-deficient clones of 32D BCR-ABL1+GFP+ cells by CRISPR/Cas9 mutagenesis (the same schematic shown as in Material and Methods Figure 3.1A, shown again for clarity of followed experimental process/pipeline). Figure created with BioRender.com. (B) Western blot analysis Rab27a protein level in wt (Parental) and Rab27a-deficient clones (C1, C13, C36) of 32D BCR-ABL1+GFP+ cells (representative of 3 experiments). (C) Nanoparticle tracking analysis of particles released by wt and Rab27a-deficient (clones C1, C13, C36) 32D BCR-ABL1+GFP+ cells. Data are from 4 experiments (n=4). Unpaired t-test with Welch's correction, single data points and mean ± SD are shown. (D) Cell cycle of wt and Rab27a-deficient 32D BCR-ABL1+GFP+ cells. Data are from 4 experiments (n=4). Unpaired t-test with Welch's correction, mean ± SD are shown. (E) Clonogenic potential of wt and Rab27a-deficient 32D BCR-ABL1+GFP+ cells. Data are from 3 experiments (n=6). Unpaired t-test with Welch's correction, single data points and mean ± SD are shown. (F) Population doubling time of wt and Rab27a-deficient 32D BCR-ABL1+GFP+ cells. Data are from 5 experiments (n=5). Unpaired t-test with Welch's correction, single data points and mean ± SD are shown.

The obtained clones were first screened for complete Rab27a knock-out (analysis by western blotting), stable GFP expression (by flow cytometry) and downregulated secretion of EVs (by nanoparticle tracking analysis). Clones 1, 13 and 36 were used for *in vitro* studies on cell growth

and clone 1 for the *in vivo* experiments. Each of these three clones had complete deficiency of Rab27a protein (Figure 4.36B) and diminished secretion of extracellular vesicles (by 30-40%), as exhibited by nanoparticle tracking analysis (Figure 4.36C). As these clones would be used for *in vivo* experiments, their basic growth parameters were first analyzed, to exclude that *in vivo* changes in the immune system or engraftment could be simply an outcome of different cell growth by Rab27a-deficient clones of 32D BCR-ABL1+GFP+ cells. Cell lines grown *in vitro* did not exhibit differences in cell cycle, population doubling time (proliferation) or clonogenicity (in a clonogenic assay in methylcellulose) (Figure 4.36D-F). Therefore, Rab27a deficiency in model cells used in this thesis does not influence basic growth parameters of leukemic cells.

4.3.3 Rab27a-deficient CML-like disease leads to CD3+ T cell compartment remodeling

The animals injected with wt and Rab27a-deficient 32D BCR-ABL1+GFP+ leukemic cells were sacrificed and blood, bone marrow and spleen were isolated. Bone marrow and spleen were used for analyses of immune cells, as I wanted to focus specifically on immunity in tissues crucial to development of CML at all stages of the disease. The main analysis was phenotyping of CD3+ T cells in these tissues, as described in Materials and Methods Chapter 3.10.4. To initially assess changes in the CD3+ T cell compartment, tSNE unsupervised cell clustering was performed on CD3+ T cells from the spleen, based on expression of 9 markers (Figure 4.37B). As the spleen contains larger numbers of T cells than the bone marrow, it enabled to obtain tSNE data of higher resolution.

First glimpse at tSNE maps from CTRL and leukemic (CML wt) animals already demonstrates how significantly the T cell compartment became remodeled by leukemia-like disease. Both CD4+ and CD8+ T cells exhibited completely different density in several regions of the tSNE map. Relevantly to the topic of this thesis, significantly more cells have localized in the region of high Foxp3 expression in mice with leukemia-like disease (Figure 4.37A-B). CD4+ and CD8+ in control mice have predominantly localized in regions of high CD62L expression, demonstrating their naive phenotype. On the other hand, in leukemic animals CD4+ T cells seemed to predominantly consist of CD44-expressing Foxp3+ Treg cells (Figure 4.37A-B). CD8+ T cells in leukemic animals have formed a new, distinct cluster of cells with high expression of CD39 and low expression of both CD62L and CD44 (marked in red on Figure 4.38A). Such CD39 expressing CD8+ T cells have been previously deemed as dysfunctional in patients with melanoma²⁶².

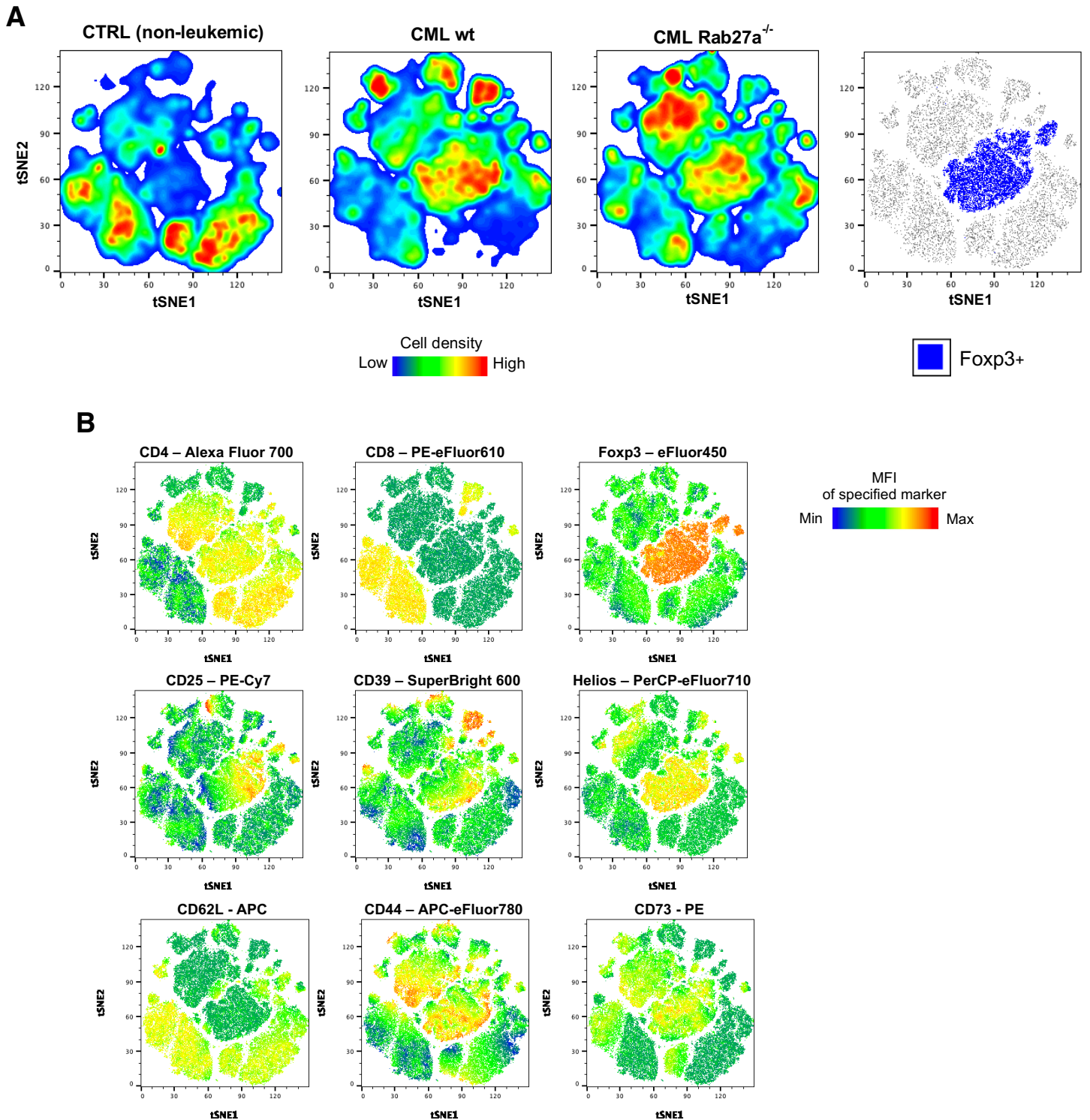


Figure 4.37 tSNE analysis reveals remodeling of CD3⁺ T cell compartment in the spleen of leukemic mice. (A) CD3⁺ T cells from spleens of either CTRL (non-leukemic) or leukemic (wt or Rab27a-deficient CML) animals were clustered using unsupervised tSNE approach. Distribution of cells in each experimental condition is shown on a separate graph. Localization of Foxp3⁺ cells (Tregs) on tSNE map is marked as a blue population on the graph on far right. tSNE was run on 90,000 cells. CD3⁺ cells were downsampled and concatenated in FlowJo to generate 30,000 cells from each experimental condition (3-4 animals per group). **(B)** Expression of specified proteins on tSNE maps.

When comparing leukemia-like disease induced by wild-type (wt) and Rab27a-deficient 32D BCR-ABL1+GFP+ cells, one can notice different clustering and density of cells in the Foxp3+ area of the tSNE map. Tregs in CML wt predominantly clustered in region of high expression of CD25, CD39 and CD44, which is not the case in Rab27a-deficient leukemia (Figure 4.37A-B). Therefore, detailed manual gating analysis of Tregs in animals was performed and is described in the next chapter. Moreover, in Rab27a-deficient leukemia, more CD4+Foxp3- cells localized in the region of high CD44 expression (marked in blue on Figure 4.38A), suggesting expansion of activated, effector CD44+ T cells, when secretion of leukemic EVs was diminished. On the other hand, it seemed like cluster of dysfunctional CD8+CD39+ cells (marked in red on Figure 4.38A) was smaller in case of Rab27a-deficient leukemia (Figure 4.38B). Both subsets were therefore analyzed by manual gating in the entire dataset of animals in both spleen and bone marrow, indeed confirming remodeling of both CD4+Foxp3-CD44+CD62L- (activated Tconv) and CD8+CD39+ (dysfunctional CD8+ cells) by CML-like disease itself, as well as partially by EVs released by leukemic cells (Figure 4.38B).

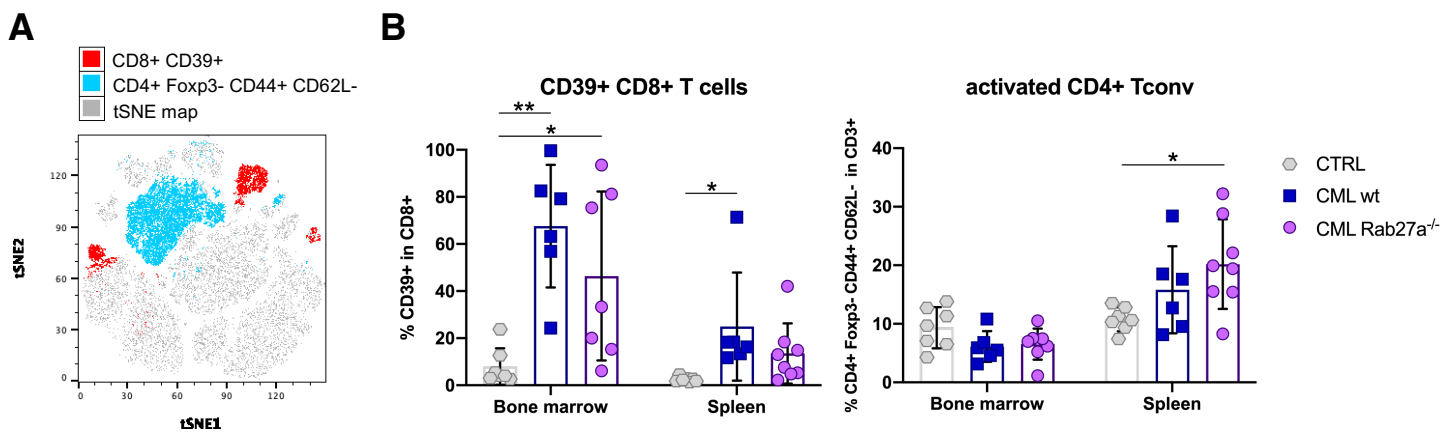


Figure 4.38 Non-Treg T cell subsets are affected *in vivo* by leukemia development and secretion of EVs by leukemic cells. (A) Localization of dysfunctional CD8+CD39+ cells and activated CD4+Foxp3-CD44+CD62L- conventional T cells on the generated tSNE map of CD3+ T cells **(B)** Amount of dysfunctional CD8+CD39+ cells and activated CD4+Foxp3-CD44+CD62L- conventional T cells in spleen and bone marrow of animals with leukemia-like disease. Data are from 3 experiments (n=7 CTRL mice, 6 CML wt mice, 8 CML Rab27a^{-/-} mice). One-way ANOVA with Tukey's posttest, single data points and mean \pm SD are shown.

Altogether, leukemia-like disease leads to remodeling of the CD3+ T cells compartment, affecting regulatory T cells and non-Treg CD4+/CD8+ T cells. Some of these changes seem to be influenced by Rab27a-dependent secretion of extracellular vesicles.

4.3.4 Rab27a-dependent EVs secretion *in vivo* modulates Tregs in the spleen and bone marrow of leukemia bearing mice

The main aim of studies using mouse model of leukemia-like disease was to assess whether Rab27a-dependent secretion of leukemic EVs may affect Treg cells *in vivo*. Therefore, Tregs from bone marrow and spleen were subjected to cell phenotyping by flow cytometry, to identify their amount, activation status and expression of suppressive molecules. As already revealed by unsupervised tSNE clustering (Figure 4.37), Foxp3⁺ Tregs undergo significant remodeling during CML-like disease in mice, which was also affected by Rab27a-dependent secretion of EVs. Thus, Tregs were analyzed in detail by manual gating and analysis of phenotypic features.

Firstly, amount of regulatory T cells was analyzed in the spleen and the bone marrow (BM). Development of CML-like disease led to significant increase in the amount of Foxp3⁺ Tregs in the bone marrow (two-fold increase compared to healthy animals) and the spleen (three-fold increase). Such trend corresponds to changes observed in patients with myeloid leukemias^{20,21,25}, therefore proving the applicability of developed mouse model for studies on Tregs in CML. Rab27a deficiency led to significantly lower amount of Tregs in the spleen of mice, but not in the bone marrow (Figure 4.39).

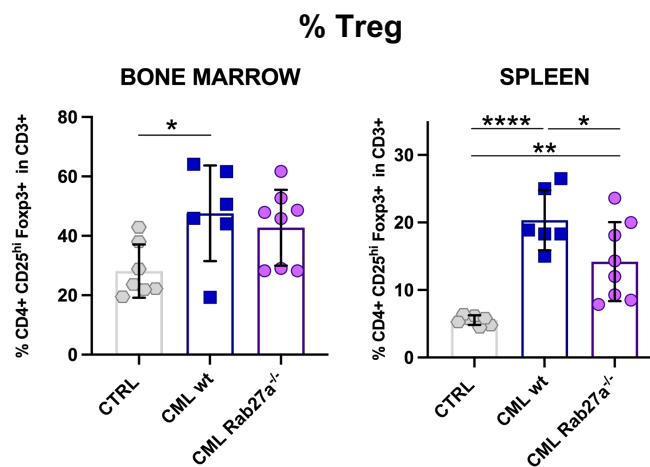


Figure 4.39 Treg levels are elevated in CML-like disease in both BM and spleen and are regulated by Rab27a-dependent EVs in the spleen. Data are from 3 experiments (n=7 CTRL mice, 6 CML wt mice, 8 CML Rab27a^{-/-} mice). One-way ANOVA with Tukey's posttest, single data points and mean \pm SD are shown. Gating strategy is shown in Figure 3.18.

In both spleen and bone marrow of animals with CML-like disease, there was a significant expansion of CD44+CD62L- activated Treg cells. Such phenotype represents Treg cells that were activated due to specific stimuli and perform suppressive function in the microenvironment which in this case corresponds to a pro-leukemic activity. On the other hand, naive Tregs were less abundant in animals with CML-like disease. In both spleen and bone marrow, deficiency of Rab27a in leukemic cells has led to decrease in the amount of activated, CD44+CD62L- Tregs. Therefore, leukemic EVs constitute a factor that promotes activity and suppressive function of Tregs *in vivo* (Figure 4.40A-B).

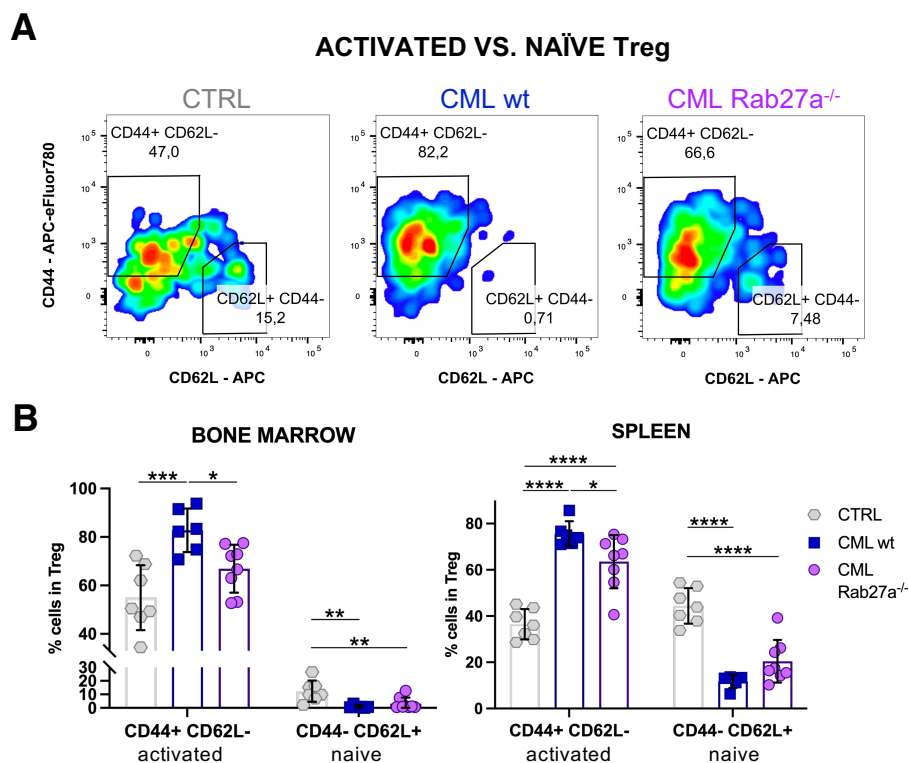


Figure 4.40 Tregs in CML-like disease exhibit an activated, CD44+CD62L- phenotype, which is driven by Rab27a-dependent EVs. (A) Representative density plots of distribution of CD44+CD62L- (activated) and CD44-CD62L+ (naive) Treg cells in the bone marrow of mice. **(B)** Amount of CD44+CD62L- (activated) and CD44-CD62L+ (naive) Treg cells in the bone marrow and spleen of mice. Data are from 3 experiments (n=7 CTRL mice, 6 CML wt mice, 8 CML Rab27a^{-/-} mice). One-way ANOVA with Tukey's posttest, single data points and mean \pm SD are shown. Gating strategy is shown in Figure 3.18.

To possibly identify specific molecules that correspond to stronger activation of Tregs *in vivo*, in the model of CML-like disease, expression of three suppressive molecules was analyzed. Expression of ectonucleosidases CD39 and CD73 and regulatory cytokine IL-10 (IL-10 only in splenic Tregs, by intracellular cytokine staining) were analyzed. All these suppressive features were elevated in Tregs in the bone marrow and spleen of animals with CML-like disease. However, their regulation by Rab27a-dependent extracellular vesicles was not as straightforward. Leukemic EVs were

partially responsible for elevated expression of CD39 in the spleen, but not in the bone marrow. On the other hand, leukemic EVs have not influenced CD73 in the spleen, but have significantly elevated levels of CD73 on Tregs in the bone marrow. Rab27a-dependent secretion of EVs was also crucial for elevated production of IL-10 by Tregs (Figure 4.41A-C). These differences in regulation of Treg suppressive features by Rab27a-dependent EVs are not straightforward and need further studies for full understanding. However, they are most likely due to different microenvironments of spleen and bone marrow. While spleen is mainly occupied by B cells and T cells, cells predominant in the bone marrow are myeloid progenitors. Therefore, Treg cells during leukemia development in either spleen or bone marrow may perform different functions and therefore be differentially modulated by leukemic EVs.

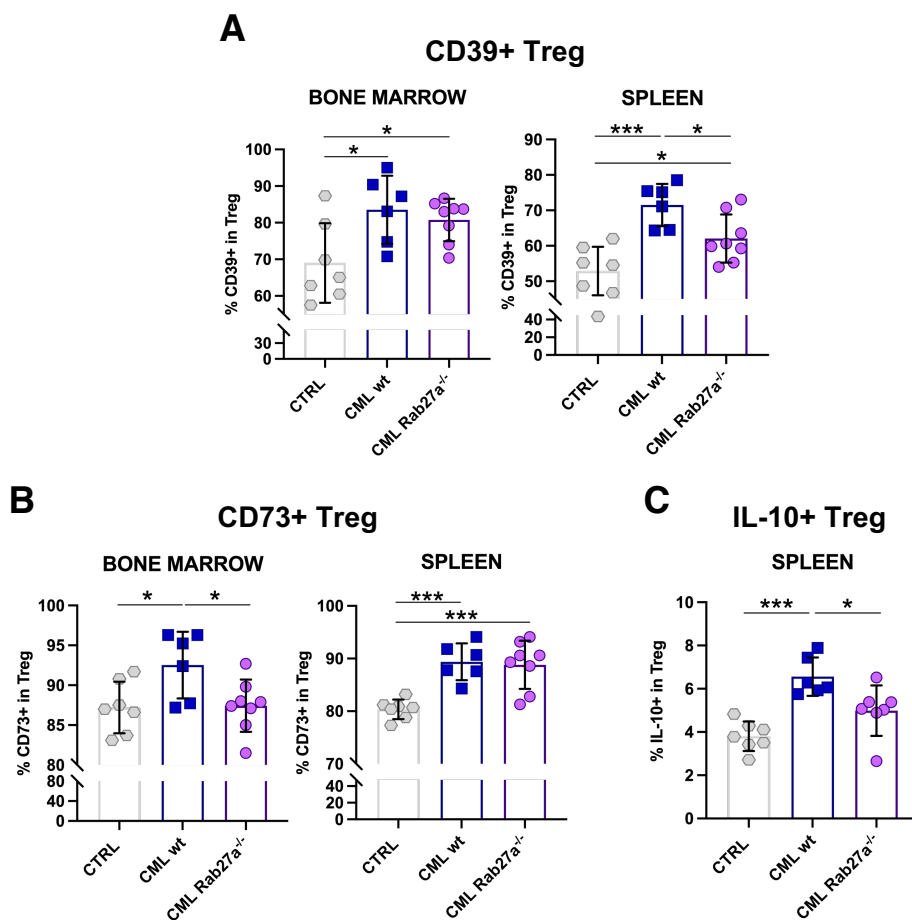


Figure 4.41 Tregs in CML-like disease exhibit elevated expression of CD39, CD73 and IL-10, which are partially driven by Rab27a-dependent EVs. Treg expression of CD39 (A), CD73 (B) and IL-10 (C) in specified tissues of animals with CML-like disease, either wt or Rab27a^{-/-}. Data are from 3 experiments (n=7 CTRL mice, 6 CML wt mice, 8 CML Rab27a^{-/-} mice). One-way ANOVA with Tukey's posttest, single data points and mean \pm SD are shown. Gating strategy is shown in Figure 3.18, 3.20.

Altogether, *in vivo* experiments in a mouse model of CML-like disease have confirmed crucial role of Treg cells in disease development. Moreover, by studies of Rab27a-deficient CML-like disease, obtained results have demonstrated the role of leukemic extracellular vesicles in several aspects of Treg suppressive, pro-leukemic activity *in vivo*.

4.3.5 Regulatory B cells and suppressive CD11b+ myeloid cells are not upregulated in CML-like disease and are not affected by Rab27a-dependent EVs

Results in the previous Chapter have demonstrated that release of Rab27a-dependent extracellular vesicles by leukemic cells is crucial for expansion of activated, suppressive Tregs in CML-like disease *in vivo*. However, this modulation does not necessarily have to be direct and could be indirect, for example via other immune cells in the microenvironment. Different immune cells, including B cells or macrophages, have been demonstrated to modulate suppressive, effector Tregs^{263,264}. Therefore, the aim of the following experiments was to check whether suppressive features of B cells or myeloid immune cells were affected by Rab27a deficiency in leukemic cells, which could implicate these subsets in the final effect on Tregs. B cells and CD11b+ constitute two most abundant immune cell subsets in the bone marrow and the spleen (except T cells) and thus could be most likely to interact with Tregs in the leukemic microenvironment.

By intracellular cytokine staining of cultured splenocytes, production of IL-10 by B cells and arginase-1 (Arg1) by CD11b+ myeloid cells were checked. IL-10-producing B cells are considered regulatory B cells with suppressive activity and potential inducers of regulatory T cells²⁶³. Arginase-1 expressing myeloid cells are often considered as "myeloid-derived suppressor cells" - an immature, highly suppressive subset of myeloid cells. However, neither expression of IL-10 in B cells or Arg1 expression in CD11b+ myeloid cells were amplified in leukemia-like disease, nor were they influenced by Rab27a deficiency in leukemic cells (Figure 4.42). While it seems like there was a trend of upregulated Arg1 expression, it was only observed in approximately 1% of myeloid cells which is rather irrelevant, especially compared to observations from other mouse models of cancer, such as lung cancer or glioma^{265,266}.

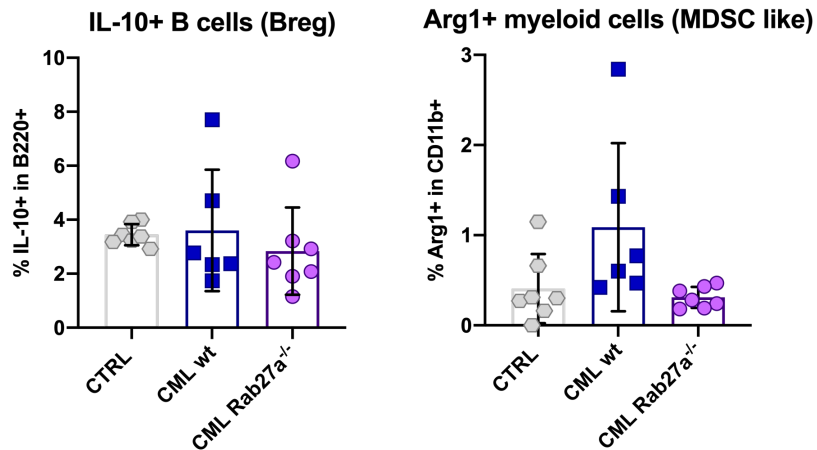


Figure 4.42 IL-10-expressing B cells and Arg1-expressing myeloid cells in the spleen are not affected by CML-like disease or Rab27a expression in leukemic cells. Data are from 3 experiments (n=7 CTRL mice, 6 CML wt mice, 7 CML Rab27a^{-/-} mice). One-way ANOVA with Tukey's posttest, single data points and mean \pm SD are shown. Gating strategy is shown in Figure 3.20.

To further investigate potential modulation by myeloid cells, phenotyping of CD11b⁺ cells from bone marrow and spleen of mice was performed. Three markers that identify immunosuppressive/immune evasive myeloid subsets were analyzed - again arginase-1, but also PD-L1 (immune checkpoint providing a co-inhibitory signal to T cells²⁶⁷) and SIRP- α (protein interacting with CD47 on tumor cells - a "don't-eat-me signal"²⁶⁸). Moreover, CD11b⁺ myeloid cells were analyzed for expression of F4/80, Ly6C and Ly6G, to potentially distinguish between suppressive subsets of tissue macrophages, monocytes or neutrophils. However, neither distribution of F4/80⁺ tissue macrophages, Ly6C⁺ monocytes and Ly6G⁺ neutrophils, nor expression of Arg1, PD-L1 and SIRP α were affected by leukemia-like disease, nor were they influenced by Rab27a deficiency in leukemic cells (Figure 4.43A-D).

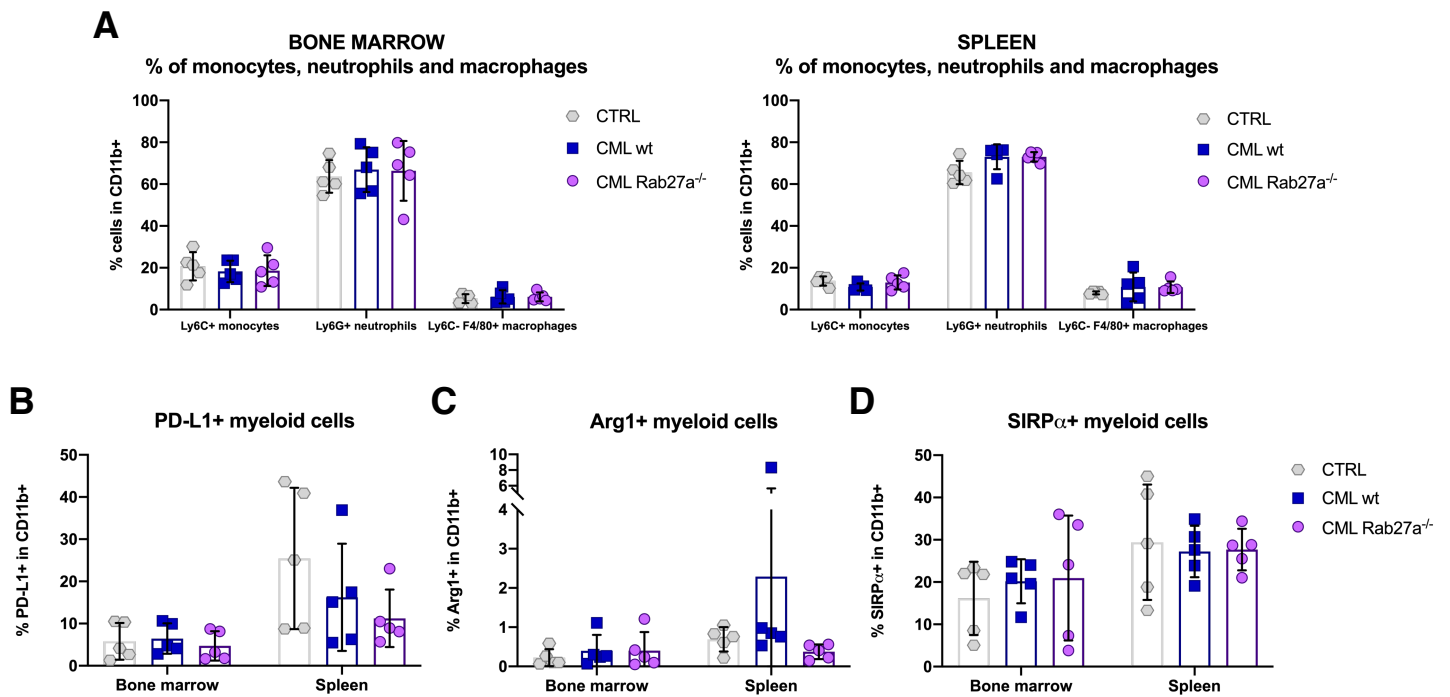


Figure 4.43 Analysis of CD11b⁺ myeloid cells in mice. (A) Distribution of myeloid cell subsets - Ly6⁺ monocytes, Ly6G⁺ neutrophils and F4/80⁺ tissue-resident macrophages in bone marrow and spleen of animals. CD11b⁺ myeloid cell expression of PD-L1 (B), arginase-1 (Arg1) (C) and SIRP- α (D) in specified tissues of animals with CML-like disease, either wt or Rab27a^{-/-}. Data are from 2 experiments (n=5 mice/each group). One-way ANOVA with Tukey's posttest, single data points and mean \pm SD are shown. Gating strategy is shown in Figure 3.19.

Altogether, these data suggest that neither regulatory B cells nor suppressive myeloid cells were engaged in elevation of activated Tregs in mouse model of CML-like disease. While this does not completely exclude a potential role of other immune and non-immune cells, it strengthens the conclusion that Rab27a-dependent EVs directly modulate Tregs and Treg activity *in vivo*.

4.3.6 Rab27a-dependent EVs secretion *in vivo* promotes leukemic engraftment

Data presented in previous Chapters have demonstrated that Rab27a-dependent leukemic extracellular vesicles drive pro-leukemic, activated phenotype of Foxp3⁺ regulatory T cells *in vivo*. The data indicate that this occurs by direct interaction between leukemic EVs and Tregs, rather than via other immune cells, such as B cells or myeloid cells. Finally, this observation was interpreted in the context of CML development in the mouse model of leukemia-like disease. To assess disease development in animals, engraftment of 32D BCR-ABL1+GFP⁺ cells (either wt or Rab27a^{-/-}) was measured by analysis of GFP-expressing cells in blood, spleen and bone marrow of animals.

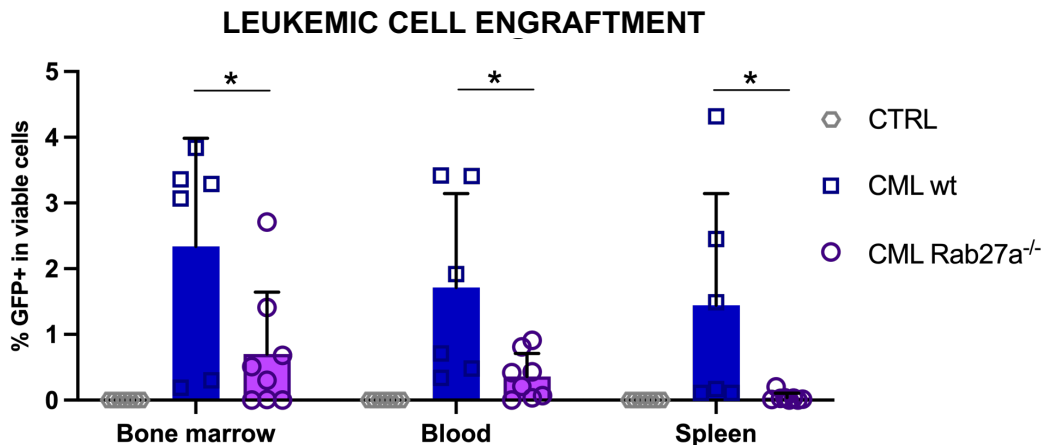


Figure 4.44 Rab27a-deficient leukemic cells demonstrate weaker engraftment into bone marrow, blood and spleen *in vivo*. Percentage of GFP-expressing leukemic cells was analyzed among viable cells in the bone marrow, blood and spleen of animals, as described in Chapter 3.10.3. Data are from 3 experiments (n=7 CTRL mice, 6 CML wt mice, 8 CML Rab27a^{-/-} mice). One-way ANOVA with Tukey's posttest, single data points and mean \pm SD are shown.

Compared to wild-type CML-like disease, Rab27a-deficient leukemic cells have exhibited significantly weaker engraftment into tissues, where CML cells typically reside - bone marrow, blood and spleen. In case of the spleen, this engraftment was barely detectable, although GFP+ cells were clearly visible during analysis of flow cytometric data (Figure 4.44). Importantly, no GFP expressing cells were detected in control, non-leukemic animals. This observation demonstrates that release of Rab27a-dependent EVs is crucial for leukemic engraftment and disease progression *in vivo* in immunocompetent animals. Importantly, as shown above, no difference in cell growth or clonogenicity was observed between wt and Rab27a-deficient leukemic cells (Figure 4.36D-F). Therefore, differences in leukemic engraftment are most likely dependent on modulation of the microenvironment by EVs. One such component are Foxp3⁺ regulatory T cells, which (as described above) were significantly affected by Rab27a deficiency in leukemic cells *in vivo*. On the other hand, other large immune cell subsets (B cells, myeloid cells) were rather not affected, thus they are most likely not implicated in influence on disease progression.

Altogether, *in vivo* studies, using mouse model of leukemia-like disease, demonstrate relevance of Rab27a-dependent secretion of extracellular vesicles in leukemia progression. Rab27a-deficiency in leukemic cells has also resulted in lower amount and less activated, suppressive phenotype of regulatory T cells in the spleen and bone marrow of animals. As other immune cells were not as significantly influenced, these changes in Tregs are likely to be directly modulated by Rab27a-dependent EVs. In conclusion, direct modulation of effector, pro-leukemic Tregs by Rab27a-dependent leukemic EVs is most probably a significant factor promoting CML development *in vivo*.

5 DISCUSSION

The main aim of the presented thesis was to investigate whether leukemic (CML- and AML-derived) extracellular vesicles can drive pro-leukemic, immunosuppressive Foxp3⁺ regulatory T cells. Experiments using several *ex vivo* models, with both human and mouse Tregs and EVs, have demonstrated direct interaction between T cells and EVs of leukemic origin. Several aspects of Treg biology were influenced - suppressive phenotype and activity, differentiation of *in vitro* induced Tregs, signaling pathways, transcriptome and expansion of effector subsets. Altogether, leukemic EVs modulated Tregs to amplify their effector capabilities, which should facilitate immunosuppression during leukemia development. Indeed, this observation was further confirmed *in vivo*, by studying disease development and Tregs in an immunocompetent mouse model of chronic myeloid leukemia. Rab27a-dependent secretion of EVs *in vivo* has facilitated regulatory T cells expansion, activation and suppressive phenotype, concurrently with stronger engraftment of leukemic cells into the bone marrow, spleen and blood.

Therefore, the obtained data are relevant to several aspects of leukemia and Treg biology. First and foremost, achieved results demonstrate a new immunosuppressive mechanism in myeloid leukemias, relevant to disease progression. Secondly, obtained data contribute to the knowledge about control of regulatory T cells in cancer, at the level of their origin, signaling and different effector subsets. Finally, proteomic and phenotypic data suggest functional relevance of 4-1BBL protein, shuttled in leukemic EVs, in tumor Tregs biology, which has not been widely explored to date. The following aspects will be discussed below.

5.1 Relevance of extracellular vesicles in driving immunosuppressive Tregs and myeloid leukemia development

Expansion and immunosuppressive influence of Foxp3⁺ regulatory T cells (Tregs) have been well documented as one of the hallmarks of cancer²⁶⁹. Depletion of Tregs in animal models has led to formation of antitumor immunity and therapeutic effects^{270,271}. However, markers that have been traditionally used to target Tregs by depleting antibodies - such as CD25 - are expressed on both Tregs and activated effector (anti-tumor) T cells. Therefore, in many cases Treg targeting has proven unsuccessful²⁷². This has urged the need to further evaluate basic principles of Treg biology in different cancers, to either find highly specific Treg markers (to increase specificity of Treg-depleting therapies) or identify factors that promote Treg expansion and activity in tumors, as such factors could be easier to target than Tregs themselves.

Similarly to solid tumors, Tregs have been recently implicated in the development of chronic and acute myeloid leukemia, as their increased amount has been observed in blood and bone marrow of leukemic patients^{21,112,118}. Also, depletion of Tregs in mouse models of AML and CML has proven

to delay leukemia development and prolong animal survival^{119,133}. Alleviation of immunosuppression (including decrease in Treg numbers) and recovery of effector immunity has been demonstrated in CML patients with treatment-free remission¹¹². Therefore, precise targeting of Tregs or Treg-driving mechanisms could also provide an attractive therapeutic option for patients in advanced, TKI-resistant blast crisis CML^{273,274}, as well as for AML patients in general, as there are no established treatments to efficiently treat the latter²⁷⁵. Again, such approach requires either identification of highly specific Treg markers or Treg-driving factors, that could be easily targeted instead.

5.1.1 Influence of leukemic extracellular vesicles on Tregs and immunosuppression

In the presented thesis, CML- and AML-derived extracellular vesicles have been identified as a factor that drives Foxp3⁺ regulatory T cells. Firstly, this has been observed (by a reductionist approach) in *ex vivo* cultures of Tregs/T cells with purified leukemic EVs. Though this approach lacks a physiological (*in vivo*) setting, it is the only approach that enables studies on direct influence of EVs on target cells (here: Tregs). Firstly, EVs released by murine 32D BCR-ABL1⁺ cells have amplified suppressive activity and Foxp3 level in mouse thymic regulatory T cells (tTregs) (Chapters 4.1.2-4.1.5). In these experiments, EVs from leukemic 32D BCR-ABL1⁺ cells have been compared to EVs from a non-malignant 32D cell line. Therefore, it clearly assigns the effect on Tregs to leukemic EVs, rather than to all EVs in general. Moreover, as exhibited on Figure 4.7B, control EVs released by 32D cells do not influence Foxp3 level at all, as compared to culture without EVs. These observations have provided initial information on biological influence of leukemic EVs on Tregs, but also provided an important experimental control. In case of studies on human EVs and Tregs, there is no control cell line to use as reference to myeloid leukemia cell lines, such as K562 (CML) or MOLM-14 (AML) and cultures without EVs were used as control. Thus, results from mouse *ex vivo* studies have provided an important experimental rationale for studies using human cells. On the other hand, *ex vivo* studies using human cells provide data much easier to translate into a clinical setting. This is for example due to some differences in Treg biology between human and mouse cells.

Indeed, experiments using EVs from human CML (K562) and AML (MOLM-14) cells have confirmed that leukemic EVs control regulatory T cell biology, by amplifying suppressive phenotype, activity, Foxp3 level and induction of human Treg cells (Chapters 4.2.3, 4.2.4). This has provided further proof that leukemic EVs are a significant factor that promotes pro-leukemic activity of Foxp3⁺ regulatory T cells. Moreover, as described in Chapter 4.2.5, human CML EVs also influence non-regulatory, effector subsets of T cells, such as non-Treg CD4⁺ and CD8⁺ T cells. Following treatment with CML EVs, these cells have exhibited an exhausted, dysfunctional phenotype, as well as attenuated effector function, observed as diminished release of proinflammatory mediators

IL-6, TNF- α , INF- γ and CCL2. This demonstrates that immunosuppressive influence of leukemic EVs is much wider than just amplification of Treg function. This observation is consistent with already published research on AML EVs, which have been shown to attenuate cytotoxic function of NK cells^{224,230} and induce apoptosis of CD8⁺ T cells²³². Therefore, therapeutic targeting of leukemic EVs could not only reverse expansion of pro-leukemic Treg cells, but also reactivate anti-tumor activity of effector T cell subsets.

Finally, to further validate the findings *ex vivo*, though in a more physiological setting, EVs isolated from plasma of CML and AML patients were isolated and used to treat human Tregs and CD25⁻ T cells (to investigate iTregs induction). Compared to control EVs from healthy (non-leukemic) donors, EVs from leukemic plasma have also led to induction of CD25^{hi}Foxp3⁺ iTregs, as well as promoted an effector phenotype of Tregs (Chapter 4.2.10). As amount of EVs in plasma of leukemic patients and healthy donors did not vary, these experiments have provided another evidence that modulation of Tregs can be assigned to EVs of leukemic origin, specifically. On the other hand, a caveat of studies on EVs from plasma is that they do not constitute a pure population of leukemic EVs, as it is in case of EVs isolated from cell line conditioned medium. Plasma EVs constitute a heterogenous mixture of EVs from platelets, leukocytes, tissues, but, importantly, also tumor cells (in case of cancer patients)^{276–278}. Nevertheless, plasma of patients contains leukemic EVs (such as EVs containing both BCR-ABL1 protein and transcript^{279–281}) and also reflects the general immunosuppressive landscape of myeloid leukemia patients. The fact that EVs from plasma of leukemic patients promoted effector Treg cells in presented experiments supports the notion that EVs released into the circulation by leukemic cells *in vivo* may drive pro-leukemic Tregs outside the bone marrow, as EVs mediate intercellular communication between faraway tissues. Therefore, extracellular vesicles released by leukemic cells residing solely in the bone marrow (during CML chronic phase) could modulate Tregs in distant tissues to facilitate immunosuppression and, among others, progression of CML to blast crisis. A similar phenomenon has been observed in several solid tumors. EVs released by cancer cells have exhibited homing to other tissues to create a premetastatic niche^{282,283}. This formation of pre-metastatic niche by tumor EVs is very often dependent on modulation of immune cells and generation of an immunosuppressive milieu. For example, in the case of pancreatic cancer, EVs promote liver metastases by driving secretion of regulatory cytokine TGF- β by Kupffer cells (liver resident macrophages) in the liver, to create a cancer permissive niche²⁸⁴. In cancers such as melanoma, tumor-derived EVs can mobilize bone marrow progenitor cells to the pre-metastatic niche in the lung, to further differentiate into immunosuppressive cells²⁸⁵.

Altogether, *ex vivo* experiments, where Tregs and T cells were cultured with leukemic EVs, have provided evidence that leukemic extracellular vesicles constitute a factor that directly promotes immunosuppressive Tregs in myeloid neoplasms. Use of several experimental models, based on

mouse and human cell lines, as well as primary material of patients, has provided concrete evidence for this observation, as different experimental models complemented each other to support the hypothesis. The obtained results have therefore pinpointed leukemic EVs as a potential therapeutic target, that could alleviate expansion of suppressive Tregs in CML and AML, as well as reinvigorate anti-tumor immunity mediated by effector T cells.

5.1.2 Influence of leukemic EVs and Tregs on myeloid leukemia development *in vivo* – EVs as potential therapeutic targets

To translate findings of this thesis into the context of disease development, as well as potential therapeutic targeting of EVs to attenuate pro-leukemic Tregs, an *in vivo* model of leukemia-like disease was developed. Importantly, the model was based on a mouse CML cell line 32D BCR-ABL1+GFP+, to facilitate stable genetic modifications of leukemic cells. This has enabled genetic targeting of EVs secretion, by deleting Rab27a protein, that is engaged in release of extracellular vesicles outside the cell. Rab27a knock-out in cancer cells has been previously used to study influence of EVs in *in vivo* tumor models, such as melanoma, breast and prostate cancer^{202,286,287}.

Firstly, the obtained data show that Rab27a-deficiency in 32D BCR-ABL1+GFP+ cells leads to significantly lower engraftment of leukemic cells into the bone marrow, spleen and blood (Chapter 4.3.6). This indeed confirms that Rab27a-secretion of leukemic extracellular vesicles contributes to disease development *in vivo* and provides an experimental rationale to target EVs in myeloid neoplasms. Importantly, in the same cohort of animals, *in vivo* secretion of Rab27a-dependent EVs has affected the biology of Treg cells, providing further evidence in support of hypothesis proposed in this thesis.

Rab27a deficiency has affected several aspects of Treg biology in the used model of CML-like disease (Chapter 4.3.4). Firstly, general activation status of Tregs was affected by Rab27a deficiency. In both spleen and bone marrow, activated, CD44+CD62L- Tregs were less abundant in Rab27a-deficient leukemia, as compared to wild-type counterparts. This was supported by downregulation of suppressive molecules in Rab27a-deficient leukemia-like disease (CD39 and IL-10 in the spleen, CD73 in the bone marrow), as well as decreased amount of Tregs in the spleen. Importantly, the effect of leukemic EVs on expression of CD39 and CD73 is consistent with the data obtained *ex vivo* in a human setting, where both CML (K562) and AML (MOLM-14) EVs led to upregulation of these molecules on Tregs (Chapter 4.2.9). CD39 and CD73 catalyze different steps of conversion of extracellular ATP to adenosine. While extracellular ATP provides a proinflammatory signal, adenosine binds different A2 receptors on effector, anti-tumor T cells, to attenuate the immune response. Indeed, A2A deletion in mice led to tumor rejection in animals²⁸⁸. Recent studies have also demonstrated that antibody-based targeting of CD39 and CD73 can

induce therapeutic benefit in mouse models of melanoma and sarcoma²⁸⁹. Therefore, CD39 and CD73 are a valid target for cancer therapy and their amplified expression on Tregs, due to leukemic EVs, is of high relevance. Moreover, CD39 on Tregs and generation of adenosine have also been implicated in quiescence of normal hematopoietic stem cells in the bone marrow^{67,68}. This observation from a normal, non-cancerous setting sets a question, whether activity of CD39 and CD73 ectoenzymes could also support leukemic stem cells, to facilitate therapy resistance in CML and AML. One intriguing aspect of results on CD39 and CD73 *in vivo* is the difference between spleen and the bone marrow, as Rab27a-dependent EVs modulated CD39 in the spleen, but not in the BM, with opposite situation in terms of CD73. At this moment, there is no clear explanation for this, other than differences in cellular composition of both tissues. While the bone marrow is dominated by myeloid (CD11b+) cells, spleen is mainly composed of T and B lymphocytes (Figure 5.1). Perhaps, EVs-mediated upregulation of CD39 or CD73 is more crucial in one tissue than the other, especially that both CD39 and CD73 can also be expressed by other cells in the niche, such as endothelial cells, fibroblasts, macrophages/myeloid cells or effector T cells²⁹⁰. Another Treg factor influenced *in vivo* by leukemic, Rab27a-dependent EVs was interleukin-10 (IL-10). IL-10 is a well-established immunosuppressive molecule in tumors, as it inhibits activity of dendritic cells and secretion of Th1 cytokines by CD4+ effector T cells²⁹¹. Recently, Treg-derived IL-10 was also implicated in development of acute myeloid leukemia by promoting stemness of leukemic cells, via PI3K/AKT signaling. Inhibition of IL-10/IL-10R signaling has affected stem properties of leukemic cells and slowed down AML progression *in vivo* in mice²⁹². The data obtained in this thesis suggest relevance of IL-10 also in CML, as well as demonstrate a potential mechanism in which leukemic cells use EVs to amplify IL-10 production by Tregs, so that Tregs could promote leukemic cell stemness via IL-10. Interestingly, our unpublished experiments have not detected soluble IL-10 in plasma of animals with leukemia-like disease. This suggests that IL-10 is especially relevant locally in the tissues, which urges more research on leukemic immunity in tissues, such as bone marrow and spleen, rather than just in peripheral blood.

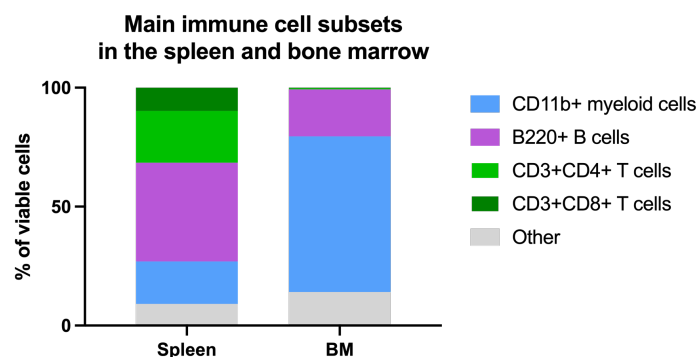


Figure 5.1 Main subsets of immune cells in the spleen and bone marrow of animals. Cells were analyzed using flow cytometry and staining of CD3, CD4, CD8 (to detect T cells), B220 (to detect B cells) and CD11b (to detect pan-myeloid cells). Data shown is from 3 animals of the C3H strain, used for *in vivo* studies presented in this thesis.

While *in vivo* experiments have confirmed relevance of EVs in both development of leukemia-like disease, as well as expansion of pro-leukemic Tregs *in vivo*, they lack direct proof that increase in Treg numbers or activated phenotype (mediated by Rab27a-dependent EVs) is responsible for increased engraftment of leukemic cells. The studies using mouse model also lack proof of direct leukemic-EVs Treg interaction. The latter has been evaluated by analysis of other significant immune cell subsets, such as B cells and immune myeloid cells (Chapter 4.3.5). Neither regulatory B cells, nor suppressive properties of myeloid cells, were upregulated in CML-like disease or affected by Rab27a-dependent release of EVs. This largely excluded involvement of other immune cells in indirect modulation of Tregs by leukemic, Rab27a-dependent, EVs *in vivo*. This strengthens data from *ex vivo* experiments that leukemic EVs directly promote pro-leukemic regulatory T cells. Moreover, an approach to track EVs *in vivo* and linking this to Treg function could contribute even more evidence. Recent advances in imaging and genetic tools have enabled fluorescent tracking of released vesicles, for studies on both EVs biogenesis and functionality. For example, fusing fluorescent proteins, such as EGFP or tdTomato, to palmitoylation signal or EV marker protein (e.g. CD63), enables generation of fluorescently-labelled EVs that could be tracked to target cells^{293,294}. Use of leukemic cells with a fluorescent reporter *in vivo* would enable flow cytometric phenotyping or functional assessment of Treg cells that have either incorporated/bound fluorescent leukemic EVs or did not exhibit such uptake, to provide further evidence for the observed effects. Further *in vivo* studies on leukemic immune microenvironment could additionally benefit from recently developed advanced techniques for single-cell analyses (scRNA-seq, CITE-seq) and spatial analyses of single cells in tissues, such as spatial transcriptomics, proteomics or molecular cartography²⁹⁵. Together with bioinformatic tools designed to identify intercellular interactions from single cell genomics datasets, such as NicheNet²⁹⁶, one could precisely identify cell-cell circuits in the leukemic niche. Recently, such approach enabled identification of a new interaction between stromal cells and monocytes in the liver²⁹⁷.

Furthermore, more complex *in vivo* models could directly link changes in Tregs, promoted by leukemic EVs, to leukemic cell engraftment and disease progression. Combining Rab27a-deficient leukemic cells with Treg depletion, by using Foxp3^{DTR} animals, would be an ideal approach, as it would enable observation if effects of diminished EVs secretion (Rab27a knock-out) and Treg depletion are additive or parallel. At this point, we were unable to conduct such experiments, as 32D BCR-ABL1+GFP+ cells originate from a C3H mouse background, whereas Foxp3^{DTR} animals are of the C57BL/6 strain. However, our lab is now starting to work with new mouse leukemic stem cell lines²⁹⁸, which are of C57BL/6 background, so such experiment could now be performed. Moreover, adoptive transfer of Tregs between animals with either wt or Rab27a-deficient could provide further evidence for observed phenomena.

Finally, extracellular vesicles, released by chronic and acute myeloid leukemia cells, have been previously implicated in remodeling of the non-immune components of the bone marrow microenvironment, including stromal cells^{221,222}, endothelium²²³, osteoblast and normal hematopoietic stem cells²¹⁹. Therefore, non-immune cells could be engaged in decreased leukemic engraftment in Rab27a-deficient leukemia-like disease (in addition or instead of Tregs). Experiments by the group of Peter Kurre, performed on mouse xenograft (immunodeficient, lacking T and B lymphocytes) models of acute myeloid leukemia, have shown that preconditioning of the bone marrow niche with AML EVs facilitates disease progression. Similar effect has been observed when immunodeficient mice were injected with human MV411 AML cells, either wt or with silenced Rab27a (by shRNA technology). Rab27a knock-down has moderately prolonged survival of animals²¹⁹. This suggests that leukemia development *in vivo*, promoted by EVs, does not necessarily have to depend on modulation of lymphocytes. On the other hand, it has been described that CML and AML cells differentially interact with the bone marrow niche (here, osteoblasts) *in vivo*, therefore mouse model studies of both types of myeloid leukemia may yield different results²⁹⁹. Studies presented in this thesis could therefore benefit from comparing leukemic engraftment between wt and Rab27a^{-/-} 32D BCR-ABL1+GFP+ cells, following injection into immunodeficient (lymphocyte deficient) animals. Such experiment would further clarify if the effect of Rab27a knock-out in leukemic cells *in vivo* depends on Treg/T cell modulation by leukemic EVs.

In the end, data presented in this thesis provides a rationale to target secretion of extracellular vesicles to delay progression of myeloid neoplasms, by alleviating Treg-driven immunosuppression and reinvigorating anti-tumor immunity. However, while genetic knock-out of Rab27a provides a straightforward approach in fundamental research experiments, it does not deliver a tangible translational approach, as genetic modification of leukemic cells in patients is clinically irrelevant. The alternative is treatment with pharmacological inhibitors of EVs biogenesis and release pathways (described in Introduction Chapter 1.3.1). To date, the focus of "EV-inhibitors" development was to target either small GTPase Rab27a or enzyme nSMase2³⁰⁰. High-throughput screening has identified Nexinhib20 compound as a small-molecule inhibitor of Rab27a, that also acts as an inhibitor of neutrophil exocytosis³⁰¹. More advanced studies have been conducted for nSMase2 inhibitor, named GW4869³⁰². GW4869 has not only proven efficient in *in vitro* cultures of cell lines, but also *in vivo*, as it has inhibited growth of colorectal cancer in mice, as well as shown potential to attenuate pathological mechanisms in neurodegenerative diseases^{303,304}. Our preliminary data from indirect (via inserts) *ex vivo* cultures of human peripheral blood mononuclear cells with either K562 or MOLM-14 cells, demonstrate that treatment of the entire culture with either Nexinhib20 or GW4869 leads to partial inhibition of Treg expansion, induced by leukemic cells. Nevertheless, use of EVs inhibitors for therapy is at very early, preclinical stages. A huge challenge in this area is that extracellular vesicles are engaged not only in pathological processes, but also

required for normal functioning of tissues, organs and the entire organism. Therefore, delivery of EV-inhibitors could lead to severe toxicity and organ failure. One alternative would be to use targeted drug delivery approach³⁰⁵, so that EV-inhibitor could specifically reach leukemic cells. On the other hand, this would require targeting of specific markers on myeloid leukemia cells, which is not straightforward. For example, CD34, often used to identify leukemic stem cells in patients, is also expressed on normal hematopoietic stem cells. Moreover, in case of some patients, leukemic stem cells do not necessarily have to express CD34 marker³⁰⁶. On the other hand, CD33 has been considered as an attractive marker to target AML cells³⁰⁷, thus it could be evaluated for specific delivery of inhibitors of EVs secretion to leukemic cells.

Nevertheless, while the strategy to target extracellular vesicles in myeloid neoplasms, to remodel and reverse the leukemia permissive, immunosuppressive microenvironment, seems attractive and has been validated using genetic targeting, there is still multiple steps for translational development of this approach.

5.2 Significance of leukemic EVs as drivers of effector, immunosuppressive Tregs, including different Treg subsets

Recent studies of immune cells in multiple cancers, using novel tools, such as single-cell genomics or 30-50 parameter cytometry, have revolutionized understanding of cancer immunity. While polarization of immune cells (usually towards immunosuppressive subsets) in cancer has been a well-recognized phenomenon, these single-cell technologies have revealed previously unrecognized heterogeneity of immune cells and existence of many different subsets, as well as new markers of these specific subsets³⁰⁸⁻³¹². This has led to significant advancements in the field of cancer immunity, improvement of therapeutic strategies and has urged the need to evaluate fundamental research discoveries in more detail, using single-cell technologies.

5.2.1 Functional relevance of effector Treg subsets driven by leukemic EVs

To evaluate potential heterogeneity and different Treg responses promoted by leukemic EVs in the presented thesis, 23-color spectral flow cytometry was applied. As described in Chapter 4.2.9, it has revealed that leukemic EVs lead to expansion of two effector subsets of Tregs, which were named effector Treg1 (eTreg1) and effector Treg2 (eTreg2). Both have constituted separate, distinct populations, as exhibited by computational analysis algorithms tSNE and FlowSOM. eTreg1 were principally characterized by high expression of markers such as CCR8, CD30 and TNFR2, whereas eTreg2 predominantly expressed TIGIT and CD39. Both subsets have expressed high levels of CCR4, which is a well-recognized marker of effector Tregs⁹². This distinct phenotype of both subsets suggests that they can differentially mediate immunosuppression in myeloid leukemias, as well as act in different tissue settings during leukemia development.

Differential expression of CCR8 chemokine receptor implicates that these two Treg subsets could exhibit homing into different tissues *in vivo*, depending on the chemoattracting cues released by different cells. CCR8 receptor can respond to different chemokines, namely CCL1, CCL8, CCL16 and CCL18³¹³. CCL1 binding by CCR8 has been shown to most efficiently amplify the suppressive function of Treg cells³¹³ and, indeed, myeloid cells in the tumor microenvironment have been shown to potently express CCL1⁹⁸. Expression of CCR8 ligands, such as CCL1, is yet to be investigated for different cells in myeloid leukemias, especially in bone marrow or the spleen, which could imply different modulation of Treg migration. Until now, Tregs have only been shown to migrate into the leukemic microenvironment via CCL3/CCR1/CCR5 and CXCL12/CXCR4 interactions¹¹⁹.

Functional significance of eTreg1 (CD30, TNFR2) and eTreg2 (CD39, TIGIT) upregulated receptors is challenging to elucidate in the leukemic microenvironment, as most of these molecules have only recently been associated with Treg cells in tumors. CD30 has been traditionally considered a costimulatory molecule, expressed on activated, effector CD4+ and CD8+ T cells³¹⁴. Recent work has identified elevated expression of CD30 on tumor Tregs in colorectal and non-small cell lung cancer⁹⁶. Primary studies have demonstrated that treatment with CD30-targeting antibody can deplete Tregs *in vitro* and *in vivo* in a xenograft model of graft-versus-host disease³¹⁵. However, functional relevance of CD30 on Tregs has not yet been dissected. Possibly, it could be responsible for activation of Tregs by immunosuppressive antigen presenting cells in the tumor milieu, rather than modulate suppressive function itself. Similarly to CD30, also TNFR2 has been mainly implicated in costimulation of T cells³¹⁴. In Treg biology, TNFR2 is involved in thymic differentiation of Foxp3+ Treg cells³¹⁶. Also, costimulation via TNFR2 contributes to Treg suppressive activity²⁴⁹. Intriguingly, costimulation of Tregs via TNFR2 induces a metabolic switch to glycolysis, simultaneously with increased suppressive activity²⁴⁹. This is contrary to most studies, which rather underline a fatty acid oxidation-based metabolism of effector Tregs in the tumor milieu¹⁰⁴. TNFR2 costimulation of Tregs has been associated with tolerogenic dendritic cells, which implicates interaction between these cells in the tumor/leukemic microenvironment³¹⁷. Again, whether expression of TNFR2 itself is relevant to suppressive function is not entirely clear. In terms of spatial localization in the tissue, expression of costimulatory molecules CD30 and TNFR2 on eTreg1 implicates their interaction with antigen presenting cells and cell circuits between Tregs and immunosuppressive myeloid cells in the tumor milieu.

Functionality of eTreg2 markers, TIGIT and CD39, has been better documented in both tumor and non-cancer setting. TIGIT is a coinhibitory receptor, which binds CD155 to block costimulation via CD226. TIGIT is highly expressed by activated Tregs, also in the tumor milieu^{94,96}, and acts primarily through inhibiting Th1 and Th17 effector CD4+ T cells⁹⁵. Interestingly, TIGIT signaling also leads to intrinsic inhibition of Th1 and Th17 cytokines³¹⁸, which can restore suppressive function of unstable, non-suppressive Th1 Tregs³¹⁹. This signifies one of the findings of the

presented thesis, that leukemic EVs maintain stability of Tregs (Chapter 4.2.7). CML EVs maintained low secretion of interferon- γ (Th1 cytokine) and interleukin-17 (Th17 cytokine) in Tregs, which is consistent with previous discoveries on the role of TIGIT in T cells, as described above. Leukemic EVs may thus upregulate TIGIT expression to stabilize Tregs, inhibit production of non-Treg cytokines and amplify suppressive activity. Moreover, another eTreg2-specific receptor, CD39, also takes part in inhibition of effector T cells function, via generation of AMP and adenosine (together with CD73)²⁹⁰, as described in the previous chapter. Based on described functions of TIGIT and CD39, eTreg2 subset, promoted by CML and AML EVs, is most likely to actively inhibit anti-tumor function of effector CD4⁺ and CD8⁺ T cells, either via coinhibitory signaling or adenosine (and A2 receptors). Moreover, as CD39 and adenosine promote quiescence of normal HSCs in the bone marrow^{67,68}, and thus potentially also support leukemic stem cells, eTreg2 population might directly interact with leukemic stem cells to promote disease development.

5.2.2 Do effector Treg subsets driven by leukemic EVs resemble Treg subsets identified in solid tumors?

An interesting aspect of identified eTreg1 and eTreg2 populations, promoted by leukemic EVs, is whether they correspond to recently described effector Treg subsets in different cancers. Initially, several studies have identified novel markers of tumor Tregs, based on bulk RNA sequencing and conventional flow cytometry^{96,98,101}. However, recent studies using single-cell genomics and high-resolution flow cytometry have added yet another layer to these data, by discovering different subsets of Tregs in tumors. Van Damme *et al.* have identified two distinct subsets of tumor-infiltrating Tregs in mouse model of Lewis lung carcinoma⁹⁹. One subset, distinguished by expression of *Ccr8* has exhibited higher expression of several effector markers, such as *Lag3*, *Tnfrsf4* (encoding OX-40), *Tnfrsf9* (encoding 4-1BB), *Il2ra*, *Areg* and *Il10*, while the second subset has exhibited a less suppressive, Th17-like phenotype. The authors have shown that functional suppressive activity of CCR8⁺ Tregs was superior in an *in vitro* suppression assay, as well as antibody-based depletion of CCR8⁺ Tregs has synergized with anti-PD-1 blockade to reduce tumor growth⁹⁹. Alvisi *et al.* have further described two subsets of Treg cells infiltrating human lung tumors, based on 27-parameter multicolor flow cytometry¹⁰². Similarly, they have identified an effector, CCR8⁺ICOS⁺ Treg subset with superior activity, as compared to the CCR8^{lo}ICOS^{lo} Tregs. Moreover, the identified effector subset was characterized by expression of transcription factor IRF4. Indeed, IRF4 was shown to be a transcriptional regulator of effector Treg gene expression and specific, tamoxifen-inducible knock-out of IRF4 in Foxp3⁺ Treg (in *Irf4^{fl/fl}FoxP3^{EGFP-cre}-ERT2* mice) has delayed growth of MC38 tumors *in vivo*. The IRF4⁺ eTreg subset has exhibited high protein expression of TIGIT, TIM-3, CD71 and gene expression of *TNFRSF9*, *TNFRSF4*, *IL1R2*, *TNFRSF8* (encoding CD30)¹⁰². Effector, CCR8-expressing Tregs, described in both mentioned studies, seem to highly overlap with the CD30⁺CCR8^{hi}TNFR2^{hi} eTreg1 subset described in this

thesis. The identified eTreg1 subset, promoted by leukemic EVs, also exhibits high expression of 4-1BB, TIM-3, CD71, OX-40, IL1R2, ICOS and, finally, IRF4 (Figure 4.27). Therefore, leukemic EVs significantly promote expansion of effector Treg1 subset, that corresponds to CCR8-expressing Treg subpopulations described in solid tumors^{99,102}. This implies that tumor extracellular vesicles in general may be engaged in driving effector Tregs in cancer in general.

Further single cell studies have identified other tumor Treg markers and specific subsets of Treg in solid tumors. Mair *et al.* have used two 30-parameter flow cytometry panels to study T cells, as well as antigen presenting cells, in head and neck squamous cell carcinoma (HNSCC). Based on NicheNet analysis they have identified ICOS and IL1R1 (receptor for IL-1 β) as specific to tumor-supportive Tregs, driven by antigen presenting cells in the microenvironment. Indeed, transcriptional profiling of single cells revealed two tumor Treg subsets distinguished by expression of IL1R1. IL1R1+ Tregs have exclusively expressed *TNFRSF9* (encoding 4-1BB), *CCR8* and *ENTPD1* (encoding CD39). On the other hand, *ICOS* and *CTLA4* were expressed by both IL1R1+ and IL1R1- Tregs³²⁰. The identified effector, IL1R1+ subset exhibits similarity to both eTreg1 and eTreg2 cells described in this thesis. While eTreg2 are primarily characterized by exclusive expression of CD39 and TIGIT, they also express CCR8 (as compared to non-effector subset Pop0+Pop3, Figure 4.27), though not as abundantly as eTreg1. Therefore, the IL1R1+ Tregs in HNSCC may be more similar to eTreg2 than eTreg1. Unfortunately, IL1R1 was not analyzed on protein level in this thesis, as it has not yet been identified as a tumor Treg marker at the point of designing the experiments. However, IL1R1 transcript level was detected in the transcriptomic dataset described in Chapter 4.2.8. As visible on the heatmap in Figure 4.24, *IL1R1* expression seems to be higher in Tregs treated with CML EVs. This implies that extracellular vesicles of tumor origin may also be implicated in driving the IL1R1+ subset of Tregs in cancer. Finally, a study by Kim *et al.* has yet again demonstrated heterogeneity of tumor Tregs, based on analyses of Tregs in renal cell carcinoma and hepatocellular carcinoma³²¹. Similarly to works described above, the authors have also identified a *CCR8*-expressing subset of human Tregs, that was further characterized by specific expression of *CD177* - a marker previously recognized in neutrophil biology. Moreover, dynamics of Treg transcriptomes and different cell fates were analyzed computationally by applying reverse graph embedding approach. This has enabled identification of two distinct cell fates of Tregs (named by the authors "Cell Fate #1" and "Cell Fate #2"), which was not revealed based on solely differential expression of Treg marker genes. While both cell fates have expressed *CCR8* and *CTLA4* (well recognized for tumor Tregs), only "Cell Fate #1" has expressed *CD177* and *TNFRSF4* (encoding OX-40). Moreover, gene set enrichment analysis of "Cell Fate #1" has indicated increased cytotoxicity, proliferation and clonality, altogether implying different functionality. Indeed, deficiency in CD177 (both in entire mice or specifically in Foxp3-expressing cells) has led to slower tumor development of Py8119 breast cancer and MC38

colon carcinoma *in vivo* in animals³²¹. This further signifies heterogeneity of Tregs in tumors and the urge to identify novel subsets by single-cell technologies. The data obtained in this thesis, using both chronic and acute myeloid leukemia-derived extracellular vesicles, strongly suggest that tumor EVs may be a factor that universally promotes effector subsets of Tregs. The performed studies could of course strongly benefit from further experiments using single-cell genomics and single-cell proteogenomic approaches, such as CITE-seq³²². An important task would be to compare Treg polarization *ex vivo*, following treatment with leukemic EVs, with single-cell analyses of Tregs/T cells in tissues *in vivo*, either from leukemia-bearing animals or patients with myeloid neoplasms. Currently, such studies are still lacking. Single-cell proteogenomic studies have already been performed on human and mouse bone marrow, including a small group of AML patients^{323,324}. However, as they were primarily focused on studying the entire bone marrow cellular composition, few T cells are present in the datasets, which does not enable high resolution clustering and analysis of Treg subsets.

The identification of Treg subsets, as well as upregulated markers, has important implications for approaches aiming to deplete Tregs, based on their specific phenotypic features. Several recent studies (as already mentioned above) have identified molecules on Treg surface for potential targeting and depletion. Chemokine receptors CCR4 and CCR8 have been of high interest. CCR4 was evaluated in earlier studies and even though animal experiments have shown anti-tumor effects of CCR4 antagonism³²⁵, a depleting, anti-CCR4 antibody mogamulizumab failed to show therapeutic benefit in clinical trials³²⁶. On the other hand, CCR8 has recently emerged as a more promising target, due to expression more specific to tumor Tregs than other cells. Indeed, animal studies have yielded promising results of CCR8-based Treg depletion in models of colon cancer³²⁷ and lung carcinoma⁹⁹. Several costimulatory and coinhibitory receptors have also been considered as attractive targets to deplete Tregs, due to high expression on these cells. This strategy, on the other hand, may suffer from also depleting activated effector T cells (with anti-tumor function), which also express these molecules. The best documented example is CTLA-4. Anti-CTLA-4 antibody, ipilimumab, has been used in the clinic in treatment of different cancers for over 10 years now, after initially proving efficient in two, large phase III clinical trials in melanoma^{328,329}. While the main rationale of CTLA-4 blockade has been to inhibit coinhibitory signal and reactivate anti-tumor immunity, ipilimumab has also been demonstrated to act by depletion of CTLA-4-expressing Tregs^{330,331}. Several molecules from TNF receptors superfamily have also been evaluated for Treg depletion in tumors. Agonistic antibody against GITR has shown synergy with anti-PD-1 antibodies in a phase I clinical trial of solid tumors³³². Preclinical studies *in vitro* and *in vivo* in mice have also demonstrated that targeting of OX-40 and TNFR2 receptors can deplete Tregs and facilitate eradication of tumor cells, although these studies have still not reached the stage of clinical trials^{269,333,334}.

Out of described molecules, CCR4, CCR8, CTLA-4 and TNFR2 were upregulated by leukemic EVs (Chapters 4.2.4, 4.2.9). Apart from being a significant observation on a fundamental research level, this also has implications for therapeutics, as it implicates molecules that may be used in Treg depletion strategies in myeloid neoplasms. This, however, requires further validation that these markers are indeed elevated on primary Tregs from leukemic patients. Studies described in literature have by far identified elevated expression of CTLA-4¹¹³ and TNFR2³³⁵ on Tregs from either blood or bone marrow of CML/AML patients. Moreover, OX-40 (TNFRSF4)¹²³ is a costimulatory receptor upregulated on Tregs in myeloid leukemias, though it was unaffected by either CML or AML EVs in studies performed in this thesis. Recent study in a mouse model of CML-like disease has demonstrated that in leukemic bone marrow, OX-40 is expressed practically solely on Tregs and treatment of mice with OX-40 depleting antibody has increased survival of animals by reactivating anti-tumor immunity (increased CD8/Treg ratio)¹³³. On the other hand, knowledge about Treg-specific markers upregulated by leukemic EVs could be an indicator for therapies using EV-inhibitors and eventual combining them with immunotherapies. In case that both types of therapies would affect Tregs in the same or different way, combined treatment is either reasonable or not. Finally, the last implication of studies in this thesis for Treg heterogeneity and potential Treg depleting therapies is that more than one effector Treg subset may be present in the tumor milieu. Presented study has identified two distinct, effector Treg subsets with different expression pattern of analyzed receptors. While both subsets express CCR4 and CCR8, eTreg1 have higher amount of these receptors and thus may be preferentially depleted by CCR4- or CCR8-targeting antibodies. Therefore, obtained data suggest that simultaneous targeting of multiple receptors may be required to efficiently deplete various subsets of Tregs in cancer.

5.2.3 Influence of leukemic EVs on Tregs of thymic and peripheral origin

An intriguing aspect of performed studies is the influence of leukemic EVs on Tregs of either thymic or non-thymic origin. Tregs in tumor tissues exhibit an effector, activated profile (Fraction II in division based on CD45RA and CD25/Foxp3, Figure 1.2)^{92,104}, suggesting they must have undergone antigen-specific stimulation via TCR. It is however still not clear, whether effector Tregs in tumors are activated, thymus-derived Tregs or Tconv, that underwent conversion into peripheral Tregs in the tumor milieu. Study using mouse model of prostate cancer has demonstrated that Tregs in tumors were predominantly specific to antigens presented in the thymus during Treg development, as Tregs with highly-overlapping antigen repertoire were present in healthy animals, including female specimens, which do not develop prostate cancer³³⁶. In mouse model of GL261 glioma, thymectomy prior to glioma cell implantation has significantly decreased amount of Tregs in tumors. Also, majority of Tregs in human glioblastoma and mouse tumors expressed Helios³³⁷. On the other hand, antigen-specific analysis of Tregs from human melanoma, gastrointestinal and

ovarian cancer has demonstrated clonal expansion of Tregs specific to mutated tumor neoantigens, suggesting that peripherally induced Tregs may be more relevant in these tumors³³⁸.

Whether Tregs in a certain cancer are thymic or peripheral is probably connected to the mutational load of tumors and abundance of novel, mutated neoantigens. Myeloid neoplasms are characterized by one of the lowest mutational burdens and thus low abundance of neoantigens³³⁹. Indeed, a HLA ligandome study of CML samples has revealed that only 4% of antigens are truly CML exclusive²⁵². Indeed, both CD8+ T cells, as well as Tregs in myeloid leukemias have been shown to be specific to antigens such as PR3, WT1 and PRAME, which are considered self-antigens and are expressed by several types of tumors^{112,340}. Consistent with that, studies performed in this thesis have demonstrated prevalence of Helios-expressing Tregs in both bone marrow and spleen of leukemia-bearing animals (Figure 4.3A), which was also documented in the bone marrow in another syngeneic model of CML¹³³. Therefore, it seems like Tregs of thymic origin, specific for self-antigens, rather the mutated tumor neoantigens, are more relevant in myeloid neoplasms. To assess whether leukemic EVs are relevant to this phenomenon, part of studies in this thesis was performed solely on pure thymic Tregs of mouse origin (Chapters 4.1.3, 4.1.5). Indeed, leukemic EVs have amplified suppressive activity and Foxp3 level in thymic regulatory T cells. On the other hand, Tregs from human blood (that contain also peripheral Tregs) were also polarized into effector cells by leukemic EVs, which suggests that not only tTregs are modulated by EVs. To further evaluate that, expression of Helios was analyzed in several experiments on human Tregs. Expression of *IKZF2* (encoding Helios) was significantly downregulated in transcriptomic RNA-seq analysis, as well as Helios-expressing cells were less abundant in 23-color flow cytometry phenotyping studies. Moreover, in our study expression of Helios did not differ between different subsets of Tregs. Both eTreg1 and eTreg2, as well as non-effector subset (Pop0+Pop3), have included both Helios+ and Helios- cells. Moreover, amount of Helios+ Tregs did not differ in spleen and bone marrow between wt and Rab27a-deficient leukemia-like disease *in vivo* (data not shown). Therefore, while leukemic EVs modulate and amplify suppressive properties of thymic regulatory T cells, there is no indication that EVs would preferentially target Tregs of thymic origin. To the contrary, data from human cells indicate that peripheral, non-thymic Tregs may be preferentially modulated by leukemic EVs.

5.2.4 Molecular pathways in Tregs influenced by leukemic EVs

Finally, Tregs in various microenvironments may undergo different molecular regulation, for example via several transcription factors. As already mentioned, Alvisi *et al.* have identified IRF4 as a crucial transcription factor that regulates effector Tregs in the tumor microenvironment¹⁰². Apart from functional experiments described above, the authors have used their RNA sequencing and ChIP (chromatin immunoprecipitation) sequencing datasets to directly demonstrate regulation

of gene expression by IRF4 and its partner BATF. Indeed, IRF4 and BATF have jointly regulated expression of *Icos*, *Tnfrsf9* and *Ikzf2*, whereas IRF4 alone has regulated *Tigit*, *Ctla4*, *Ccr8* and *Tnfrsf8*. Moreover, bioinformatic analysis of transcription factor binding motifs in differentially expressed genes in RNA sequencing datasets has implicated several other transcription factors, such as NRF1, TFDP1, GABPA and ATF1¹⁰². Similar analysis by Magnuson *et al.* has revealed another set of transcription factors, such as FOXM1, NR1H3 and E2F4¹⁰¹. These differences in top hits of such analysis suggest different modes of transcriptional Treg regulation in several cancers (in this case: lung vs colon). Similar analysis of transcription factor binding motifs was also performed in the presented thesis, based on differentially expressed genes in the RNA sequencing dataset (Figure 4.23, same methodology as Alvisi *et al.*¹⁰²). 31 transcription factors were identified as potential regulators of different transcriptomes between control and leukemic EVs-treated Tregs. Expression (RNA level) of three of the identified transcription factors was additionally upregulated in EVs-treated Tregs - EGR1, EGR3 and ZNF740, suggesting they are most likely to be engaged in effects driven in Tregs by leukemic EVs. EGR3 in Tregs has been previously described as responsible for modulating TGF- β 3 secretion and prevention of excess autoimmunity in mouse model of lupus-like autoimmune disease²⁵⁷. *EGR1* has been one of the most differentially expressed genes in CD177-expressing effector Tregs identified in cancer by Kim *et al.*, in work described above³²¹. These data signify relevance of EGR1 and EGR3 for Treg function and strongly implicate these transcription factors in modulating Tregs after treatment with leukemic EVs. Among other transcription factors identified in the performed analysis, also E2F4¹⁰¹, ZBTB7A/LRF²⁵⁶ and TFDP1¹⁰² have been previously implicated in Treg function or development. On the other hand, identification of HIF1A as a potential regulatory factor, but upregulated in control Tregs, may seem surprising, as one could expect it to be somehow engaged in Treg modulation in the hypoxic microenvironment of leukemic bone marrow³⁴¹. Nevertheless, while bioinformatic analysis of transcription factor binding motifs indicated potential molecular regulators of observed functional differences, final conclusions would need to be validated, either by chromatin immunoprecipitation (to demonstrate binding of transcription factor to target genes) or by pharmacological/genetic targeting of chosen factors. Recently, CRISPR/Cas9 methodology was also applied to primary human lymphocytes³⁴², which could facilitate such studies.

Moreover, potential regulatory pathways modulated by leukemic EVs were also identified by analysis of phosphorylated signaling proteins by flow cytometry (Chapter 4.2.6). STAT5 phosphorylation (which was potentiated by leukemic EVs) is a well-recognized driver of *Foxp3* expression, by targeting intronic element CNS2 in the *Foxp3* gene³⁴³. STAT5 phosphorylation is classically modulated by IL-2 binding to CD25, although it may be IL-2 independent³⁴⁴. As leukemic EVs do not contain IL-2, they probably regulate STAT5 phosphorylation in a different manner, which is not clear by far. One of hypotheses evaluated in my project (though not shown in this thesis) was

that BCR-ABL1, contained in leukemic EVs, could modulate STAT5 in Tregs, as STAT5 is a prominent partner of BCR-ABL1 in leukemic cells³⁴⁵. BCR-ABL1 protein was detected in EVs from both mouse 32D BCR-ABL1+ cells and human K562 cells, but inhibition of BCR-ABL1+ kinase activity by imatinib, in cultures of EVs with human Tregs, did not influence effects of leukemic EVs. Another pathway influenced by leukemic EVs was mTOR-S6, although in this case phosphorylation of proteins was downregulated. However, contrary to STAT5, mTOR signaling negatively modulates Treg differentiation and function^{69,80}. Therefore, downregulation of mTOR-S6 by leukemic EVs is consistent with immunosuppressive Treg-promoting influence. An interesting aspect of mTOR-S6 signaling is its influence on T cell metabolism, as this pathway is a crucial regulator of glycolysis^{249,346}. Strong downregulation of mTOR-S6 signaling suggests that leukemic EVs may also influence Treg metabolism. Finally, it is worth mentioning that SMAD signaling (downstream of TGF- β) was not affected by leukemic EVs (Chapter 4.2.6). This is especially intriguing in experiments where EVs have potently induced Foxp3 in conventional, non-regulatory T cells, as this process is usually modulated by TGF- β /SMAD signaling⁴⁹. This suggests a novel, previously undescribed pathway that leads to *in vitro* Treg induction, possibly by coordinated phosphorylation of STAT5 and dephosphorylation of mTOR-S6, as observed in this study.

5.3 Significance of 4-1BBL, shuttled by EVs, in leukemia and activity of Tregs

Extracellular vesicles have been previously implicated in modulation of Treg cells in solid tumors. However, different proteins in EVs have been involved in this regulation. Initial study by Szajnik *et al.* has identified that TGF- β 1 and IL-10 in ovarian cancer extracellular vesicles have promoted expansion of Foxp3-expressing regulatory T cells²⁰⁷. Mrizak *et al.* have identified chemokine CCL20 in EVs released by nasopharyngeal carcinoma and its role in facilitating migration of Tregs towards the tumor niche²¹¹. Other studies have pinpointed microRNAs, rather than proteins, as components of EVs that modulate Treg cells. MicroRNA miR-24-3p in nasopharyngeal carcinoma EVs was engaged in Foxp3 induction in non-regulatory, conventional T cells^{209,210}, whereas miR-214, shuttled in lung carcinoma EVs, has promoted expression of Foxp3 and IL-10 in Treg cells²¹².

Studies performed in this thesis have evaluated protein composition of CML EVs and identified 4-1BBL/CD137L/TNFSF9 protein as a molecule that is engaged in effects of leukemic EVs on Foxp3+ regulatory T cells (Chapters 4.2.11, 4.2.12). This establishes a previously undescribed mechanism of Treg modulation by tumor EVs. 4-1BBL expression has been primarily described on antigen presenting cells^{347,348} and delivers costimulatory signal to activate effector, non-regulatory T cells³⁴⁹. On the other hand, receptor for 4-1BBL - 4-1BB, has been well recognized as a marker of effector tumor Tregs. Bulk RNA-sequencing studies of several human tumors have demonstrated elevated expression of *TNFRSF9* (encoding 4-1BB) on tumor Tregs (suggesting it to be a pan-cancer marker of tumor Tregs), as compared to Tregs from peripheral blood of patients³⁵⁰.

Also single-cell studies (described in previous chapter) have identified *TNFRSF9* expression in effector subsets of tumor Tregs^{99,102,320,321}. Even more significantly, antibody-based targeting of 4-1BB expressing cells in mouse model of CT26 colorectal carcinoma has led to depletion of Tregs and reduced tumor burden, without significantly affecting CD8+ T cells³⁵⁰. Therefore, 4-1BBL in leukemic EVs can target 4-1BB-expressing effector Tregs to further maintain their activation and amplify suppressive function. On the other hand, this influence may indeed be dedicated only to 4-1BB-expressing Tregs. Also in our experiments, only a fraction of entire Treg population has expressed 4-1BB (as visible on representative analysis of control sample, Figure 5.2). In FlowSOM analysis of 23-color phenotyping data, 4-1BB was primarily expressed by the eTreg1 subset (Figure 4.27). Further studies could benefit from comparing influence of 4-1BBL-containing (leukemic) EVs on different subsets of Tregs, such as 4-1BB+ and 4-1BB- Tregs, that would be separated by sorting before experiments. Additionally, comparing effect on Tregs from healthy donors/tissues and leukemic bone marrow could provide compelling observations.

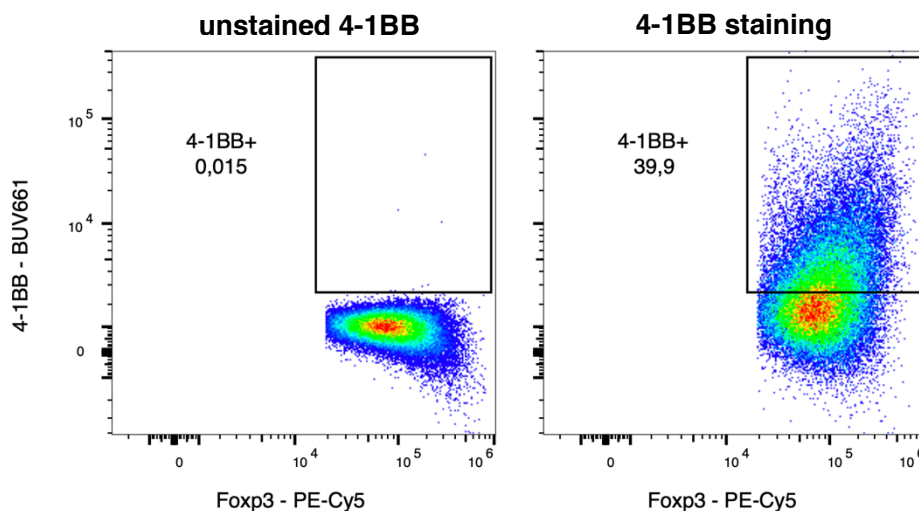


Figure 5.2 Expression of 4-1BB receptor on human regulatory T cells cultured *ex vivo*. Tregs were cultured as described in Chapter 3.6.3. Presented representative sample is from 23-color phenotyping experiments (Chapter 4.2.9).

While expression of 4-1BB receptor on tumor Tregs has become a well-established phenomenon, the functional relevance of 4-1BB/4-1BBL signaling on Tregs has been a poorly investigated matter. First evidence of functional relevance of this pathway came from studies on RelA (p65-NF κ B) transcription factor, which is activated by TNF family receptors, including 4-1BB. RelA was localized in the nucleus of Tregs, suggesting its involvement in transcriptional regulation. Indeed, RelA deficiency in Tregs (in *Rela^{fl/fl}Foxp3^{Cre}* mice) has led to severe autoimmunity and excess activation of effector CD4+ and CD8+ cells. Indeed, RelA-deficient Tregs have lacked effector signature and downregulated expression of genes such as *Tigit*, *Icos*, *Areg* and *Il10*. Importantly, control of Tregs by RelA was independent of TCR-mediated IRF4 regulation⁸¹. RelA in Tregs was engaged in

differentiation of intestinal ROR γ t+ Tregs and prevention of colitis^{81,83}. RelA signaling in Tregs has been directly linked to the activity of TNF family receptors, as stimulation of RelA knock-out Tregs with 4-1BB, TNFR2 and GITR agonists has exhibited weaker influence on proliferation and survival, as compared to wild-type Tregs. Stimulation of Tregs with 4-1BB, TNFR2, GITR and DR3 agonists has led to NF κ B activation and RelA was shown to interact with NF κ B in Tregs activated by 4-1BB agonist. Functionally, stimulation of Tregs via 4-1BB has promoted proliferation and survival of Tregs, as well as profound transcriptomic differences (for example upregulation of *Areg* and *Ebi3*, encoding IL-35)⁸². Tregs treated with TNFR agonists also exhibited increased capacity to prevent colitis *in vivo* in mice upon adoptive transfer⁸², which is consistent with *in vivo* data from animals with RelA deficiency in Tregs^{81,83}.

Collectively, expression of 4-1BB (receptor for 4-1BBL) on tumor Tregs has been well documented, as well as the role of 4-1BBL/4-1BB and RelA signaling in effector Tregs has been recently described. However, the functional relevance of this pathway in cancer has not been elucidated. Analysis of transcription factor binding motifs in RNA-sequencing datasets of IRF4+CCR8+ICOS+ Tregs has detected REL, RELA and RELB as potential transcriptional regulators of tumor Treg gene expression¹⁰². This has provided first evidence that these pathways and signaling downstream of TNF family receptors (TNFRSFs) may be functionally relevant in Tregs in cancer. Data obtained in this thesis indeed confirm that 4-1BBL (contained in leukemic EVs) can promote effector phenotype of Tregs in cancer, such as expression of TNFR2, CD30 and LAG-3. On the other hand, phosphorylation of RelA (p65-NF κ B) transcription factor was not influenced by leukemic EVs (Chapter 4.2.6). However, phosphorylation of RelA seems not to be an effector signaling mechanism downstream of 4-1BB⁸¹, which acts rather by promoting RelA binding to NF κ B and subsequent activation of the latter, as exhibited in experiments using EMSA technique. Investigation of Tregs treated with leukemic, 4-1BBL containing EVs, by supershift analysis of NF κ B with antibodies specific to RelA, RelB or cRel would be of high importance and could provide further details of molecular events mediated by 4-1BBL in leukemic EVs. Relevance of 4-1BBL in myeloid leukemias is further signified by observation that AML blasts express 4-1BBL and that it correlates with lower probability of overall survival in AML patients³⁵¹. Stimulation of 4-1BBL on AML cells has promoted secretion of TNF- α and IL-10 by leukemic blasts. 4-1BBL on AML blasts has also induced dysfunction of NK cells, by binding 4-1BB on NK cell surface³⁵². Moreover, low levels of soluble 4-1BBL in sera of AML patients correlate with probability of achieving and sustaining complete remission, whereas high soluble 4-1BBL correlated with progression of the disease, further signifying potential relevance of 4-1BBL in AML development. In the described study, analyzed sera were not depleted of EVs, therefore 4-1BBL in leukemic EVs could be a factor in these observations³⁵³.

While 4-1BB receptor expression has been recognized as a tumor Treg marker and has been initially evaluated to deplete Tregs and inhibit tumor growth³⁵⁰, therapeutic efforts in the clinic in the past few years have been rather focused on 4-1BB agonistic antibodies, to provide costimulatory signal to effector, non-Treg CD4⁺ and CD8⁺ T cells and reinvigorate anti-tumor immunity. Stimulation of CD8⁺ T cells with 4-1BB agonists has promoted their activation and generation of stable memory³⁵⁴. In human glioblastoma, 4-1BB-expressing CD8⁺ cells have exhibited improved functionality (such as IFN- γ production), despite PD-1 expression³⁵⁵. Agonism of 4-1BB in a mouse model of CT2A glioblastoma has restored functionality of CD8⁺ cells *in vivo* and provided survival benefit of mice, when combined with PD-1 blockade^{355,356}. 4-1BB stimulation in mouse tumor models has also provided therapeutic effects in models of B cell lymphoma or melanoma^{357,358}. Interestingly, combined, sequential use of 4-1BB-targeting antibodies of different isotype and Fc γ R availability has enabled to both deplete 4-1BB-expressing Tregs and stimulate 4-1BB-expressing CD8⁺ effector T cells, leading to significantly decreased tumor growth in mouse model of CT26 colon carcinoma³⁵⁹. Finally, in mouse models of acute myeloid leukemia (AML-ETO9a and MLL-AF9), 4-1BB agonism has provided a significant therapeutic outcome in combination with a NKT cell based vaccine³⁶⁰, again confirming relevance of 4-1BBL/4-1BB signaling in myeloid neoplasms. Promising data in animal studies have led to initial clinical trials of 4-1BB agonistic antibodies in human tumors. Two 4-1BB agonistic antibodies, urelumab and utomilumab, have been evaluated by far and have failed to provide promising results. Utomilumab has provided very low efficiency, while urelumab, though exhibited some anti-tumor efficiency, has led to severe liver toxicity and thus could not be further evaluated^{361,362}. Expression of 4-1BB on both effector non-Treg cells and Treg cells is an important consideration and needs to be studied further in different types of cancer, including myeloid neoplasms. Such studies need to assess whether 4-1BB expression is more relevant for Treg pro-leukemic activity or non-Treg anti-leukemic function. *In vivo* mouse studies using 4-1BBL-deficient leukemic cells could elucidate whether expression of this TNF family molecule is relevant to disease progression and stimulation of different T cell subsets.

Finally, presence of 4-1BBL in leukemic EVs, as documented in the presented thesis, could also be of clinical significance as a potential biomarker in myeloid leukemias. As described above, levels of soluble 4-1BBL have been already implicated as a negative prognostic marker in AML³⁵³. In that study, total level of soluble 4-1BBL was measured in serum by ELISA, without distinguishing different particles in serum, such as EVs. Studies in the presented thesis have identified 4-1BBL in EVs released by both chronic and acute myeloid leukemia cell lines K562 and MOLM-14. Future studies could benefit from a wider panel of cell lines, as well as primary samples from patients. Moreover, comparison to EVs from other leukemias and solid tumors would be an interest study. 4-1BBL is best recognized as expressed on antigen presenting cells^{347,348}, therefore myeloid

leukemias, which originate from myeloid progenitors, may be considered as "predisposed" to express 4-1BBL, whereas epithelial cancers would not be expected to express this ligand. Analysis of specific or upregulated proteins in tumor-derived EVs is an attractive approach for biomarker development. Liquid biopsies based on analysis of EVs are well justified, as plasma (source of EVs) is easy and non-invasive to obtain³⁶³. Moreover, plasma and EVs could be probed at different stages of disease, as well as during remission, which might provide indication of a potential relapse. This is a reasonable approach in myeloid neoplasms that arise in the bone marrow - while leukemic cells still reside exclusively in the bone marrow, leukemic EVs should be already present in the circulation. Though most potential biomarkers in cancer EVs are constituted by miRNAs and DNA fragments, proteins have also been evaluated. Glypican-1 (GPC1) was discovered as a potential biomarker in pancreatic cancer³⁶⁴. The authors have used antibody-based detection and flow cytometric analysis of EVs bound to beads to evaluate expression of GPC1. GPC1 was present in EVs from plasma of 190 pancreatic cancer patients and was absent in EVs of 100 healthy donors. Moreover, GPC1 level in plasma EVs has decreased following tumor resection and correlated with patient survival³⁶⁴. Another study in pancreatic cancer has indicated that presence of MIF protein in EVs can be a predictor of liver metastasis²⁸⁴. While use of plasma EVs as a biomarker is a promising approach in further clinical applications, it still needs advanced studies. One of the biggest obstacles is the fact that tumor EVs may often constitute a small fraction of EVs in plasma²⁸² which urges the need to develop reliable methods to rapidly and precisely analyze EVs from plasma, for example by EV-flow cytometry platforms³⁶⁵.

Collectively, 4-1BBL protein in leukemic extracellular vesicles is likely to be a driver of regulatory T cells and myeloid leukemia development, though it needs validation by applying *in vivo* leukemia models. Another aspect, potentially applicable in the clinic, is that presence of 4-1BBL in leukemic EVs could be validated as a biomarker of immunosuppression and disease development (or recurrence) in myeloid neoplasms.

6 SUMMARY AND CONCLUSIONS

Immunosuppression is one of the key microenvironmental factors that support progression of cancer, including chronic and acute myeloid leukemia (CML, AML). One of the key immunosuppressive components in CML and AML are Foxp3⁺ regulatory T cells (Tregs). Tregs are elevated in patients suffering from myeloid leukemias and have been shown to directly promote leukemia progression in animal models. However, mechanisms that drive Tregs in CML and AML are poorly understood. Therefore, the aim of the presented thesis was to evaluate if extracellular vesicles (EVs), released by myeloid leukemia cells, may be a factor that drives immunosuppression and, specifically, pro-leukemic Foxp3⁺ regulatory T cells. In the presented thesis, first two parts of the performed studies, using *ex vivo* models, aimed at studying direct effects of purified leukemic EVs on mouse and human Treg cells. This was followed by studies in a mouse model of leukemia-like disease, to assess influence of Rab27a-dependent secretion of EVs on regulatory T cells and leukemia progression *in vivo*.

The performed studies and experiments have led to following results and conclusions (summed up on Figure 6.1).

Results:

1. Leukemic extracellular vesicles (EVs) upregulate suppressive activity and Foxp3 level in mouse and human regulatory T cells, as well as induce Foxp3 expression in human non-regulatory cells, leading to differentiation of induced Foxp3⁺ regulatory T cells (iTregs).
2. CML EVs lead to exhausted, dysfunctional phenotype and attenuated secretion of inflammatory mediators by human effector CD4⁺ (non-Treg) and CD8⁺ T cells.
3. CML EVs upregulate phosphorylation of STAT5 and downregulate mTOR-S6 signaling, to induce Foxp3 and upregulate suppressive activity of human Tregs.
4. Transcriptome of human regulatory T cells is significantly affected by CML EVs, including upregulation of genes involved in RNA metabolism and tumor Treg signature.
5. Regulatory T cells, driven by leukemic EVs, exhibit an effector phenotype signature, characterized by expression of CD30, CCR8, TNFR2, CCR4, IL21R, CD39 and TIGIT and include two effector subsets: CD30⁺CCR8^{hi}TNFR2^{hi} eTreg1 and CD39⁺TIGIT^{hi} eTreg2.
6. Leukemic EVs contain a costimulatory 4-1BBL/CD137 protein, which upregulates expression of CD30, TNFR2 and LAG-3 on human regulatory T cells.
7. Foxp3⁺ regulatory T cells are upregulated and exhibit an activated, suppressive phenotype *in vivo* in a mouse model of CML-like disease.
8. In CML-like disease induced by Rab27a-deficient leukemic cells (with diminished secretion of EVs), Foxp3⁺ regulatory T cells are less abundant in the spleen and exhibit a less activated, less suppressive phenotype, compared to the wild-type leukemia counterparts.

9. Rab27a deficiency and diminished secretion of leukemic EVs *in vivo* (in a mouse model of CML-like disease) attenuate engraftment and development of leukemia.

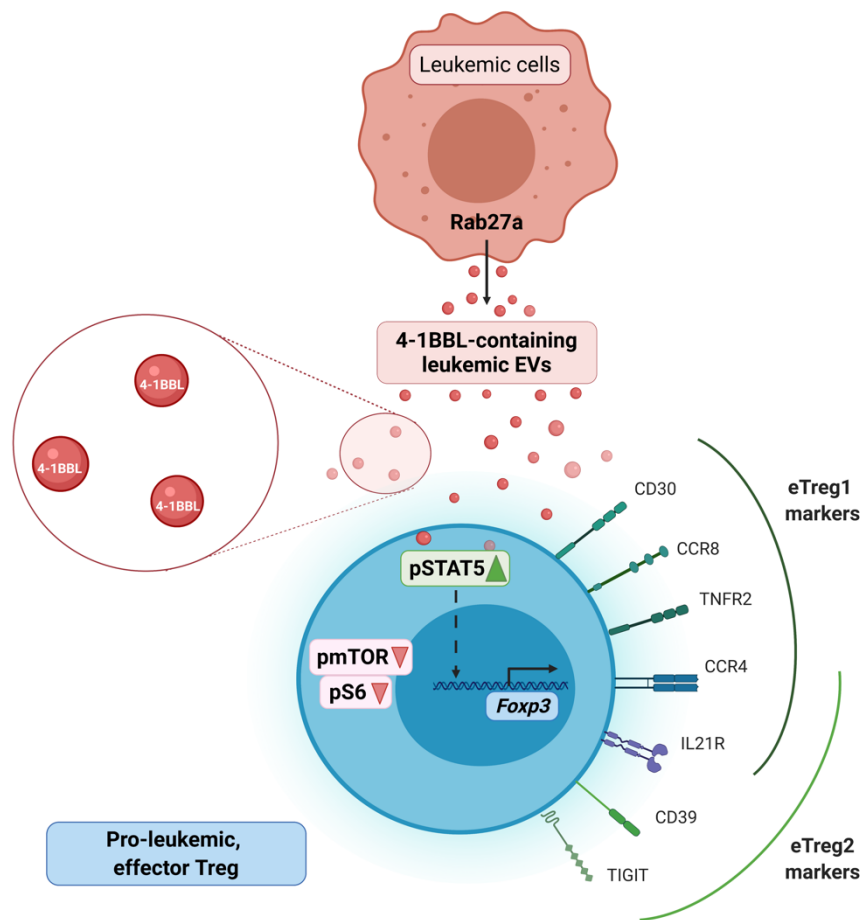


Figure 6.1 A schematic model showing regulation of Foxp3⁺ regulatory T cells by leukemic extracellular vesicles, based on results obtained in the presented thesis.

Conclusion:

Altogether, chronic and acute myeloid leukemia-derived extracellular vesicles promote effector, pro-leukemic Foxp3⁺ regulatory T cells which pinpoints a novel immunosuppressive mechanism in myeloid neoplasms. Leukemic EVs affect several aspects of Treg biology, such as Foxp3 induction, suppressive activity, transcriptome, signaling pathways and expansion of effector subsets. Based on *in vivo* experiments, it can be concluded that interaction between Rab27a-dependent EVs and Tregs is relevant for chronic myeloid leukemia development. We postulate that Rab27a and leukemic EVs-Tregs interaction could be therapeutically targeted in myeloid leukemias.

7 LITERATURE

1. Smith, D. L., Burthem, J. & Whetton, A. D. Molecular pathogenesis of chronic myeloid leukaemia. *Expert Rev. Mol. Med.* **5**, 1–27 (2003).
2. Siegel, R. L., Miller, K. D. & Jemal, A. Cancer statistics, 2019. *CA. Cancer J. Clin.* **69**, 7–34 (2019).
3. Dong, Y. *et al.* Leukemia incidence trends at the global, regional, and national level between 1990 and 2017. *Exp. Hematol. Oncol.* **9**, 14 (2020).
4. Shallis, R. M., Wang, R., Davidoff, A., Ma, X. & Zeidan, A. M. Epidemiology of acute myeloid leukemia: Recent progress and enduring challenges. *Blood Rev.* **36**, 70–87 (2019).
5. Hehlmann, R. & Hochhaus, A. Chronic myeloid leukaemia. **370**, 9 (2007).
6. De Kouchkovsky, I. & Abdul-Hay, M. 'Acute myeloid leukemia: a comprehensive review and 2016 update'. *Blood Cancer J.* **6**, e441–e441 (2016).
7. Döhner, H., Weisdorf, D. J. & Bloomfield, C. D. Acute Myeloid Leukemia. *N. Engl. J. Med.* **373**, 1136–1152 (2015).
8. Survival | Chronic myeloid leukaemia (CML) | Cancer Research UK. <https://www.cancerresearchuk.org/about-cancer/chronic-myeloid-leukaemia-cml/survival>.
9. Carter, J. L. *et al.* Targeting multiple signaling pathways: the new approach to acute myeloid leukemia therapy. *Signal Transduct. Target. Ther.* **5**, 288 (2020).
10. Daver, N., Venugopal, S. & Ravandi, F. FLT3 mutated acute myeloid leukemia: 2021 treatment algorithm. *Blood Cancer J.* **11**, 104 (2021).
11. Druker, B. J. *et al.* Effects of a selective inhibitor of the Abl tyrosine kinase on the growth of Bcr–Abl positive cells. *Nat. Med.* **2**, 561–566 (1996).
12. Chereda, B. & Melo, J. V. Natural course and biology of CML. *Ann. Hematol.* **94**, 107–121 (2015).
13. Chomel, J.-C. & Turhan, A. G. Chronic myeloid leukemia stem cells in the era of targeted therapies: resistance, persistence and long-term dormancy. *Oncotarget* **2**, 713–727 (2011).
14. Papaemmanuil, E. *et al.* Genomic Classification and Prognosis in Acute Myeloid Leukemia. *N. Engl. J. Med.* **374**, 2209–2221 (2016).
15. Bonnet, D. & Dick, J. E. Human acute myeloid leukemia is organized as a hierarchy that originates from a primitive hematopoietic cell. *Nat. Med.* **3**, 730–737 (1997).
16. Houshmand, M. *et al.* Chronic myeloid leukemia stem cells. *Leukemia* **33**, 1543–1556 (2019).
17. Taussig, D. C. *et al.* Leukemia-initiating cells from some acute myeloid leukemia patients with mutated nucleophosmin reside in the CD34 χ fraction. **115**, 10 (2010).
18. Swatler, J., Turos-Korgul, L., Kozłowska, E. & Piwocka, K. Immunosuppressive Cell Subsets and Factors in Myeloid Leukemias. *Cancers* **13**, 1203 (2021).
19. Hornick, N. I. *et al.* AML suppresses hematopoiesis by releasing exosomes that contain microRNAs targeting c-MYB. *Sci. Signal.* **9**, ra88–ra88 (2016).
20. Brück, O. *et al.* Immune cell contexture in the bone marrow tumor microenvironment impacts therapy response in CML. *Leukemia* **32**, 1643–1656 (2018).
21. Brück, O. *et al.* Immune profiles in acute myeloid leukemia bone marrow associate with patient age, T-cell receptor clonality, and survival. *Blood Adv.* **4**, 274–286 (2020).
22. Lamble, A. J. *et al.* Reversible suppression of T cell function in the bone marrow microenvironment of acute myeloid leukemia. *Proc. Natl. Acad. Sci.* **117**, 14331–14341 (2020).
23. Li, Z., Philip, M. & Ferrell, P. B. Alterations of T-cell-mediated immunity in acute myeloid leukemia. *Oncogene* **39**, 3611–3619 (2020).
24. Le Dieu, R. *et al.* Peripheral blood T cells in acute myeloid leukemia (AML) patients at diagnosis have abnormal phenotype and genotype and form defective immune synapses with AML blasts. *Blood* **114**, 3909–3916 (2009).
25. Hughes, A. & Yong, A. S. M. Immune Effector Recovery in Chronic Myeloid Leukemia and Treatment-Free Remission. *Front. Immunol.* **8**, 469 (2017).
26. Zha, X. *et al.* Alternative expression of TCR ζ related genes in patients with chronic myeloid leukemia. *J. Hematol. Oncol. J Hematol Oncol* **5**, 74 (2012).
27. Fauriat, C. *et al.* Deficient expression of NCR in NK cells from acute myeloid leukemia: evolution during leukemia treatment and impact of leukemia cells in NCRdull phenotype induction. *Blood* **109**, 323–330 (2007).
28. Ilander, M., Hekim, C. & Mustjoki, S. Immunology and Immunotherapy of Chronic Myeloid Leukemia. *Curr. Hematol. Malign. Rep.* **9**, 17–23 (2014).
29. Dufva, O. *et al.* Immunogenomic Landscape of Hematological Malignancies. *Cancer Cell* **38**, 380–399.e13 (2020).

30. Mumprecht, S., Schürch, C., Schwaller, J., Solenthaler, M. & Ochsenbein, A. F. Programmed death 1 signaling on chronic myeloid leukemia-specific T cells results in T-cell exhaustion and disease progression. *Blood* **114**, 1528–1536 (2009).
31. Sakaguchi, S., Fukuma, K., Kuribayashi, K. & Masuda, T. Organ-specific autoimmune diseases induced in mice by elimination of T cell subset. I. Evidence for the active participation of T cells in natural self-tolerance; deficit of a T cell subset as a possible cause of autoimmune disease. *J. Exp. Med.* **161**, 72–87 (1985).
32. Sakaguchi, S., Sakaguchi, N., Asano, M., Itoh, M. & Toda, M. Immunologic self-tolerance maintained by activated T cells expressing IL-2 receptor alpha-chains (CD25). Breakdown of a single mechanism of self-tolerance causes various autoimmune diseases. *J. Immunol.* **155**, 1151 (1995).
33. Hori, S. Control of Regulatory T Cell Development by the Transcription Factor Foxp3. *Science* **299**, 1057–1061 (2003).
34. Fontenot, J. D., Gavin, M. A. & Rudensky, A. Y. Foxp3 programs the development and function of CD4+CD25+ regulatory T cells. *Nat. Immunol.* **4**, 330–336 (2003).
35. Hori, S. FOXP3 as a master regulator of Treg cells. *Nat. Rev. Immunol.* **21**, 618–619 (2021).
36. Khattri, R., Cox, T., Yasayko, S.-A. & Ramsdell, F. An essential role for Scurfin in CD4+CD25+ T regulatory cells. *Nat. Immunol.* **4**, 337–342 (2003).
37. Feuerer, M., Hill, J. A., Mathis, D. & Benoist, C. Foxp3+ regulatory T cells: differentiation, specification, subphenotypes. *Nat. Immunol.* **10**, 689–695 (2009).
38. Barra, M. M., Richards, D. M., Hofer, A.-C., Delacher, M. & Feuerer, M. Premature Expression of Foxp3 in Double-Negative Thymocytes. *PLOS ONE* **10**, e0127038 (2015).
39. Kraj, P. & Ignatowicz, L. The mechanisms shaping the repertoire of CD4 + Foxp3 + regulatory T cells. *Immunology* **153**, 290–296 (2018).
40. Wojciech, L. *et al.* The same self-peptide selects conventional and regulatory CD4+ T cells with identical antigen receptors. *Nat. Commun.* **5**, 5061 (2014).
41. Owen, D. L., Sjaastad, L. E. & Farrar, M. A. Regulatory T Cell Development in the Thymus. *J. Immunol.* **203**, 2031–2041 (2019).
42. Hsieh, C.-S. *et al.* Recognition of the Peripheral Self by Naturally Arising CD25+ CD4+ T Cell Receptors. *Immunity* **21**, 267–277 (2004).
43. Cheng, M. & Anderson, M. S. Thymic tolerance as a key brake on autoimmunity. *Nat. Immunol.* **19**, 659–664 (2018).
44. Chen, W. *et al.* Conversion of Peripheral CD4+CD25– Naive T Cells to CD4+CD25+ Regulatory T Cells by TGF- β Induction of Transcription Factor Foxp3. *J. Exp. Med.* **198**, 1875–1886 (2003).
45. Josefowicz, S. Z., Lu, L.-F. & Rudensky, A. Y. Regulatory T Cells: Mechanisms of Differentiation and Function. *Annu. Rev. Immunol.* **30**, 531–564 (2012).
46. Arpaia, N. & Rudensky, A. Y. Microbial metabolites control gut inflammatory responses: Fig. 1. *Proc. Natl. Acad. Sci.* **111**, 2058–2059 (2014).
47. Abbas, A. K. *et al.* Regulatory T cells: recommendations to simplify the nomenclature. *Nat. Immunol.* **14**, 307–308 (2013).
48. Wing, J. B., Tanaka, A. & Sakaguchi, S. Human FOXP3+ Regulatory T Cell Heterogeneity and Function in Autoimmunity and Cancer. *Immunity* **50**, 302–316 (2019).
49. Zheng, Y. *et al.* Role of conserved non-coding DNA elements in the Foxp3 gene in regulatory T-cell fate. *Nature* **463**, 808–812 (2010).
50. Yadav, M. *et al.* Neuropilin-1 distinguishes natural and inducible regulatory T cells among regulatory T cell subsets in vivo. *J. Exp. Med.* **209**, 1713–1722 (2012).
51. Thornton, A. M. *et al.* Helios + and Helios – Treg subpopulations are phenotypically and functionally distinct and express dissimilar TCR repertoires. *Eur. J. Immunol.* **49**, 398–412 (2019).
52. Szurek, E. *et al.* Differences in Expression Level of Helios and Neuropilin-1 Do Not Distinguish Thymus-Derived from Extrathymically-Induced CD4+Foxp3+ Regulatory T Cells. *PLOS ONE* **10**, e0141161 (2015).
53. Ito, T. *et al.* Two Functional Subsets of FOXP3+ Regulatory T Cells in Human Thymus and Periphery. *Immunity* **28**, 870–880 (2008).
54. Opstelten, R. *et al.* GPA33: A Marker to Identify Stable Human Regulatory T Cells. *J. Immunol.* **204**, 3139–3148 (2020).
55. Floess, S. *et al.* Epigenetic Control of the foxp3 Locus in Regulatory T Cells. *PLoS Biol.* **5**, e38 (2007).
56. Plitas, G. & Rudensky, A. Y. Regulatory T Cells: Differentiation and Function. *Cancer Immunol.*

- Res.* **4**, 721–725 (2016).
57. Ohkura, N. *et al.* Regulatory T Cell-Specific Epigenomic Region Variants Are a Key Determinant of Susceptibility to Common Autoimmune Diseases. *Immunity* **52**, 1119–1132.e4 (2020).
 58. Liu, Z. *et al.* Immune homeostasis enforced by co-localized effector and regulatory T cells. *Nature* **528**, 225–230 (2015).
 59. Wing, K. *et al.* CTLA-4 Control over Foxp3+ Regulatory T Cell Function. *Science* **322**, 271–275 (2008).
 60. Hodi, F. S. *et al.* Improved Survival with Ipilimumab in Patients with Metastatic Melanoma. *N. Engl. J. Med.* **363**, 711–723 (2010).
 61. Deaglio, S. *et al.* Adenosine generation catalyzed by CD39 and CD73 expressed on regulatory T cells mediates immune suppression. *J. Exp. Med.* **204**, 1257–1265 (2007).
 62. Borsellino, G. *et al.* Expression of ectonucleotidase CD39 by Foxp3+ Treg cells: hydrolysis of extracellular ATP and immune suppression. *Blood* **110**, 1225–1232 (2007).
 63. Li *et al.* - 2019 - Dysfunctional CD8 T Cells Form a Proliferative, Dy.pdf.
 64. Le, B. V. *et al.* TGF β R-SMAD3 Signaling Induces Resistance to PARP Inhibitors in the Bone Marrow Microenvironment. *Cell Rep.* **33**, 108221 (2020).
 65. Huber, S. *et al.* Th17 Cells Express Interleukin-10 Receptor and Are Controlled by Foxp3– and Foxp3+ Regulatory CD4+ T Cells in an Interleukin-10-Dependent Manner. *Immunity* **34**, 554–565 (2011).
 66. Cao, X. *et al.* Granzyme B and Perforin Are Important for Regulatory T Cell-Mediated Suppression of Tumor Clearance. *Immunity* **27**, 635–646 (2007).
 67. Campbell, C. & Rudensky, A. Roles of Regulatory T Cells in Tissue Pathophysiology and Metabolism. *Cell Metab.* **31**, 18–25 (2020).
 68. Hirata, Y. *et al.* CD150high Bone Marrow Tregs Maintain Hematopoietic Stem Cell Quiescence and Immune Privilege via Adenosine. *Cell Stem Cell* **22**, 445–453.e5 (2018).
 69. Lu, L., Barbi, J. & Pan, F. The regulation of immune tolerance by FOXP3. *Nat. Rev. Immunol.* **17**, 703–717 (2017).
 70. Kwon, H.-K., Chen, H.-M., Mathis, D. & Benoist, C. Different molecular complexes that mediate transcriptional induction and repression by FoxP3. *Nat. Immunol.* **18**, 1238–1248 (2017).
 71. Zheng, Y. *et al.* Regulatory T-cell suppressor program co-opts transcription factor IRF4 to control TH2 responses. *Nature* **458**, 351–356 (2009).
 72. Ono, M. *et al.* Foxp3 controls regulatory T-cell function by interacting with AML1/Runx1. *Nature* **446**, 685–689 (2007).
 73. Wu, Y. *et al.* FOXP3 Controls Regulatory T Cell Function through Cooperation with NFAT. *Cell* **126**, 375–387 (2006).
 74. Dominguez-Villar, M. & Hafler, D. A. Regulatory T cells in autoimmune disease. *Nat. Immunol.* **19**, 665–673 (2018).
 75. Chen, C., Rowell, E. A., Thomas, R. M., Hancock, W. W. & Wells, A. D. Transcriptional Regulation by Foxp3 Is Associated with Direct Promoter Occupancy and Modulation of Histone Acetylation. *J. Biol. Chem.* **281**, 36828–36834 (2006).
 76. Ohkura, N. *et al.* T Cell Receptor Stimulation-Induced Epigenetic Changes and Foxp3 Expression Are Independent and Complementary Events Required for Treg Cell Development. *Immunity* **37**, 785–799 (2012).
 77. Huehn, J., Polansky, J. K. & Hamann, A. Epigenetic control of FOXP3 expression: the key to a stable regulatory T-cell lineage? *Nat. Rev. Immunol.* **9**, 83–89 (2009).
 78. Nair, V. S., Song, M. H., Ko, M. & Oh, K. I. DNA Demethylation of the Foxp3 Enhancer Is Maintained through Modulation of Ten-Eleven-Translocation and DNA Methyltransferases. *Mol. Cells* **39**, 888–897 (2016).
 79. Gerriets, V. A. *et al.* Foxp3 and Toll-like receptor signaling balance Treg cell anabolic metabolism for suppression. *Nat. Immunol.* **17**, 1459–1466 (2016).
 80. Delgoffe, G. M. *et al.* The mTOR Kinase Differentially Regulates Effector and Regulatory T Cell Lineage Commitment. *Immunity* **30**, 832–844 (2009).
 81. Vasanthakumar, A. *et al.* The TNF Receptor Superfamily-NF- κ B Axis Is Critical to Maintain Effector Regulatory T Cells in Lymphoid and Non-lymphoid Tissues. *Cell Rep.* **20**, 2906–2920 (2017).
 82. Lubrano di Ricco, M. *et al.* Tumor necrosis factor receptor family costimulation increases regulatory T-cell activation and function via NF- κ B. *Eur. J. Immunol.* **50**, 972–985 (2020).
 83. Ronin, E. *et al.* The NF- κ B RelA Transcription Factor Is Critical for Regulatory T Cell Activation

- and Stability. *Front. Immunol.* **10**, 2487 (2019).
84. Chen, Z. *et al.* The Ubiquitin Ligase Stub1 Negatively Modulates Regulatory T Cell Suppressive Activity by Promoting Degradation of the Transcription Factor Foxp3. *Immunity* **39**, 272–285 (2013).
 85. Wang, L. *et al.* Ubiquitin-specific Protease-7 Inhibition Impairs Tip60-dependent Foxp3 + T-regulatory Cell Function and Promotes Antitumor Immunity. *EBioMedicine* **13**, 99–112 (2016).
 86. Bates, G. J. *et al.* Quantification of Regulatory T Cells Enables the Identification of High-Risk Breast Cancer Patients and Those at Risk of Late Relapse. *J. Clin. Oncol.* **24**, 5373–5380 (2006).
 87. Sato, E. *et al.* Intraepithelial CD8+ tumor-infiltrating lymphocytes and a high CD8+/regulatory T cell ratio are associated with favorable prognosis in ovarian cancer. *Proc. Natl. Acad. Sci.* **102**, 18538–18543 (2005).
 88. Shimizu, J., Yamazaki, S. & Sakaguchi, S. Induction of Tumor Immunity by Removing CD25+CD4+ T Cells: A Common Basis Between Tumor Immunity and Autoimmunity. *J. Immunol.* **163**, 5211 (1999).
 89. Liu, J. *et al.* Assessing Immune-Related Adverse Events of Efficacious Combination Immunotherapies in Preclinical Models of Cancer. *Cancer Res.* **76**, 5288–5301 (2016).
 90. Taylor, N. A. *et al.* Treg depletion potentiates checkpoint inhibition in claudin-low breast cancer. *J. Clin. Invest.* **127**, 3472–3483 (2017).
 91. Teng, M. W. L. *et al.* Conditional Regulatory T-Cell Depletion Releases Adaptive Immunity Preventing Carcinogenesis and Suppressing Established Tumor Growth. *Cancer Res.* **70**, 7800–7809 (2010).
 92. Tanaka, A. & Sakaguchi, S. Targeting Treg cells in cancer immunotherapy. *Eur. J. Immunol.* **49**, 1140–1146 (2019).
 93. Andrews, L. P., Marciscano, A. E., Drake, C. G. & Vignali, D. A. A. LAG3 (CD223) as a cancer immunotherapy target. *Immunol. Rev.* **276**, 80–96 (2017).
 94. Lucca, L. E. & Dominguez-Villar, M. Modulation of regulatory T cell function and stability by co-inhibitory receptors. *Nat. Rev. Immunol.* **20**, 680–693 (2020).
 95. Joller, N. *et al.* Treg Cells Expressing the Coinhibitory Molecule TIGIT Selectively Inhibit Proinflammatory Th1 and Th17 Cell Responses. *Immunity* **40**, 569–581 (2014).
 96. De Simone, M. *et al.* Transcriptional Landscape of Human Tissue Lymphocytes Unveils Uniqueness of Tumor-Infiltrating T Regulatory Cells. *Immunity* **45**, 1135–1147 (2016).
 97. Mizukami, Y. *et al.* CCL17 and CCL22 chemokines within tumor microenvironment are related to accumulation of Foxp3+ regulatory T cells in gastric cancer. *Int. J. Cancer* **122**, 2286–2293 (2008).
 98. Plitas, G. *et al.* Regulatory T Cells Exhibit Distinct Features in Human Breast Cancer. *Immunity* **45**, 1122–1134 (2016).
 99. Van Damme, H. *et al.* Therapeutic depletion of CCR8 + tumor-infiltrating regulatory T cells elicits antitumor immunity and synergizes with anti-PD-1 therapy. *J. Immunother. Cancer* **9**, e001749 (2021).
 100. Azizi, E. *et al.* Single-Cell Map of Diverse Immune Phenotypes in the Breast Tumor Microenvironment. *Cell* **174**, 1293–1308.e36 (2018).
 101. Magnuson, A. M. *et al.* Identification and validation of a tumor-infiltrating Treg transcriptional signature conserved across species and tumor types. *Proc. Natl. Acad. Sci.* **115**, E10672–E10681 (2018).
 102. Alvisi, G. *et al.* IRF4 instructs effector Treg differentiation and immune suppression in human cancer. *J. Clin. Invest.* **130**, 3137–3150 (2020).
 103. Wang, H. *et al.* CD36-mediated metabolic adaptation supports regulatory T cell survival and function in tumors. *Nat. Immunol.* **21**, 298–308 (2020).
 104. Kumagai, S. *et al.* An Oncogenic Alteration Creates a Microenvironment that Promotes Tumor Progression by Conferring a Metabolic Advantage to Regulatory T Cells. *Immunity* **53**, 187–203.e8 (2020).
 105. Pacella, I. *et al.* Fatty acid metabolism complements glycolysis in the selective regulatory T cell expansion during tumor growth. *Proc. Natl. Acad. Sci.* **115**, E6546–E6555 (2018).
 106. Watson, M. J. *et al.* Metabolic support of tumour-infiltrating regulatory T cells by lactic acid. *Nature* **591**, 645–651 (2021).
 107. Zappasodi, R. *et al.* CTLA-4 blockade drives loss of Treg stability in glycolysis-low tumours. *Nature* **591**, 652–658 (2021).
 108. Newton, R., Priyadarshini, B. & Turka, L. A. Immunometabolism of regulatory T cells. *Nat.*

- Immunol.* **17**, 618–625 (2016).
109. Ha, D. *et al.* Differential control of human Treg and effector T cells in tumor immunity by Fc-engineered anti-CTLA-4 antibody. *Proc. Natl. Acad. Sci.* **116**, 609–618 (2019).
 110. Sugiyama, D. *et al.* Anti-CCR4 mAb selectively depletes effector-type FoxP3+CD4+ regulatory T cells, evoking antitumor immune responses in humans. *Proc. Natl. Acad. Sci.* **110**, 17945–17950 (2013).
 111. Dong, Q. *et al.* Levels and Clinical Significance of Regulatory B Cells and T Cells in Acute Myeloid Leukemia. *BioMed Res. Int.* **2020**, 1–6 (2020).
 112. Hughes, A. *et al.* CML patients with deep molecular responses to TKI have restored immune effectors and decreased PD-1 and immune suppressors. *Blood* **129**, 1166–1176 (2017).
 113. Szczepanski, M. J. *et al.* Increased Frequency and Suppression by Regulatory T Cells in Patients with Acute Myelogenous Leukemia. *Clin. Cancer Res.* **15**, 3325–3332 (2009).
 114. Wan, Y. *et al.* Hyperfunction of CD4 CD25 regulatory T cells in de novo acute myeloid leukemia. *BMC Cancer* **20**, 472 (2020).
 115. Tao, Q. *et al.* Regulatory T cells-derived IL-35 promotes the growth of adult acute myeloid leukemia blasts: IL-35 in the pathogenesis of AML. *Int. J. Cancer* **137**, 2384–2393 (2015).
 116. Rojas, J. M. *et al.* Naturally occurring CD4+ CD25+ FOXP3+ T-regulatory cells are increased in chronic myeloid leukemia patients not in complete cytogenetic remission and can be immunosuppressive. *Exp. Hematol.* **38**, 1209–1218 (2010).
 117. Tian, T. *et al.* The Profile of T Helper Subsets in Bone Marrow Microenvironment Is Distinct for Different Stages of Acute Myeloid Leukemia Patients and Chemotherapy Partly Ameliorates These Variations. *PLOS ONE* **10**, e0131761 (2015).
 118. Brück, O. *et al.* Immune cell contexture in the bone marrow tumor microenvironment impacts therapy response in CML. *Leukemia* **32**, 1643–1656 (2018).
 119. Wang, R. *et al.* Blocking migration of regulatory T cells to leukemic hematopoietic microenvironment delays disease progression in mouse leukemia model. *Cancer Lett.* **469**, 151–161 (2020).
 120. Zahran, A. M., Badrawy, H. & Ibrahim, A. Prognostic value of regulatory T cells in newly diagnosed chronic myeloid leukemia patients. *Int. J. Clin. Oncol.* **19**, 753–760 (2014).
 121. Lamble, A. J. & Lind, E. F. Targeting the Immune Microenvironment in Acute Myeloid Leukemia: A Focus on T Cell Immunity. *Front. Oncol.* **8**, 213 (2018).
 122. Yang, W. & Xu, Y. Clinical significance of Treg cell frequency in acute myeloid leukemia. *Int. J. Hematol.* **98**, 558–562 (2013).
 123. Williams, P. *et al.* The distribution of T-cell subsets and the expression of immune checkpoint receptors and ligands in patients with newly diagnosed and relapsed acute myeloid leukemia. *Cancer* **125**, 1470–1481 (2019).
 124. Delia, M. *et al.* After Treatment Decrease of Bone Marrow Tregs and Outcome in Younger Patients with Newly Diagnosed Acute Myeloid Leukemia. *J. Immunol. Res.* **2020**, 1–11 (2020).
 125. Govindaraj, C. *et al.* Reducing TNF Receptor 2 + Regulatory T Cells via the Combined Action of Azacitidine and the HDAC Inhibitor, Panobinostat for Clinical Benefit in Acute Myeloid Leukemia Patients. *Clin. Cancer Res.* **20**, 724–735 (2014).
 126. Lu, Z. *et al.* Therapeutic immune monitoring of CD4+CD25+ T cells in chronic myeloid leukemia patients treated with tyrosine kinase inhibitors. *Oncol. Lett.* **14**, 1363–1372 (2017).
 127. Najima, Y. *et al.* Regulatory T cell inhibition by dasatinib is associated with natural killer cell differentiation and a favorable molecular response—The final results of the D-first study. *Leuk. Res.* **66**, 66–72 (2018).
 128. Irani, Y. D. *et al.* Successful treatment-free remission in chronic myeloid leukaemia and its association with reduced immune suppressors and increased natural killer cells. *Br. J. Haematol.* **191**, 433–441 (2020).
 129. Tanaka, A. *et al.* Tyrosine kinase inhibitor imatinib augments tumor immunity by depleting effector regulatory T cells. *J. Exp. Med.* **217**, e20191009 (2020).
 130. Larmonier, N. *et al.* Imatinib Mesylate Inhibits CD4 + CD25 + Regulatory T Cell Activity and Enhances Active Immunotherapy against BCR-ABL - Tumors. *J. Immunol.* **181**, 6955–6963 (2008).
 131. Delluc, S. *et al.* Dramatic efficacy improvement of a DC-based vaccine against AML by CD25 T cell depletion allowing the induction of a long-lasting T cell response. *Cancer Immunol. Immunother.* **58**, 1669–1677 (2009).
 132. Zhou, Q. *et al.* Depletion of endogenous tumor-associated regulatory T cells improves the efficacy

- of adoptive cytotoxic T-cell immunotherapy in murine acute myeloid leukemia. *Blood* **114**, 3793–3802 (2009).
133. Hinterbrandner, M. *et al.* Tnfrsf4-expressing regulatory T cells promote immune escape of chronic myeloid leukemia stem cells. *JCI Insight* (2021) doi:10.1172/jci.insight.151797.
 134. Curti, A. *et al.* Modulation of tryptophan catabolism by human leukemic cells results in the conversion of CD25 α into CD25 γ T regulatory cells. **109**, 7 (2007).
 135. Mansour, I., Zayed, R. A., Said, F. & Latif, L. A. Indoleamine 2,3-dioxygenase and regulatory T cells in acute myeloid leukemia. *Hematology* **21**, 447–453 (2016).
 136. Han, Y. *et al.* Acute Myeloid Leukemia Cells Express ICOS Ligand to Promote the Expansion of Regulatory T Cells. *Front. Immunol.* **9**, 2227 (2018).
 137. Dong, Y. *et al.* PD-L1 Is Expressed and Promotes the Expansion of Regulatory T Cells in Acute Myeloid Leukemia. *Front. Immunol.* **11**, 1710 (2020).
 138. Zhou, Q. *et al.* Coexpression of Tim-3 and PD-1 identifies a CD8 γ T-cell exhaustion phenotype in mice with disseminated acute myelogenous leukemia. **117**, 10 (2011).
 139. Coles, S. J. *et al.* Increased CD200 expression in acute myeloid leukemia is linked with an increased frequency of FoxP3+ regulatory T cells. *Leukemia* **26**, 2146–2148 (2012).
 140. Colombo, M., Raposo, G. & Théry, C. Biogenesis, Secretion, and Intercellular Interactions of Exosomes and Other Extracellular Vesicles. *Annu. Rev. Cell Dev. Biol.* **30**, 255–289 (2014).
 141. van Niel, G., D'Angelo, G. & Raposo, G. Shedding light on the cell biology of extracellular vesicles. *Nat. Rev. Mol. Cell Biol.* **19**, 213–228 (2018).
 142. Swatler, J., Dudka, W. & Piwocka, K. Isolation and Characterization of Extracellular Vesicles from Cell Culture Conditioned Medium for Immunological Studies. *Curr. Protoc. Immunol.* **129**, (2020).
 143. Kowal, J. *et al.* Proteomic comparison defines novel markers to characterize heterogeneous populations of extracellular vesicle subtypes. *Proc. Natl. Acad. Sci.* **113**, E968–E977 (2016).
 144. Tkach, M. *et al.* Qualitative differences in T-cell activation by dendritic cell-derived extracellular vesicle subtypes. *EMBO J.* **36**, 3012–3028 (2017).
 145. Mathieu, M., Martin-Jaular, L., Lavieu, G. & Théry, C. Specificities of secretion and uptake of exosomes and other extracellular vesicles for cell-to-cell communication. *Nat. Cell Biol.* **21**, 9–17 (2019).
 146. Trajkovic, K. *et al.* Ceramide Triggers Budding of Exosome Vesicles into Multivesicular Endosomes. *Science* **319**, 1244–1247 (2008).
 147. Ostrowski, M. *et al.* Rab27a and Rab27b control different steps of the exosome secretion pathway. *Nat. Cell Biol.* **12**, 19–30 (2010).
 148. Van Deun, J. *et al.* The impact of disparate isolation methods for extracellular vesicles on downstream RNA profiling. *J. Extracell. Vesicles* **3**, 24858 (2014).
 149. Kang, M., Jordan, V., Blenkiron, C. & Chamley, L. W. Biodistribution of extracellular vesicles following administration into animals: A systematic review. *J. Extracell. Vesicles* **10**, (2021).
 150. Wiklander, O. P. B. *et al.* Extracellular vesicle in vivo biodistribution is determined by cell source, route of administration and targeting. *J. Extracell. Vesicles* **4**, 26316 (2015).
 151. Kamerkar, S. *et al.* Exosomes facilitate therapeutic targeting of oncogenic KRAS in pancreatic cancer. *Nature* **546**, 498–503 (2017).
 152. Zitvogel, L. *et al.* Eradication of established murine tumors using a novel cell-free vaccine: dendritic cell derived exosomes. *Nat. Med.* **4**, 594–600 (1998).
 153. Valadi, H. *et al.* Exosome-mediated transfer of mRNAs and microRNAs is a novel mechanism of genetic exchange between cells. *Nat. Cell Biol.* **9**, 654–659 (2007).
 154. Pan, B.-T. & Johnstone, R. M. Fate of the transferrin receptor during maturation of sheep reticulocytes in vitro: Selective externalization of the receptor. *Cell* **33**, 967–978 (1983).
 155. Bebelman, M. P. *et al.* Real-time imaging of multivesicular body–plasma membrane fusion to quantify exosome release from single cells. *Nat. Protoc.* **15**, 102–121 (2020).
 156. Verweij, F. J. *et al.* Live Tracking of Inter-organ Communication by Endogenous Exosomes In Vivo. *Dev. Cell* **48**, 573–589.e4 (2019).
 157. Théry, C., Amigorena, S., Raposo, G. & Clayton, A. Isolation and Characterization of Exosomes from Cell Culture Supernatants and Biological Fluids. *Curr. Protoc. Cell Biol.* **30**, (2006).
 158. Raposo, G. *et al.* B lymphocytes secrete antigen-presenting vesicles. *J. Exp. Med.* **183**, 1161–1172 (1996).
 159. Gardiner, C. *et al.* Techniques used for the isolation and characterization of extracellular vesicles: results of a worldwide survey. *J. Extracell. Vesicles* **5**, 32945 (2016).
 160. Shelke, G. V., Lässer, C., Gho, Y. S. & Lötvall, J. Importance of exosome depletion protocols to

- eliminate functional and RNA-containing extracellular vesicles from fetal bovine serum. *J. Extracell. Vesicles* **3**, 24783 (2014).
161. Karimi, N. *et al.* Detailed analysis of the plasma extracellular vesicle proteome after separation from lipoproteins. *Cell. Mol. Life Sci.* **75**, 2873–2886 (2018).
 162. Lötvall, J. *et al.* Minimal experimental requirements for definition of extracellular vesicles and their functions: a position statement from the International Society for Extracellular Vesicles. *J. Extracell. Vesicles* **3**, 26913 (2014).
 163. Théry, C. *et al.* Minimal information for studies of extracellular vesicles 2018 (MISEV2018): a position statement of the International Society for Extracellular Vesicles and update of the MISEV2014 guidelines. *J. Extracell. Vesicles* **7**, 1535750 (2018).
 164. Mateescu, B. *et al.* Obstacles and opportunities in the functional analysis of extracellular vesicle RNA – an ISEV position paper. *J. Extracell. Vesicles* **6**, 1286095 (2017).
 165. Welsh, J. A. *et al.* MIFlowCyt-EV: a framework for standardized reporting of extracellular vesicle flow cytometry experiments. *J. Extracell. Vesicles* **9**, 1713526 (2020).
 166. Lener, T. *et al.* Applying extracellular vesicles based therapeutics in clinical trials – an ISEV position paper. *J. Extracell. Vesicles* **4**, 30087 (2015).
 167. EV-TRACK Consortium *et al.* EV-TRACK: transparent reporting and centralizing knowledge in extracellular vesicle research. *Nat. Methods* **14**, 228–232 (2017).
 168. Théry, C. *et al.* Indirect activation of naïve CD4+ T cells by dendritic cell-derived exosomes. *Nat. Immunol.* **3**, 1156–1162 (2002).
 169. Marar, C., Starich, B. & Wirtz, D. Extracellular vesicles in immunomodulation and tumor progression. *Nat. Immunol.* **22**, 560–570 (2021).
 170. Zeng, F. & Morelli, A. E. Extracellular vesicle-mediated MHC cross-dressing in immune homeostasis, transplantation, infectious diseases, and cancer. *Semin. Immunopathol.* **40**, 477–490 (2018).
 171. Driedonks, T. A. P. *et al.* Immune stimuli shape the small non-coding transcriptome of extracellular vesicles released by dendritic cells. *Cell. Mol. Life Sci.* **75**, 3857–3875 (2018).
 172. Cai, Z. *et al.* Immunosuppressive exosomes from TGF- β 1 gene-modified dendritic cells attenuate Th17-mediated inflammatory autoimmune disease by inducing regulatory T cells. *Cell Res.* **22**, 607–610 (2012).
 173. Torralba, D. *et al.* Priming of dendritic cells by DNA-containing extracellular vesicles from activated T cells through antigen-driven contacts. *Nat. Commun.* **9**, 2658 (2018).
 174. Tung, S. L. *et al.* Regulatory T cell-derived extracellular vesicles modify dendritic cell function. *Sci. Rep.* **8**, 6065 (2018).
 175. Okoye, I. S. *et al.* MicroRNA-Containing T-Regulatory-Cell-Derived Exosomes Suppress Pathogenic T Helper 1 Cells. *Immunity* **41**, 89–103 (2014).
 176. Robbins, P. D. & Morelli, A. E. Regulation of immune responses by extracellular vesicles. *Nat. Rev. Immunol.* **14**, 195–208 (2014).
 177. Gowen, A., Shahjin, F., Chand, S., Odegaard, K. E. & Yelamanchili, S. V. Mesenchymal Stem Cell-Derived Extracellular Vesicles: Challenges in Clinical Applications. *Front. Cell Dev. Biol.* **8**, 149 (2020).
 178. Chen, G. *et al.* Exosomal PD-L1 contributes to immunosuppression and is associated with anti-PD-1 response. *Nature* **560**, 382–386 (2018).
 179. Haderk, F. *et al.* Tumor-derived exosomes modulate PD-L1 expression in monocytes. *Sci. Immunol.* **2**, eaah5509 (2017).
 180. Gabrusiewicz, K. *et al.* Glioblastoma stem cell-derived exosomes induce M2 macrophages and PD-L1 expression on human monocytes. *OncolImmunology* **7**, e1412909 (2018).
 181. Salimu, J. *et al.* Dominant immunosuppression of dendritic cell function by prostate-cancer-derived exosomes. *J. Extracell. Vesicles* **6**, 1368823 (2017).
 182. Park, J. E. *et al.* Hypoxia-induced tumor exosomes promote M2-like macrophage polarization of infiltrating myeloid cells and microRNA-mediated metabolic shift. *Oncogene* **38**, 5158–5173 (2019).
 183. Berchem, G. *et al.* Hypoxic tumor-derived microvesicles negatively regulate NK cell function by a mechanism involving TGF- β and miR23a transfer. *OncolImmunology* **5**, e1062968 (2016).
 184. Skog, J. *et al.* Glioblastoma microvesicles transport RNA and proteins that promote tumour growth and provide diagnostic biomarkers. *Nat. Cell Biol.* **10**, 1470–1476 (2008).
 185. Tanaka, Y. *et al.* Clinical impact of serum exosomal microRNA-21 as a clinical biomarker in human esophageal squamous cell carcinoma: Exosomal MicroRNA-21 Expression in ESCC.

- Cancer* **119**, 1159–1167 (2013).
186. Kalluri, R. The biology and function of exosomes in cancer. *J. Clin. Invest.* **126**, 1208–1215 (2016).
 187. Park, J. E. *et al.* Hypoxic Tumor Cell Modulates Its Microenvironment to Enhance Angiogenic and Metastatic Potential by Secretion of Proteins and Exosomes. *Mol. Cell. Proteomics* **9**, 1085–1099 (2010).
 188. Peinado, H. *et al.* Melanoma exosomes educate bone marrow progenitor cells toward a pro-metastatic phenotype through MET. *Nat. Med.* **18**, 883–891 (2012).
 189. Zhou, W. *et al.* Cancer-Secreted miR-105 Destroys Vascular Endothelial Barriers to Promote Metastasis. *Cancer Cell* **25**, 501–515 (2014).
 190. Naito, Y. *et al.* Cancer extracellular vesicles contribute to stromal heterogeneity by inducing chemokines in cancer-associated fibroblasts. *Oncogene* **38**, 5566–5579 (2019).
 191. Webber, J. P. *et al.* Differentiation of tumour-promoting stromal myofibroblasts by cancer exosomes. *Oncogene* **34**, 290–302 (2015).
 192. Boelens, M. C. *et al.* Exosome Transfer from Stromal to Breast Cancer Cells Regulates Therapy Resistance Pathways. *Cell* **159**, 499–513 (2014).
 193. Dourado, M. R. *et al.* Extracellular vesicles derived from cancer-associated fibroblasts induce the migration and invasion of oral squamous cell carcinoma. *J. Extracell. Vesicles* **8**, 1578525 (2019).
 194. Kalluri, R. The biology and function of exosomes in cancer. *J. Clin. Invest.* **126**, 1208–1215 (2016).
 195. Hoshino, D. *et al.* Exosome Secretion Is Enhanced by Invadopodia and Drives Invasive Behavior. *Cell Rep.* **5**, 1159–1168 (2013).
 196. Mu, W., Rana, S. & Zöller, M. Host Matrix Modulation by Tumor Exosomes Promotes Motility and Invasiveness. *Neoplasia* **15**, 875-IN4 (2013).
 197. Becker, A. *et al.* Extracellular Vesicles in Cancer: Cell-to-Cell Mediators of Metastasis. *Cancer Cell* **30**, 836–848 (2016).
 198. Clayton, A., Al-Taei, S., Webber, J., Mason, M. D. & Tabi, Z. Cancer Exosomes Express CD39 and CD73, Which Suppress T Cells through Adenosine Production. *J. Immunol.* **187**, 676–683 (2011).
 199. Czystowska-Kuzmicz, M. *et al.* Small extracellular vesicles containing arginase-1 suppress T-cell responses and promote tumor growth in ovarian carcinoma. *Nat. Commun.* **10**, 3000 (2019).
 200. Ludwig, S. *et al.* Suppression of Lymphocyte Functions by Plasma Exosomes Correlates with Disease Activity in Patients with Head and Neck Cancer. *Clin. Cancer Res.* **23**, 4843–4854 (2017).
 201. Muller, L. *et al.* Human tumor-derived exosomes (TEX) regulate Treg functions via cell surface signaling rather than uptake mechanisms. *Oncolimmunology* **6**, e1261243 (2017).
 202. Poggio, M. *et al.* Suppression of Exosomal PD-L1 Induces Systemic Anti-tumor Immunity and Memory. *Cell* **177**, 414–427.e13 (2019).
 203. Theodoraki, M.-N., Yerneni, S. S., Hoffmann, T. K., Gooding, W. E. & Whiteside, T. L. Clinical Significance of PD-L1 + Exosomes in Plasma of Head and Neck Cancer Patients. *Clin. Cancer Res.* **24**, 896–905 (2018).
 204. Troyer, R. M. *et al.* Exosomes from Osteosarcoma and normal osteoblast differ in proteomic cargo and immunomodulatory effects on T cells. *Exp. Cell Res.* **358**, 369–376 (2017).
 205. Muller, L., Mitsuhashi, M., Simms, P., Gooding, W. E. & Whiteside, T. L. Tumor-derived exosomes regulate expression of immune function-related genes in human T cell subsets. *Sci. Rep.* **6**, 20254 (2016).
 206. Ricklefs, F. L. *et al.* Immune evasion mediated by PD-L1 on glioblastoma-derived extracellular vesicles. *Sci. Adv.* **4**, eaar2766 (2018).
 207. Szajnik, M., Czystowska, M., Szczepanski, M. J., Mandapathil, M. & Whiteside, T. L. Tumor-Derived Microvesicles Induce, Expand and Up-Regulate Biological Activities of Human Regulatory T Cells (Treg). *PLoS ONE* **5**, e11469 (2010).
 208. Wieckowski, E. U. *et al.* Tumor-Derived Microvesicles Promote Regulatory T Cell Expansion and Induce Apoptosis in Tumor-Reactive Activated CD8 + T Lymphocytes. *J. Immunol.* **183**, 3720–3730 (2009).
 209. Ye, S. *et al.* Tumor-derived exosomes promote tumor progression and T-cell dysfunction through the regulation of enriched exosomal microRNAs in human nasopharyngeal carcinoma. *Oncotarget* **5**, 5439–5452 (2014).
 210. Ye, S.-B. *et al.* Exosomal miR-24-3p impedes T-cell function by targeting *FGF11* and serves as

- a potential prognostic biomarker for nasopharyngeal carcinoma: Role of exosomal miR-24 in immune regulation of nasopharyngeal carcinoma. *J. Pathol.* **240**, 329–340 (2016).
211. Mrizak, D. *et al.* Effect of Nasopharyngeal Carcinoma-Derived Exosomes on Human Regulatory T Cells. *JNCI J. Natl. Cancer Inst.* **107**, (2015).
 212. Yin, Y. *et al.* Tumor-secreted miR-214 induces regulatory T cells: a major link between immune evasion and tumor growth. *Cell Res.* **24**, 1164–1180 (2014).
 213. Raimondo, S. *et al.* Chronic myeloid leukemia-derived exosomes promote tumor growth through an autocrine mechanism. *Cell Commun. Signal.* **13**, 8 (2015).
 214. Min, Q.-H. *et al.* Exosomes derived from imatinib-resistant chronic myeloid leukemia cells mediate a horizontal transfer of drug-resistant trait by delivering miR-365. *Exp. Cell Res.* **362**, 386–393 (2018).
 215. Nehrbas, J., Butler, J. T., Chen, D.-W. & Kurre, P. Extracellular Vesicles and Chemotherapy Resistance in the AML Microenvironment. *Front. Oncol.* **10**, 90 (2020).
 216. Mudgapalli, N. *et al.* The role of exosomes and MYC in therapy resistance of acute myeloid leukemia: Challenges and opportunities. *Mol. Aspects Med.* **70**, 21–32 (2019).
 217. Cai, J. *et al.* Transferred BCR/ABL DNA from K562 Extracellular Vesicles Causes Chronic Myeloid Leukemia in Immunodeficient Mice. *PLoS ONE* **9**, e105200 (2014).
 218. Jurj, A., Pasca, S., Teodorescu, P., Tomuleasa, C. & Berindan-Neagoe, I. Basic knowledge on BCR-ABL1-positive extracellular vesicles. *Biomark. Med.* bmm-2019-0510 (2020) doi:10.2217/bmm-2019-0510.
 219. Kumar, B. *et al.* Acute myeloid leukemia transforms the bone marrow niche into a leukemia-permissive microenvironment through exosome secretion. *Leukemia* **32**, 575–587 (2018).
 220. Huan, J. *et al.* Coordinate regulation of residual bone marrow function by paracrine trafficking of AML exosomes. *Leukemia* **29**, 2285–2295 (2015).
 221. Doron, B. *et al.* Transmissible ER stress reconfigures the AML bone marrow compartment. *Leukemia* **33**, 918–930 (2019).
 222. Corrado, C. *et al.* Exosome-mediated crosstalk between chronic myelogenous leukemia cells and human bone marrow stromal cells triggers an Interleukin 8-dependent survival of leukemia cells. *Cancer Lett.* **348**, 71–76 (2014).
 223. Mineo, M. *et al.* Exosomes released by K562 chronic myeloid leukemia cells promote angiogenesis in a src-dependent fashion. *Angiogenesis* **15**, 33–45 (2012).
 224. Szczepanski, M. J., Szajnik, M., Welsh, A., Whiteside, T. L. & Boyiadzis, M. Blast-derived microvesicles in sera from patients with acute myeloid leukemia suppress natural killer cell function via membrane-associated transforming growth factor- 1. *Haematologica* **96**, 1302–1309 (2011).
 225. Benites, B. D. *et al.* Exosomes in the serum of Acute Myeloid Leukemia patients induce dendritic cell tolerance: Implications for immunotherapy. *Vaccine* **37**, 1377–1383 (2019).
 226. Jafarzadeh, N. *et al.* Alteration of cellular and immune-related properties of bone marrow mesenchymal stem cells and macrophages by K562 chronic myeloid leukemia cell derived exosomes: JAFARZADEH ET AL. *J. Cell. Physiol.* **234**, 3697–3710 (2019).
 227. Giallongo, C. *et al.* Monocytic myeloid-derived suppressor cells as prognostic factor in chronic myeloid leukaemia patients treated with dasatinib. *J. Cell. Mol. Med.* (2017) doi:10.1111/jcmm.13326.
 228. Pyzer, A. R. *et al.* MUC1-mediated induction of myeloid-derived suppressor cells in patients with acute myeloid leukemia. *Blood* **129**, 1791–1801 (2017).
 229. Tohumeken, S. *et al.* Palmitoylated Proteins on AML-Derived Extracellular Vesicles Promote Myeloid-Derived Suppressor Cell Differentiation via TLR2/Akt/mTOR Signaling. *Cancer Res.* **80**, 3663–3676 (2020).
 230. Hong, C.-S. *et al.* Circulating exosomes carrying an immunosuppressive cargo interfere with cellular immunotherapy in acute myeloid leukemia. *Sci. Rep.* **7**, 14684 (2017).
 231. Hong, C.-S. *et al.* Human acute myeloid leukemia blast-derived exosomes in patient-derived xenograft mice mediate immune suppression. *Exp. Hematol.* **76**, 60-66.e2 (2019).
 232. Moussa Agha, D. *et al.* Impact of Bone Marrow miR-21 Expression on Acute Myeloid Leukemia T Lymphocyte Fragility and Dysfunction. *Cells* **9**, 2053 (2020).
 233. Kolba, M. D. *et al.* Tunneling nanotube-mediated intercellular vesicle and protein transfer in the stroma-provided imatinib resistance in chronic myeloid leukemia cells. *Cell Death Dis.* **10**, 817 (2019).
 234. Podszycwalow-Bartnicka, P. *et al.* Increased phosphorylation of eIF2 α in chronic myeloid leukemia

- cells stimulates secretion of matrix modifying enzymes. *Oncotarget* **7**, 79706–79721 (2016).
235. Podszwywalow-Bartnicka, P. *et al.* Characteristics of live parameters of the HS-5 human bone marrow stromal cell line cocultured with the leukemia cells in hypoxia, for the studies of leukemia-stroma cross-talk: Monitoring Stromal Cells in the Leukemia Coculture. *Cytometry A* **93**, 929–940 (2018).
 236. Keeshan, K., Mills, K., Cotter, T. & McKenna, S. Elevated Bcr-Abl expression levels are sufficient for a haematopoietic cell line to acquire a drug-resistant phenotype. *Leukemia* **15**, 1823–1833 (2001).
 237. Lozzio, C. & Lozzio, B. Human chronic myelogenous leukemia cell-line with positive Philadelphia chromosome. *Blood* **45**, 321–334 (1975).
 238. Matsuo, Y. *et al.* Two acute monocytic leukemia (AML-M5a) cell lines (MOLM-13 and MOLM-14) with interclonal phenotypic heterogeneity showing MLL-AF9 fusion resulting from an occult chromosome insertion, ins(11;9)(q23;p22p23). *Leukemia* **11**, 1469–1477 (1997).
 239. Quentmeier, H., Reinhardt, J., Zaborski, M. & Drexler, H. G. FLT3 mutations in acute myeloid leukemia cell lines. *Leukemia* **17**, 120–124 (2003).
 240. Yuana, Y., Levels, J., Grootemaat, A., Sturk, A. & Nieuwland, R. Co-isolation of extracellular vesicles and high-density lipoproteins using density gradient ultracentrifugation. *J. Extracell. Vesicles* **3**, 23262 (2014).
 241. Böing, A. N. *et al.* Single-step isolation of extracellular vesicles by size-exclusion chromatography. *J. Extracell. Vesicles* **3**, 23430 (2014).
 242. Swatler, J. *et al.* Chronic myeloid leukemia-derived extracellular vesicles increase Foxp3 level and suppressive activity of thymic regulatory T cells. *Eur. J. Immunol.* **50**, 606–609 (2020).
 243. Cossarizza, A. *et al.* Guidelines for the use of flow cytometry and cell sorting in immunological studies (second edition). *Eur. J. Immunol.* **49**, 1457–1973 (2019).
 244. Brummelman, J. *et al.* Development, application and computational analysis of high-dimensional fluorescent antibody panels for single-cell flow cytometry. *Nat. Protoc.* **14**, 1946–1969 (2019).
 245. Belkina, A. C. *et al.* Automated optimized parameters for T-distributed stochastic neighbor embedding improve visualization and analysis of large datasets. *Nat. Commun.* **10**, 5415 (2019).
 246. Van Gassen, S. *et al.* FlowSOM: Using self-organizing maps for visualization and interpretation of cytometry data: FlowSOM. *Cytometry A* **87**, 636–645 (2015).
 247. Collison, L. W. & Vignali, D. A. A. In Vitro Treg Suppression Assays. in *Regulatory T Cells* (eds. Kassiotis, G. & Liston, A.) vol. 707 21–37 (Humana Press, 2011).
 248. Schmidt, A., Eriksson, M., Shang, M.-M., Weyd, H. & Tegnér, J. Comparative Analysis of Protocols to Induce Human CD4+Foxp3+ Regulatory T Cells by Combinations of IL-2, TGF-beta, Retinoic Acid, Rapamycin and Butyrate. *PLOS ONE* **11**, e0148474 (2016).
 249. de Kivit, S. *et al.* Stable human regulatory T cells switch to glycolysis following TNF receptor 2 costimulation. *Nat. Metab.* **2**, 1046–1061 (2020).
 250. La Trobe University, Bundoora, Victoria. ExoCarta: EXOSOME PROTEIN, RNA AND LIPID DATABASE. <http://exocarta.org/index.html>. Accessed 27 July 2021. <http://exocarta.org/query.html>.
 251. Rezvani, K. *et al.* Functional leukemia-associated antigen-specific memory CD8+ T cells exist in healthy individuals and in patients with chronic myelogenous leukemia before and after stem cell transplantation. *Blood* **102**, 2892–2900 (2003).
 252. Bilich, T. *et al.* The HLA ligandome landscape of chronic myeloid leukemia delineates novel T-cell epitopes for immunotherapy. 16.
 253. Haribhai, D. *et al.* Regulatory T Cells Dynamically Control the Primary Immune Response to Foreign Antigen. *J. Immunol.* **178**, 2961–2972 (2007).
 254. Lin, W. *et al.* Regulatory T cell development in the absence of functional Foxp3. *Nat. Immunol.* **8**, 359–368 (2007).
 255. Saeys, Y., Van Gassen, S. & Lambrecht, B. N. Computational flow cytometry: helping to make sense of high-dimensional immunology data. *Nat. Rev. Immunol.* **16**, 449–462 (2016).
 256. Carpenter, A. C. *et al.* The Transcription Factors Thpok and LRF Are Necessary and Partly Redundant for T Helper Cell Differentiation. *Immunity* **37**, 622–633 (2012).
 257. Morita, K. *et al.* Egr2 and Egr3 in regulatory T cells cooperatively control systemic autoimmunity through Ltbp3-mediated TGF-β3 production. *Proc. Natl. Acad. Sci.* **113**, E8131–E8140 (2016).
 258. Schmidt, A. *et al.* Time-resolved transcriptome and proteome landscape of human regulatory T cell (Treg) differentiation reveals novel regulators of FOXP3. *BMC Biol.* **16**, 47 (2018).
 259. Van Etten, R. A. Studying the pathogenesis of BCR-ABL+ leukemia in mice. *Oncogene* **21**, 8643–

- 8651 (2002).
260. Koschmieder, S. *et al.* Inducible chronic phase of myeloid leukemia with expansion of hematopoietic stem cells in a transgenic model of BCR-ABL leukemogenesis. *Blood* **105**, 324–334 (2005).
 261. Bertilaccio, M. T. S. *et al.* Xenograft models of chronic lymphocytic leukemia: problems, pitfalls and future directions. *Leukemia* **27**, 534–540 (2013).
 262. Li, H. *et al.* Dysfunctional CD8 T Cells Form a Proliferative, Dynamically Regulated Compartment within Human Melanoma. *Cell* **176**, 775–789.e18 (2019).
 263. Olkhanud, P. B. *et al.* Tumor-Evoked Regulatory B Cells Promote Breast Cancer Metastasis by Converting Resting CD4⁺ T Cells to T-Regulatory Cells. *Cancer Res.* **71**, 3505–3515 (2011).
 264. Sun, W. *et al.* A positive-feedback loop between tumour infiltrating activated Treg cells and type 2-skewed macrophages is essential for progression of laryngeal squamous cell carcinoma. *Br. J. Cancer* **117**, 1631–1643 (2017).
 265. Pilanc, P. *et al.* A Novel Oral Arginase 1/2 Inhibitor Enhances the Antitumor Effect of PD-1 Inhibition in Murine Experimental Gliomas by Altering the Immunosuppressive Environment. *Front. Oncol.* **11**, 703465 (2021).
 266. Sosnowska, A. *et al.* Inhibition of arginase modulates T-cell response in the tumor microenvironment of lung carcinoma. *Oncolimmunology* **10**, 1956143 (2021).
 267. Swatler, J. & Kozłowska, E. Immunoterapie nowotworów działające na punkty kontrolne układu odpornościowego. *Postepy Hig Med Dosw* **18**.
 268. Chao, M. P., Weissman, I. L. & Majeti, R. The CD47–SIRP α pathway in cancer immune evasion and potential therapeutic implications. *Curr. Opin. Immunol.* **24**, 225–232 (2012).
 269. Plitas, G. & Rudensky, A. Y. Regulatory T Cells in Cancer. **21** (2020).
 270. Green, J. A., Arpaia, N., Schizas, M., Dobrin, A. & Rudensky, A. Y. A nonimmune function of T cells in promoting lung tumor progression. *J. Exp. Med.* **214**, 3565–3575 (2017).
 271. Onda, M., Kobayashi, K. & Pastan, I. Depletion of regulatory T cells in tumors with an anti-CD25 immunotoxin induces CD8 T cell-mediated systemic antitumor immunity. *Proc. Natl. Acad. Sci.* **116**, 4575–4582 (2019).
 272. Jacobs, J. F. M. *et al.* Dendritic Cell Vaccination in Combination with Anti-CD25 Monoclonal Antibody Treatment: A Phase I/II Study in Metastatic Melanoma Patients. *Clin. Cancer Res.* **16**, 5067–5078 (2010).
 273. Hehlmann, R. How I treat CML blast crisis. *Blood* **120**, 737–747 (2012).
 274. Bonifacio, M., Stagno, F., Scaffidi, L., Krampera, M. & Di Raimondo, F. Management of Chronic Myeloid Leukemia in Advanced Phase. *Front. Oncol.* **9**, 1132 (2019).
 275. Daver, N. *et al.* New directions for emerging therapies in acute myeloid leukemia: the next chapter. *Blood Cancer J.* **10**, 107 (2020).
 276. Vitale, S. R. *et al.* Detection of tumor-derived extracellular vesicles in plasma from patients with solid cancer. *BMC Cancer* **21**, 315 (2021).
 277. Li, Y. *et al.* EV-origin: Enumerating the tissue-cellular origin of circulating extracellular vesicles using exLR profile. *Comput. Struct. Biotechnol. J.* **18**, 2851–2859 (2020).
 278. Kuravi, S. J. *et al.* Changes in the pattern of plasma extracellular vesicles after severe trauma. *PLOS ONE* **12**, e0183640 (2017).
 279. Bernardi, S. *et al.* Feasibility of tumor-derived exosome enrichment in the onco-hematology leukemic model of chronic myeloid leukemia. *Int. J. Mol. Med.* (2019) doi:10.3892/ijmm.2019.4372.
 280. Kang, K.-W. *et al.* The Potential of Exosomes Derived from Chronic Myelogenous Leukaemia Cells as a Biomarker. *Anticancer Res.* **38**, 3935–3942 (2018).
 281. Trino, S. *et al.* Clinical relevance of extracellular vesicles in hematological neoplasms: from liquid biopsy to cell biopsy. *Leukemia* **35**, 661–678 (2021).
 282. Xu, R. *et al.* Extracellular vesicles in cancer — implications for future improvements in cancer care. *Nat. Rev. Clin. Oncol.* **15**, 617–638 (2018).
 283. Becker, A. *et al.* Extracellular Vesicles in Cancer: Cell-to-Cell Mediators of Metastasis. *Cancer Cell* **30**, 836–848 (2016).
 284. Costa-Silva, B. *et al.* Pancreatic cancer exosomes initiate pre-metastatic niche formation in the liver. *Nat. Cell Biol.* **17**, 816–826 (2015).
 285. Peinado, H. *et al.* Melanoma exosomes educate bone marrow progenitor cells toward a pro-metastatic phenotype through MET. *Nat. Med.* **18**, 883–891 (2012).
 286. Bobrie, A. *et al.* Rab27a Supports Exosome-Dependent and -Independent Mechanisms That

- Modify the Tumor Microenvironment and Can Promote Tumor Progression. *Cancer Res.* **72**, 4920–4930 (2012).
287. Guo, D. *et al.* RAB27A promotes melanoma cell invasion and metastasis *via* regulation of pro-invasive exosomes. *Int. J. Cancer* **144**, 3070–3085 (2019).
 288. Ohta, A. *et al.* A2A adenosine receptor protects tumors from antitumor T cells. *Proc. Natl. Acad. Sci.* **103**, 13132–13137 (2006).
 289. Perrot, I. *et al.* Blocking Antibodies Targeting the CD39/CD73 Immunosuppressive Pathway Unleash Immune Responses in Combination Cancer Therapies. *Cell Rep.* **27**, 2411–2425.e9 (2019).
 290. Moesta, A. K., Li, X.-Y. & Smyth, M. J. Targeting CD39 in cancer. *Nat. Rev. Immunol.* **20**, 739–755 (2020).
 291. Sato, T. *et al.* Interleukin 10 in the tumor microenvironment: a target for anticancer immunotherapy. *Immunol. Res.* **51**, 170–182 (2011).
 292. Xu, Y. *et al.* Regulatory T cells promote the stemness of leukemia stem cells through IL10 cytokine-related signaling pathway. *Leukemia* (2021) doi:10.1038/s41375-021-01375-2.
 293. Lai, C. P. *et al.* Visualization and tracking of tumour extracellular vesicle delivery and RNA translation using multiplexed reporters. *Nat. Commun.* **6**, 7029 (2015).
 294. Verweij, F. J. *et al.* The power of imaging to understand extracellular vesicle biology in vivo. *Nat. Methods* **18**, 1013–1026 (2021).
 295. Guilliams, M. *et al.* *Spatial proteogenomics reveals distinct and evolutionarily-conserved hepatic macrophage niches.* <http://biorxiv.org/lookup/doi/10.1101/2021.10.15.464432> (2021) doi:10.1101/2021.10.15.464432.
 296. Browaeys, R., Saelens, W. & Saeys, Y. NicheNet: modeling intercellular communication by linking ligands to target genes. *Nat. Methods* **17**, 159–162 (2020).
 297. Bonnardel, J. *et al.* Stellate Cells, Hepatocytes, and Endothelial Cells Imprint the Kupffer Cell Identity on Monocytes Colonizing the Liver Macrophage Niche. *Immunity* **51**, 638–654.e9 (2019).
 298. Doma, E. *et al.* A robust approach for the generation of functional hematopoietic progenitor cell lines to model leukemic transformation. *Blood Adv.* **5**, 39–53 (2021).
 299. Krause, D. S. *et al.* Differential regulation of myeloid leukemias by the bone marrow microenvironment. *Nat. Med.* **19**, 1513–1517 (2013).
 300. Zhang, H., Lu, J., Liu, J., Zhang, G. & Lu, A. Advances in the discovery of exosome inhibitors in cancer. *J. Enzyme Inhib. Med. Chem.* **35**, 1322–1330 (2020).
 301. Johnson, J. L. *et al.* Identification of Neutrophil Exocytosis Inhibitors (Nexinhibs), Small Molecule Inhibitors of Neutrophil Exocytosis and Inflammation. *J. Biol. Chem.* **291**, 25965–25982 (2016).
 302. Essandoh, K. *et al.* Blockade of exosome generation with GW4869 dampens the sepsis-induced inflammation and cardiac dysfunction. *Biochim. Biophys. Acta BBA - Mol. Basis Dis.* **1852**, 2362–2371 (2015).
 303. Wang, B., Wang, Y., Yan, Z., Sun, Y. & Su, C. Colorectal cancer cell-derived exosomes promote proliferation and decrease apoptosis by activating the ERK pathway. **11**.
 304. Tallon, C. *et al.* Nipping disease in the bud: nSMase2 inhibitors as therapeutics in extracellular vesicle-mediated diseases. *Drug Discov. Today* **26**, 1656–1668 (2021).
 305. Manzari, M. T. *et al.* Targeted drug delivery strategies for precision medicines. *Nat. Rev. Mater.* **6**, 351–370 (2021).
 306. Quek, L. *et al.* Genetically distinct leukemic stem cells in human CD34+ acute myeloid leukemia are arrested at a hemopoietic precursor-like stage. *J. Exp. Med.* **213**, 1513–1535 (2016).
 307. O’Hear, C., Heiber, J. F., Schubert, I., Fey, G. & Geiger, T. L. Anti-CD33 chimeric antigen receptor targeting of acute myeloid leukemia. *Haematologica* **100**, 336–344 (2015).
 308. Ochocka, N. *et al.* Single-cell RNA sequencing reveals functional heterogeneity of glioma-associated brain macrophages. *Nat. Commun.* **12**, 1151 (2021).
 309. Katzenelenbogen, Y. *et al.* Coupled scRNA-Seq and Intracellular Protein Activity Reveal an Immunosuppressive Role of TREM2 in Cancer. *Cell* **182**, 872–885.e19 (2020).
 310. Li, H. *et al.* Dysfunctional CD8 T Cells Form a Proliferative, Dynamically Regulated Compartment within Human Melanoma. *Cell* **176**, 775–789.e18 (2019).
 311. Cohen, Y. C. *et al.* Identification of resistance pathways and therapeutic targets in relapsed multiple myeloma patients through single-cell sequencing. *Nat. Med.* **27**, 491–503 (2021).
 312. Massalha, H. *et al.* A single cell atlas of the human liver tumor microenvironment. *Mol. Syst. Biol.* **16**, (2020).
 313. Barsheshet, Y. *et al.* CCR8 + FOXP3 + T_{reg} cells as master drivers of immune regulation. *Proc.*

- Natl. Acad. Sci.* **114**, 6086–6091 (2017).
314. Ward-Kavanagh, L. K., Lin, W. W., Šedý, J. R. & Ware, C. F. The TNF Receptor Superfamily in Co-stimulating and Co-inhibitory Responses. *Immunity* **44**, 1005–1019 (2016).
 315. Heiser, R. A., Grogan, B. M., Manlove, L. S. & Gardai, S. J. Abstract 1789: CD30⁺T regulatory cells, but not CD30⁺CD8⁺ T cells, are impaired following brentuximab vedotin treatment in vitro and in vivo. *Cancer Res.* **78**, 1789 (2018).
 316. Mahmud, S. A. *et al.* Costimulation via the tumor-necrosis factor receptor superfamily couples TCR signal strength to the thymic differentiation of regulatory T cells. *Nat. Immunol.* **15**, 473–481 (2014).
 317. Kleijwegt, F. S. *et al.* Critical Role for TNF in the Induction of Human Antigen-Specific Regulatory T Cells by Tolerogenic Dendritic Cells. *J. Immunol.* **185**, 1412–1418 (2010).
 318. Lozano, E., Dominguez-Villar, M., Kuchroo, V. & Hafler, D. A. The TIGIT/CD226 Axis Regulates Human T Cell Function. *J. Immunol.* **188**, 3869–3875 (2012).
 319. Lucca, L. E. *et al.* TIGIT signaling restores suppressor function of Th1 Tregs. *JCI Insight* **4**, e124427 (2019).
 320. Mair, F. *et al.* *Extricating human tumor-unique immune alterations from non-malignant tissue inflammation.* <https://www.researchsquare.com/article/rs-356214/v1> (2021) doi:10.21203/rs.3.rs-356214/v1.
 321. Kim, M.-C. *et al.* CD177 modulates the function and homeostasis of tumor-infiltrating regulatory T cells. *Nat. Commun.* **12**, 5764 (2021).
 322. Stoeckius, M. *et al.* Simultaneous epitope and transcriptome measurement in single cells. *Nat. Methods* **14**, 865–868 (2017).
 323. Baccin, C. *et al.* Combined single-cell and spatial transcriptomics reveal the molecular, cellular and spatial bone marrow niche organization. *Nat. Cell Biol.* **22**, 38–48 (2020).
 324. Triana, S. H. *et al.* *Single-cell proteo-genomic reference maps of the hematopoietic system enable the purification and massive profiling of precisely defined cell states.* <http://biorxiv.org/lookup/doi/10.1101/2021.03.18.435922> (2021) doi:10.1101/2021.03.18.435922.
 325. Pere, H. *et al.* A CCR4 antagonist combined with vaccines induces antigen-specific CD8₂ T cells and tumor immunity against self antigens. **118**, 10 (2011).
 326. Kurose, K. *et al.* Phase Ia Study of FoxP3 + CD4 Treg Depletion by Infusion of a Humanized Anti-CCR4 Antibody, KW-0761, in Cancer Patients. *Clin. Cancer Res.* **21**, 4327–4336 (2015).
 327. Villarreal, D. O. *et al.* Targeting CCR8 Induces Protective Antitumor Immunity and Enhances Vaccine-Induced Responses in Colon Cancer. *Cancer Res.* **78**, 5340–5348 (2018).
 328. Hodi, F. S. *et al.* Improved Survival with Ipilimumab in Patients with Metastatic Melanoma. *N. Engl. J. Med.* **363**, 711–723 (2010).
 329. Robert, C. *et al.* Ipilimumab plus Dacarbazine for Previously Untreated Metastatic Melanoma. *N. Engl. J. Med.* **364**, 2517–2526 (2011).
 330. Romano, E. *et al.* Ipilimumab-dependent cell-mediated cytotoxicity of regulatory T cells ex vivo by nonclassical monocytes in melanoma patients. *Proc. Natl. Acad. Sci.* **112**, 6140–6145 (2015).
 331. Tarhini, A. A. *et al.* Immune Monitoring of the Circulation and the Tumor Microenvironment in Patients with Regionally Advanced Melanoma Receiving Neoadjuvant Ipilimumab. *PLoS ONE* **9**, e87705 (2014).
 332. Siu, L. L. *et al.* Preliminary results of a phase I/IIa study of BMS-986156 (glucocorticoid-induced tumor necrosis factor receptor–related gene [GITR] agonist), alone and in combination with nivolumab in pts with advanced solid tumors. *J. Clin. Oncol.* **35**, 104–104 (2017).
 333. Torrey, H. *et al.* Targeting TNFR2 with antagonistic antibodies inhibits proliferation of ovarian cancer cells and tumor-associated T_{regs}. *Sci. Signal.* **10**, eaaf8608 (2017).
 334. Marabelle, A. *et al.* Depleting tumor-specific Tregs at a single site eradicates disseminated tumors. *J. Clin. Invest.* **123**, 2447–2463 (2013).
 335. Wang, M. *et al.* Increased Regulatory T Cells in Peripheral Blood of Acute Myeloid Leukemia Patients Rely on Tumor Necrosis Factor (TNF)-α–TNF Receptor-2 Pathway. *Front. Immunol.* **9**, 1274 (2018).
 336. Malchow, S., Leventhal, D. S. & Savage, P. A. Organ-specific regulatory T cells of thymic origin are expanded in murine prostate tumors. *Oncol Immunology* **2**, e24898 (2013).
 337. Wainwright, D. A., Sengupta, S., Han, Y. & Lesniak, M. S. Thymus-derived rather than tumor-induced regulatory T cells predominate in brain tumors. *Neuro-Oncol.* **13**, 1308–1323 (2011).
 338. Ahmadzadeh, M. *et al.* Tumor-infiltrating human CD4⁺ regulatory T cells display a distinct TCR repertoire and exhibit tumor and neoantigen reactivity. *Sci. Immunol.* **4**, eaao4310 (2019).

339. Chalmers, Z. R. *et al.* Analysis of 100,000 human cancer genomes reveals the landscape of tumor mutational burden. *Genome Med.* **9**, 34 (2017).
340. Dermime, S. *et al.* CD4+ Regulatory T Cells Specific for the WT1 Antigen Are Present in Acute Myeloid Leukemia Patients: Implication for Immunotherapy. *Blood* **112**, 1933–1933 (2008).
341. Benito, J., Zeng, Z., Konopleva, M. & Wilson, W. R. Targeting hypoxia in the leukemia microenvironment. *Int. J. Hematol. Oncol.* **2**, 279–288 (2013).
342. Wolf, T. *et al.* Dynamics in protein translation sustaining T cell preparedness. *Nat. Immunol.* **21**, 927–937 (2020).
343. Feng, Y. *et al.* Control of the Inheritance of Regulatory T Cell Identity by a cis Element in the Foxp3 Locus. *Cell* **158**, 749–763 (2014).
344. Antov, A., Yang, L., Vig, M., Baltimore, D. & Van Parijs, L. Essential Role for STAT5 Signaling in CD25 + CD4 + Regulatory T Cell Homeostasis and the Maintenance of Self-Tolerance. *J. Immunol.* **171**, 3435–3441 (2003).
345. Kollmann, S. *et al.* Twins with different personalities: STAT5B—but not STAT5A—has a key role in BCR/ABL-induced leukemia. *Leukemia* **33**, 1583–1597 (2019).
346. Salmond, R. J. mTOR Regulation of Glycolytic Metabolism in T Cells. *Front. Cell Dev. Biol.* **6**, 122 (2018).
347. Mbanwi, A. N. & Watts, T. H. Costimulatory TNFR family members in control of viral infection: Outstanding questions. *Semin. Immunol.* **26**, 210–219 (2014).
348. Wortzman, M. E., Clouthier, D. L., McPherson, A. J., Lin, G. H. Y. & Watts, T. H. The contextual role of TNFR family members in CD8 + T-cell control of viral infections. *Immunol. Rev.* **255**, 125–148 (2013).
349. Bartkowiak, T. & Curran, M. A. 4-1BB Agonists: Multi-Potent Potentiators of Tumor Immunity. *Front. Oncol.* **5**, (2015).
350. Freeman, Z. T. *et al.* A conserved intratumoral regulatory T cell signature identifies 4-1BB as a pan-cancer target. *J. Clin. Invest.* **130**, 1405–1416 (2020).
351. Schmohl, J. U. *et al.* Expression of 4-1BB and its ligand on blasts correlates with prognosis of patients with AML. *J. Investig. Med.* **64**, 1252 (2016).
352. Baessler, T. *et al.* CD137 ligand mediates opposite effects in human and mouse NK cells and impairs NK-cell reactivity against human acute myeloid leukemia cells. *Blood* **115**, 3058–3069 (2010).
353. Hentschel, N. *et al.* Serum levels of sCD137 (4-1BB) ligand are prognostic factors for progression in acute myeloid leukemia but not in non-Hodgkin's lymphoma. *Eur. J. Haematol.* **77**, 91–101 (2006).
354. Willoughby, J. E. *et al.* Differential Impact of CD27 and 4-1BB Costimulation on Effector and Memory CD8 T Cell Generation following Peptide Immunization. *J. Immunol.* **193**, 244–251 (2014).
355. Woroniecka, K. I. *et al.* 4-1BB Agonism Averts TIL Exhaustion and Licenses PD-1 Blockade in Glioblastoma and Other Intracranial Cancers. *Clin. Cancer Res.* **26**, 1349–1358 (2020).
356. Woroniecka, K. & Fecci, P. E. 4-1BB Agonism as a strategy to license immune checkpoint blockade in glioblastoma. *Oncoscience* **7**, 34–35 (2020).
357. Weigelin, B. *et al.* Focusing and sustaining the antitumor CTL effector killer response by agonist anti-CD137 mAb. *Proc. Natl. Acad. Sci.* **112**, 7551–7556 (2015).
358. Kobayashi, T., Doff, B. L., Rearden, R. C., Leggatt, G. R. & Mattarollo, S. R. NKT cell-targeted vaccination plus anti-4-1BB antibody generates persistent CD8 T cell immunity against B cell lymphoma. *OncolImmunology* **4**, e990793 (2015).
359. Buchan, S. L. *et al.* Antibodies to Costimulatory Receptor 4-1BB Enhance Anti-tumor Immunity via T Regulatory Cell Depletion and Promotion of CD8 T Cell Effector Function. *Immunity* **49**, 958–970.e7 (2018).
360. Kerage, D. *et al.* Therapeutic vaccination with 4-1BB co-stimulation eradicates mouse acute myeloid leukemia. *OncolImmunology* **7**, e1486952 (2018).
361. Chester, C., Sanmamed, M. F., Wang, J. & Melero, I. Immunotherapy targeting 4-1BB: mechanistic rationale, clinical results, and future strategies. *Blood* **131**, 49–57 (2018).
362. Qi, X. *et al.* Optimization of 4-1BB antibody for cancer immunotherapy by balancing agonistic strength with FcγR affinity. *Nat. Commun.* **10**, 2141 (2019).
363. Siravegna, G., Marsoni, S., Siena, S. & Bardelli, A. Integrating liquid biopsies into the management of cancer. *Nat. Rev. Clin. Oncol.* **14**, 531–548 (2017).
364. Melo, S. A. *et al.* Glypican-1 identifies cancer exosomes and detects early pancreatic cancer.

- Nature* **523**, 177–182 (2015).
365. Libregts, S. F. W. M., Arkesteijn, G. J. A., Németh, A., Nolte-'t Hoen, E. N. M. & Wauben, M. H. M. Flow cytometric analysis of extracellular vesicle subsets in plasma: impact of swarm by particles of non-interest. *J. Thromb. Haemost.* **16**, 1423–1436 (2018).

8 PUBLICATIONS - OUTCOME OF THE THESIS

The following publications have been created while conducting studies for the presented thesis and include the described results:

Original papers:

- **Swatler J.**, Dudka W., Bugajski L., Brewinska-Olchowik M., Kozłowska E. & Piwocka K., 2020. Chronic myeloid leukemia-derived extracellular vesicles increase Foxp3 level and suppressive activity of thymic regulatory T cells, *European Journal of Immunology* (50(4):606-609)
- **Swatler J.**, Dudka W., Piwocka K., 2020. Isolation and characterization of extracellular vesicles from cell culture conditioned medium for immunological studies, *Current Protocols in Immunology* (129(1): e96)
- **Swatler J.**, Turos-Korgul L., Brewinska-Olchowik M., De Biasi S., Dudka W., Le BV., Kominek A., Cyranowski S., Pilanc-Kudlek P., Mohammadi E., Cysewski D., Kozłowska E., Grabowska-Pyrzewicz W., Wojda U., Basak G., Mieczkowski J., Skorski T., Cossarizza A. & Piwocka K., 4-1BBL-containing leukemic extracellular vesicles promote immunosuppressive effector regulatory T cells, in revision in *Blood Advances*

Review paper:

- **Swatler J.**, Turos-Korgul L., Kozłowska E., Piwocka K., 2021. Immunosuppressive Cell Subsets and Factors in Myeloid Leukemias, *Cancers* (13(6), 1203)